DR-1911

ANL/ES-CEN-1011

ANNUAL REPORT

ON

A DEVELOPMENT PROGRAM ON PRESSURIZED FLUIDIZED-BED COMBUSTION

Contract No. 14-32-0001-1780

ARGONNE NATIONAL LABORATORY

July 1975

Annual Report for Period

July 1, 1974 - June 30, 1975

Prepared For

OFFICE OF FOSSIL ENERGY

UNITED STATES ENERGY RESEARCH AND DEVELOPMENT ADMINISTRATION

WASHINGTON, D. C. 20545

DISCLAIMER

Printed in the United States of America
Available from
National Technical Information Service
U. S. Department of Commerce
5285 Port Royal Road
Springfield, Virginia 22161
Price: Printed Copy $7.60; Microfiche $2.25

ANL/ES-CEN-1011
Distribution Category UC-90e

A DEVELOPMENT PROGRAM ON PRESSURIZED FLUIDIZED-BED COMBUSTION

Annual Report
July 1, 1974 - June 30, 1975

G. J. Vogel, P. Cunningham, J. Fischer, B. Hubble, S. Lee, J. Lenc, J. Montagna, A. Panek, C. Schoffstoll, S. Siegel, G. Smith, S. Smith, R. Snyder, S. Saxena, J. Stockbar, W. Swift, G. Teats, I. Wilson, and A. A. Jonke

ARGONNE NATIONAL LABORATORY
9700 South Cass Avenue
Argonne, Illinois 60439

July 1975

PREPARED FOR THE UNITED STATES
ENERGY RESEARCH AND DEVELOPMENT ADMINISTRATION
Under Contract No. 14-32-0001-1780

BIBLIOGRAPHIC DATA SHEET	1. Report No. ANL/ES-CEN-1011	2.	3. Recipient's Accession No.

4. Title and Subtitle

A Development Program on Pressurized Fluidized-Bed Combustion

5. Report Date: July 1975

6.

7. Author(s) G. Vogel, P. Cunningham, J. Lenc, B. Hubble, J. Montagna, A. Panek, C. Schoffstoll, S. Siegel, G. Smith, S. Saxena, S. Smith, R. Snyder, W. Swift, G. Teats, I. Wilson, J. Stockbar, J. Fischer, S. Lee, and A. A. Jonke

8. Performing Organization Rept. No. ANL/ES-CEN-1011

10. Project/Task/Work Unit No.

9. Performing Organization Name and Address

Argonne National Laboratory
9700 South Cass Avenue
Argonne, Illinois 60439

11. Contract/Grant No. 14-32-0001-1780

12. Sponsoring Organization Name and Address

U.S. Energy Research and Development Administration

13. Type of Report & Period Covered: Annual, July 1974 - June 1975

14.

15. Supplementary Notes

16. Abstract: The feasibility of using fluidized-bed combustors in power and steam plants is being evaluated. The concept involves burning fuels such as coal in a fluidized bed of either a naturally occurring, calcium-containing limestone or dolomite or in a synthetically prepared calcium-containing stone. The calcium oxide in the stone reacts with the sulfur released during combustion to form calcium sulfate, which remains in the bed, thus decreasing the level of SO_2 in the flue gas. Levels of NO_x in the flue gas are also low. The effect of operating variables and type of stone on the levels of SO_2 and NO_x is being determined. Behavior of trace elements during combustion has been preliminarily evaluated. The properties of a fluidized bed at minimum fluidization at different temperature and pressures have been determined.

The $CaSO_4$ produced in the combustion process is regenerated to CaO for reuse in the combustor by reductive decomposition at 1095°C/2000°F. The effects of operating variables on sulfur release during regeneration are being evaluated. Another regeneration process, solid-solid reaction of $CaSO_4$ with CaS, is also being investigated.

Fundamental investigations of the kinetics of sulfation and regeneration reactions for the natural and synthetic stones are continuing. A model for the sulfation reaction is presented.

The status of the new combustor and ancillary regeneration equipment is discussed.

17. Key Words and Document Analysis

Air Pollution
Fluidized-Bed Processing
Sulfur Oxides
Dolomite
Fossil Fuel
Combustion
Coal
Calcium Sulfates
Additives
Sulfur
Kerosene
Sulfation
Mercury
Regenerator
Regeneration
Carbonation

17a.

Calcium Oxides
Calcium Carbonate
Flue Gas
X-ray Diffraction
Methane
Aluminum Oxide
Carbon Monoxide
Roasting
Calcium Sulfide
Limestone
Nitrogen Oxide
Combustion Efficincy
Fly Ash

17b. Identifiers/Open-Ended Terms

Air Pollution Control
Stationary Sources
Fluidized-Bed Combustion
Supported Additives
Additive Regeneration
Combined-cycle Power Generation

17c. COSATI Field/Group 13B

18. Availability Statement	19. Security Class (This Report) UNCLASSIFIED	21. No. of Pages
	20. Security Class (This Page) UNCLASSIFIED	22. Price

TABLE OF CONTENTS

TABLE OF CONTENTS (Cont'd)

LIST OF FIGURES

LIST OF FIGURES (Cont'd)

LIST OF FIGURES (Cont'd)

LIST OF FIGURES (Cont'd)

LIST OF FIGURES (Cont'd)

LIST OF TABLES

LIST OF TABLES (Cont'd)

LIST OF TABLES (Cont'd.)

ABSTRACT

The feasibility of using fluidized-bed combustors in power and steam plants is being evaluated. The concept involves burning fuels such as coal in a fluidized bed of either a naturally occurring, calcium-containing limestone or dolomite or in a synthetically prepared calcium-containing stone. The calcium oxide in the stone reacts with the sulfur released during combustion to form calcium sulfate, which remains in the bed, thus decreasing the level of SO_2 in the flue gas. Levels of NO_x in the flue gas are also low. The effect of operating variables and type of stone on the levels of SO_2 and NO_x is being determined. Behavior of trace elements during combustion has been preliminarily evaluated. The properties of a fluidized bed at minimum fluidization at different temperatures and pressures have been determined.

The $CaSO_4$ produced in the combustion process is regenerated to CaO for reuse in the combustor by reductive decomposition at 1095°C/2000°F. The effects of operating variables on sulfur release during regeneration are being evaluated. Another regeneration process, solid-solid reaction of $CaSO_4$ with CaS, is also being investigated.

Fundamental investigations of the kinetics of sulfation and regeneration reactions for the natural and synthetic stones are continuing. A model for the sulfation reaction is presented.

The status of the new combustor and ancillary regenerator equipment is discussed.

SUMMARY

In fluidized-bed combustion, coal is completely combusted in a bed of partially sulfated additive using an excess of oxygen. Sulfur contained in the coal is released during combustion as SO_2, which in the excess-oxygen environment reacts with the additive to form $CaSO_4$. The additive can be a naturally occurring calcium-containing limestone/dolomite or it may be a synthetically prepared material consisting of calcium oxide-impregnated on a support material. Fresh additive is continuously added to the combustor and sulfated material is continuously withdrawn to keep the level of the bed constant. The sulfated material can be regenerated (an alternative to discarding the sulfated material) to obtain (1) CaO that can be returned to the combustor for reuse and (2) SO_2 that can be converted either to sulfur or to sulfuric acid. The regeneration process of main interest consists of reacting the $CaSO_4$ with a reductant at ∿1095°C/∿2000°F. Other regeneration reactions are also being studied.

The current program on regeneration consists of studying (1) the effects of operating variables on the reductive decomposition of $CaSO_4$ to CaO, (2) the regeneration-sulfation of synthetic additives, (3) the possible use of other regeneration reactions such as the solid-solid, $CaSO_4$-CaS reaction, and (4) the chemistry of the sulfation-regeneration reactions. Combustion studies have been made to determine (1) the effect of operating variables and different additives on SO_2 and NO_x emissions, (2) the behavior of biologically hazardous elements--Hg, Be, F, and Pb--during combustion and the fate of elements such as Na which are potentially corrosive to turbine blade and equipment metals. Another study pertinent to the program is determining the effects of temperature and pressure on minimum fluidization velocities of particles. The status of equipment design and construction is described.

One-Step Regeneration Experiments

One-step or reductive decomposition regeneration experiments were completed to evaluate the effects of experimental conditions on the regeneration of CaO from sulfated Tymochtee dolomite additive. The reduction of $CaSO_4$ to CaO is favored by high temperatures (≥1900°F/1038°C) and mildly reducing conditions.

$$CaSO_4 + CO \rightarrow CaO + SO_2 + CO_2 \quad (1)$$

$$CaSO_4 + H_2 \rightarrow CaO + SO_2 + H_2O \quad (2)$$

At lower temperatures (∿870-925°C/∿1600-1700°F) and under more highly reducing conditions, the following reactions are favored:

$$CaSO_4 + 4CO \rightarrow CaS + 4CO_2 \quad (3)$$

$$CaSO_4 + 4H_2 \rightarrow CaS + 4H_2O \quad (4)$$

The effects of temperature, residence time, total concentration of reducing gas (H_2, CO, or CH_4) in the fluidized bed, and height of fluidized bed on the regeneration of CaO from $CaSO_4$ were evaluated.

Sulfated Tymochtee dolomite containing either ∿7 or 10.2 wt % S was egenerated in the one-step regeneration experiments. The sulfated material ad been produced in combustion experiments. Experiments were made in the 3-in.-dia fluidized-bed regenerator.

One-Step Regeneration with the *In Situ* Combustion of Kerosene Under Reducing Conditions. In these experiments, the reducing gases were generated by the combustion of kerosene under reducing conditions. The maximum SO_2 concentration in the off-gas was 3%. Plugging of the bed overflow line and the off-gas system was encountered in most of the regeneration experiments; this caused the experiments to be terminated before steady state conditions could be established. Heavy petroleum byproducts were found in the plugging material.

One-Step Regeneration with the *In Situ* Combustion of Methane. In situ partial combustion of methane (instead of kerosene, which had caused operating problems) was used in these experiments to provide the heat and the reducing gas (CO, H_2, and excess CH_4) necessary for the regeneration of CaO from sulfated additive. Results obtained in eleven regeneration experiments, in which sulfated Tymochtee dolomite containing 10.2 wt % S was regenerated, have shown the following:

(1) When replicating one experiment three times the sulfur regeneration results agreed within 8%, ranging from 57 to 65%. The difference in completeness of regeneration was due mainly to small differences in the fluidizing-gas velocity at which these experiments were performed.

(2) Deeper beds resulted in poorer regeneration. The effect of fluidized-bed heights of 2.5 ft and 1.5 ft were evaluated.

(3) Poorer regeneration was obtained at lower bed temperatures. Fluidized-bed temperatures ranged from 1010°C (1850°F) to 1093°C (2000°F).

(4) Increasing the fluidizing gas velocity adversely affected regeneration. Data from an experiment at a fluidizing velocity of 3.0 ft/sec were compared with one at 2.2 ft/sec.

(5) When the residence time of the solid in the bed was effectively doubled by regenerating a previously regenerated batch of sulfated dolomite, the regeneration rate remained high in the second regeneration. The combined material from the first regeneration had a sulfur concentration of ∿5.8 wt %. After the second regeneration it was 2.7 wt %.

Material and Energy Balances. An experimental program is being initiated to develop and demonstrate the technical feasibility of one-step regeneration at atmospheric pressure. A technical objective of the program is ultimately to reduce sulfated additive in a fluidized bed by the in situ partial combustion of coal. Additive particles will be processed, using a high solids throughput, *i.e.*, short reactor residence times (surface utilization only).

Material and energy balances have been determined for three sets of base conditions to assess the potential operating capabilities of the unit at high solids throughput. The energy balances clearly emphasize the penalty imposed by not preheating the reactants (and inerts). Approximately 50 to 60% of the heat input to the unit is required to raise the temperature of the reactants to the design operating temperature of 2000°F, and only 15 to 25% of the fuel is required to carry out the reduction reaction.

Preparation, Sulfation, and Regeneration of Calcium Oxide-Impregnated Supported Additives

A research program is in progress to determine the feasibility of using supported additives for removing SO_2 from the combustion gas. Various supports will be studied, with the major candidate being α-Al_2O_3. Currently, only CaO and K_2O are being considered as additives. Methods for impregnating an α-Al_2O_3 support with an additive are described.

Pellets (catalyst support material) containing 6.6% CaO have been sulfated and regenerated in a thermal gravimetric analysis (TGA) unit to determine the rates of sulfation and regeneration, the percent calcium oxide utilization during sulfation, and the effects of the various gases on the kinetics of the reactions. Results of sulfation at 900°C, using gas streams containing as little as 0.3% SO_2, show that more than 60% of the calcium oxide is utilized for SO_2 capture within 40 min. The sulfation rate is proportional to the SO_2 gas composition (0.3 to 3% SO_2), but the order of the reaction has not been determined at this time. A minimum of 75% of the calcium oxide was utilized within 4 hr at the SO_2 gas compositions used.

One-step regeneration studies have been performed at 1100°C using carbon monoxide at concentrations of 0.5 to 6%. In all cases, complete reduction of the $CaSO_4$ was obtained. The regeneration reaction rate was approximately first order and very rapid--only $\sim$5 min being required to reduce the $CaSO_4$ in the pellets using 6% CO in N_2.

In preliminary fluidization experiments using only air and calcium oxide-impregnated supports, no decrepitation of pellets or calcium loss from the pellets were observed.

Sulfur Emission Control Chemistry

The fundamental aspects of the chemical reactions and structural properties related to the cyclic use of limestone and other reagents to control sulfur emissions are being investigated. A number of exploratory experiments have been conducted to determine those factors that influence reaction rates, the degree of reagent utilization, the ease of sorbent regeneration, and the extent of decrepitation. Techniques to obtain the experimental data include thermogravimetric analyses (TGA), differential thermal analyses (DTA), X-ray diffraction, optical microscopy, electron microscopy, electron microprobe, and infrared spectroscopy.

A rudimentary mathematical model has been developed to assist in interpreting the experimental data. This model successfully fits much of the sulfation data presently available, but certain parameters are still without physical significance. Nevertheless, this model has been useful for suggesting lines of investigation and will serve as a point of departure for a more satisfactory model.

The sulfation of half-calcined dolomite has been studied by several experimental approaches. Detailed analysis of the crystallographic structure and morphology of the stone before and after sulfation has provided considerable insight into the nature of the sulfation process on a microscale. Similar structural studies of the calcination reaction suggest that the crystallographic nature of the calcined stone is determined by the calcining conditions and that properties desirable in subsequent reactions can be selectively produced.

An alternative one-step regeneration process based on the solid-solid reaction of CaS and $CaSO_4$ has been explored. In other work, the structural and morphological character of the various sorbent reagents has been examined on a microscale in an effort to determine those factors that contribute to stone hardness and thereby influence decrepitation rates.

Bench-Scale, Pressurized, Fluidized-Bed Combustion Experiments

In earlier fluidized-bed combustion studies, the effects of bed temperature (788-899°C), gas velocity (2-5 ft/sec), and Ca/S mole ratio (1-3) on the sulfur retention, NO level in the flue gas, and particulate solids loading in the flue gas were evaluated using Tymochtee dolomite additive and operating at a system pressure of 8 atm. The studies have been extended to evaluating the effects of a higher bed temperature, precalcination of additive, a different additive (limestone), and the amount of excess air.

Combustion experiments were performed using a highly caking, high-volatile bituminous, Pittsburg seam coal from the Consolidation Coal Company's Arkwright mine.

Tymochtee dolomite obtained from C. E. Duff and Sons, Huntsville, Ohio, was used in some of the experiments, and limestone No. 1359 obtained from M. J. Grove Co., Stephen City, VA., was used for the remainder of the combustion experiments. Prerun treatment of the additive consisted of air-drying and screening.

The ANL bench-scale equipment, designed for operation at pressures up to 10 atm, consists of a 6-in.-dia fluidized-bed combustor, a compressor for supplying fluidizing-combustion air, a preheater for the fluidizing-combustion air, coal and additive feeders, and an off-gas system (cyclones, filters, gas-sampling equipment, and pressure let-down valve). The system is thoroughly instrumented and is equipped with an automatic data logging system.

Effect of Bed Temperature of 955°C (1750°F) at Different Ca/S Mole Ratios on Sulfur Retention and NO Flue-Gas Level. At a CO_2 concentration of ~15% in the combustor, a system pressure of 8 atm absolute, and a bed temperature of 955°C, Tymochtee dolomite and limestone No. 1359 calcine fully, *i.e.*, any contained $CaCO_3$ and $MgCO_3$ are converted to their respective oxides. BET

surface area measurements were made for -25 +35 mesh Tymochtee dolomite and limestone No. 1359. Dolomite in the air-dried, half-calcined, and fully calcined states had surface areas of 2.14, 4.05, and 8.23 m^2/g, respectively. Limestone in the air-dried and fully calcined states had surface areas of 0.35 and 3.56 m^2/g. Calcination does create larger internal openings in the additive particles and should, therefore, increase their capability to react with SO_2. Experiments at 955°C (where full calcination of the additive occurs) and at 900°C (where partial calcination occurs) were performed with Tymochtee dolomite. In two tests, the total sulfur retention decreased from 96% to 87% upon lowering of the Ca/S mole ratio from 1.5 to 1.1 at 955°C. The predicted sulfur retentions for these two experiments are 89% and 82%, respectively. These predicted values are based on an empirical correlation for half-calcined dolomite ($MgCO_3$ only is calcined) in the VAR-series of experiments reported earlier. To check the VAR results an experiment was performed at a combustor temperature of 900°C and a Ca/S mole ratio of 1.2 using Tymochtee dolomite additive. A total sulfur retention of 82% was measured which was in agreement with the empirically predicted sulfur retention of 83%. The NO concentration in the flue gas (~130 ppm) was relatively constant in these experiments.

Using limestone No. 1359 instead of dolomite and experimental conditions similar to those used in the dolomite experiments, two experiments were performed. When the Ca/S mole ratio was decreased from 1.8 to 1.4 at 955°C, sulfur retention dropped from 72% to 63%. At 900°C and with a Ca/S mole ratio of 1.5, a sulfur retention of 62% was obtained.

To test the effect of precalcination (calcining the additive prior to feeding it into the combustor) on the sulfur retention capability, an experiment was performed with precalcined limestone at a bed temperature of 900°C and a Ca/S mole ratio of 1.4. Total sulfur retention was only 56%. Precalcination apparently does not improve limestone performance. The average additive particle diameter for the precalcined limestone was 850 microns, in comparison with 700 microns for the uncalcined feed limestone. This may explain the lower sulfur retention of this experiment in comparison with the experiment at 900°C with uncalcined limestone.

The NO concentration in the dry flue gas ranged from 130 to 135 ppm in the experiments with dolomite and from 84 to 110 ppm in the limestone experiments.

Comparison of the Sulfur Retention Capabilities of Limestone and Dolomite. Comparison of the performance of the two additives was made in experiments that were performed mainly at 955°C, a pressure of 8 atm, a gas velocity of 3.5 ft/sec, and a nominal particle size distribution of -14 +100 mesh. Tymochtee dolomite was found to be superior to limestone No. 1359 as a sulfur-retaining additive on both a molar-feed and a mass-feed basis. The mass-feed ratio, (lb stone fed)/(lb sulfur in coal), was varied from 5 to 9.5 with dolomite and from 4.6 to 13 with limestone. The sulfur retention varied from 75 to 95% for dolomite and from 63 to 85% for limestone.

The NO concentrations in the dry flue gas ranged from 130 to 135 ppm using dolomite and from 84 to 150 ppm using limestone. The additive type does not seem to affect NO emission from a fluidized coal combustor.

Effect of Percent Excess Combustion Air on Sulfur Retention. The EA-series of experiments was designed to test the effect of Ca/S mole feed ratio on the sulfur retention capability of Tymochtee dolomite at several excess air combustion conditions. These experiments were performed at 900°C, 8 atm, and a nominal fluidizing-gas velocity of 4.5 ft/sec.

With 17% excess air, a sulfur retention of 83% was obtained at a Ca/S mole ratio of 1.4. With 44% excess air, as the Ca/S mole ratio was varied from 1.1 to 2.9, sulfur retention was 76 to 93%. With 75% excess air, a sulfur retention variation of 57 to 92% was found as the Ca/S mole ratio was varied from 1.3 to 2.9.

At all of the excess-air levels studied, increasing the Ca/S mole ratio generally resulted in improved sulfur retention. However, no meaningful effect of excess-air condition on the sulfur retention capability of dolomite was found in the excess-air range of 17 to 75%.

The NO concentration in the dry flue gas generally increased with oxygen concentration, as expected. At ∿3% oxygen in the dry flue gas, the NO concentration was 160 ppm; at 6%, it averaged 200 ppm; and at ∿9%, it averaged 220 ppm.

Combustion Efficiency and Carbon Balance Calculations for Excess Air and Dolomite-Limestone Experiments. Carbon balances and combustion efficiencies have been calculated for some of the experiments to study the effects of excess air, dolomite, and limestone. The calculated carbon balances for these experiments ranged from 97 to 114 percent. The combustion efficiency in the excess air experiments ranged from 85 to 97 percent, increasing in proportion to the quantity of excess air. Combustion efficiencies in the experiments comparing dolomite and limestone, which were made at bed temperatures of 900°C and 955°C and with 17% excess air, ranged from 88 to 97%.

Concentration of COS in Flue Gas. In six combustion experiments, the COS concentration in the flue gas was found to be below the detectability limit of 100 ppm.

Processing of Combustor Data. Programs for plotting data collected in combustion experiments are being rewritten to allow usage of Integrated Software Corporation's plotting package. Examples of plots are given.

Coal Combustion Reactions

Determination of the Inorganic Constituents in the Effluent Gas from Coal. Work has begun on a laboratory-scale investigation to determine inorganic constituents in the effluent gas from coal combustion. The study is necessary to determine which species exist in the vapor phase or are carried as particulates that may be deleterious to turbine components in a combined-cycle power generation system. Analyses will be performed on feed materials, particulates retained on a filter, and materials condensed in a cold trap in order to obtain a complete material balance. The initial apparatus, now being designed, will consist of a fixed-bed coal combustion unit, a hot filter, a cold trap, appropriate analytical instruments, and ancillary equipment.

Systematic Study of the Volatility of Trace Elements in Coal. A study to obtain data on the volatility of trace elements in coal at practical coal combustion and gasification conditions is under way. This work is also intended to obtain data supporting the study on the determination of the inorganic constituents in the effluent gas from coal combustion.

The procedure will be to ash coal at various temperatures under both combustion and gasification conditions. The resulting ashes will be analyzed for the trace elements of interest. The variables of temperature, time, and the composition of feed gases will be studied to evaluate their effects on the volatility of trace elements.

Trace-Element Distribution Studies

The process of coal combustion releases trace elements, *e.g.*, Hg, Pb, Be, F, to the environment as vapors and/or in association with particulate emissions. Although a substantial fraction of the trace elements is retained with the fly ash removed by emission control devices, significant quantities of trace elements (such as mercury) may still be emitted as vapors or in association with submicron size particles that are not efficiently removed by present-day devices.

Since fluidized-bed combustion is carried out at temperatures of 845-955°C (1550-1750°F), which are well below those of conventional coal-fired power plants, and in the presence of a chemically reactive additive for sulfur dioxide removal, an evaluation was made of the potential of fluidized-bed combustion for reducing trace element emissions as compared with conventional combustors. Mass balances were made around ANL's 6-in.-dia, pressurized, fluidized-bed combustor for the following trace and minor elements: Hg, F, Be, Pb, As, Br, Co, Cr, Fe, K, La, Mn, Na, and Sc.

Results are presented here for a total of four combustion experiments made to assess the behavior of trace elements during combustion. The operating conditions varied were bed temperature (845 or 900°C), system pressure (8 or 10 atm), and oxygen content of the flue gas (3 or 4%). To assess the effect of additive, one experiment at each set of conditions involved the combustion of coal in a fluidized bed of alumina; the other experiment involved the combustion of coal in a fluidized bed of dolomite.

Material Balance Results. The extent of retention of the relatively volatile elements (Hg, As, F, and Br) in the solid samples indicated a definite potential for reduction of their emission by fluidized-bed combustion. The average retention of 34% for mercury in the solid effluents from the combustor compares favorably with the 10% retention reported for a large conventional coal-fired power plant. The average retention of 85% for arsenic is considerably better than the 35-50% recovery reported for a conventional boiler and for a high-Btu gasification pilot plant. The average retention of fluorine and bromine in the combustion experiments with dolomite (59 and 36%, respectively) was compared with retention in the combustion experiments in an alumina bed (14 and 0%, respectively). This indicates that the dolomite additive used for sulfur dioxide removal is also effective in reducing the emissions of these two elements.

Of the remaining ten elements reported on, seven (Pb, Co, Fe, K, La, Na, nd Sc) had average material balances of 100 ± 10%, indicating essentially o losses by volatilization. Average recoveries of beryllium and chromium were 69 and 74%, respectively, but are suspect since complete recoveries of chromium have been reported for much higher temperature coal-processing units and beryllium is reportedly less volatile than chromium. With the exception of one unaccountably high recovery for manganese, it also exhibited a recovery of 100 ± 10%.

The concentrations of the trace elements in the coal and fly-ash samples from successive stages of gas-cleaning devices (primary cyclone, secondary cyclone, and filter) were adjusted to a combustible-matter-free basis and compared for significant differences in concentration between coal and ash samples and among successively finer samples of ash. The concentrations of several elements (such as Ba, Co, Fe, K, La, Na, and Sc) had slight tendencies to increase with decreasing particle size. The lower combustion temperatures of fluidized-bed combustion are apparently effective, however, in reducing the preferential concentration of trace elements in the finer ash particles, which has been observed in conventional coal-fired power plants.

Testing of Mercury Sampling Train. Because of low mercury recoveries observed in the experiments, an evaluation of the mercury sampling train used to measure the levels of volatilized mercury in the flue gas was made. Essentially complete recovery of mercury was observed when known quantities of mercury were added to a nitrogen carrier stream and to a flue-gas carrier stream. Therefore, further experimentation is required.

The Properties of a Dolomite Bed of a Range of Particle Sizes and Shapes at Minimum Fluidization

A two-phase model to describe the combustion of coal in a fluidized bed of dolomite would be critically influenced by the properties, at minimum fluidization, of bed materials of a range of particle sizes and shapes. To aid in developing the model, experiments have been performed with dolomite particles of a size distribution in the range of 88 to 1410 μm in a 6-in.-dia fluidized-bed reactor. The bed voidage at minimum fluidization and the minimum fluidizing air velocities were determined as a function of temperature (20-425°C/ 70-800°F) and pressure (26-121 psia). The experimental data suggest that at a given temperature, the minimum fluidization velocity decreases with increasing pressure and that at a given pressure, the minimum fluidization velocity is almost independent of temperature. These data were correlated using the Ergun relation. The mean sphericity of the particles required in the Ergun correlation was determined from experimental pressure drop data at low Reynolds number.

Other methods often employed for predicting the minimum fluidization velocity of a bed of single size spherical particles were examined with appropriate modifications for their applicability to a bed consisting of a wide range of particle sizes and shapes. Specific recommendations have been made as to the applicability of the different methods for calculating minimum fluidization velocities.

Revamping of the Bench-Scale, Pressurized, Fluidized-Bed Combustion System

The existing 6-in.-dia, pressurized, fluidized-bed combustor is limited to operation at combustion temperatures ranging from 790 to 955°C (1450 to 1750°F), fluidizing-gas velocities of 2 to 5 ft/sec, bed depths of 3 to 4 ft, and additive particle sizes below 14 U.S. mesh. The off-gas from the combustor cools several hundred degrees Centigrade in the freeboard area of the combustor, and the off-gas system is not designed to withstand combustion-zone temperatures. A new 6-in.-dia combustor is being designed for isntallation and use in studying the effects of higher gas velocities (6 to 10 ft/sec), deeper beds (6 to 8 ft), and larger additive particle sizes (up to 0.25 in.). With the installation of the new combustor, the present combustor off-gas system (piping, cyclones, and filters) will be replaced with equipment suitable for operation at temperatures up to 900°C (1650°F). Preliminary design characteristics of the new combustor and flue-gas system are presented.

Separation of Combustion and Regeneration Systems

The pressurized, fluidized-bed combustor and the regenerator currently utilize several common components. Because of the dual function of these components, the two units cannot be operated simultaneously. To physically separate the two units so as to permit concurrent investigations of both the combustion process and the regeneration process, modification of both units and installation of additional equipment is in progress.

A new regenerator support structure with associated access platforms was erected. The existing regenerator will be located in the new structure, with the combustor remaining in its present location. Plans were formulated for installation of the process piping and electrical services required for the new system, and work related to these services was started.

INTRODUCTION

Fluidized-bed combustion has the potential for contributing significantly to the solution of the nation's urgent energy problem without polluting the atmosphere. For the past six years, the Chemical Engineering Division has been cooperating with other organizations in this country and abroad in developing this technique for burning high-sulfur coal. The program has been sponsored by the Office of Coal Research, U.S. Energy Research and Development Agency.

In the fluidized-bed process, small particles of limestone or dolomite are held in a dense suspension by a stream of air passing upward through them. The fluidized bed is heated to about 1600°F (870°C), and finely crushed coal is injected into it. As the coal mixes with the bed material, it burns, generating heat. This heat is transferred by the moving particles to steam tubes immersed in the bed, and the steam is used to generate electric power. In more advanced versions of the process that operate at elevated pressures, a portion of the power is generated by a gas turbine operating on the hot, pressurized flue gases or on air heated in tubes immersed in the bed.

Crushed limestone or dolomite is added continuously to the bed at a suitable rate. The $CaCO_3$ (or CaO if the $CaCO_3$ is calcined) in the limestone reacts with the sulfur dioxide released by the burning of the coal to produce calcium sulfate, which is discharged from the bed. To avoid creating a solid waste problem from this discharged stone, methods for regenerating the spent stone so that it may be reused many times are being developed. A favored process is a one-step reductive decomposition of $CaSO_4$ to CaO at ∿2000°F (∿1095°C) using a reductant (for example, CO) according to the following reaction:

$$CaSO_4 + CO \rightarrow CaO + SO_2 + CO_2 \qquad (1)$$

In the experimental investigation reported here on the combustion and regeneration process, the following were studied:

1. The effect of regeneration operating variables (bed temperature, reducing gas concentration, gas velocity, and bed height) on SO_2 concentration in the off-gas.

2. The conditions for preparation of and the regeneration properties of pellets consisting of CaO impregnated in an Al_2O_3 matrix.

3. The effectiveness, in a preliminary investigation, of the solid-solid ($CaSO_4$-CaS) reaction for producing SO_2.

4. The effect of the basic chemical and structural properties of reagent materials on their reactivity, regenerability, and physical properties.

5. The effect on sulfur retention in the bed and NO level in the flue gas of significant variables and materials outside the range used in previous studies. The combustor has been operated using a higher bed temperature (955°C/1750°F), higher levels of excess combustion air (to ∿75%), and with limestone as well as dolomite.

6. The equipment (now being fabricated) and the procedure to identify and to determine the concentrations of inorganic species in the vapor phase or carried as particulates in the flue gas. This is of interest if the flue gas is to be passed through a turbine.

7. The distribution and emission of biologically hazardous trace elements from the combustion system.

8. The minimum fluidization velocity, as a function of temperature and pressure, for particles in the size range used in the beds of the combustor and regenerator.

Information is also presented on the status of the construction of the regeneration system (which will have feeding and off-gas equipment separate from that of the combustor) and on the design considerations for the new system for hot flue gas to be constructed.

ONE-STEP ADDITIVE REGENERATION EXPERIMENTS

One-step additive regeneration experiments were completed to evaluate the effects of various experimental conditions on the regeneration of CaO from sulfated Tymochtee dolomite. The reduction of $CaSO_4$ to CaO is favored by high temperatures ($\geq$1900°F/1038°C) and mildly reducing conditions.

$$CaSO_4 + CO \rightleftarrows CaO + SO_2 + CO_2 \quad (1)$$

$$CaSO_4 + H_2 \rightleftarrows CaO + SO_2 + H_2O \quad (2)$$

At lower temperatures (∿1600-1700°F/∿870-925°C) and under more highly reducing conditions, the following reactions are favored:

$$CaSO_4 + 4CO \rightarrow CaS + 4CO_2 \quad (3)$$

$$CaSO_4 + 4H_2 \rightarrow CaS + 4H_2O \quad (4)$$

The effects of temperature, residence time, total reducing gas (H_2, CO, or CH_4) concentration in the fluidized bed, and height of fluidized bed on the regeneration of CaO from $CaSO_4$ are being evaluated.

Materials

Tymochtee dolomite, which had been sulfated (∿7 wt % S) in the VAR-series experiments, was regenerated in experiments R-14, R-15A, R-15B. Kerosene from the ANL stock was used to heat the regenerator to 1900°F, and its combustion under reducing conditions was used to generate the necessary reductants (CO, CH_4, and H_2) for these experiments and for experiment KB-2. The characteristics of the Alundum used in KB-2 are given in Table A-1 in Appendix A.

For the FAC-series of experiments, sulfated Tymochtee dolomite (10.2 wt % S) from the C- and EA- combustion experiments was regenerated. The *in situ* combustion of methane was used to generate the heat and provide reductant gases.

Equipment

The experimental system used for regeneration experiments R-14, R-15A, R-15B, and KB-2 is shown in Ref. 1, p. 7. This system was modified to that shown in Fig. 1 and was used in the FAC-series. Modifications included the addition of a multipoint gas injection system for methane in the regenerator and removal of the low-efficiency cyclone and the two in-series filters in the off-gas system to reduce the residence time of the off-gas. This modification prevented the gas from reaching its water dew point before it was exhausted and eliminated plugging caused by buildups of moisture and solid particles in the off-gas lines.

The regeneration system consists of a 3-in.-dia fluidized-bed regenerator, a peripherally sealed rotary feeder for metering solids transported into the regenerator, and the equipment for removing solids from the off-gas. Some of the fluidizing gas and the preheating gas (used in startup only) is preheated in an electrically heated pipe heat exchanger. For experiments R-14, R-15A, -15B, and KB-2, an off-gas sample was continuously removed, dewatered, and analyzed for SO_2, NO, CH_4, CO, and O_2; it was intermittently analyzed for CO_2.

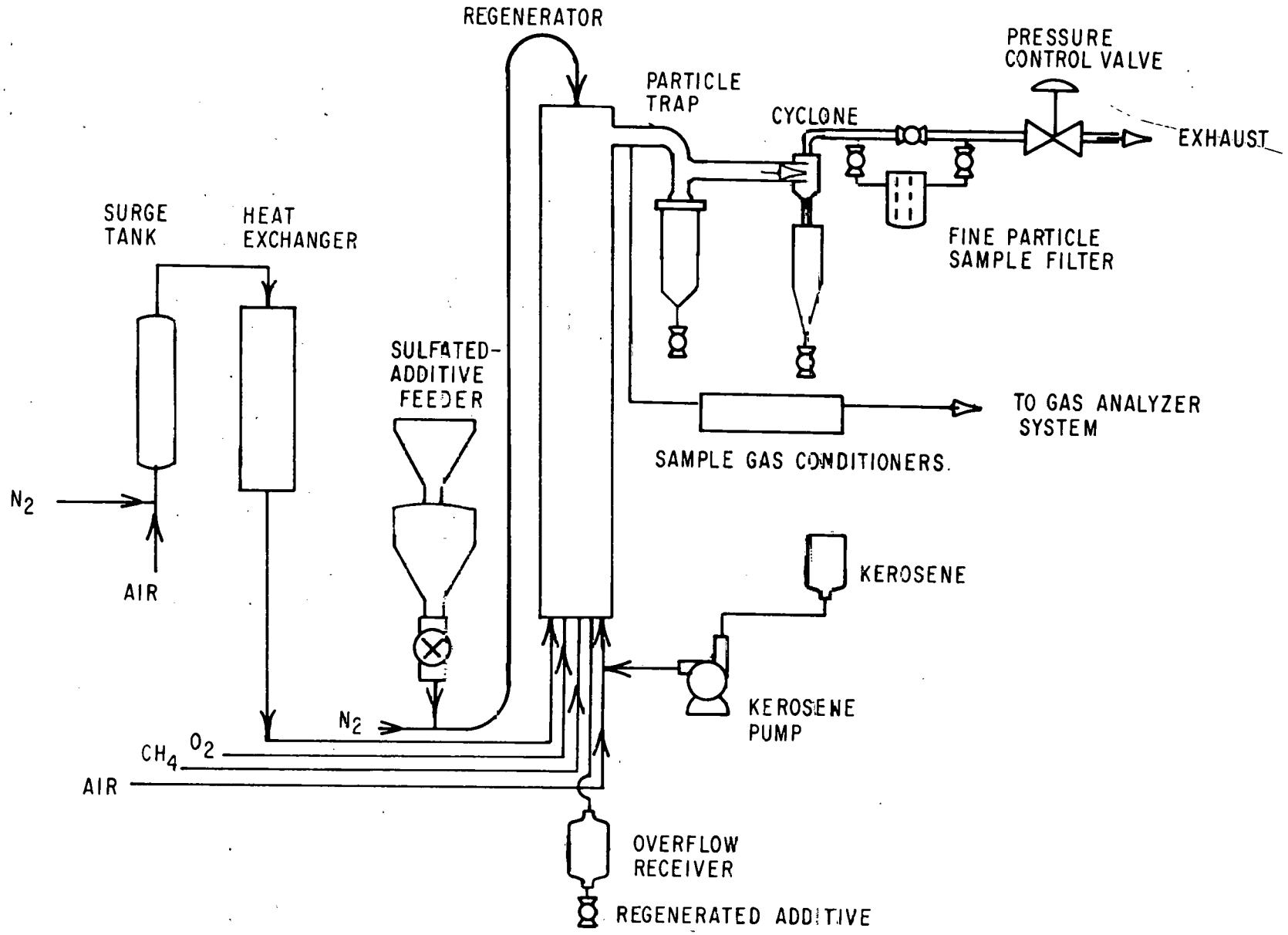

Fig. 1. Schematic Diagram of the Modified Fluidized-Bed Regeneration System

For the FAC-series, in addition, off-gas samples from each experiment were analyzed for H_2S, H_2, and some trace gases using a mass spectrograph.

The 3-in.-dia pressurized, fluidized-bed regenerator shown schematically in Fig. 2 consists of 2 1/2-in. Plibrico castable refractory encased in a 8-in.-dia Schedule 40 pipe (Type 316 SS), approximately 7 1/2 ft long, with almost its entire length contained within a 12-in.-dia Schedule 20 carbon steel pipe. Differential thermal expansion between the inner and outer pipes is accommodated by the use of packing glands on lines entering the bottom flange of the unit. The unit has a balanced-pressure design. The annular chamber between the two pipes can be maintained under pressure to prevent a large pressure differential across the hot inner-pipe wall when the unit is operated at pressures up to the design limit of 10 atm absolute.

One-Step Regeneration with the *In Situ* Combustion of Kerosene Under Reducing Conditions

In the kerosene combustion experiments, sulfated Tymochtee dolomite containing ∿7 wt % S was regenerated by the one-step regeneration process. The starting procedure consisted of heating the fluidized bed (to ∿800°F or 427°C) with preheated air. The fluidizing air was then replaced with oxygen and preheated nitrogen. The bed temperature was increased to the desired operating temperature by burning kerosene in an oxidizing atmosphere (the oxygen concentration in the off-gas was greater than 10%). Kerosene and oxygen were introduced through separate inlets. The oxygen flowrate was decreased until the oxygen concentration in the off-gas was less than 2%. The resulting incomplete combustion produced the reductants (CO, CH_4, and H_2) required for the reductive decomposition of $CaSO_4$. At steady operating conditions, feeding of the sulfated additive was initiated.

In experiment R-14, sulfated dolomite was regenerated at an average pressure of 1.6 atm absolute, a fluidizing-gas velocity of ∿5 ft/sec, a bed temperature of ∿1900°F, and an additive feed rate of ∿10 lb/hr, with an initial bed of 4.1 kg of sulfated dolomite. The nominal fluidized-bed height was fixed at 36 in. with an internal standpipe. The input gas feed rates and the flue-gas analysis for R-14 are presented in Fig. 3 and 4. The CO concentration in the gas above the fluidized bed varied from 0.3 to 7.1%, CH_4 varied from 0.6 to 1.3%, and SO_2 varied from 1.2 to 2.6%. During this experiment, a major fraction of the solids fed to the regenerator was elutriated because of the relatively high fluidizing-gas velocity (∿5 ft/sec). The remaining regeneration experiments were performed with a lower fluidizing gas velocity (3.7 ft/sec) to eliminate this problem.

Experiment R-15A was performed at a pressure of 1.5 atm absolute, and sulfated dolomite was fed intermittently at an average rate of 6.4 lb/hr for a period of 3.75 hr. The input gas flowrates and the flue-gas analysis for R-15A are presented in Figs. 5 and 6. Graphs (*e.g.*, Fig. 6) of bed temperature and concentrations of above bed off-gas constituents are computer plots of data acquired at 10-min intervals. The variations of the concentrations in the gas above the bed were 0.1 to 4.4% for CO, 0.2 to 2.2% for CH_4, and 0.1 to 3.3% for SO_2. Plugging of the bed overflow line caused termination of this experiment.

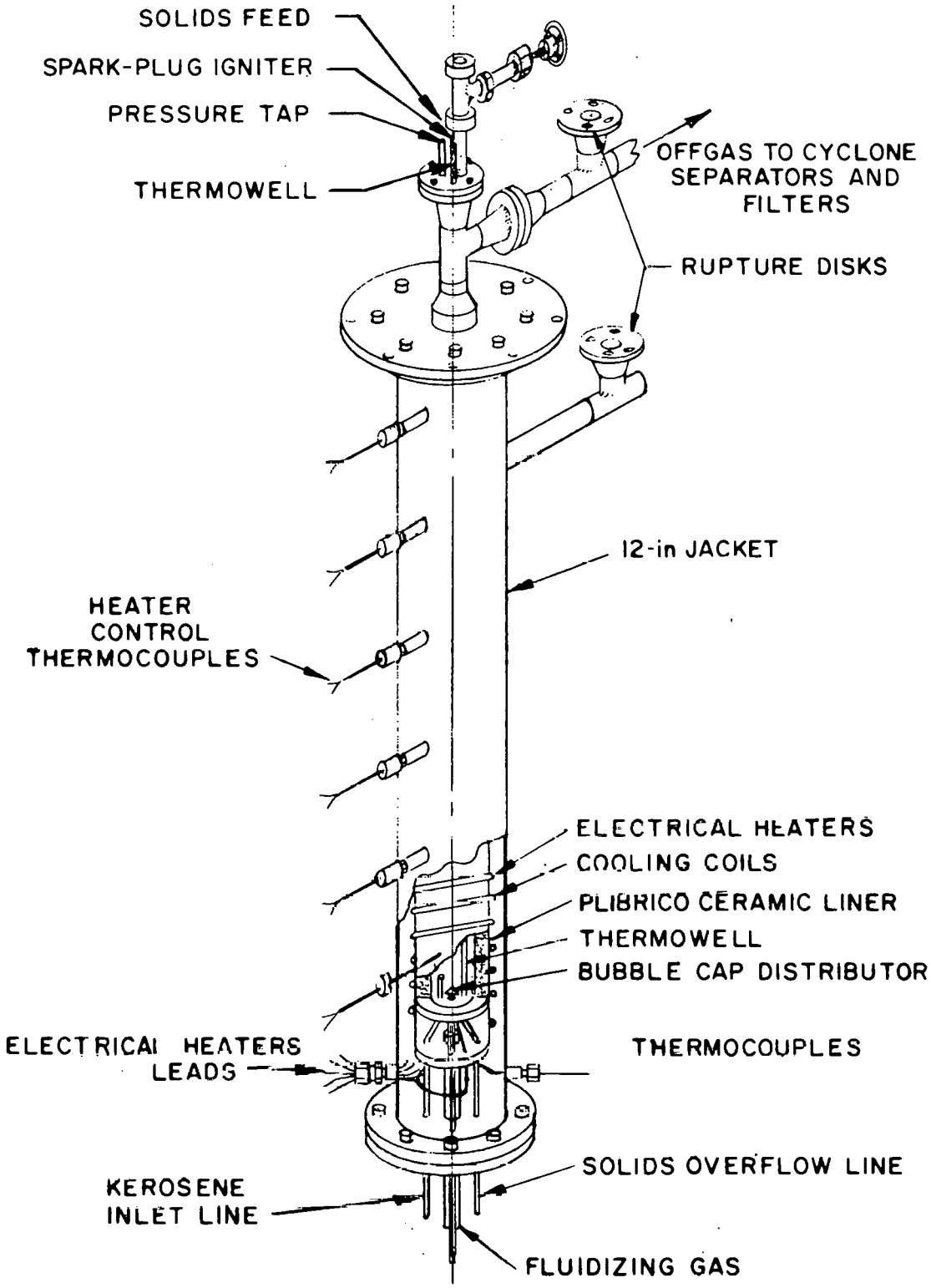

Fig. 2. Three-inch-diameter Fluidized-Bed Regenerator

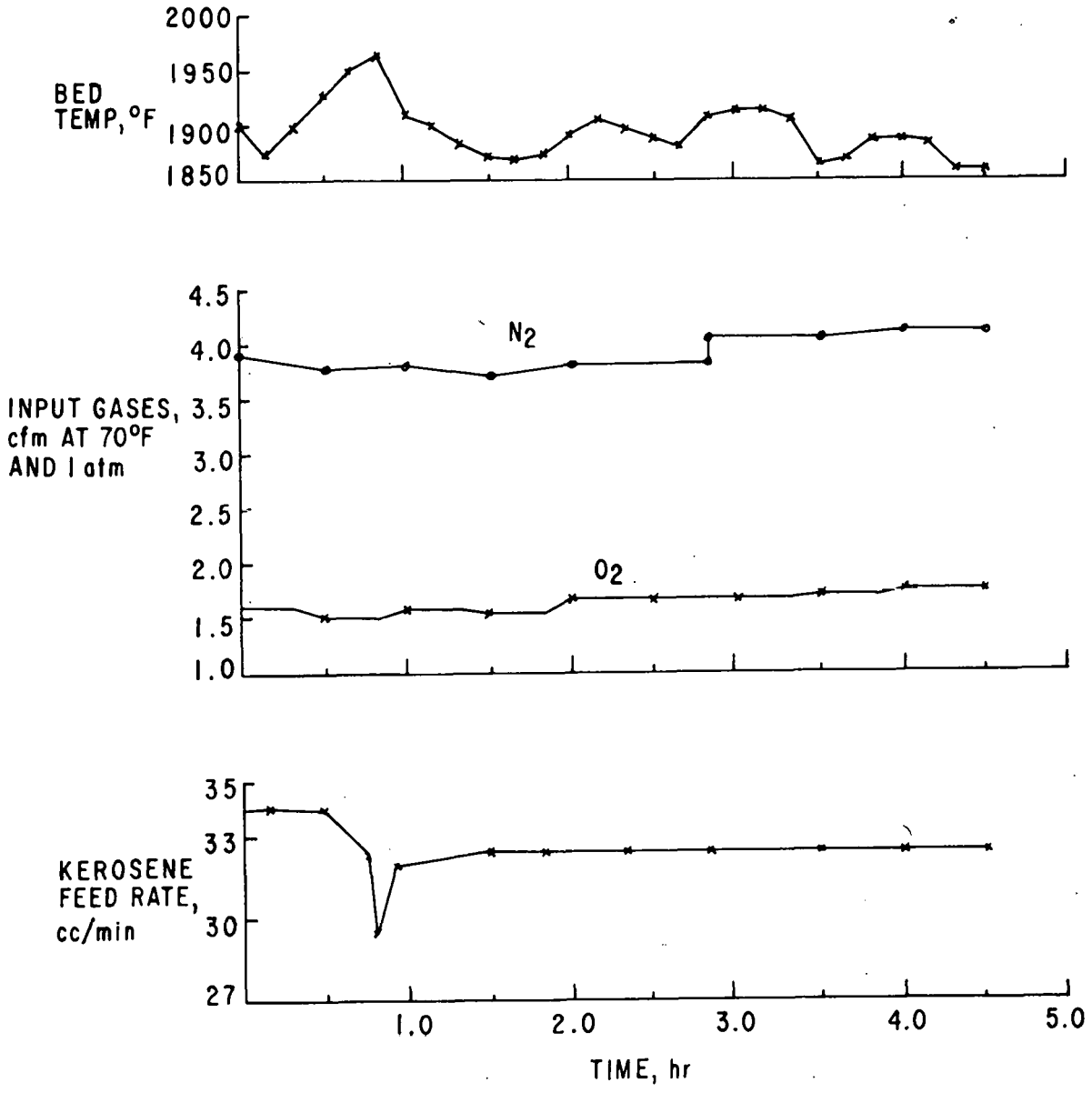

Fig. 3. Input Flow Rates of Oxygen, Nitrogen, Kerosene, and Bed Temperatures for Experiment R-14

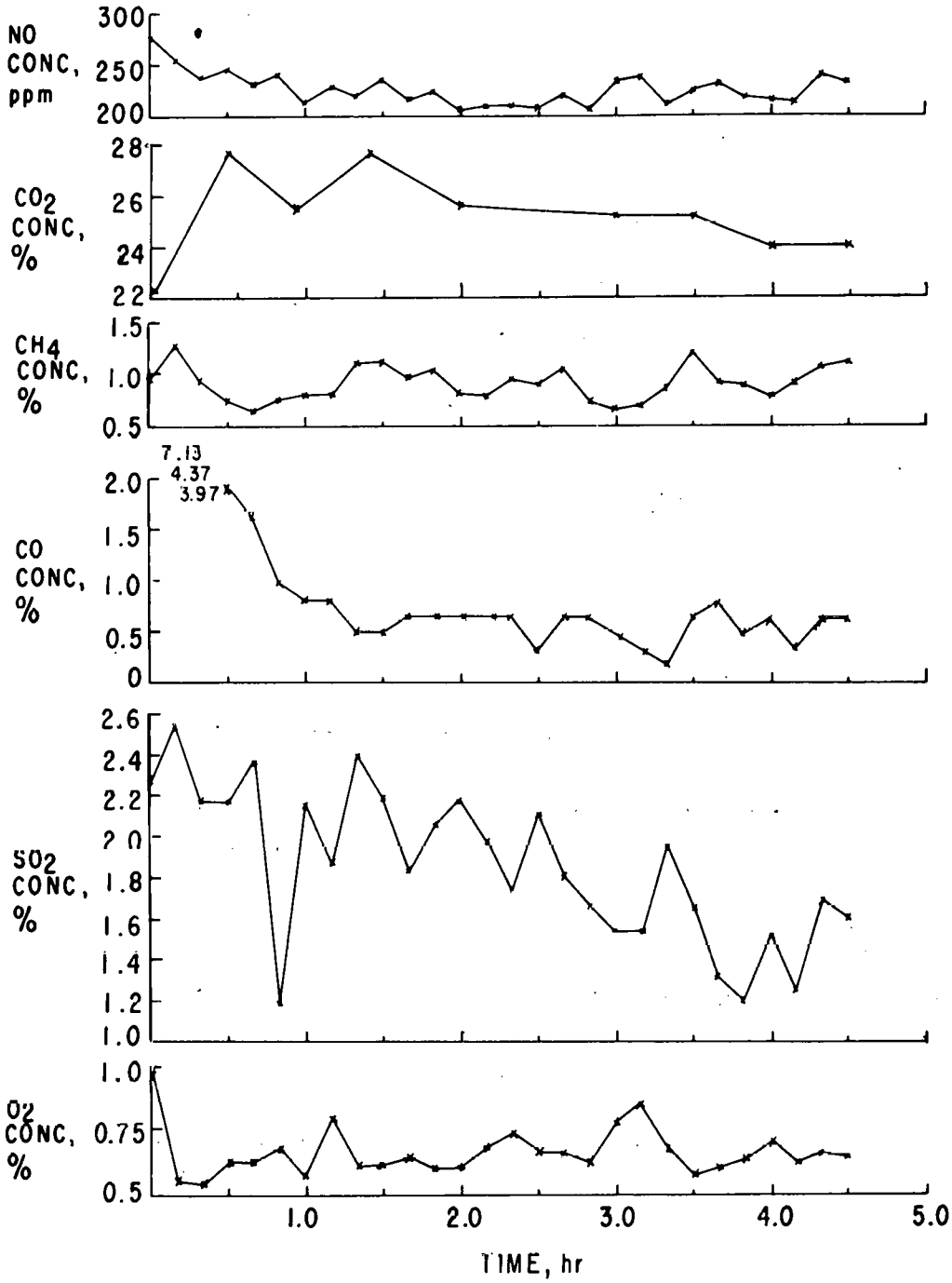

Fig. 4. Off-Gas Composition Above the Fluidized Bed for Experiment R-14

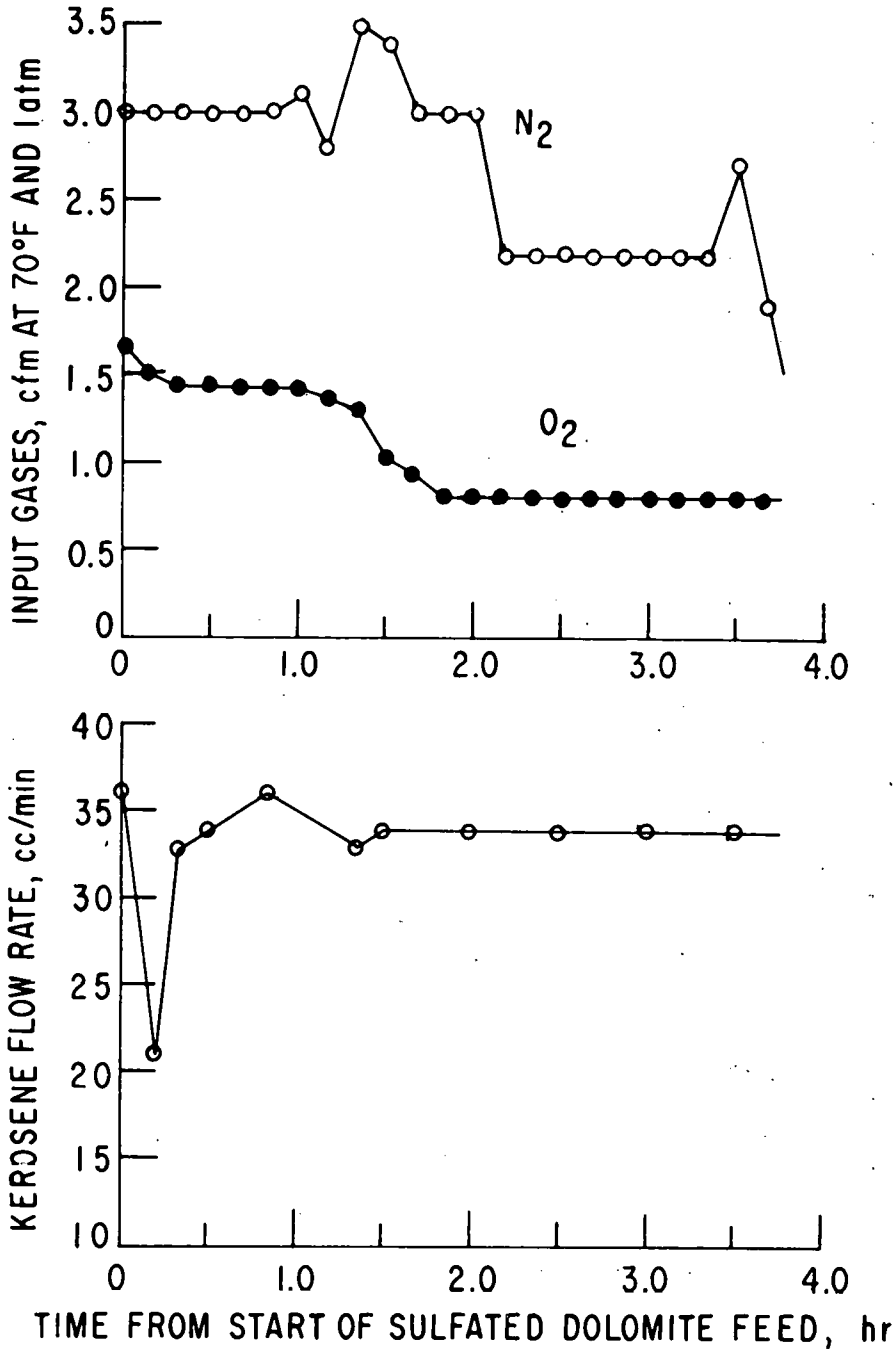

Fig. 5. Input Flow Rates of Oxygen, Nitrogen, and Kerosene for Experiment R-15A

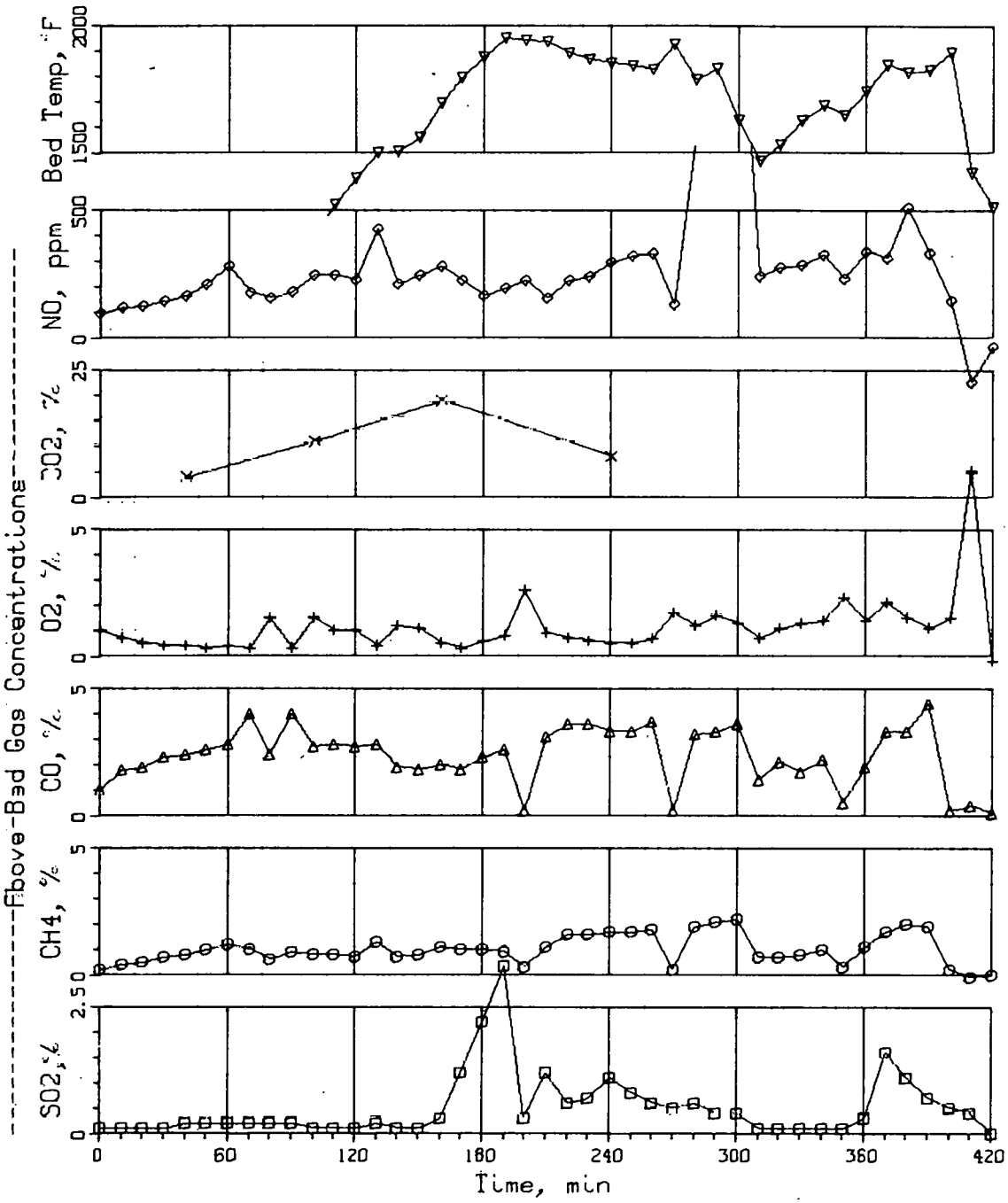

Fig. 6. Bed Temperature and Concentrations of Off-Gas Constituents, Experiment R-15A

In preparing the unit for this test, it was discovered that the bed-overflow line had developed a crack in the section of the line that is enclosed in the gas-distributor housing. This crack provided a path for fluidizing gas to flow up through the 36-in.-high, bed-overflow line instead of following its normal route through the bubble-cap gas distributors. This defect, which was corrected before the next experiment, resulted in two deleterious effects during experiments R-14 and R-15A: (1) the degree of fluidization of the bed was significantly reduced because of the decreased flow of gas through the bubble-cap distributors and (2) the amount of solids entrained in the off-gas was markedly increased by the gas stream jetting out of the 36-in.-high, bed-overflow line.

The purpose of the kerosene-burning test (KB-2) was twofold: (1) to establish operating procedures for maintaining a uniform bed temperature of 1040°C (∿1900°F) under reducing conditions without any regenerative-type reactions occurring and (2) to determine whether the CO concentration of the gas in the regenerator could be increased by increasing the kerosene flow-rate without upsetting the bed temperature. The bed for this test consisted of 6.3 kg of 30-mesh alumina (∿2-ft static-bed height). The input flow-rates of oxygen, nitrogen, and kerosene for the test are shown in Fig. 7; bed temperature and concentrations of constituents of the off-gas are shown in Fig. 8. Steady operating conditions at 1920°F (1050°C) were achieved with a kerosene flowrate of 29.5 cc/min. The gas velocity through the bed was ∿4 ft/sec. The off-gas above the bed (dry basis) during this period of constant conditions contained ∿1.5 O_2 and ∿7% CO. Increasing the kerosene feed rate to 32.6 cc/min decreased the O_2 concentration in the dry off-gas to 0.3% and increased the CO concentration to 11%. The bed temperature increased slightly to ∿1940°F (1060°C). The results of this part of the test show that a constant bed temperature of ∿1900°F can be maintained and that the concentration of reductant CO in the off-gas can be significantly increased without upsetting the bed temperature by increasing the kerosene flowrate.

In the same experiment (KB-2), efforts to duplicate the above results a lower bed temperature (∿1800°F or 982°C) were not as successful. Steady operating conditions at 970°C or 1780°F were achieved with a kerosene flowrate of 22 cc/min. The gas velocity through the bed was 3.6 ft/sec and the dry off-gas during this period of constant conditions contained 1.2% O_2 and 5% CO. Increasing the kerosene flowrate to 25 cc/min increased the CO concentration in the dry off-gas to 6% but did not change the 1.2% O_2 concentration. The bed temperature decreased to 1760°F (960°C).

In experiment R-15B, sulfated Tymochtee dolomite from the VAR-series pressurized combustion experiments was regenerated at an average pressure of 1.5 atm absolute, a bed temperature of ∿1040°C or ∿1900°F, and a fluidizing-gas velocity of 3.2 ft/sec. Sulfated dolomite was fed to the fluidized bed at an average rate of 8.4 lb/hr during a 4-hr period.

The input flowrates of oxygen, nitrogen, and kerosene during the 4-hr period in which the sulfated dolomite was fed to the regenerator are shown in Fig. 9. Plots of the bed temperature and of the concentrations of O_2, SO_2, CO, CH_4, CO_2, and NO in the gas above the fluidized bed for the duration of the experiment are shown in Fig. 10.

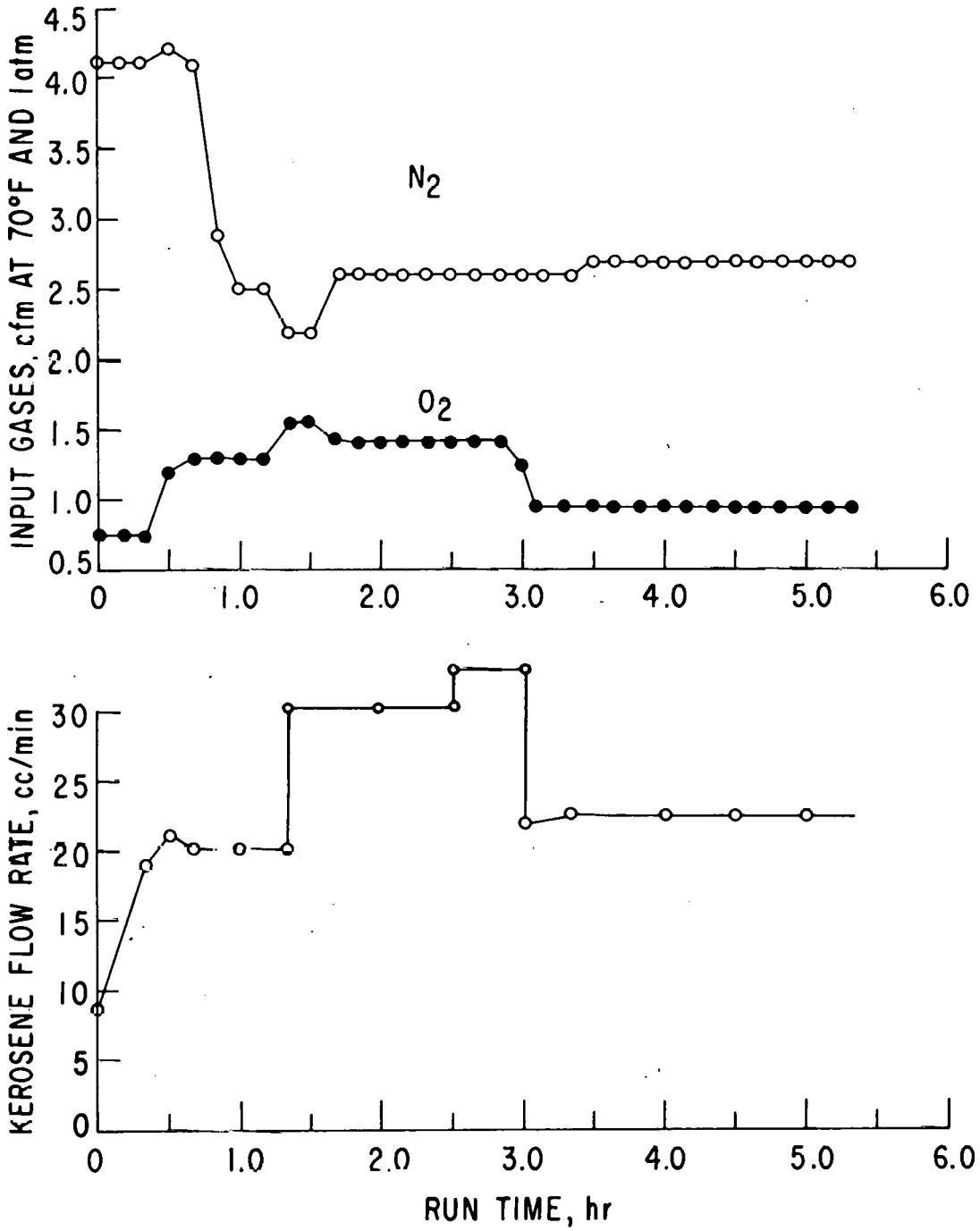

Fig. 7. Input Flow Rates of Oxygen, Nitrogen, and Kerosene in Experiment KB-2

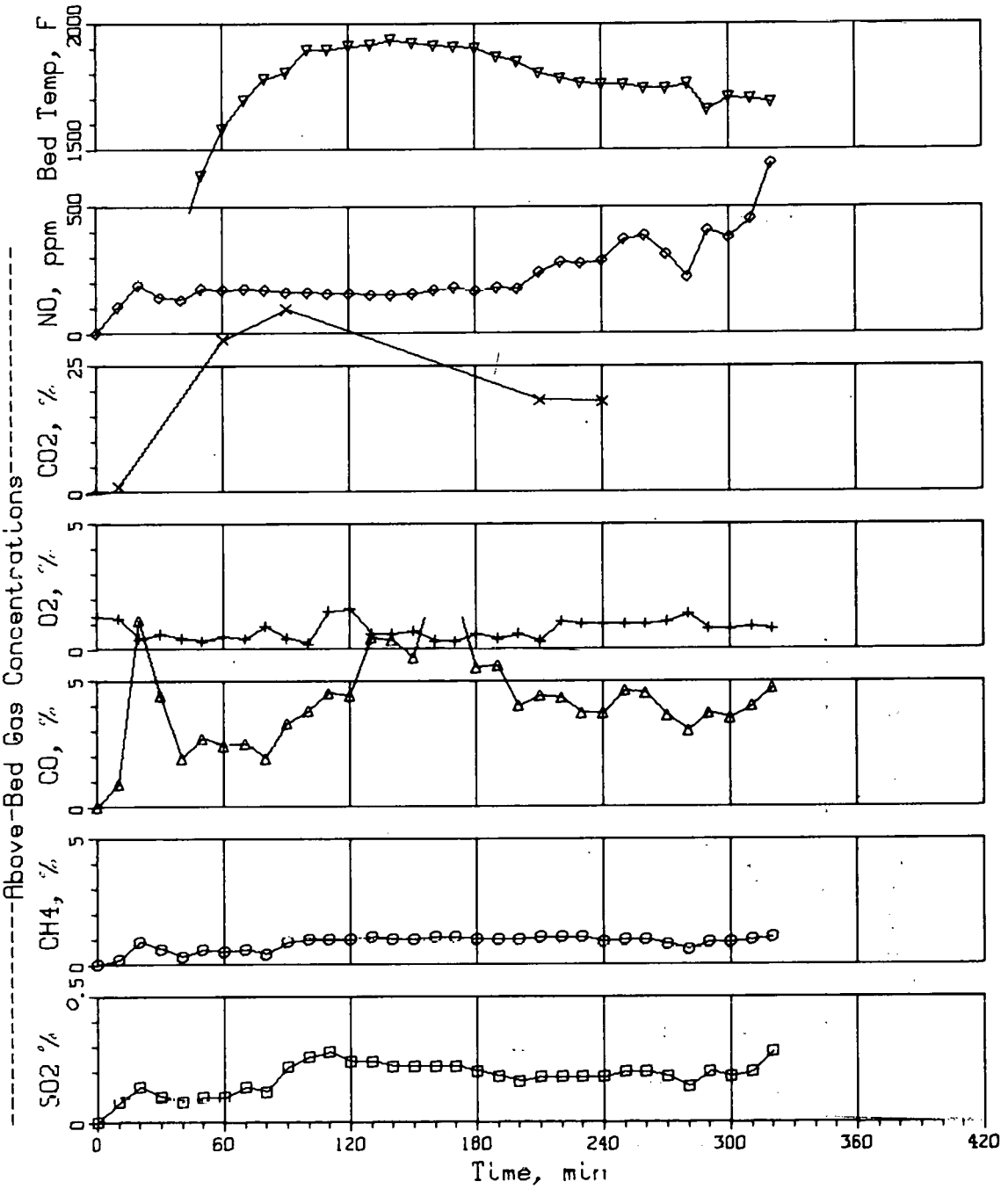

Fig. 8. Bed Temperature and Concentrations of Constituents of Off-Gas, Experiment KB-2

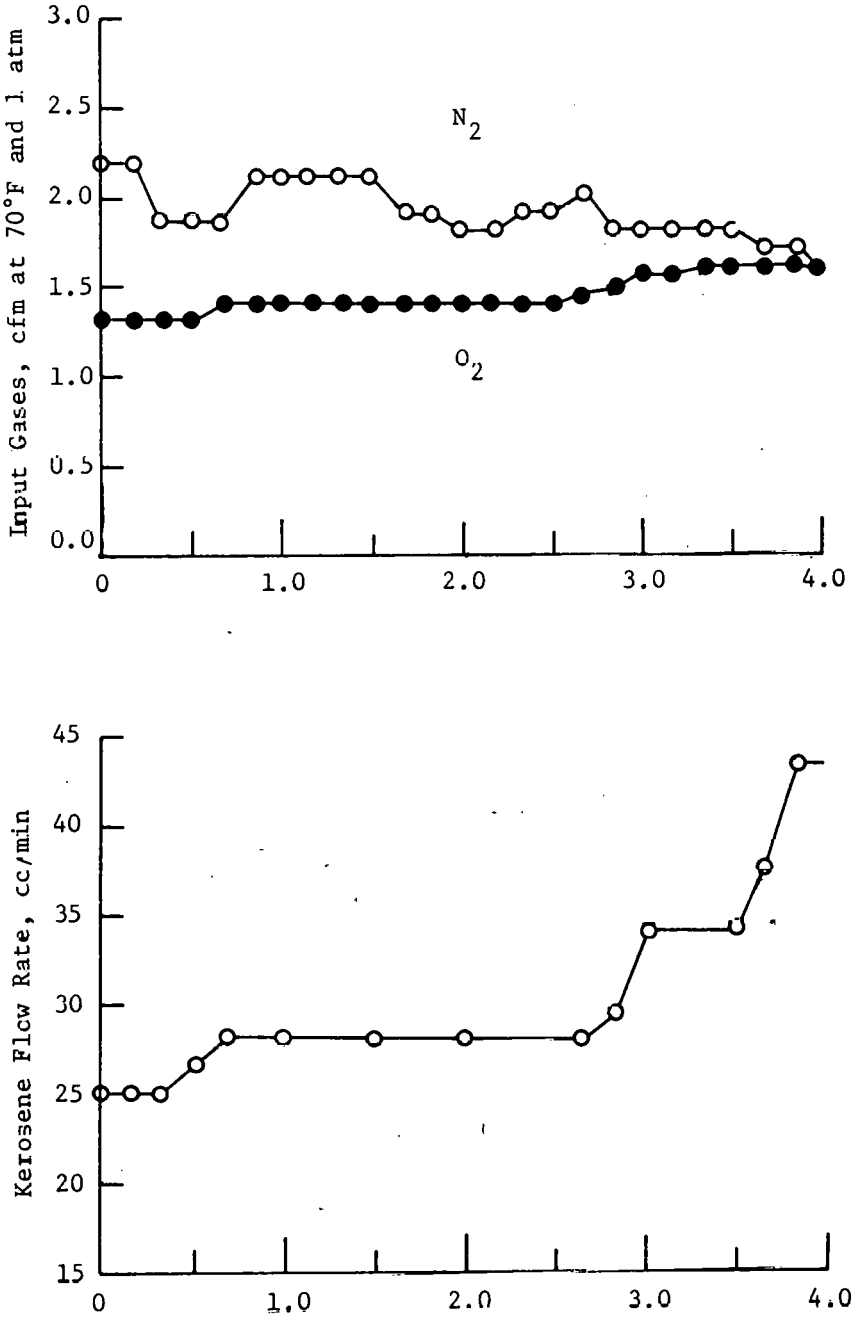

Fig. 9. Input Flow Rates of Oxygen, Nitrogen, and Kerosene for Experiment R-15B

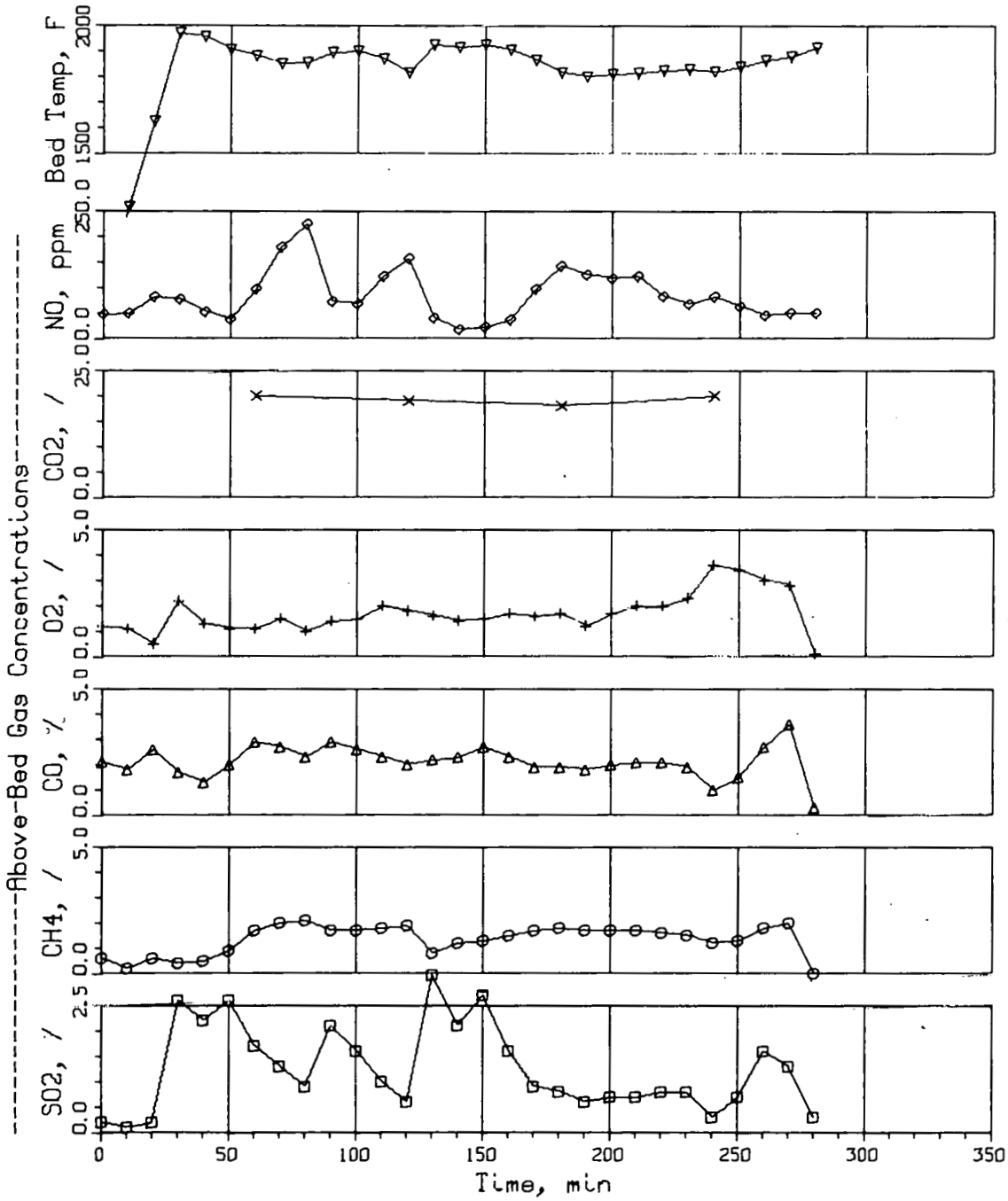

Fig. 10. Bed Temperature and Concentrations of Constituents of Off-Gas, Experiment R-15B

Plugging, which occurred initially in the bed-overflow line and subsequently in the off-gas particulate removal system, caused termination of experiment R-15B. Examination of the plugging material revealed a mixture of the bed material, kerosene degradation products, and moisture.

One-Step Regeneration with the *In Situ* Combustion of Methane

In the experiments described above (R-14, R-15A, R-15B), steady state conditions were never really achieved because of recurring problems. One of the problems was plugging of equipment and lines in the off-gas system and the overflow pipe due to buildup of unburned hydrocarbons and water from the combustion of kerosene. Another problem was excursion of the bed temperature to >1095°C (>2000°F), probably caused by poor fluidization. To overcome most of these problems, the experimental system was modified as indicated above (Fig. 1), and methane instead of kerosene was combusted under reducing conditions in the FAC-series of experiments described below.

As in previous experiments, to start the unit, kerosene was combusted *in situ* under oxidizing conditions to raise the temperature of the bed in the regenerator to ∿1600°F. Methane was then introduced under oxidizing conditions at two different bed heights through a dual-point injection system, lowering the hot spot temperatures at the injectors in comparison with a single-point injection system. The temperature of the fluidized bed was allowed to increase to ∿1800°F, at which temperature reducing conditions were established. The final reducing conditions and operating temperature of each experiment were approached slowly so that the fluidized bed experienced no abrupt changes in conditions at the high temperature. The combustion of CH_4 under reducing conditions provided the necessary heat and reducing gases for regeneration. Both of the following combustion reactions occur at different zones in the fluidized bed:

$$\text{Oxidizing Zone:} \quad CH_4 + 2\,O_2 \rightarrow CO_2 + 2H_2O \tag{5}$$

$$\text{Reducing Zone:} \quad CH_4 + O_2 \rightarrow CO + H_2 + H_2O \tag{6}$$

The excess methane serves as a reductant in addition to CO and H_2. The solid-gas reactions by which regeneration of sulfated dolomite occurs can be summarized by the following reactions:

$$CaSO_4 + CO \rightarrow CaO + CO_2 + SO_2 \tag{7}$$

$$CaSO_4 + H_2 \rightarrow CaO + H_2O + SO_2 \tag{8}$$

$$4\,CaSO_4 + CH_4 \rightarrow 4\,CaO + 2\,H_2O + CO_2 + 4\,SO_2 \tag{9}$$

At lower temperatures (<1040°C/<1900°F) and with a reducing atmosphere, CaS is formed.

A series of experiments was performed using *in situ* combustion of methane to evaluate the effects of temperature, residence time (controlled by feed rate and bed height), height of fluidized bed, and total reducing gas conditions. From past thermodynamic studies,[2] the expected effects are that increasing the bed temperature and reducing gas concentration should increase the amount of regeneration. Increasing the residence time (by decreasing the feed rates or increasing the fluidized-bed height) should also increase the amount of regeneration because the reaction time is extended.

The original statistical design for this series was modified as a result of problems that occurred because of equipment limitations. As an example, experiment FAC-2 (see Table 1) was attempted four times; during each attempt, partial caking of the sulfated dolomite bed occurred, leading to termination of the experiment. Operating conditions for this experiment were a bed temperature of 1095°C and a 15% reducing gas concentration in the effluent. It is believed that upsets in the fluidization of the additive bed caused local temperatures to rise higher than the measured operating temperature. It was reported by Wheelock and Boylen[3] that the surface of $CaSO_4$ became glassy upon regeneration at 1250°C (2300°F). If localized temperatures in the regenerator momentarily exceeded this temperature, the additive particles would begin to adhere and to restrict the gas flow. A regenerator with a larger cross section would not be hampered as readily by small bed cakes. The planned experimental program did not permit further modifications or attempts to perform experiments with extreme conditions such as those used in FAC-2. Therefore, the experimental plans were modified to accommodate the experimental capabilities of the existing regenerator system, *i.e.*, conditions were selected to avoid the fusing of bed solids or the formation of cakes, which would hinder fluidization.

Sulfated Tymochtee dolomite containing 10.2 wt % S from combustion experiments was regenerated. Operating data and regeneration results are shown in Table 1.

Replicate Experiments. Replicate experiments FAC-1, FAC-1R1, and FAC-1R2 were performed at 1040°C and a low total reducing gas concentration in the effluent, ∿3% (near-stoichiometric CH_4 in the feed gas), with an additive feed rate of 6 lb/hr, and with a nominal fluidized-bed height of 1.5 ft. The amount of sulfur regenerated as SO_2 was 65% for FAC-1, 61% for FAC-1R1, and 57% for FAC-1R2 of that contained in the sulfated Tymochtee dolomite. The SO_2 concentration in the wet flue gas varied from 3.0% in FAC-1 to 2.3% in FAC-1R2. The difference in these results is due mainly to slight differences in the fluidizing-gas velocities. Operating conditions for FAC-1 are presented in Fig. 11 and 12 and for the remainder of the FAC-experiments in Appendix B.

Effect of Fluidized-Bed Height at a Constant Additive Feed Rate. Experiment FAC-5 was performed at 1040°C (1900°F), an additive feed rate of 10 lb/hr (residence time of ∿30 min), a nominal fluidized-bed height of 2.5 ft, and a total nominal reducing gas concentration of 15% in the effluent. A sulfur regeneration of 54% was obtained, with a SO_2 concentration of 3.5% in the wet effluent gas. This experiment can be compared with FAC-3, which was performed at the same additive feed rate and total reducing gas concentration in the effluent but with a shorter fluidized-bed height of 1.5 ft (residence time of ∿18 min). A higher sulfur regeneration of 62% was obtained for FAC-3. This indicates that increasing the fluidized-bed height from 1.5 ft to 2.5 ft was detrimental to sulfur regeneration.

Fluidization and mixing in the 2.5-ft bed may be less effective than in the 1.5-ft bed. As gas bubbles rise in the fluidized bed, they coalesce and grow larger. In deeper beds, larger gas bubbles are formed and thus a greater degree of segregation between the gas phase and the well-fluidized phase takes place. Transport of the reducing gases from the gas phase to the well-fluidized

Table 1. Design Experimental Conditions for the FAC-Series and Sulfur Regeneration Results Obtained

Pressure, psig: 12
Additive: Sulfated Tymochtee Dolomite (10.2 % S)

Exp.	Temp (°C)	Design Conditions				Fluidizing Velocity (ft/sec)	Measured SO_2[b] in Effluent (%wet)/(% dry)	Sulfur Regeneration (%)
		Additive Feed Rate (lb/hr)	Residence Time (min)	Bed Height (ft)	Total Reducing Gas in Effluent,[a] %			
FAC-1	1040	6	30	1.5	3	2.2	3.0 / 4.0	65
FAC-1R1	1040	6	30	1.5	3	2.4	2.6 / 3.6	61
FAC-1R2	1040	6	30	1.5	3	2.5	2.3 / 2.9	57
FAC-2	1095	6	30	1.5	15	Experiment could not be completed		
FAC-3	1040	10	18	1.5	15	2.6	4.1 / 5.7	62
FAC-4	1095	10	18	1.5	3	2.5	5.3 / 7.3	73
FAC-5	1040	10	30	2.5	15	2.7	3.5 / 4.4	54
FAC-7	1040	10	30	2.5	3	2.5	2.7 / 3.3	40
FAC-8	1010	5	30	1.5	3	2.3	0.65/ 0.78	14
FAC-9	1040	6	30	1.5	3	2.5	1.3 / 1.7	55
FAC-9A	1040	6	30	1.5	3	3.0	1.3 / 1.5	38

[a] The actual reducing gas concentrations were within 15% of the design levels.

[b] Determined by I.R. SO_2 analysis of the dry flue gas.

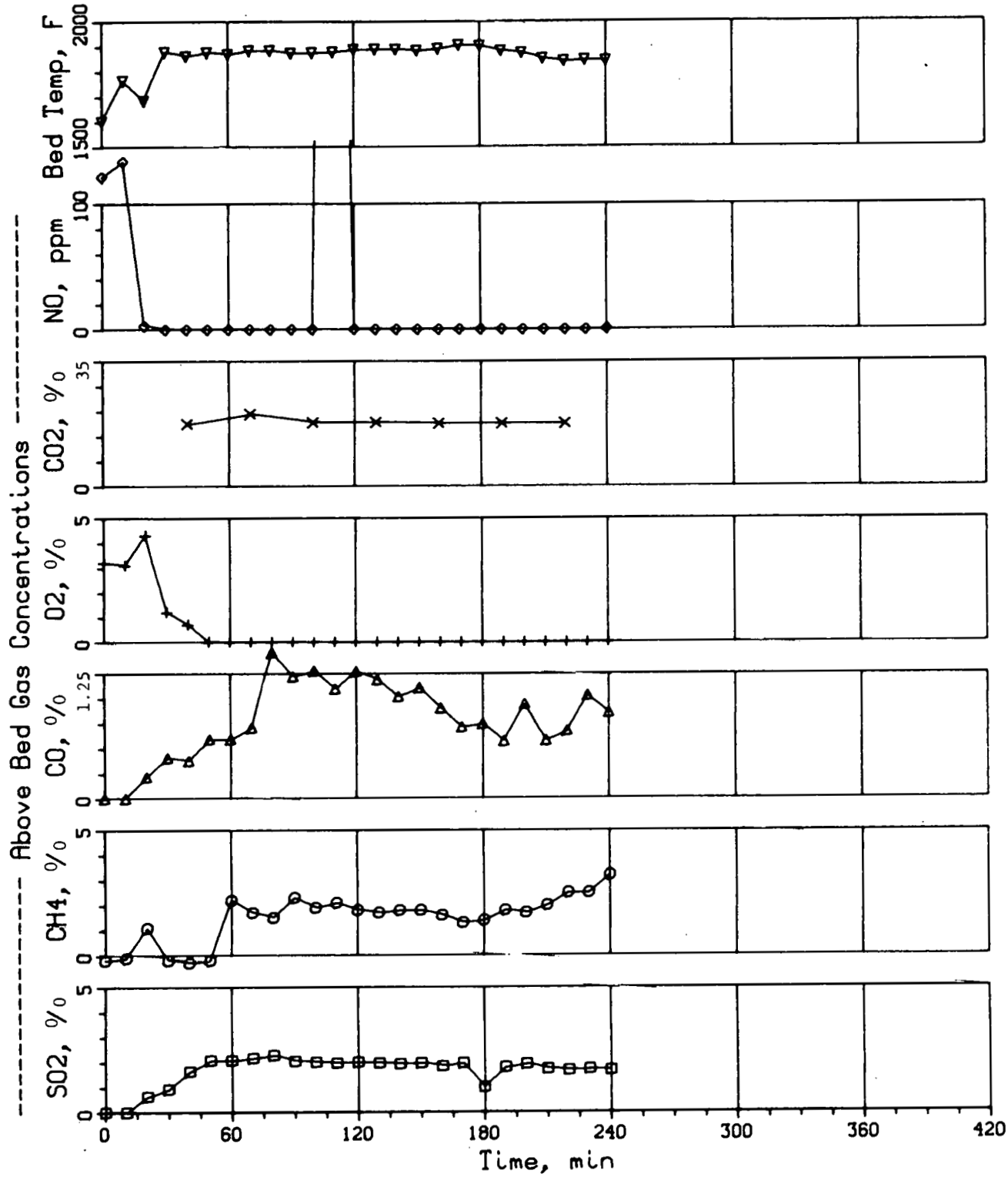

Fig. 11. Bed Temperature and Gas Concentrations in Off-Gas, Experiment FAC-1

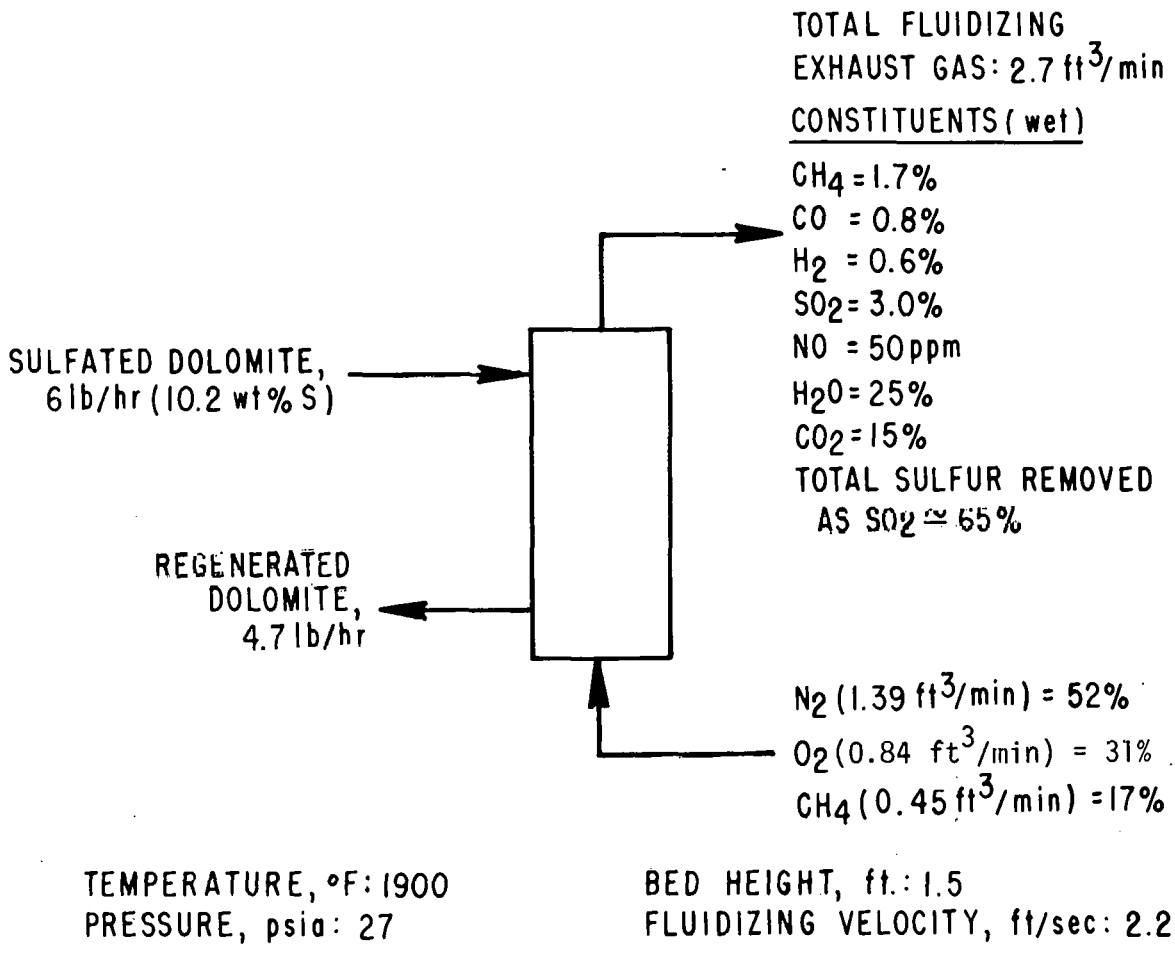

Fig. 12. Operating Conditions and Experimental Flow Diagram with Results for FAC-1

phase becomes increasingly difficult. This could reduce the regeneration rates. Also, because the additive is dropped into the top of the fluidized bed (where the entrance to the overflow pipe is located), poor mixing could prevent the sulfated additive from circulating throughout the entire bed and reaction would take place only in the upper (more segregated) portion of the fluidized bed. This would result in shorter actual residence times.

Effect of Fluidized-Bed Height at a Constant Solids Residence Time. FAC-7 was designed to test the effect of increasing the fluidized-bed height from 1.5 to 2.5 ft while the solids residence time was fixed at ~30 min. It is compared with experiment FAC-1R2, which was performed at the same fluidizing-gas velocity of 2.5 ft/sec, a bed temperature of 1040°C, and a total reducing gas concentration of 3% in the effluent gas. In experiment FAC-7, at a fluidized-bed height of 2.5 ft, a sulfur regeneration of 40% was obtained with a SO_2 concentration of 2.7% in the wet effluent. In FAC-1R2, at a fluidized-bed height of 1.5 ft, a much higher sulfur regeneration was obtained (57%).

As in experiment FAC-5, less effective fluidization and solids mixing in the 2.5 ft-high bed may have caused the actual residence time of the additive in FAC-7 to be less than that in FAC-1R2, resulting in less sulfur regeneration.

Effect of Low Regeneration Temperature (<1040°C). FAC-8 was designed to test the effect on sulfur regeneration of a regeneration temperature lower than 1040°C. The results are compared with the results of FAC-1R1, performed at 1040°C. Both experiments were performed with an additive feed rate of 6 lb/hr, a fluidized-bed height of 1.5 ft, and a total effluent reducing gas concentration of 3%.

Sulfur regeneration was 14% in FAC-8, in which the regeneration temperature was 1010°C. The SO_2 concentration in the wet effluent was 0.65%. In comparison, sulfur regeneration was 61% for FAC-1R1 and the SO_2 concentration was 2.6%. At the lower temperature, the formation of CaS is favored in a reducing atmosphere. Chemical analysis of the regenerated additive is under way to determine the quantitative difference in sulfide formation between FAC-8 and FAC-1R1.

Effect of Fluidizing-Gas Velocity. The effect of fluidizing-gas velocity on regeneration was evaluated by performing FAC-9A with a fluidizing-gas velocity of 3 ft/sec and comparing the results with the results of FAC-1, which was performed with a fluidizing-gas velocity of 2.2 ft/sec. A sulfur regeneration of 38% was obtained in FAC-9A in comparison with 65% in FAC-1. At the higher gas velocity, sulfur regeneration decreased. At higher fluidizing-gas velocities, the bubble phase in the fluidized bed increases and the transport of reducing gas from the bubble phase to the additive becomes more difficult. In effect, this could result in a reduced effective reducing gas concentration and less sulfur regeneration. Also, at higher fluidizing velocities, solids mixing may be less effective due to the geometry of the fluidized bed (height of bed/bed diameter = 6).

Effect of Residence Time on Regeneration Rate. The regenerated additive from FAC-1 and FAC-1R1 was used as feed material in FAC-9, as illustrated in Fig. 13. This experiment (FAC-9) was performed to evaluate the effect of doubling the residence time in the fluidized bed. The actual sulfur content of this feed material was ∿5.8 wt %. A sulfur regeneration of ∿55% was obtained in FAC-9 with 1.3% SO_2 in the wet effluent gas. The regeneration rate remained high, comparing favorably with that in FAC-1 and -1R1, but the SO_2 concentration in the effluent gas decreased. The above combined regeneration results for FAC-9 and FAC-1 are better than might be expected if the residence time in a well-mixed fluidized-bed regenerator were double that of either FAC-9 or FAC-1. In FAC-9 (illustrated in Fig. 13), fresh fluidizing reducing gas (>3% total) containing no SO_2 was fed to the regenerator. (More complete regeneration data for all FAC experiments are being obtained by chemical analysis of regenerated products.)

As stated above, experiment FAC-1R2 was performed at the following experimental conditions: bed temperature of 1040°C (1900°F), system pressure of 12 psig, nominal fluidized-bed height of 1.5 ft, additive feed rate of 6 lb/hr (residence time of ∿30 min), and total reducing gas concentration in the effluent of ∿3%, *i.e.*, near-stoichiometric CH_4 in the feed mixture. A sulfur regeneration of 57% for FAC-1R2 was obtained with a SO_2 concentration of 2.3% in the wet flue gas. In experiment FAC-3, the sulfated additive feed rate was increased to 10 lb/hr (residence time of 18 min), and the total reducing gas concentration in the effluent was increased to 14%. A sulfur regeneration of 62% was obtained, and the SO_2 concentration in the wet flue gas was 4.1%.

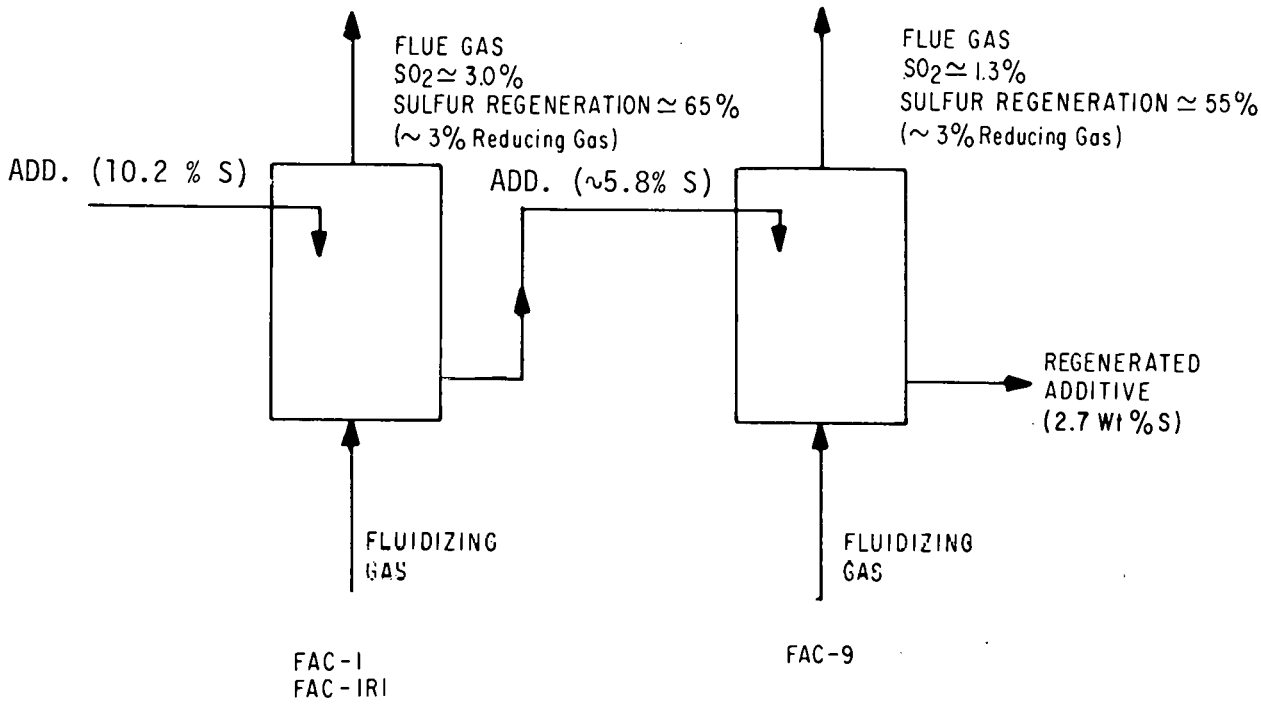

TEMPERATURE, °C: 1040 BED HEIGHT, ft: 1.5

PRESSURE, psia: 27 FLUIDIZING VELOCITY, ft/sec: 2.5

Fig. 13. Experimental Flow Diagram for FAC-9 with Regeneration Results

A comparison indicates that the detrimental effect on sulfur regeneration of decreasing the residence time from ~30 to ~18 min was less effective than the beneficial effect of increasing the total reducing gas concentration in the effluent from 3% to 14%.

Effect of Higher Regeneration Temperature (1095°C). Experiment FAC-4 was performed at 2000°F, an additive feed rate of 10 lb/hr, and with a low-level total reducing gas concentration (~3%) in the effluent gas. A sulfur regeneration of 73% was obtained and a SO_2 concentration of 7.3% in the dry flue gas at steady state. A higher sulfur regeneration has been obtained in FAC-4 than in FAC-3 (at 1900°F), which was performed with the same feed rate (residence time of 18 min) and with a high concentration of reducing gas in the effluent. The higher temperature (2000°F) of FAC-4 increased the regeneration of sulfated dolomite more than lowering the reducing gas concentration decreased it, in comparison to FAC-3.

Material and Energy Balances for the One-Step Regeneration Scheme

An objective of part of the experimental program at ANL is to develop and demonstrate the technical feasibility of one-step regeneration at atmospheric pressure. In some experiments being performed in the existing 3-in.-dia, fluidized-bed regeneration unit, the *in situ* partial combustion of methane is employed to provide the necessary heat and reducing gases for regeneration. Future experimentation in a 4-in.-dia, fluidized-bed reactor will investigate the feasibility of using the *in situ* partial combustion of coal to provide the heat and reducing gases for regeneration.

Technical Considerations

The concentration of SO_2 in the off-gas from the regenerator needs to be sufficiently high (~10%) for economic further processing and recovery of the sulfur. The use of *in situ* combustion to provide both the heat and reducing gases necessary for regeneration tends to dilute the SO_2 level in the off-gas if the sulfated additive is insufficiently preheated.

Serious decrepitation problems have been encountered during regeneration of sulfated additive. It has been proposed, therefore, that only the surface of the additive particles be utilized, where the kinetics are favorable (not diffusion limited); short residence times in the processing units (combustor and regenerator) would then be sufficient. This also bears directly on the need for sufficient preheat of the high throughput of solids in the regenerator to prevent excessive dilution of the off-gas by an additional heat load on the *in situ* combustion.

Existing Capabilities. Material and energy balances have been made around the ANL 3-in.-dia fluidized-bed regeneration unit to assess the existing operating capabilities at a high solids throughput, *i.e.*, short reactor residence times. The calculations are of a preliminary nature and are intended as a guide for setting up an experimental program and for making equipment modifications to meet the technical considerations of the proposed process. Equilibrium limitations were not considered in this preliminary effort as such limitations are not believed to affect seriously the overall balances. Kinetic limitations are much more likely to be a limiting factor in the process. The process flowsheet for material and energy balances is shown in Fig. 14.

The reactants enter the regenerator at ambient temperature and 2 atm abs. pressure. Fully calcined and partially sulfated limestone (20% utilization) was used as the basis for the calculations. To compensate for the lack of preheat of the reactants and the relatively large heat loss from a small unit, an oxygen-nitrogen mix would be fed to the regenerator to increase the amount of fuel which could be burned at a given flowrate.

Three cases were considered. Case 1 involved operating the regenerator at a gas velocity of 4 ft/sec using a mixture of 50% oxygen and 50% nitrogen. For Case 2 the mixture was 40% oxygen and 60% nitrogen. Case 3 involved regeneration at 2.25 ft/sec and a 75% oxygen and 25% nitrogen gas mix. A heat loss of 13,500 Btu/hr was estimated for all three base cases. The resulting material and energy balances are presented in Tables 2 and 3, respectively.

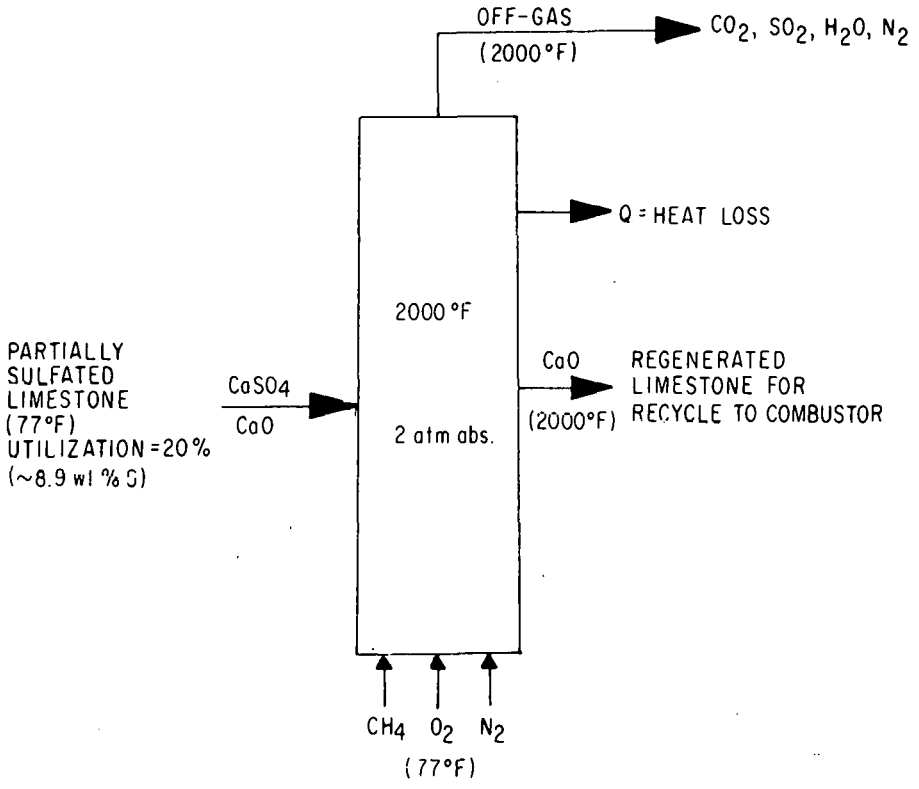

Fig. 14. Process Flow Sheet Used in Making Material and Energy Balances Around Existing ANL 3-in.-dia, Fluidized-Bed Regenerator

All three cases indicate a solids residence time of from 9-15 minutes, assuming fluidized-bed weight of ~6 lb (~3 ft fluidized-bed height). Unfavorable kinetics would necessitate increasing the solids residence time.

Data in Table 2 show a definite advantage of higher gas velocities in that higher nitrogen levels can be used to reduce the percentage of H_2O in the off-gas, which has caused operational problems in previous regeneration experiments.

Information in Table 3 clearly emphasizes the penalty imposed by not preheating the reactants. Approximately 50 to 60% of the heat input is used to raise the reactants (plus inerts) to temperature, and another 25 to 35% compensates for heat losses. Only 15 to 20% of the heat supplied by *in situ* fuel combustion is used for the reduction reaction. Preheating of the reactants would permit the use of additional nitrogen to further reduce the operational problems of water in the off-gas with no loss in the percentage of SO_2 obtained.

Table 2. Material Balances for Three Postulated Cases of Regenerator Operating Conditions

Operating Temp: 2000°F Limestone: 8.9 wt % sulfur
Operating Pressure: 2 atm abs

	Case 1		Case 2		Case 3	
Operating Conditions:						
Velocity, ft/sec	4		4		2.25	
O_2:N_2 mole ratio	1:1		2:3		3:1	
Material Balance:						
In, lb/hr						
$CaSO_4$	12.9		8.9		9.4	
CaO	21.2		14.7		15.5	
Total Solids		34.1		23.6		24.9
CH_4	3.0		2.4		2.2	
O_2	9.9		8.4		7.6	
N_2	8.7		11.0		2.2	
Total Gas		21.6		21.8		12.0
Total In		55.7		45.4		36.9
Out, lb/hr						
CaO	26.6		18.4		19.4	
N_2	8.7	(33%)[a]	11.0	(44%)	2.2	(14%)
CO	7.9	(19%)	6.5	(16%)	6.0	(25%)
SO_2	6.1	(10%)	4.2	(7%)	4.4	(12%)
H_2O	6.5	(38%)	5.3	(33%)	4.9	(49%)
Total Cut	55.8	(100%)	45.4	(100%)	36.9	(100%)

[a] Gas composition in mole %

Table 3. Energy Balances for Three Postulated Cases of Regenerator Operating Conditions

Operating Temp: 2000°F Limestone containing 8.9 wt % sulfur
Operating Pressure: 2 atm abs

	Case 1	Case 2	Case 3
Heat Source, Btu/hr			
CH_4 Combustion	53,200	45,300	41,000
Heat Sinks, Btu/hr			
Heat $CaSO_4$ to 2000°F	6,600 (12%)[a]	4,600 (10%)	4,800 (12%)
Heat CaO to 2000°F	8,900 (17%)	6,100 (13%)	6,500 (16%)
Heat Gases to 2000°F	14,500 (27%)	13,900 (31%)	8,600 (21%)
Reduction Reaction	10,200 (19%)	7,000 (16%)	7,400 (18%)
Heat Loss	13,500 (25%)	13,500 (30%)	13,500 (33%)
	53,700 (100%)	45,100 (100%)	40,800 (100%)

[a] Contribution to total heat load in percent.

PREPARATION, SULFATION, AND REGENERATION OF CALCIUM OXIDE-IMPREGNATED SUPPORTED ADDITIVES

Naturally occurring limestone and dolomite are the only materials that have been energetically evaluated for removing sulfur dioxide from flue gas, primarily due to their low cost. However, during regeneration of sulfated dolomite at other sites, decrepitation of the particles has occurred. A structure that would be sufficiently strong to eliminate decrepitation would be desirable.

A research program has been initiated to determine methods of supporting calcium oxide in a highly dispersed state in a matrix of a high-strength, inert material. Calcium oxide is probably more reactive in a dispersed state than is massive CaO, and the inert support material would supply the strength needed to eliminate the decrepitation problem. In this program, the capability of supported calcium oxide to react with sulfur dioxide and of the resulting $CaSO_4$ to be regenerated is being studied, using calcium oxide impregnated in α-alumina support (pellets).

One-step regeneration experiments (which require a temperature above 950°C), as well as sulfation experiments, were completed on a newly constructed high-temperature TGA system described below. In other experiments, pellets were fluidized in air to determine the effect on their integrity. Two types of support materials have been selected for testing: Alumina (Al_2O_3) compounds similar to those used in conventional catalytic processes are being studied now; silicates will be studied later. Both calcium- and potassium-impregnated alumina pellets have been prepared. Methods of impregnation are described below.

Materials

Porous alumina supports have surface areas that range from 5 to 250 m^2/g and a void space (volume of pores x 100/volume of pellet) that is approximately 50 percent of the support volume. The supports currently being used in our studies have a surface area of 5-10 m^2/g. Supports that have a small surface area per gram usually contain larger pores than support materials having a large surface area. The supports (obtained from Girdler Chemical Co.) were cylindrical pellets 1/8 in. in dia by 1/8 in. long. This and other sizes of pellets are readily available commercially in large quantity.

Reagents used in preparing impregnated pellets were of a chemically pure grade.

Preparation of Supported Additives

Calcium Oxide-Impregnated Additive. Four methods of placing calcium oxide in the pores of 1/8-in. cylindrical alumina pellets have been studied. The only process that evenly distributed calcium oxide through the pores of the pellet involved first contacting the alumina in an aqueous solution of calcium nitrate. The solution was refluxed for approximately eight hours to ensure that the calcium nitrate solution was evenly distributed in the pores. The solution was then cooled, and the pellets were removed and placed in a drying oven, where they were heated slowly to 800°C. During heating, the water was vaporized, the

calcium nitrate decomposed, and calcium aluminates ($5Al_2O_3 \cdot 3CaO$) formed by the reaction of CaO with Al_2O_3. Two samples were prepared for sulfation and regeneration tests. A solution of 50 g of $Ca(NO_3)_2 \cdot 4H_2O$ in 25 g of H_2O yielded a support containing 17% CaO; a solution of 50 g of $Ca(NO_3)_2 \cdot 4H_2O$ in 100 g of water yielded a support containing 6.6% CaO.

X-ray diffraction results showed that not all of the CaO had reacted to form calcium aluminates. The ratio of calcium in the oxide to the calcium in the aluminate has not been determined. It is believed that the ratio depends on the time and temperature of heat-treating the pellets during the impregnation and calcining process. Calcium is thought to react with the alumina when the calcium nitrate is in the liquid state and calcium ions exist. To gain greater insight into the reaction mechanism, solid calcium oxide powder and alumina powder were mixed and heated at 800°C for 4 hr. X-ray diffraction analysis of the resultant powder showed that only a very minor amount of calcium aluminates formed, with the major portion of the powder remaining as calcium oxide and aluminum oxide. This implies that the solid-solid reaction is slow and that the aluminates may form by another mechanism.

Thermodynamic considerations indicate that calcium aluminates will react with sulfur dioxide. Therefore, this calcium bonding may be acceptable, depending on the kinetics of the reaction of SO_2 with calcium aluminates. In fact, the bonding of calcium with alumina could be useful for stabilizing the CaO on the internal surfaces of the alumina.

In a second preparation method, alumina supports were placed in molten calcium nitrate (m.p., 561°C) for 4 hr. The calcium nitrate flowed into the pores, where it slowly decomposed to nitrogen oxides and to calcium oxide that reacted with alumina to form calcium aluminates. The pellets, which contained 27 wt % CaO, were sulfated at a temperature of 750°C with an inlet gas of 0.39% SO_2 in N_2. Approximately 35% of the original total void space in the support was occupied by CaO. After 4 hr, only 2% of the calcium oxide had reacted to form calcium sulfate. It is believed that the low percentage of sulfation resulted because of blockage of the pores. Therefore, this method of preparing supported additives has been rejected.

A third preparation technique is based on the precipitation of calcium carbonate in the pores by the reaction of sodium carbonate with calcium chloride in an aqueous solution. Pellets of alumina were placed in a saturated aqueous sodium carbonate solution for 12 hr. This allowed the aqueous sodium carbonate solution to enter the pores of the pellets. The solution was then cooled to precipitate the sodium carbonate from the solution. The pellets were removed and heated to remove water and were then placed in a saturated aqeuous solution of calcium chloride. As the sodium carbonate reentered the solution and reacted with $CaCl_2$, the calcium carbonate precipitated because of its low solubility in water. The pellets were removed, washed, and dried. Only minimum success was attained; the calcium carbonate was found to be unevenly distributed.

The fourth preparation technique studied is based on the reaction of sulfuric acid with calcium carbonate to form calcium sulfate, which would then be reduced to CaO. Alumina pellets were placed in a solution of concentrated sulfuric acid and calcium carbonate and were heated for four hours. After cooling, the pellets were removed and heated to 800°C to remove sulfuric acid. The X-ray diffraction results showed that, although calcium sulfate was present in the

pores, it was not evenly distributed throughout the pellet. Approximately three-fourths of the pellets contained calcium sulfate, but no calcium was found at the center. Possibly, a longer reaction time might allow the calcium sulfate to permeate the pellet. This method was not evaluated further.

Potassium Oxide-Impregnated Additive. The use of alkali metal oxides for the removal of SO_2 from a combustion gas stream is being considered. The alkali metal oxides have the greatest affinity for sulfur but may be difficult to regenerate economically. Potassium oxide has been placed in α-alumina pellets by refluxing, for 4 hr, a solution of 50 g KNO_3-100 g H_2O into which α-alumina pellets had been placed; the pellets were then removed and were heat-treated at 1000°C for 12 hr. X-ray diffraction results indicated that all of the potassium was in the form of an aluminate. The concentration of the contained potassium oxide was approximately 3%. These pellets will be sulfated later on the TGA.

Thermal Gravimetric Analysis (TGA) System

The new TGA system is depicted in Fig. 15.

The reactant gas mixture, which is prepared by controlling the flow of each constituent or mixture by means of a diaphragm-type regulator and calibrated rotameters, flows upward through the heated reaction tube, past the sample, and exits through a condenser and a series of scrubbers. Total flow rate can be controlled in the range from 200 to 4000 cc/min with an accuracy for the total flow and for each constituent of about ±2%. The sample (contained in a wire mesh platinum basket) is suspended from one arm of a recording balance. The balance, which provides continuous weight data over the range from 0.2 to 1.0 g with an accuracy of ±0.1 mg, is protected from corrosive gases by a purge flow of nitrogen. The temperature in the reaction zone of the Marshall furnace is controlled to an accuracy of ±5°C up to about 1500°C and is recorded, along with the sample weight, on a recorder.

Sulfation Experiments

In preliminary sulfation experiments, it was found that in pellets containing 27% CaO, only 2% of the calcium oxide was sulfated, probably because of pore blockage. The pellets were sulfated at 750°C with a gas mixture containing 0.39% SO_2.

Pellets containing ~6.6% CaO were sulfated at 750°C with a gas mixture containing 1% SO_2 in N_2. Weight measurements obtained on the pellets before and after sulfation indicated that all of the calcium oxide had reacted to form $CaSO_4$. Scanning electron microscope (SEM) experiments were performed on the sulfated pellets, and an even sulfur distribution was found throughout the pellets. Consequently, pellets using this concentration of CaO were used in subsequent tests.

Sulfation Operability Experiments. Calcium oxide-impregnated pellets were sulfated (1) to test the operating performance of the high-temperature TGA unit, (2) to determine the reproducibility of sulfation experiments, (3) to compare the use of premixed and blended gases, and (4) to determine if the reaction was SO_2-limited. The starting material in each sulfation experiment

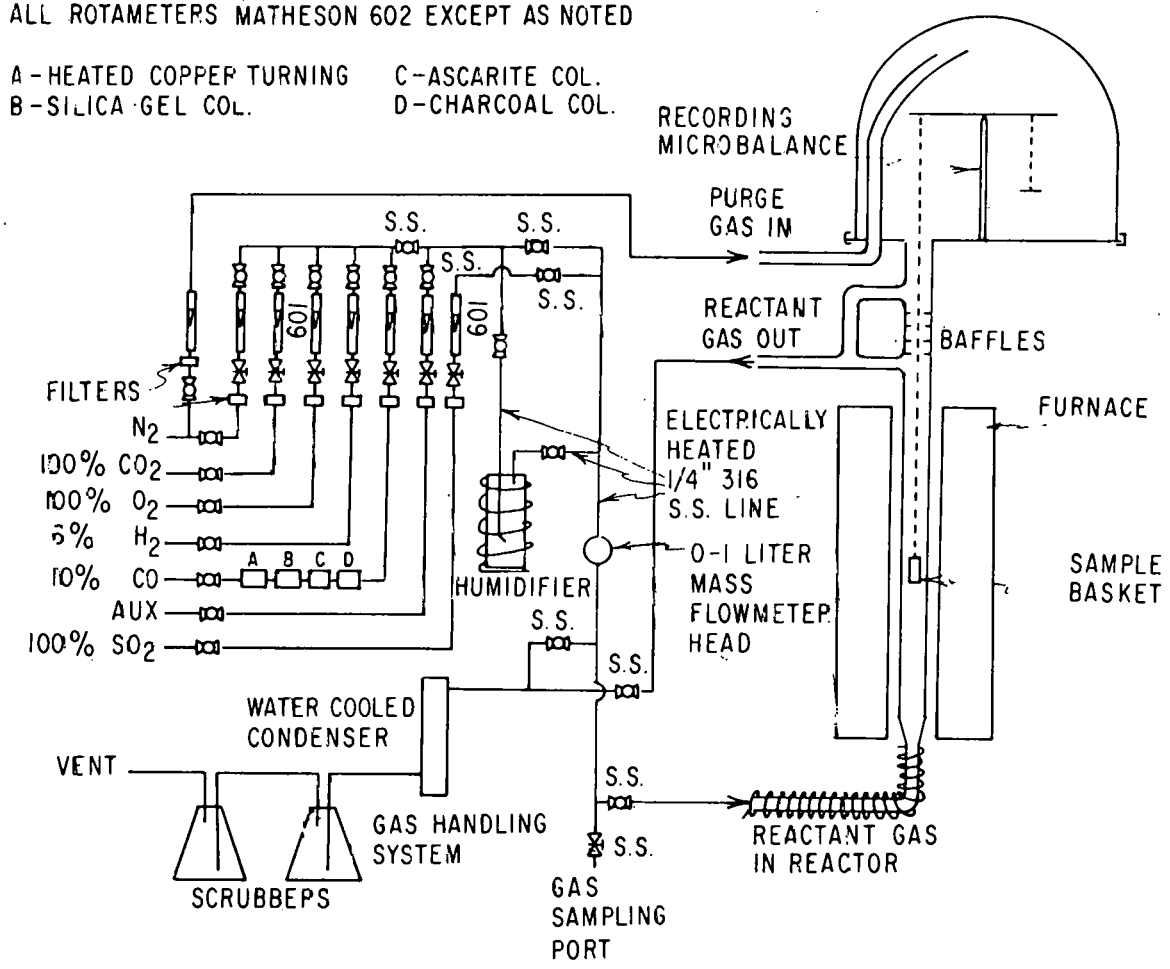

Fig. 15. Schematic Diagram of the Modified TGA Apparatus

was α-alumina cylindrical pellets, 1/8 in. by 1/8 in., containing an average f 6.64% CaO and weighing 35 to 40 mg apiece. The CaO concentration of the ellets ranged from 6 to 7%.

Sulfation runs 16 to 18 were performed using a premixed gas from a cylinder containing 3% SO_2, 5% O_2, 40% CO_2, and 52% N_2. In experiment 19, gases were blended using rotameters to give 3% SO_2, 5% O_2, and 92% N_2. The results of these four experiments are shown in Fig. 16 and 17, where the percent conversion of CaO to $CaSO_4$ is plotted as a function of time. Because of the inhomogeneity of the α-alumina pellets, different amounts of CaO are contained in different pellets and the exact quantity of SO_2 needed for 100% sulfation is unknown. Hence the data are plotted on the basis of two alternative assumptions. Figure 16 data assume that the pellets contained an average of 6.64% CaO; Fig. 17 data assume that all of the CaO was sulfated during each sulfation experiment. Samples of the sulfated pellets have been submitted for calcium and sulfur analyses to learn the percentage of calcium utilized. This should yield information as to whether Fig. 16 or Fig. 17 better represents the data.

In experiments 16 and 18, the reproducibility of results was demonstrated. In experiment 17, 12 pellets instead of 6 were used and the data were compared with the data for experiments 16 and 18 to show that the reaction was not SO_2-limited. Experiment 19 was made to show that blending of SO_2 and O_2 by use of the TGA system rotameters would give the same results as does the premixed gas. In experiment 19, CO_2 was absent. However, in all experiments, $CaCO_3$ would not form at these conditions; therefore, the presence of CO_2 should not have affected the reaction rate.

X-ray diffraction results here confirmed that the CaO in the pellets reacted with SO_2 to form $CaSO_4$, as given below:

$$CaO + SO_2 + 1/2\ O_2 \rightarrow CaSO_4$$

SEM results have shown an even distribution of calcium and sulfur throughout the pellets, which indicates that the Ca/S ratio was constant within a pellet. This implies that the same percent calcium utilization was being achieved and that Fig. 17 is possibly more representative of the data.

Figure 18 shows the SEM sulfur and calcium peaks at four different locations on a pellet from experiment 17. The top curve (No. 1) is for a scan at the center of the pellet; the bottom curve (No. 4) is for a scan near the surface of the pellet. Figure 19 shows the polished cross section of the same sulfated pellet from experiment 17 (for which scans are shown in Fig. 18). Figures 19b and 19c illustrate the calcium and sulfur distributions throughout the same pellet, respectively. The white dots in Fig. 19b represent only calcium, while in Fig. 19c the white dots represent only sulfur. The one-to-one correspondence of calcium to sulfur in Fig. 19b and 19c can be observed easily.

Effect of SO_2 Concentration on Sulfation Rate. Data on the effect of the SO_2 gas concentration on the rate of the sulfation reaction at 900°C at SO_2 concentrations ranging from 0.3% to 3% are shown in Fig. 20. Experiments will also be run at SO_2 concentrations below 0.3. These experiments were done using pellets from the same batch as in the previous series, with an average CaO concentration of 6.6%. The rate of reaction increased with increasing O_2 concentration. Modeling efforts will begin soon to quantify the data.

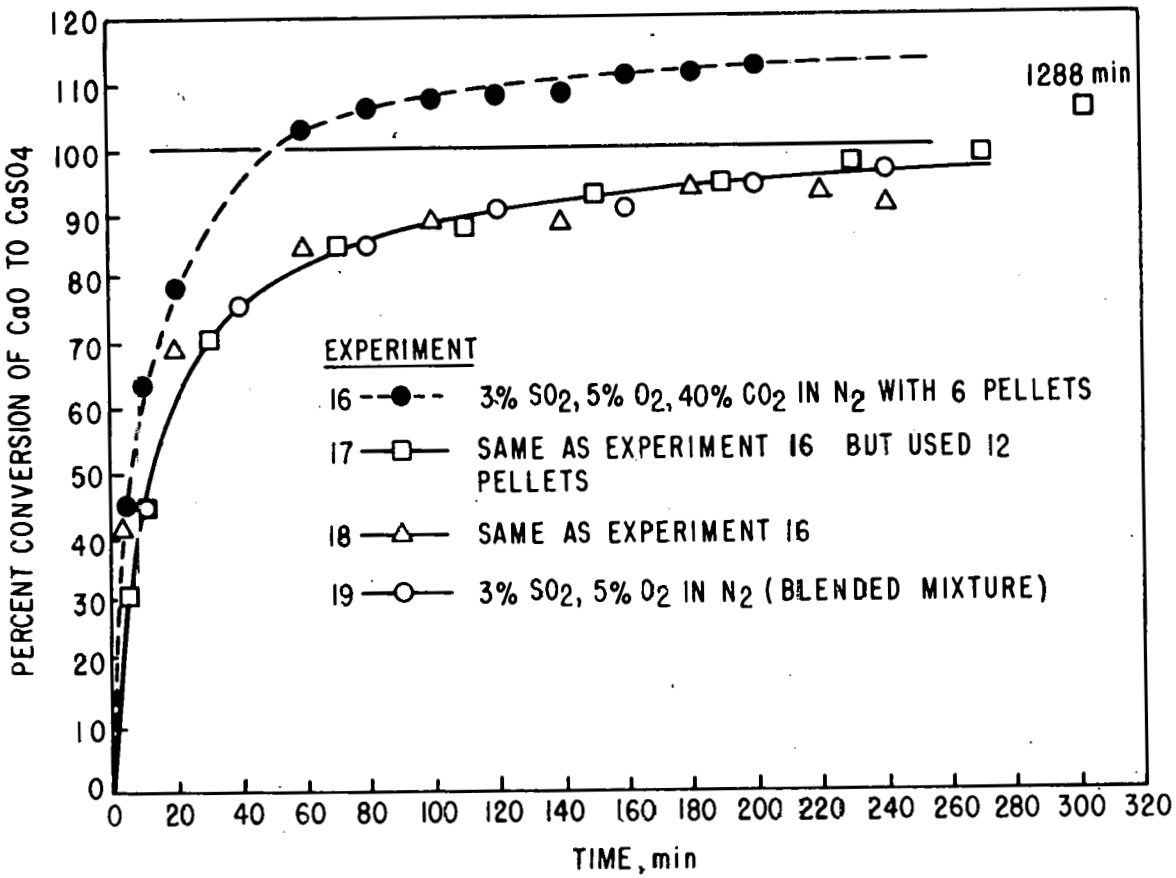

Fig. 16. Sulfation of 6.6% $CaO-Al_2O_3$ at 850°C with 3% SO_2 in Feed Gas

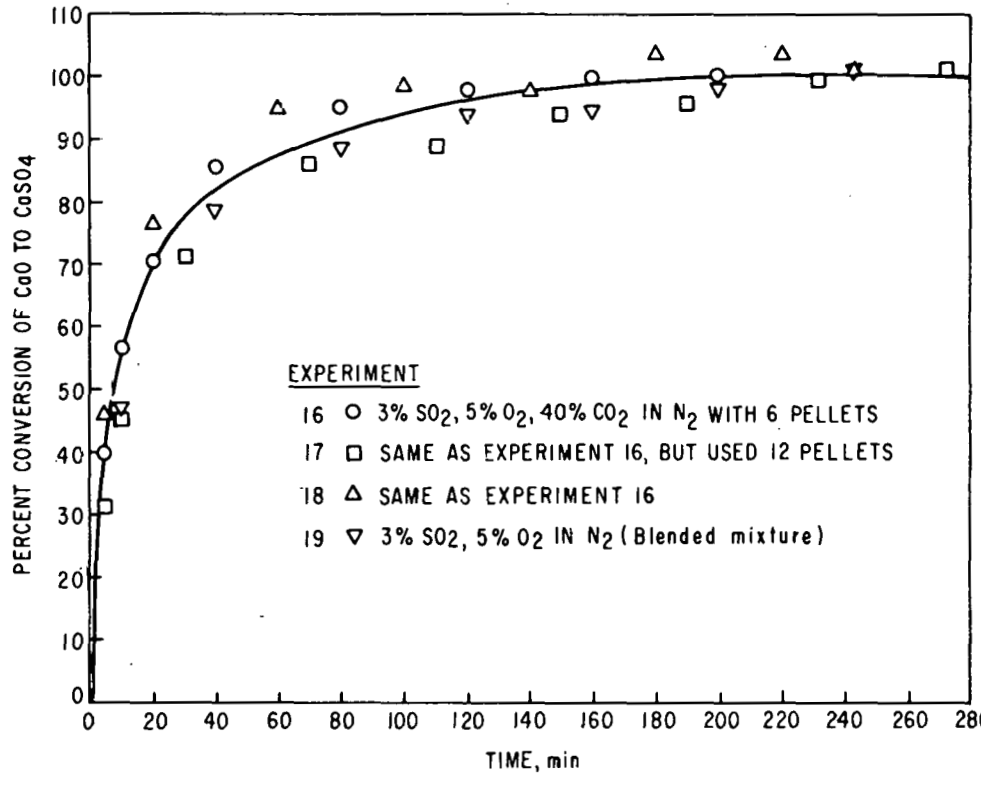

Fig. 17. Sulfation of 6.6% $CaO-Al_2O_3$, at 850°C with 3% SO_2 5% O_2 in N in the Feed Gas; 100% Sulfation is Assumed.

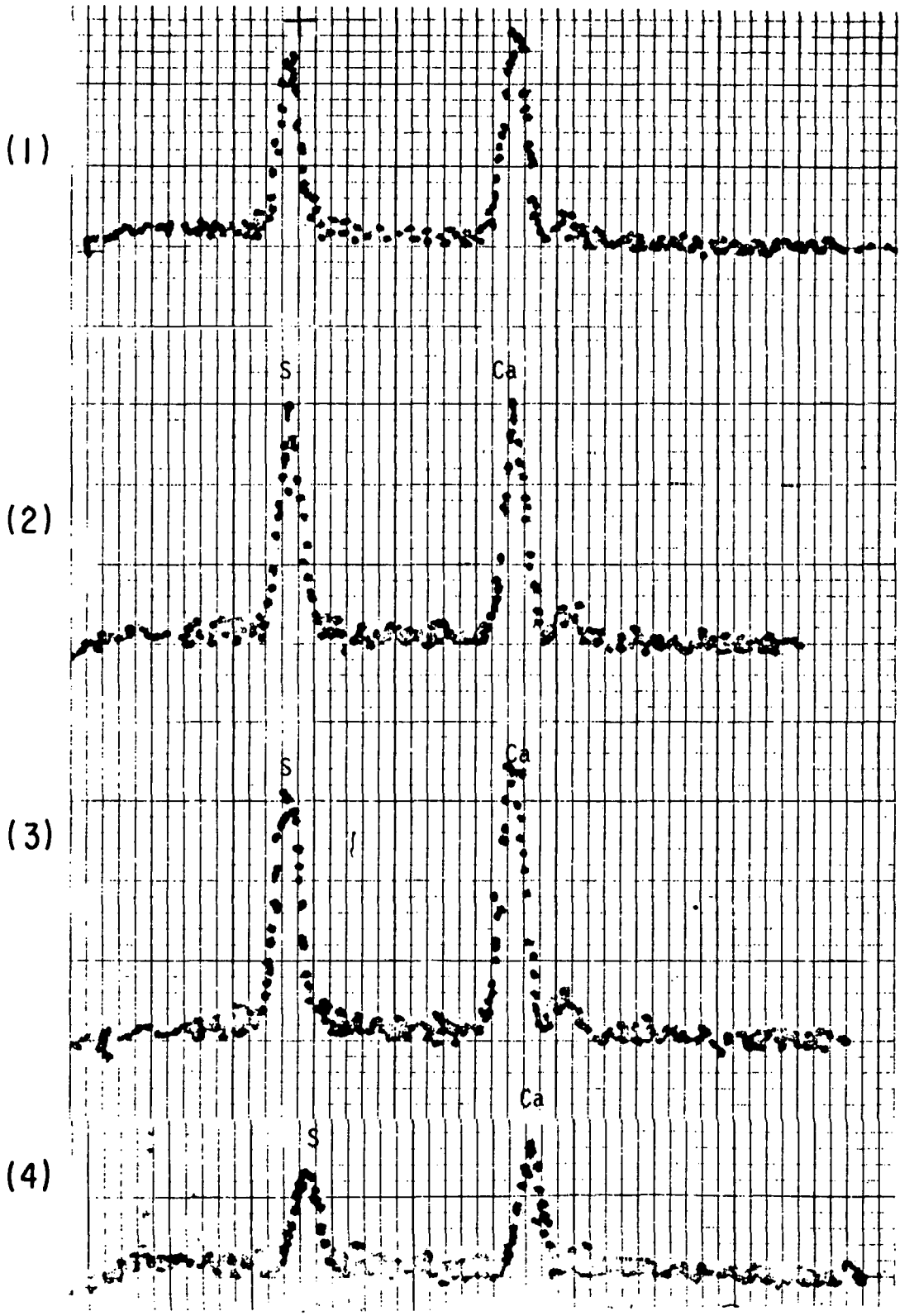

Fig. 18. SEM Results on Sulfated 6.6% CaO-α-alumina

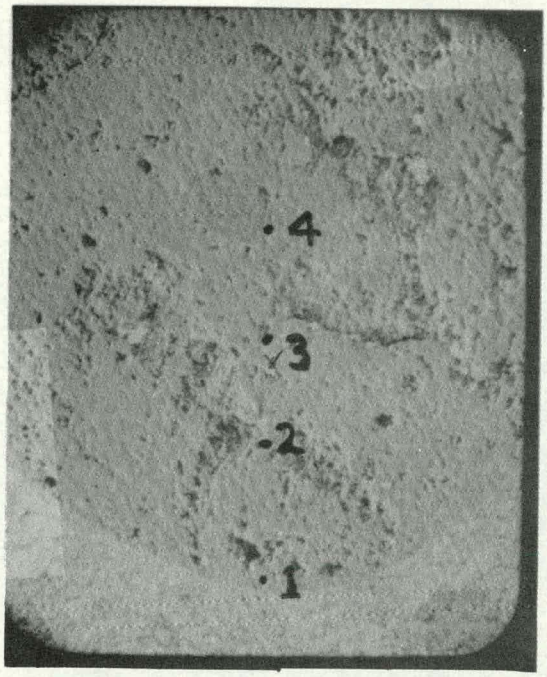

a. Polished Cross Section of a Sulfated 6.6% CaO-αAlumina Pellet from Experiment 17. The numbered dots are the locations where SEM analyses were taken. Mag. 40X.

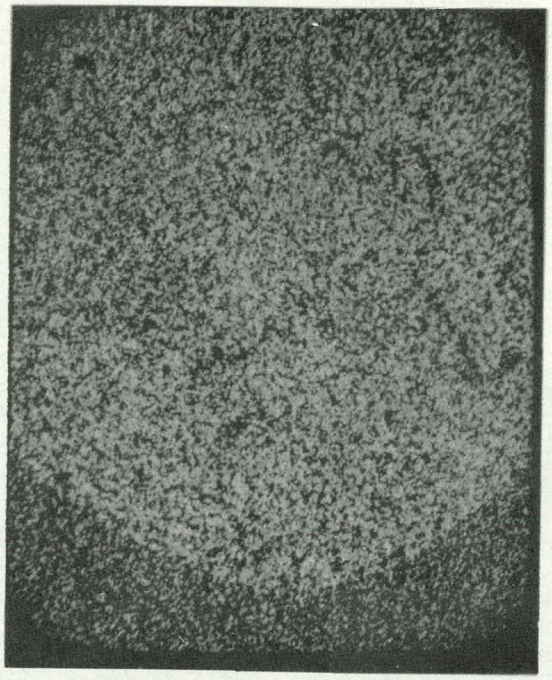

b. Distribution of Calcium in Sulfated 6.6% CaO-αAlumina Pellet. Mag. 40X.

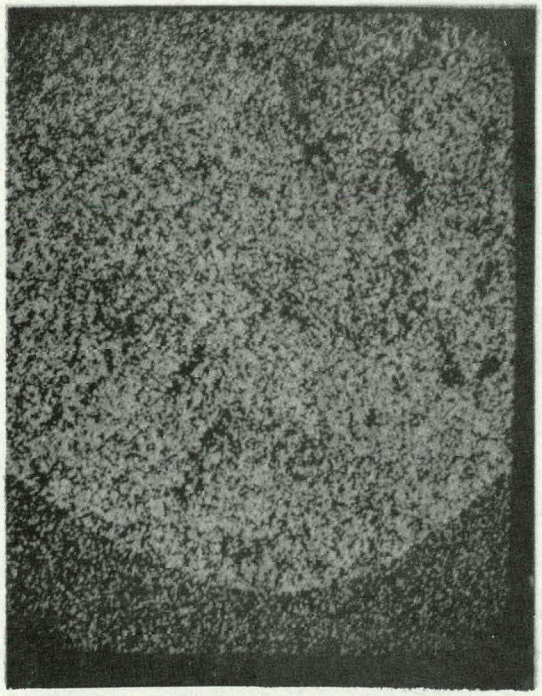

. Distribution of Sulfur in Sulfated 6.6% CaO-αAlumina Pellet. Mag. 40X.

Fig. 19. Sulfated 6.6% CaO-α-Alumina Pellet (Experiment 17)

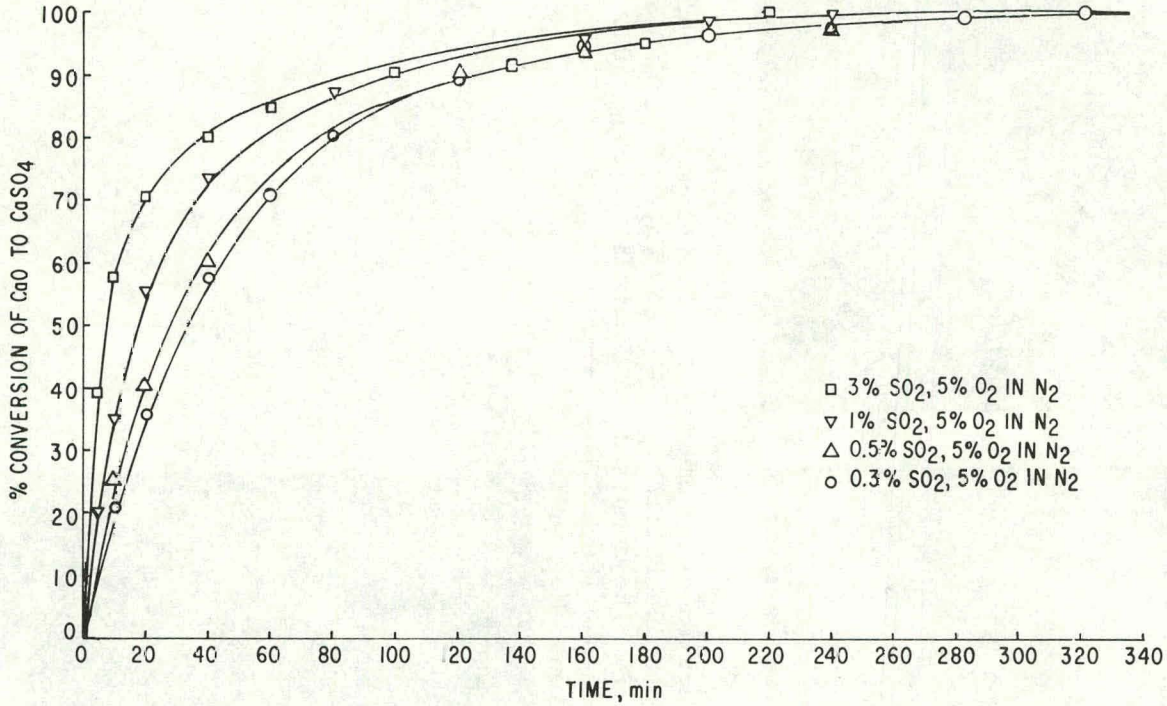

Fig. 20. Sulfation of 6.6% CaO-α-Alumina at 900°C

It should be noted that the reaction was more than 60% completed after about) min, but that it took approximately 4 hr to reach 100% sulfation. This _raph, like the Fig. 17 graph, assumes that 100% sulfation occurred. If it is assumed instead that 6.6% CaO was in each sample, the extent of reaction (on the basis of weight gains) would be 85, 78, 75, and 90% for the reactions using 0.3, 0.5, 1.0, and 3% SO_2, respectively. The sulfated pellets have been submitted for wet chemical analysis so that the extent of reaction can be clarified.

One-Step Regeneration Experiments

The $CaSO_4$-α-alumina pellets used in the regeneration experiments were taken from a batch of 225 pellets that had been sulfated at 900°C, using 3% SO_2, for 22 hr.

Regeneration Operability Experiments. Four experiments were performed using 6% CO at 1100°C and varying the number of pellets and the gas flow rate (i.e., the CO/CaO ratio) to determine if the regeneration reaction was CO-limited. Figure 21 presents these results, which are based on the assumption of complete reduction of $CaSO_4$ to CaO.

In the experiment with the lowest CO/CaO ratio, eleven pellets and a gas flow rate of 400 cc/min were used; in the experiment with the highest CO/CaO ratio, two pellets and 800 cc/min were used. Possibly, the reaction of eleven pellets with a 400 cc/min flow rate was CO-limited. However, in the other three experiments the CO/CaO ratio was sufficiently high and the reaction was not CO-limited. In fact, the reaction rates with two and five pellets at 800 cc/min were somewhat lower than the rate using five pellets at 400 cc/min. This difference is within experimental error for this rate of reaction.

Effect of CO Concentration on Regeneration of Sulfated Pellets. To determine the effect of CO concentration on regeneration, the $CaSO_4$-α-alumina pellets were reduced at 1100°C, using various CO concentrations in N_2. The results are given in Fig. 22, which shows the percentage conversion of $CaSO_4$ back to CaO as a function of time. In plotting the data, the assumption was made that at the end of the experiment, the $CaSO_4$ was completely reduced to CaO. This seems reasonable on the basis of the theoretical and experimental weight losses since if it is assumed that the CaO in the pellets was completely sulfated to $CaSO_4$, the percent conversions of $CaSO_4$ back to CaO during reduction would be 102, 102, 101, and 108% for experiments using 6, 3, 1, and 0.5% CO, respectively. The reaction was almost first order in CO concentration. The rate of regeneration was fast compared with that of sulfation, only 4-5 min being required to reduce the pellets with 6% CO.

X-ray diffraction results on the product indicate that only $CaO \cdot 2Al_2O_3$ and $CaO \cdot Al_2O_3$ were present. Quantitative analysis and SEM results will be used to verify that $CaSO_4$ is reduced to CaO and that CaS is absent. In all experiments, five pellets and a gas flow rate of 800 cc/min were used, and thus the reaction rate should not be CO-limited. To verify this, the experiment using 3% CO was repeated using only two pellets at 800 cc/min, and the same rate of reaction was obtained as in the experiment with five pellets.

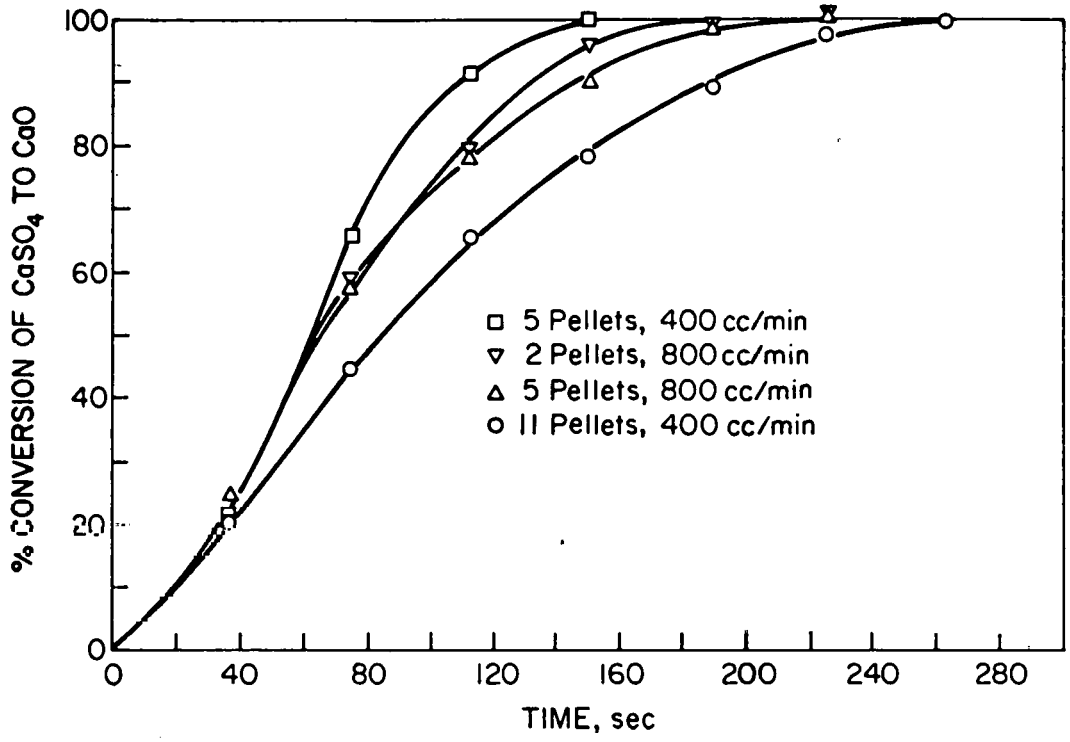

Fig. 21. Reduction of Sulfated Pellets with 6% CO at 1100°C

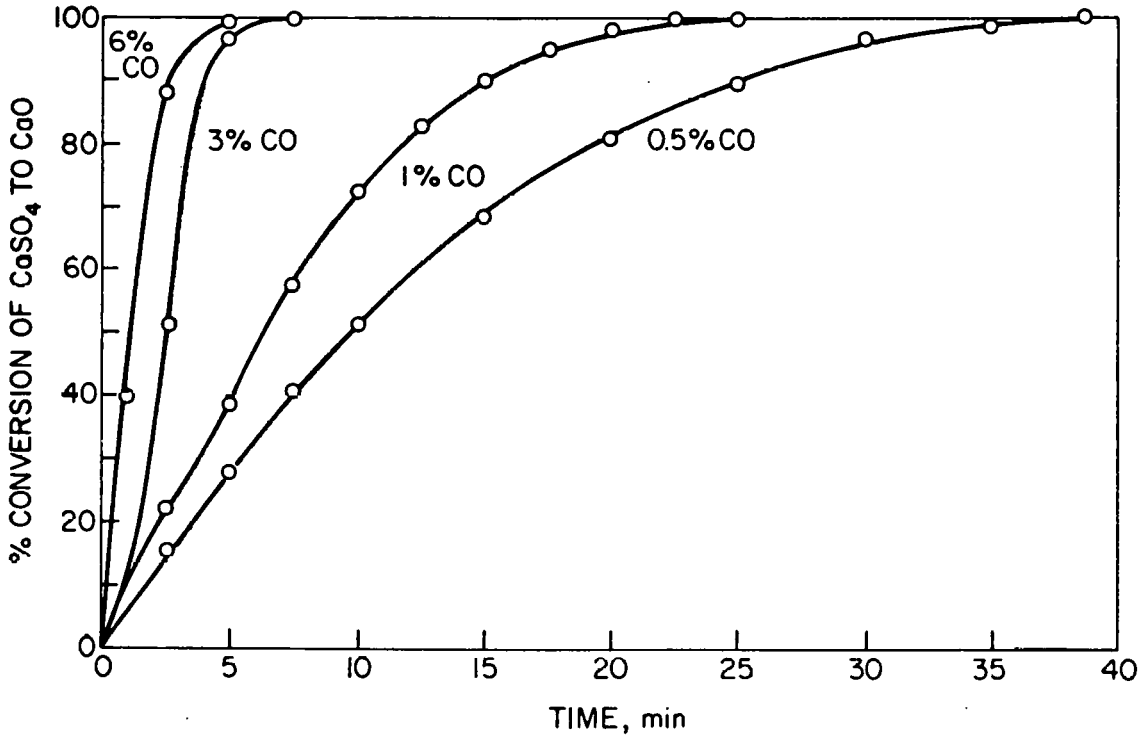

Fig. 22. Reduction of Sulfated Pellets with CO at 1100°C

Fluidization of Pellets

Preliminary fluidization experiments with air were performed to determine the integrity of the pellets. When α-alumina pellets containing no CaO were fluidized, they showed no decrepitation. Other pellets containing 6% CaO were fluidized for approximately 7 hr at 900°C and were then submitted for wet chemical analysis for calcium and for SEM analysis. SEM results showed uniform distribution of calcium throughout the pellets after fluidization, with no observable loss of calcium at the surface.

SULFUR EMISSION CONTROL CHEMISTRY*

Study of the fundamental aspects of the chemical reactions involved in the use of limestones or other reagents to control sulfur emissions from fluidized-bed combustors provides information that can be used to optimize the performance of the environmental control-related portions of these power-producing systems. This section describes activities carried out to gain insight into basic chemical and structural properties of reagent materials that may affect their reactivity, regenerability, and physical properties.

The sorbent reagent that has received principal emphasis in this program is dolomite in the half-calcined form, which is prepared as indicated by Eq. 1:

$$[CaCO_3.MgCO_3] \rightarrow [CaCO_3 \cdot MgO] + CO_2 \quad (1)$$

The half-calcined dolomite reacts with SO_2 as indicated by Eq. 2

$$[CaCO_3 \cdot MgO] + SO_2 + 0.5\ O_2 \rightarrow [CaSO_4 \cdot MgO] + CO_2 \quad (2)$$

For obvious economic and environmental reasons, it is desirable to regenerate the reactive sorbent material from the product. Two such regeneration schemes that are of greatest interest at this time are indicated by Eq. 3, 4, and 5.

$$[CaSO_4 \cdot MgO] + 4H_2 \rightarrow [CaS \cdot MgO] + 4H_2O \quad (3a)$$

$$[CaSO_4 \cdot MgO] + 4CO \rightarrow [CaS \cdot MgO] + 4CO_2 \quad (3b)$$

$$[CaS \cdot MgO] + H_2O + CO_2 \rightarrow [CaCO_3 \cdot MgO] + H_2S \quad (4)$$

$$[CaSO_4 \cdot MgO] + H_2 \rightarrow [CaO \cdot MgO] + SO_2 \quad (5)$$

Eq. 3 and 4 represent a two-step regeneration scheme that can be performed at lower temperatures than the one-step, higher temperature process represented by Eq. 5. However, other regeneration schemes may be feasible. For example, preliminary results are presented on another scheme, represented by Eq. 6:

$$3[CaSO_4 \cdot MgO] + [CaS \cdot MgO] \rightarrow 4[CaO \cdot MgO] + SO_2 \quad (6)$$

An important goal in any regeneration scheme is to obtain an off-gas that contains H_2S (or SO_2) at a sufficiently high concentration to permit economic sulfur recovery in a Claus plant.

Reactions, such as those described by Eq. 1 through 6, serve to define the scope of sulfur emission control chemistry relevant to this work. The goal of the program is to develop an understanding of this chemistry. Specifically, chemical reaction rates, extents of reactions, structural changes that take place in the solid reagents during these reactions, and the effect that these factors have on relevant chemistry are the types of information sought.

* The work reported in this section is supported in part by the U.S. Energy Research and Development Administration Division of Physical Research.

It is also considered desirable to develop a mechanistic model that is consistent with experimental results and can be used to predict the behavior of dolomite and other reagents under various reaction conditions. Finally, it is believed that synthetic reagents will provide a valuable means of testing reaction theories and may also serve as alternative sorbent materials.

Emphasis has been placed on the examination of those factors that will ultimately have a bearing on the rates of reaction and on limitations of yield. A review of the extensive literature on the effects of stone type, particle and pore sizes, reacting gas pressures and temperatures, and chemical reaction rates indicates that a more detailed knowledge of the structural and morphological characteristics of the sorbent is required. To that end, a basic study has been initiated which it is hoped will lead to a clearer picture of the various structural and morphological changes associated with sulfation and regeneration. Such an approach should improve our understanding of the reaction mechanisms and supply detailed information for refined mathematical modeling.

Experimental

The primary experimental tool for our work is the thermogravimetric apparatus (TGA) used for the kinetic studies. This equipment allows us to introduce reaction gases and to monitor weight changes at known temperatures. However, we recognize that multiple chemical processes and changing morphology are going on within our sorbent; accordingly optical microscopy, probe techniques, and X-ray diffraction methods are used in conjunction with the TGA experiments.

TGA Experimental Techniques. The thermogravimetric unit used for most of the experiments reported herein has been described previously.[4] In that system, the reactant gas mixture is prepared by controlling the flow of each constituent by means of a diaphragm-type regulator and calibrated rotameters. Total flow was controlled in the range from 300 to 400 cm^3/min. The water content of the reactant gas was controlled by a thermostated humidifier, with sulfur dioxide added to the stream after humidification. The sample, contained in a platinum basket, was suspended from one arm of an Ainsworth Model RVA balance, which provides continuous weight data over the range from 0.2 to 1.0 g with an accuracy of ±0.1 mg; it is protected from corrosive gases by a purge flow of helium. Temperature in the reaction zone up to about 950°C, controlled by a Marshall furnace with an accuracy of ±5°C, is recorded along with sample weight on a recorder. The apparatus was fabricated from quartz and type 304 stainless steel.

Improvements in the TGA Apparatus. Considerable emphasis has been placed on improving the accuracy and reproducibility of TGA experiments. Figure 23 is a schematic diagram of the apparatus which includes the modifications being introduced to accomplish this goal. Prepared mixtures containing the low concentrations of reactant gases replace the approach of blending the reactant gas stream from the pure constituents by the use of rotameters. In addition, an improved procedure for the introduction of H_2O vapor into reactive gas streams is being adopted. Instead of water introduction by the thermostated humidifier technique, water is pumped into the system at a constant rate, then evaporated and finally mixed

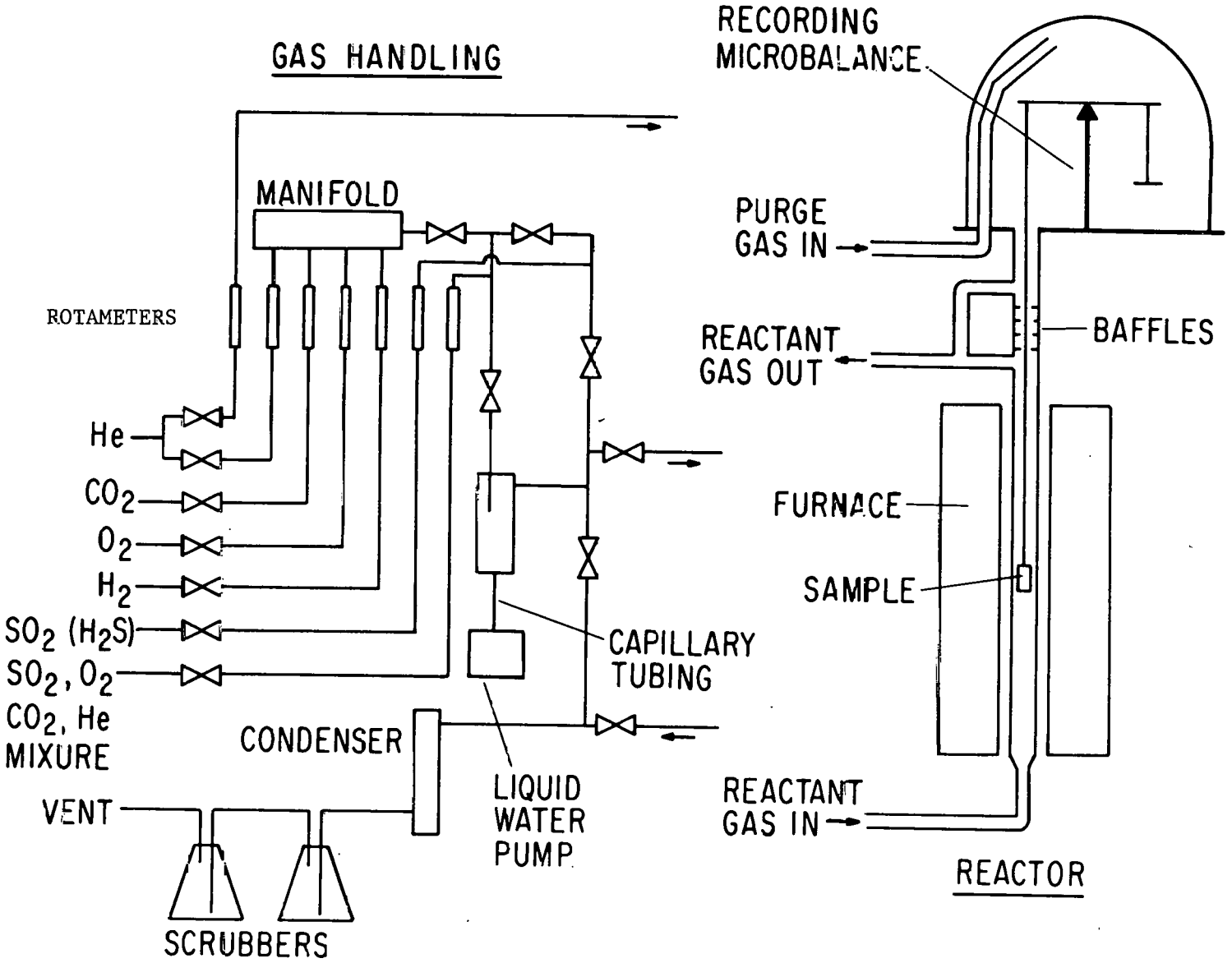

Fig. 23. Schematic Diagram of the Modified Apparatus for Kinetic Studies

with the remaining components of the reactive gas mixture before being carried to the reaction tube. These changes in the apparatus should lead to improvement in the accuracy and reproducibility of the TGA data and will be completed in the near future.

Methods for Structural and Morphological Analysis. Techniques employed in these investigations to obtain structural information center on the use of aliquots of reagent stones removed at various stages of the reaction of interest. Room-temperature X-ray powder diffraction patterns of a random selection of stones from such an aliquot provide information on the chemical phases present at that stage of reaction, as well as details of crystallite size, preferred orientation, disordering, etc. Optical microscopic investigation of random stones from an aliquot provides information on chemical phases present, crystal sizes, distribution of phases within a stone, and general morphological features. Electron microprobe studies are made on random stones from aliquots to determine the presence of Ca, Mg, and S as a function of position within a cross section of the stone. The various techniques serve to complement each other and provide an excellent overall picture of the structural changes that take place during the course of reactions under study.

Mathematical Modeling of Kinetic Data

This section presents the results of efforts to develop a mathematical model that will describe the kinetic data available. Since the sulfation reaction, Eq. 2, has been studied the most extensively, these modeling efforts have been directed toward this reaction. A description of assumptions, development of the model, and testing of the model follows. The results presented suggest that limited success has been achieved in these initial efforts on the modeling aspect of the overall program.

A particle of half-calcined dolomite is known to be quite porous and to comprise a mixture of small crystallites of $CaCO_3$ and MgO. It is assumed in developing this model that macropore diffusion in the particle can be neglected, *i.e.*, that the concentration of gaseous reactants at the surface of the $CaCO_3$ crystallites is the same as that in the reactant-gas stream. Further, it is assumed that the $CaCO_3$ crystallites are platelets (see Fig. 24) and that the reacting gases diffuse through a product layer of $CaSO_4$ to a moving reaction interface. The diffusion rate is assumed to be high compared with the movement of the reacting interface so that steady-state diffusion conditions exist within the product layer, with SO_2 diffusion being the rate-limiting process. The intrinsic reaction rate, r_1, for sulfation (Eq. 2) is given by

$$r_1 = k_1 \left(C_{O_2}\right)^m \left(C^*_{SO_2}\right) \tag{7}$$

where it is assumed that the reaction is first order with respect to the sulfur dioxide concentration.[4]

By using Eq. 7, and the steady-state assumption mentioned above, and by imposing suitable boundary conditions, we can represent the concentration of sulfur dioxide at the reaction interface, $C^*_{SO_2}$, as follows:

$$C^*_{SO_2} = \frac{C^\circ_{SO_2}}{1 + \frac{k_1 (C_{O_2})^m}{D_e} (\ell - \ell^*)} \tag{8}$$

where D_e is the effective diffusion coefficient, $C^\circ_{SO_2}$ is the sulfur dioxide concentration in the reactant-gas stream, and ℓ and ℓ^* are characteristic dimensions in the platelet (see Fig. 24). If it is now assumed that the effective diffusion coefficient for SO_2 diffusing through the product layer of calcium sulfate is linearly dependent on the extent of the reaction, *i.e.*, $D_e = \xi^* D^\circ_e$ with $\xi^* \equiv \ell^*/\ell$, Eq. 8 can be rewritten as

$$C^*_{SO_2} = \frac{C^\circ_{SO_2}}{1 + \left(\frac{\ell k_1 (C_{O_2})^m}{D^\circ_e}\right)\left(\frac{(1-\xi^*)}{\xi^*}\right)} \tag{9}$$

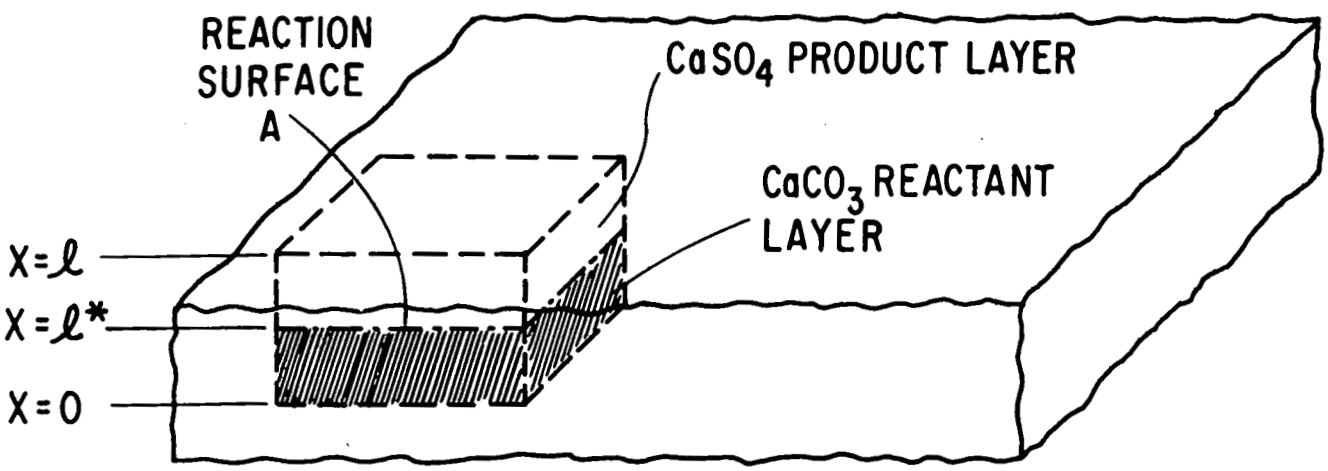

Fig. 24. Schematic of a $CaCO_3$ Crystallite, Assumed to be of Rectangular Platelet Geometry, Found in Half-Calcined Dolomite Stone.

The material balance for the reaction can be written as

$$\frac{d}{dt}\left[A\ell^* C_{CaCO_3}\right] = -Ak_1 \left[C_{O_2}\right]^m \left[C^*_{SO_2}\right] \tag{10}$$

where C_{CaCO_3} is the calcium carbonate concentration in the crystallite. Substituting Eq. 9 into Eq. 10 and rearranging terms gives

$$\frac{d\,\xi^*}{dt} = -\left\{\frac{k_1 \left[C_{O_2}\right]^m \left[C^\circ_{SO_2}\right]}{\ell C_{CaCO_3}}\right\} \left\{\frac{1}{1+\left[\frac{\ell k_1 \left(C_{O_2}\right)^m}{D^\circ_e}\right]\left[\frac{1-\xi^*}{\xi^*}\right]}\right\} \tag{11}$$

which can now be integrated to give

$$\frac{-\ln(1-\Psi)}{\Psi} = \frac{1}{\tau_D}\left(\frac{t}{\Psi}\right) - \left(\frac{\tau_R}{\tau_D} - 1\right) \tag{12}$$

where $\Psi \equiv 1 - \xi^*$, t is the time, and physical constants associated with characteristic times for the reaction and diffusion have been collected so that

$$\frac{1}{\tau_R} = \frac{k_1 \left[C_{O_2}\right]^m \left[C^\circ_{SO_2}\right]}{\ell\, C_{CaCO_3}} \tag{13}$$

$$\frac{1}{\tau_D} = \frac{D^\circ_e \left[C^\circ_{SO_2}\right]}{\ell^2\, C_{CaCO_3}} \tag{14}$$

The success of the model can be tested by ascertaining whether linear plots of $-\ln(1 - \Psi)/\Psi$ versus t/Ψ are obtained for the experimental data. This has been done for the sulfation reaction data previously reported,[4] and Figs. 25 and 26 show that the model does indeed fit the data. In addition, Fig. 27 shows that the model also provides a reasonable fit for preliminary data obtained for the carbonation reaction (Eq. 4), which is discussed more fully below. Equation 14 suggests a method whereby the order of the reaction with respect to SO_2 concentration may be calculated via the model; that is, the slope of a plot of $\ln(1/\tau_D)$ versus $\ln C^\circ_{SO_2}$ is equal to the order of the reaction with respect to SO_2 concentration:

$$\ln(1/\tau_D) = \ln C^\circ_{SO_2} + \ln D^\circ_e/\ell^2 C_{CaCO_3} \tag{15}$$

Figure 28 shows the results of such a calculation. For the sulfation reaction data with H_2O present in the simulated flue gas, the slope is 0.99; for the sulfation reaction data without H_2O vapor, the slope is 0.85. The previously reported values[1] for this parameter, which were obtained from an analysis based on the initial reaction-rate model, are 1.08 for the sulfation reaction with H_2O vapor present and 0.77 for the sulfation

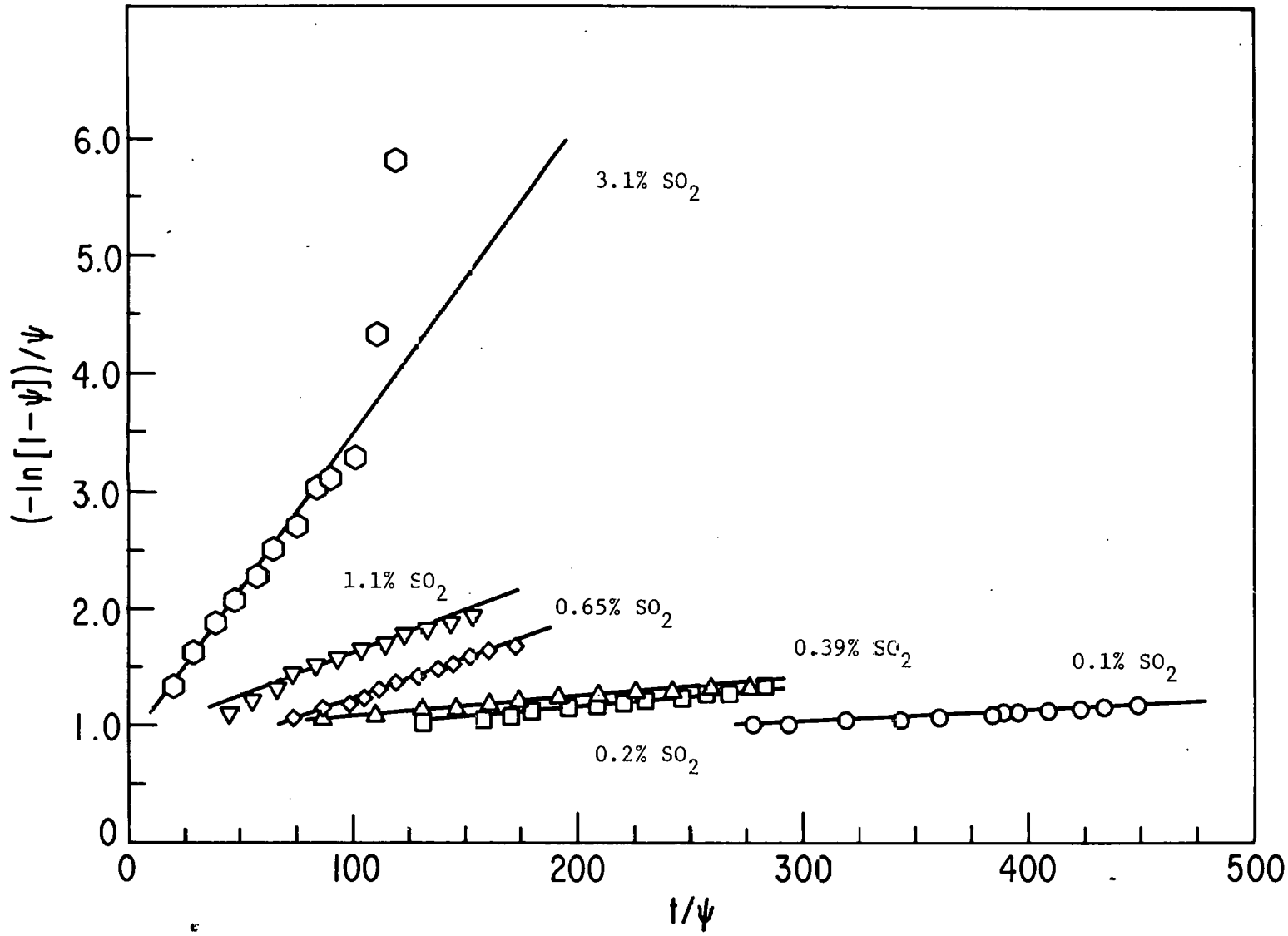

Fig. 25. Plots of $(-\ln[1 - \Psi])/\Psi$ vs t/Ψ Employing Kinetic data for Sulfation Reaction with H_2O Vapor Present in Reaction Gas Stream. Reaction Conditions: Temperature: 750°C; CO_2: 15%; O_2: 5%; SO_2: listed; H_2O: 2.9%; N_2: balance

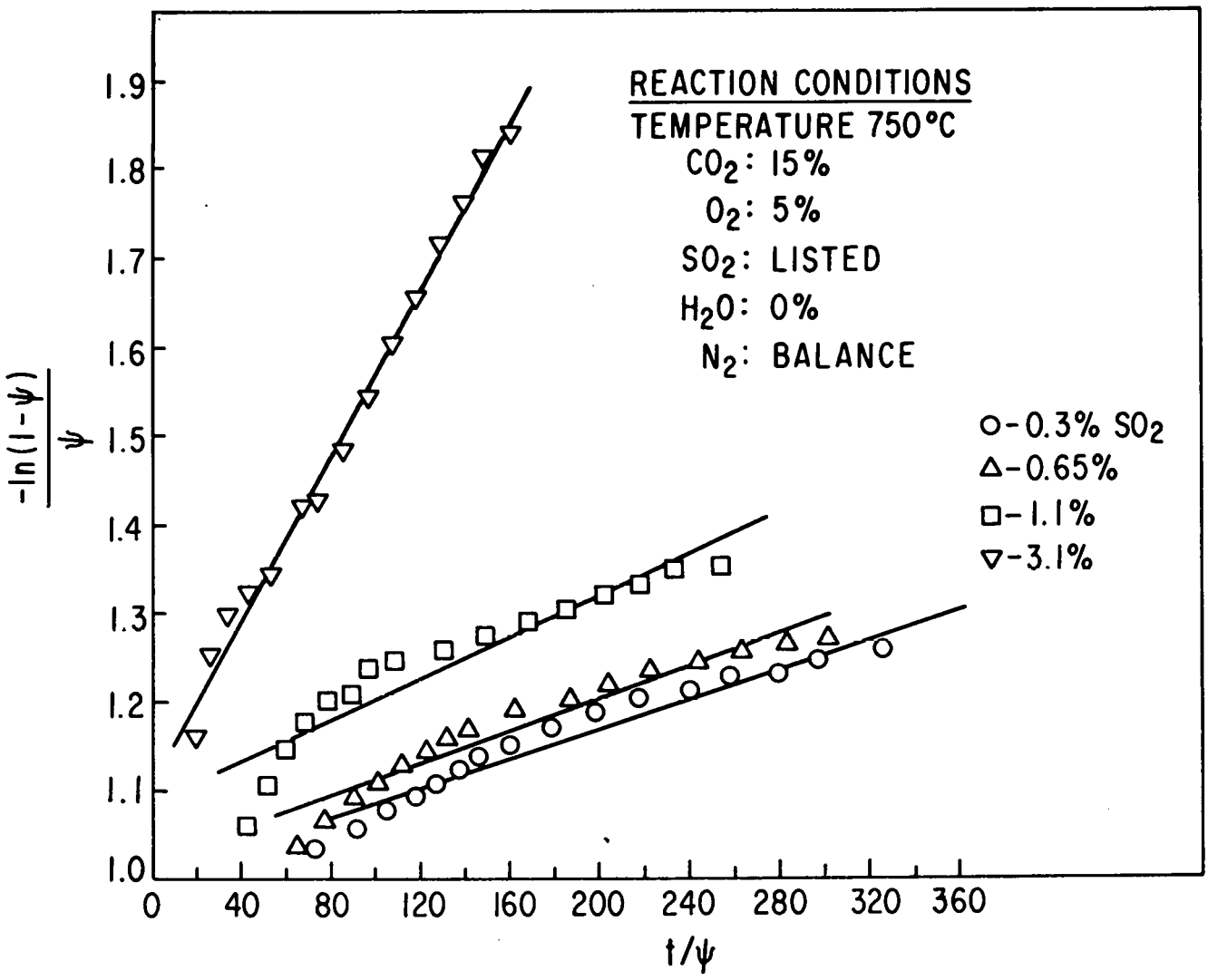

Fig. 26. $-\ln(1-\psi)/\psi$ vs t/ψ Plots, Employing Kinetic Data for Sulfation Reaction without H_2O Vapor Present in Reactive Gas Stream

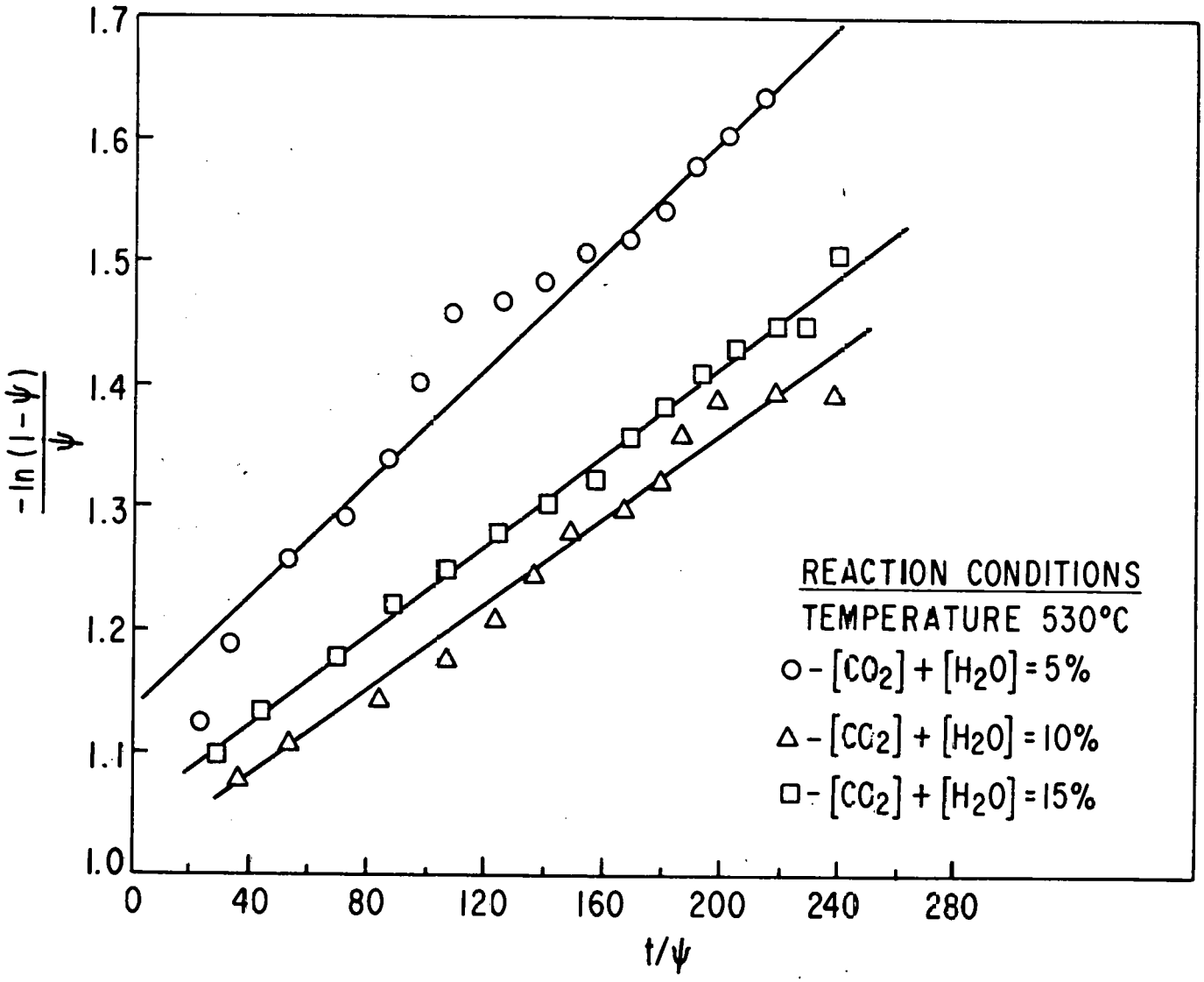

Fig. 27. Plot of $-\ln(1-\Psi)/\Psi$ vs. t/Ψ, Employing Kinetic Data Obtained for Carbonation Reaction

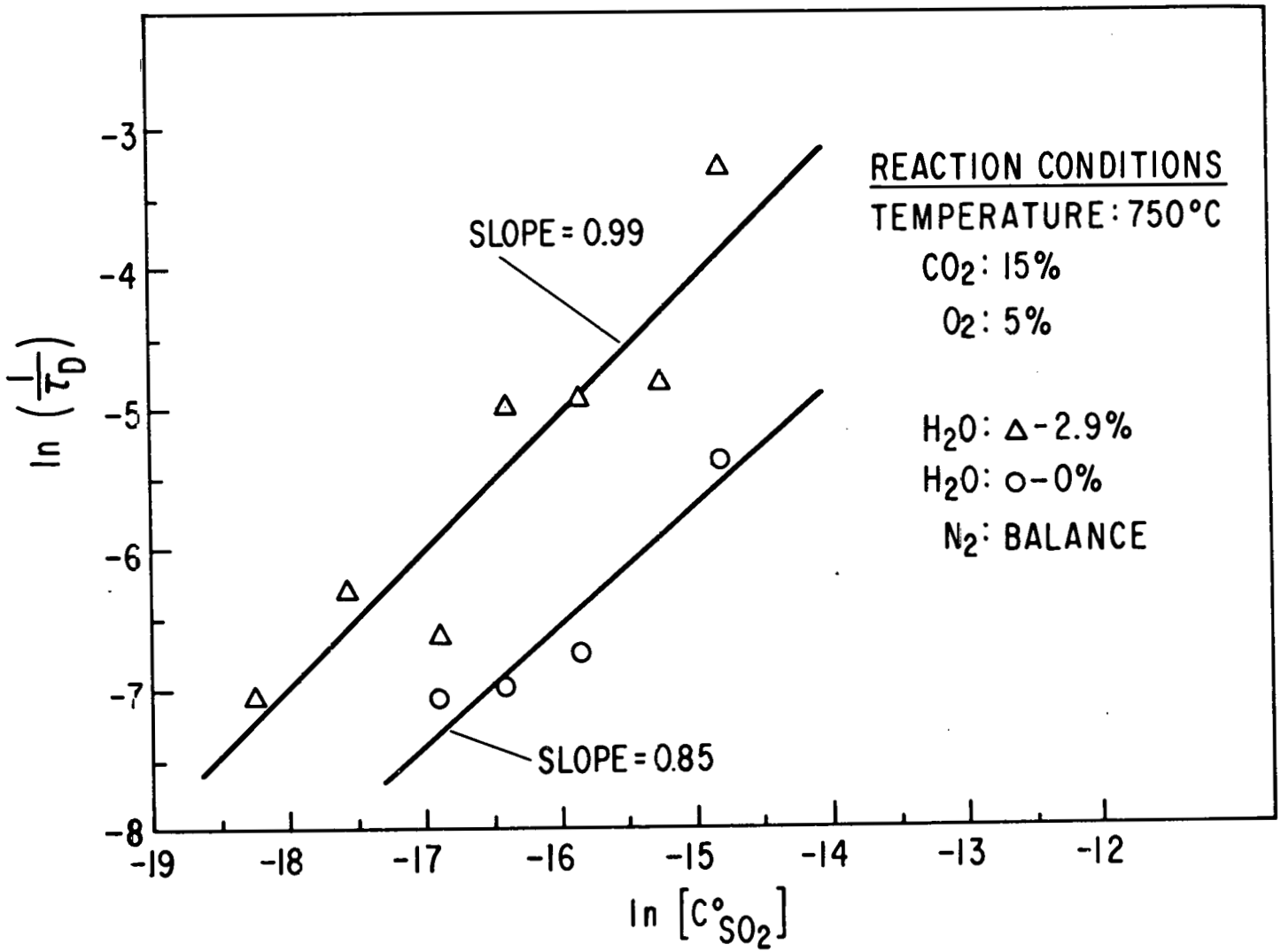

Fig. 28. $\ln(1/\tau_D)$ vs. $\ln[C^\circ_{SO_2}]$, Employing Kinetic Data For Sulfation Reaction

reaction data with no H_2O vapor present in the simulated flue gas. The agreement of the results obtained with the two models is surprisingly good, especially in light of the fact that the mathematical model calculation of this parameter is based on kinetic data over the entire reaction time period.

Values of the model parameters of interest, τ_D and τ_R, can be obtained from the slopes and intercepts of plots of Eq. 12. Table 4 summarizes the results of such calculation, obtained by analyzing the kinetic data for the sulfation reaction. From this table it is obvious that neither the τ_D nor τ_R parameter is a constant from experiment to experiment, but varies with the SO_2 and H_2O concentrations. Equations 13 and 14 suggest that these model parameters should be a function of SO_2 concentration only, since C_{O_2} is the same for each experiment reported in Table 4. The last two columns in Table 4 contain the values obtained when the values for τ_D and τ_R are multiplied by the $C^{\circ}_{SO_2}$ values; according to Eq. 13 and 14, the values in the last two columns should be constant from experiment to experiment. However, an order of magnitude spread is found in the values, suggesting that the simple SO_2 concentration dependence implied by Eq. 13 and 14 does not exist. The results shown in Fig. 28 suggest a log-log SO_2 concentration dependence of the model parameters.

Due to the formulation of the model, it is not possible to compute values of k_1 and D°_e separately, but instead only the ratio $D^{\circ}_e/\ell k_1$ may be obtained from values of the intercept of plots of Eq. 12, *i.e.*,

$$\tau_R/\tau_D = D^{\circ}_e/\ell k_1 [C_{O_2}]^m \tag{16}$$

where the quantity $(C_{O_2})^m$ is the same for each experiment. The value for C_{O_2} is given in Table 4. Computed τ_R/τ_D ratios are also given in this table,[2] where it is seen that, if more than one significant figure is considered, the τ_R/τ_D values are not constant from experiment to experiment.

In the development of the model, the effect of H_2O concentration on the reaction rate observed experimentally[4] was ignored by assuming

$$\text{rate} = k_1 [C^{*}_{SO_2}] \; [C_{O_2}]^m \tag{7}$$

where $C^{*}_{SO_2}$ is the SO_2 concentration at the reaction interface. However, it should be possible to separate the effect of H_2O concentration on the reaction rate by the following analysis. In Eq. 7, it is implied that the C_{H_2O} effect is included in the rate constant k_1, *i.e.*,

$$k_1 = k_s (C_{H_2O})^n \tag{17}$$

where k_s is the "true" intrinsic rate constant, C_{H_2O} is the gas-phase concentration of H_2O, and n is the order of the reaction with respect to water concentration. Equation 17 suggests that for reactions with H_2O vapor present in the simulated flue gas, Eq. 13 should be modified as follows:

Table 4. Summary of the Values Obtained for the Model Parameters, τ_D and τ_R

SO_2, %	$C^{\circ}_{SO_2}$, mole/cc	$C^{\circ}_{H_2O}$, mole/cc	C_{O_2}, mole/cc	τ_R/τ_D	τ_D	τ_R	$\tau_D[C^{\circ}_{SO_2}]$	$\tau_R[C^{\circ}_{SO_2}]$
0.1	1.19×10^{-8}	3.47×10^{-7}	5.95×10^{-7}	1.77	1170	2070	1.39×10^{-5}	2.46×10^{-5}
0.2	2.38×10^{-8}	3.47×10^{-7}	5.95×10^{-7}	1.80	562	1010	1.34×10^{-5}	2.40×10^{-5}
0.39	4.64×10^{-8}	3.47×10^{-7}	5.95×10^{-7}	1.95	746	1460	3.46×10^{-5}	6.77×10^{-5}
0.39	4.64×10^{-8}	0	5.95×10^{-7}	2.00	1190	2380	5.52×10^{-5}	1.10×10^{-4}
0.65	7.74×10^{-8}	3.47×10^{-7}	5.95×10^{-7}	1.55	148	229	1.14×10^{-5}	1.77×10^{-5}
0.65	7.74×10^{-8}	0	5.95×10^{-7}	2.02	1080	2180	8.36×10^{-5}	1.69×10^{-4}
1.1	1.31×10^{-7}	3.47×10^{-7}	5.95×10^{-7}	1.86	136	253	1.78×10^{-5}	3.31×10^{-5}
1.1	1.31×10^{-7}	0	5.95×10^{-7}	2.08	842	1750	1.10×10^{-4}	2.29×10^{-4}
3.1	3.69×10^{-7}	3.47×10^{-7}	5.95×10^{-7}	1.26	27	34	9.96×10^{-6}	1.26×10^{-5}
3.1	3.69×10^{-7}	0	5.95×10^{-7}	2.10	215	452	7.93×10^{-5}	1.79×10^{-4}

$$(1/\tau_R)_{C_{H_2O}\neq 0} = k_s (C_{H_2O})^n (C_{O_2})^m (C^{\circ}_{SO_2})/\ell (C_{CaCO_3}) \quad (18)$$

which suggests

$$(\tau_R)_{C_{H_2O}=0} / (\tau_R)_{C_{H_2O}\neq 0} = (C_{H_2O})^n \quad (19)$$

Table 5 summarizes the results of the calculations of such an analysis for the kinetic data in Table 4. The results show that the $(C_{H_2O})^n$ values are not constant from experiment to experiment. However, the values of n, found in the last column, are in fairly good agreement with the experimentally determined value of n, which is zero.[4]

The parameters included in a model should possess certain qualities. Because the parameters are ratios of physical constants of the system under investigation, the values of these parameters should be a constant and should not vary from experiment to experiment in an unexplainable fashion. Moreover, such parameters should provide information that can be interpreted physically. From the above analysis, it is difficult to draw conclusions that support the merit of the model. The results do not completely discredit the model, but strongly suggest that it is not complete as presently formulated. The situation of not clearly supporting or discrediting the model may change when more kinetic data become available for analysis and when further structural data are obtained.

Table 5. Summary of Data on Effect of Water Concentration on Reaction Rate

C_{SO_2}, %	C_{H_2O}, mole/cc	τ_R	$\frac{(\tau_R)_{C_{H_2O}=0}}{(\tau_R)_{C_{H_2O}\neq 0}} = (C_{H_2O})^n$	n
0.39	3.47×10^{-7}	1460		
0.39	0	2370	1.623	-0.03
0.65	3.47×10^{-7}	229		
0.65	0	2180	8.65	-0.14
1.1	3.47×10^{-7}	252		
1.1	0	1754	6.96	-0.13
3.1	3.47×10^{-7}	250		
3.1	0	453	1.81	-0.04

It must be emphasized that the limited success of this model does not mean that it is an accurate description of the physical processes actually taking place in these reactions. It is, in fact, very difficult to rationalize, on the basis of some physical phenomena, the dependence of the effective diffusion coefficient on the degree of reaction. Nevertheless, the model does provide a mathematical description for the reaction under a variety of conditions and can serve as a point of departure for the development of a more satisfactory model by suggesting further experiments. The extent to which this process has already begun is pointed out in later sections where kinetic results not explained by this early model are presented. In addition, structural results are presented which indicate that the assumptions of the model are not correct. These structural results suggest a more realistic model.

Sulfation Reaction of Half-Calcined Dolomite

Initial TGA Experiments. The initial results obtained for the sulfation reaction (Eq. 2) were presented in an earlier report,[4] but are summarized again here for completeness. They indicate that the reaction is first order with respect to SO_2 concentration when H_2O vapor is present in the reactive-gas stream, and that the rate varies with the three-fourths power of SO_2 concentration when H_2O vapor is not present. Thus, it appears that the rate-determining step is different, depending on whether or not water is present in the reactive gas. With water present, the reaction is 0.22 order with respect to oxygen concentration in the reactive-gas stream. An apparent activation energy of 7.3 kcal/mol was found; such a value does not point conclusively to a mechanism in which a chemical reaction is rate controlling, but is somewhat greater than one might expect if the reaction were diffusion controlled.

A number of other studies have now been performed on the sulfation reaction, Eq. 2, employing type 1337 dolomite. These experiments are described below and have been performed (1) to test the simple mathematical model described above, and (2) to initiate a study of the structural changes in the solid reagent that are associated with this reaction.

TGA Kinetic Experiments to Test Mathematical Model. The experimental procedure employed is the same as that used in the earlier study,[4] that is, with the TGA apparatus before it was modified to the form shown in Fig. 23. The studies completed include the following: (a) experiments at low SO_2 concentrations in the reactant gas mixture (0.39% and 0.65% SO_2) to determine whether the $CaCO_3$ available in half-calcined dolomite stones can be completely converted to $CaSO_4$ at low SO_2 concentrations, (b) experiments in which the SO_2 concentration in the reactant-gas mixture was stepped up from an initially low value (0.39% or 0.65%) to a high value of (3.1%) at a later stage of the sulfation reaction, and (c) an experiment to test the effect on the reaction rate that might be caused by crushing the stone after it had been partially sulfated. The results of these investigations are shown in Fig. 29. For comparison, results obtained earlier[4] for 3.1% SO_2 are also included.

From curves c and d in Fig. 29, it is evident that, at the low SO_2 concentrations of 0.39% and 0.65%, the conversion of $CaCO_3$ in the dolomite stone to $CaSO_4$ stops after a finite reaction time and that conversion is less than complete. The data obtained in the earlier work, shown as curve a,

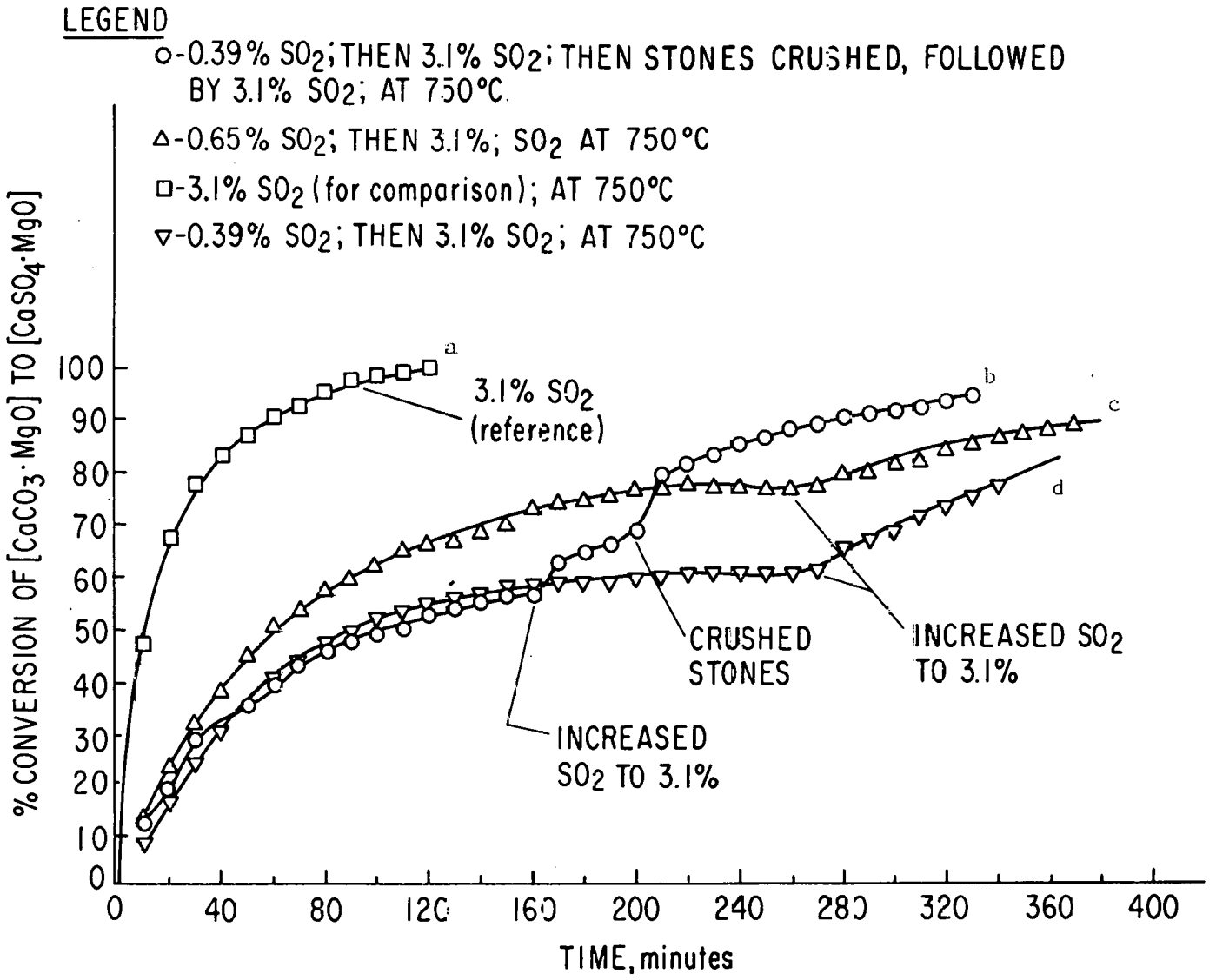

Fig. 29. Plots of % Conversion *vs* Time for the Sulfation Reaction of Half-Calcined 1337 Dolomite Under the Reaction Conditions Described in the Legend

indicate that with 3.1% SO_2 in the reacting-gas mixture, essentially complete conversion can be obtained. These preliminary results suggest that the extent of conversion of $CaCO_3$ to $CaSO_4$ might be a function of the SO_2 concentration in the reactant-gas mixture. It should be noted that in the kinetic model described above, the assumption is made that complete conversion of $CaCO_3$ in the half-calcined dolomite stones will always occur.

It could be suggested that the incomplete conversion of the $CaCO_3$ in the half-calcined dolomite stones at low SO_2 concentrations might possibly involve some process whereby a structural change in the $CaSO_4$ product layer occurs that, in effect, blocks diffusion of the SO_2 through the $CaSO_4$ product layer. This possible simple explanation led to the step experiments (curves c and d). If by some process, SO_2 diffusion is indeed blocked, then one would expect that once the reaction has stopped at some fractional conversion value, it would not proceed even if the SO_2 concentration is increased. Curves c and d in Fig. 29 show that reaction does indeed start again upon increasing the SO_2 concentration. However, the reaction rate after the SO_2 concentration was increased to 3.1% was much lower than that observed when fresh half-calcined dolomite stones were sulfated with a 3.1% SO_2 gas mixture from the beginning to the end of the reaction (see curve a). The mathematical model in its present simple form is incapable of explaining these experimental results.

From curve b, it is evident that after the half-calcined, partially sulfated stones were crushed, the reaction rate was higher than before crushing. This effect is probably due to exposure of new $CaCO_3$ surfaces as a result of crushing.

Structural and Morphological Studies of Sulfation. Crystal-chemical considerations based on X-ray diffraction and optical microscopy studies have given new insight into the structural and morphological details associated with sulfation and regeneration. The following discussion is related to observations made on stones that have undergone the sulfation reaction.

Figure 30 shows the course of a sulfation reaction experiment with time under the following conditions. A sample at point A is the half-calcined (at 800°C) starting material. Sample point B represents the sample condition after reacting with 0.39% SO_2 for 70 minutes at 750°C. Sample point C represents the state of the material at 750°C but with no SO_2 in the reactive gas stream. At sample point D, the SO_2 concentration of 0.39% has been restored and maintained for an additional 90 minutes. The SO_2 was omitted for the 168-minute interval between sampling points B and C in order to note any structural or morphological changes (changes in composition or crystallite size) that might occur as a result of sintering during this interval. Aliquots of stones were removed at points A, B, C, and D for X-ray, microscopic, and electron microprobe studies.

X-ray Diffraction Studies. The diffraction pattern of the initial 1337 dolomite shows it to be very crystalline, with a small amount of fine material. (The crystals are readily observed under low magnification with an optical microscope.) The stones are fairly soft, but nevertheless, the dolomite crystals within the stone are fused together in a random (crystallographic) orientation to produce an adherence.

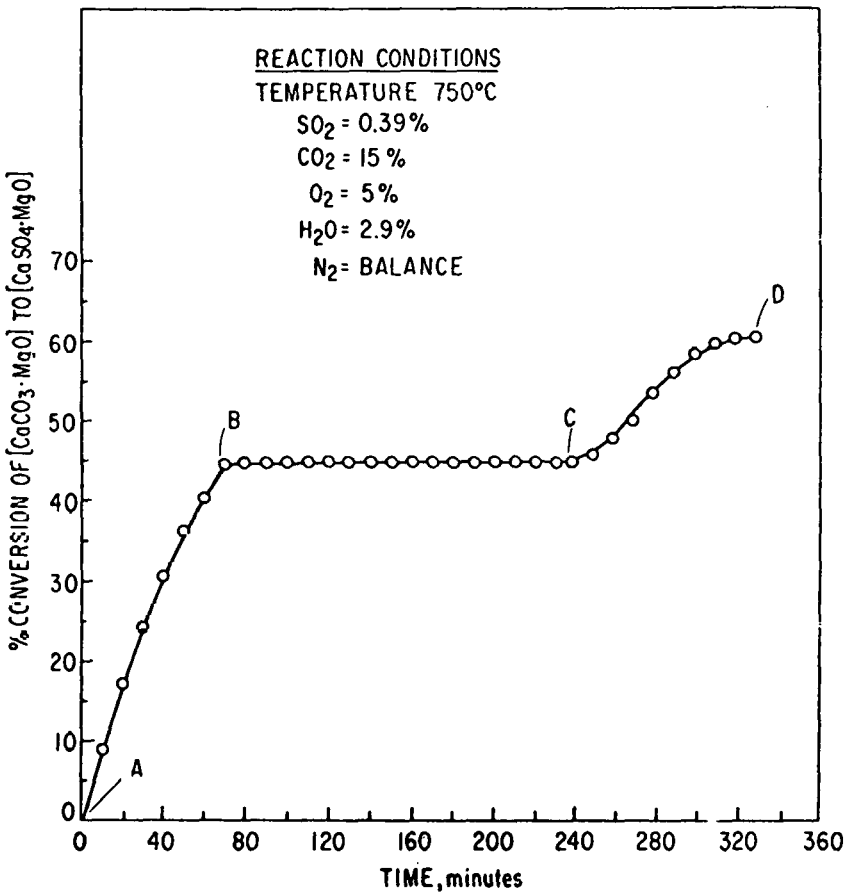

Fig. 30. Course of Sulfation Reaction.

All X-ray diffraction observations have been made at room temperature. The removal of a TGA sample produces a rapid quench, and it is assumed that the quenched sample represents the condition of the material at elevated temperatures. X-ray measurements at elevated temperatures are planned in order to check the validity of this assumption.

In sample A, the X-ray diffraction pattern shows MgO and $CaCO_3$, both exhibiting very small crystallites, but with the $CaCO_3$ probably disordered. The MgO crystallites are of the order of 1000 Å or smaller. The lack of resolution of the CuKα doublet for $CaCO_3$ indicates crystallite sizes of 300-1000 Å, but the rapid drop-off in intensity with angle strongly suggests some disorder or thermal effect. There is a tendency for ordering on the 104 planes (natural cleavage faces) of $CaCO_3$. The ordering is so pronounced that clusters of large "crystals" are produced. Under some half-calcining conditions, the $CaCO_3$ crystals may show more or less tendency for preferred orientation as indicated below in the section on half-calcination. Nevertheless, the characteristics described above may be quite general, for they agree fairly well with studies made by Wilsdorf and Haul[5,6] on transparent single crystals of dolomite.

In sample B, MgO is present, with $CaSO_4$ appearing with the $CaCO_3$. MgO is still present in sample C. The volume of $CaSO_4$ has decreased substantially over the amount observed in sample B. This is a result of the nonuniformity of behavior of individual stones.

In sample D, the results are essentially unchanged from those of sample C.

The $CaSO_4$ seems to be in the same condition (small crystallite size or disorder, or both) as the $CaCO_3$ from which it was derived. In addition, the preferred orientation of the $CaCO_3$ (and the sizes of the associated pseudo crystals) decreases as sulfation progresses. Following sulfation, the stones become harder; under low-power magnification, they seem to exhibit the same characteristic coarse pore structure observed in the dolomite stage.

Microscopy and SEM Studies. Optical examination of the untreated dolomite shows a crystal size range between 30 and 300 microns. Upon half-calcining, it is found that the single crystals of dolomite are replaced by grains -- that is, a crystal seems to convert to a grain of about the same shape, with the grains still held together to produce a coarse pore structure similar to that found in the original dolomite.

MgO cannot be detected with certainty. It would be expected, according to the X-ray results, that aggregates of MgO could be seen but that single crystals of MgO would be below the limit of visibility. Calcite crystals are observed, however, that have a size range of 1-15 microns and an average size of about 3 microns (30,000 Å). Extinction in polarized light of the calcite crystals is always undulatory, indicating strain or disorder. In view of the small sizes of these crystals, it is a question whether stresses would be present. It is quite possible that the origin of these crystals lies in the tendency of small crystallites to align in preferred orientation to simulate a larger "single crystal", as indicated in the X-ray diffraction patterns. The undulatory nature of the extinction would then arise from incomplete and inexact alignment along crystallographic directions.

Oil-immersed calcite grains viewed in transmitted light show narrow rivulets or stringers about 1 micron in width which exhibit high relief when the calcite grain is in a position of zero relief. It is suspected that these stringers are MgO, but their small size precludes a refractive index determination. Additional studies should lead to an understanding of the nature of the MgO distribution, but for the time being, we consider the stringers distributed in the calcite "crystals" to be MgO.

Following sulfation, microscopic examination shows that these calcite crystals are reduced in size, in accordance with the X-ray observations. However, a most interesting morphological change is found optically: the calcite cyrstals do not sulfate uniformly. In Fig. 31a, the drawing depicts an irregularly shaped calcite crystal that exhibits the nonuniform extinction. Upon sulfation, a crystal will be found to exhibit both $CaSO_4$ and $CaCO_3$ crystallites adhering together as shown in Fig. 31b. This condition

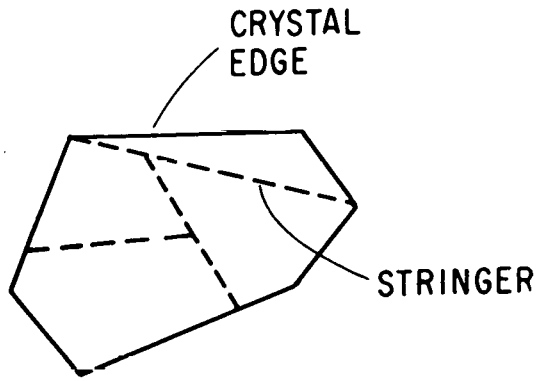

Fig. 31 (a) Appearance of Stringers in a Calcite Crystal Exhibiting Nonuniform Extinction.

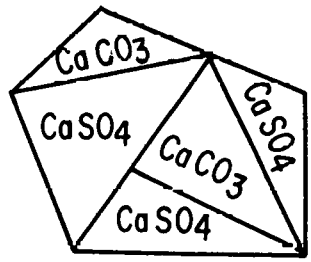

Fig. 31 (b) Distribution of Aggregated $CaCO_3$ and $CaSO_4$ Crystals after Partial Sulfation

is found even on the periphery of stone that is about 50-60% sulfated.

Figure 32 shows a 75X magnification of the edge of a stone removed from point D, Fig. 30. The individual grains are apparent. The band along the periphery, in which the grains are pronounced, constitutes the region of primary sulfation. SEM studies confirm the observation that the peripheries of stones are being sulfated first. Figures 33 and 34 show typical SEM results. These were obtained on a stone taken from point C in Fig. 30, corresponding to about 45% sulfation. Figure 33a shows a Ca scan across the entire stone; Fig. 33b, a S scan across the entire stone; and Fig. 33c outlines five areas on the stone that were analyzed in detail for Ca, Mg, and S. Figure 34 gives the results of the analysis of these five areas. It is apparent that even though Ca and Mg are uniformly distributed across the stone, S, for the most part, is distributed only on its periphery. With this information, we can set up a tentative model for the sulfation process.

Development of Structural Model. In Fig. 35a, the dolomite is represented as composed of macroscopic crystals of $CaMg(CO_3)_2$. The irregular shapes represent individual crystals, and the arrows indicate that the crystallographic directions of the crystals are random. The total aggregate of the crystals constitute the dolomite stone. Voids between the crystals, labelled a, contain some finely divided dolomite crystals, so small as to be a powder. It is assumed that the single crystals of dolomite are held together by some intergrowth of the crystals, or perhaps by some tendency of the powder to grow into the larger crystals. Alternatively, a hydrate could be responsible. After half-calcining, the single crystals become grains, as indicated in Fig. 35b. It is quite possible that the initial voids a are maintained at this stage, for the grains are still held together to maintain a good adherence. Each of these grains is now composed of the $CaCO_3$ + MgO aggregate. We have remarked that X-ray studies indicate that the calcite crystallites aggregate by preferred orientation into large pseudo crystals. As Haul and Wilsdorf[5,6] have observed, a single crystal of dolomite will serve as a base against which the $CaCO_3$ will develop and orient. Hence, as long as single crystals of dolomite are present as shown in Fig. 35a, we would expect each dolomite crystal to serve as a base for developing the oriented calcite crystallites into aggregates. This is consistent with the crystal structures of both dolomite and calcite, as will be described below. A single grain of half-calcined dolomite is shown in Fig. 35c, and this figure represents a speculated view of the make-up of the grain.

In Fig. 35c, individual crystallites of $CaCO_3$ are shown to tend to align along a crystallographic direction. This is a simple view, since the symmetry of $CaCO_3$ allows three equivalent directions. The black shading in the individual $CaCO_3$ crystallite represents MgO, and the black shadings between the aggregated crystallites are also intended to represent MgO, but as isolated material. Regions marked b are new voids, now within the grain (and between crystals of $CaCO_3$), as distinct from voids a which are formed between the grains. Figure 35d shows a view of a "single crystal" of $CaCO_3$ as consisting of an aggregate of crystallites tending to order. As described below, the single crystallite of $CaCO_3$ could show stacking disorder, containing extended sheets of entrapped MgO (the stringers). The entrapped MgO as before is

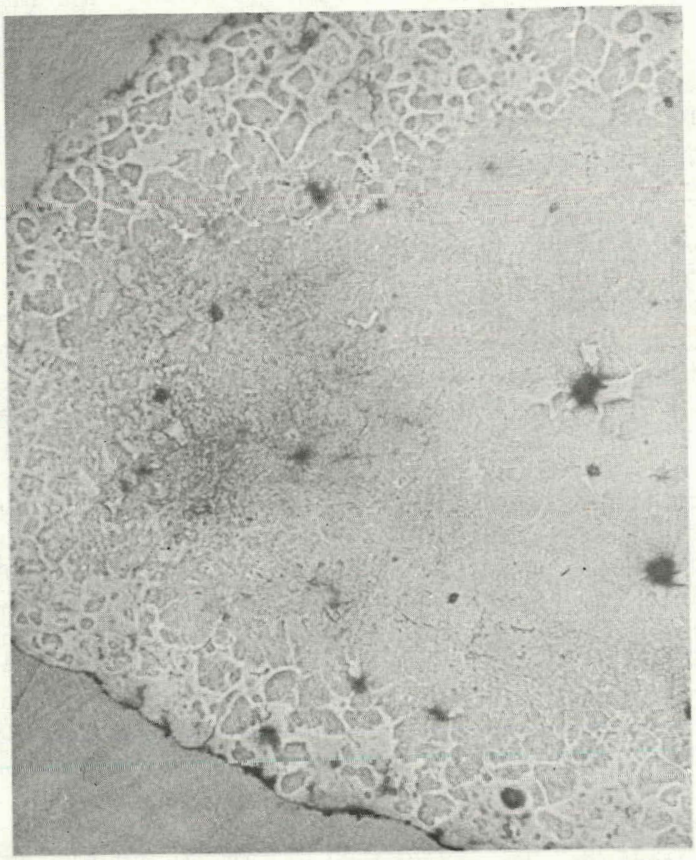

Fig. 32. Stone Removed from Point D, Fig. 30. Individual grains of stone apparent. The band, along the periphery of stone, where grains are most pronounced, is the region of primary sulfation

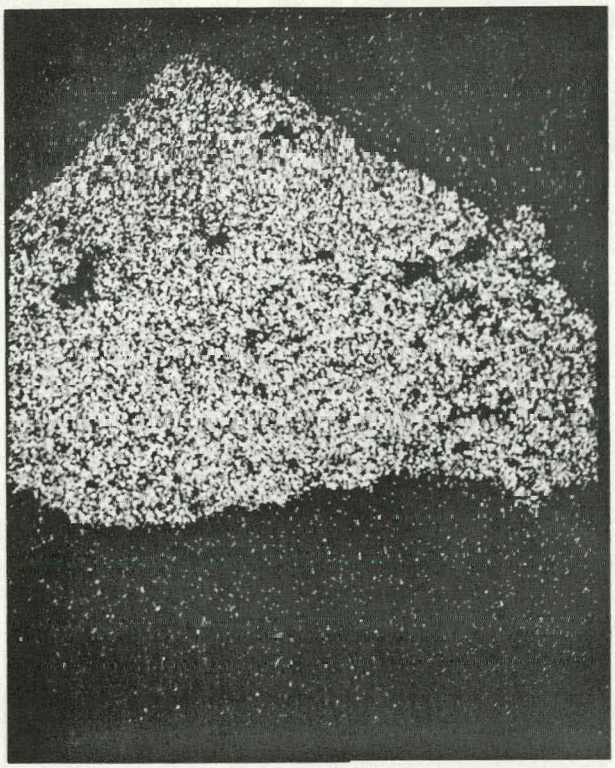

(a)

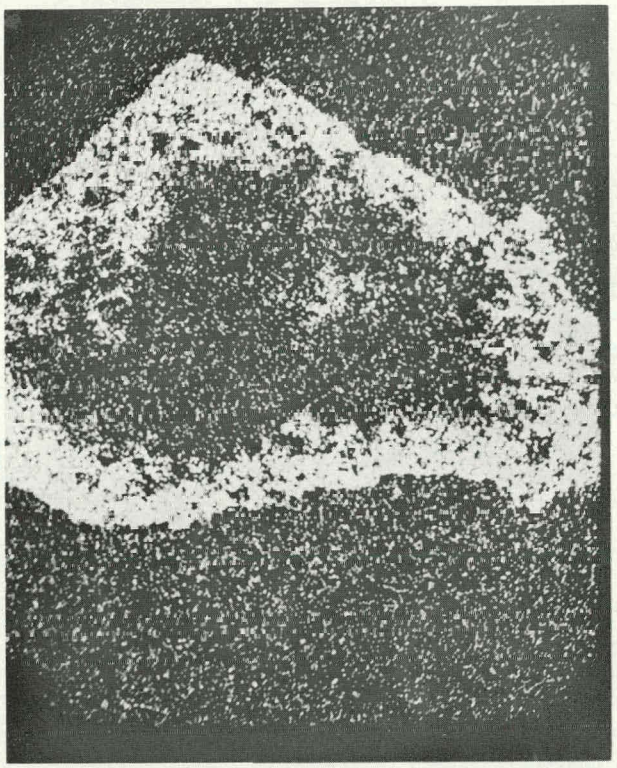

(b)

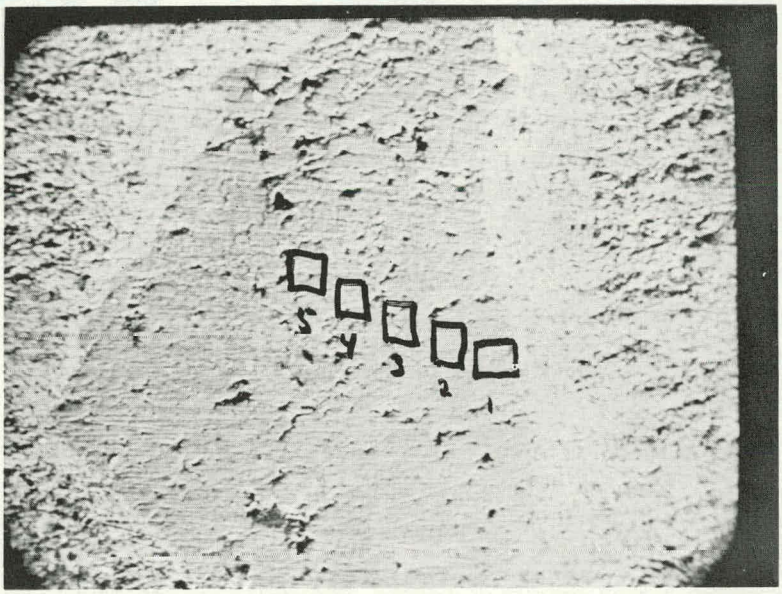

(c)

Fig. 33. SEM Results on a Stone Taken from Point C in Fig. 30. Fig. 33a shows a Ca X-ray scan across the entire stone, Fig. 33b a S X-ray scan across the entire stone, and Fig. 33c outlines five areas on the stone analyzed in detail for the presence of Ca, Mg, and S (see Fig. 34)

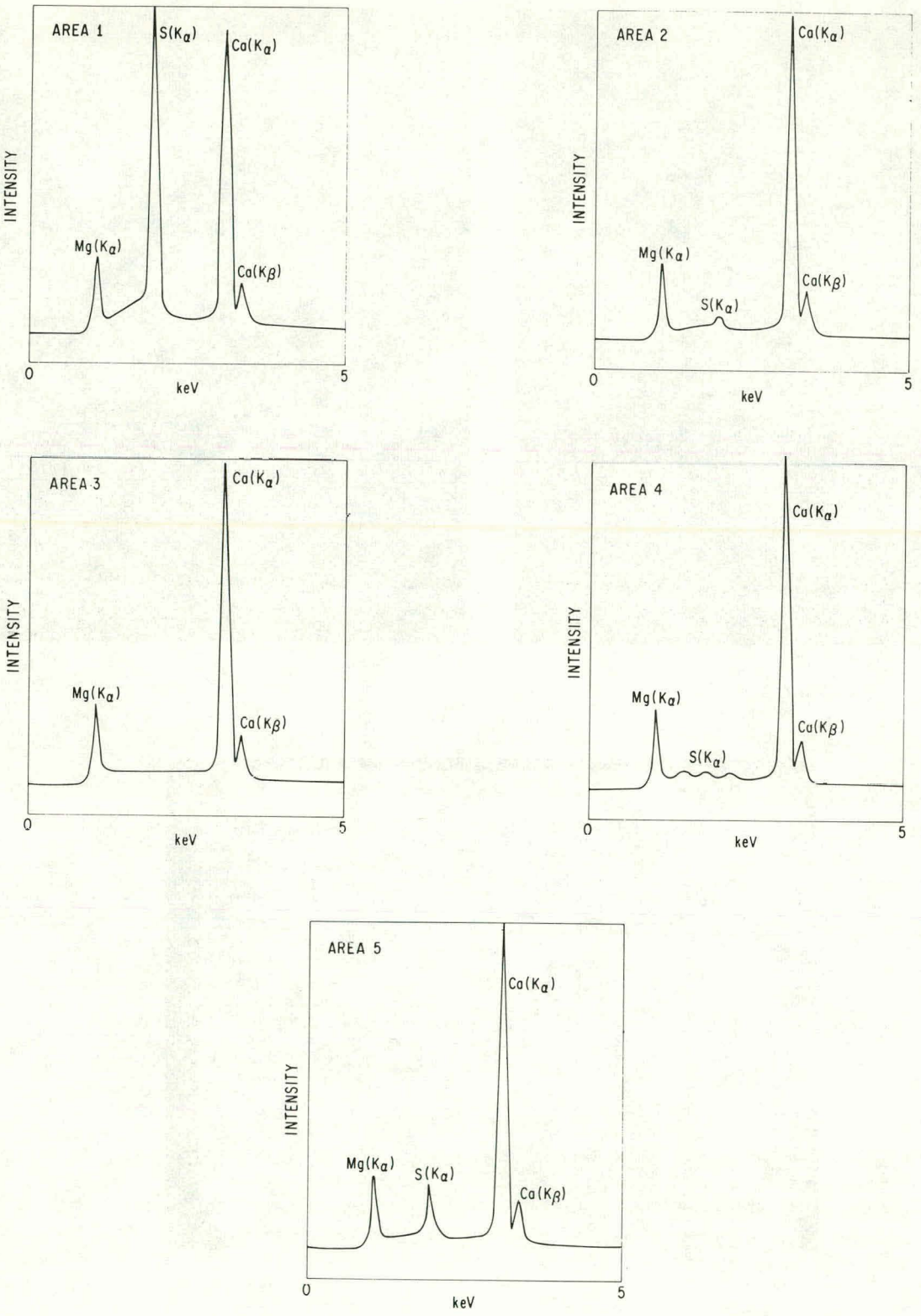

Fig. 34. SEM Results of Analysis for Presence of Ca, Mg, and S in the Five Areas of the Stone Described in Fig. 33c

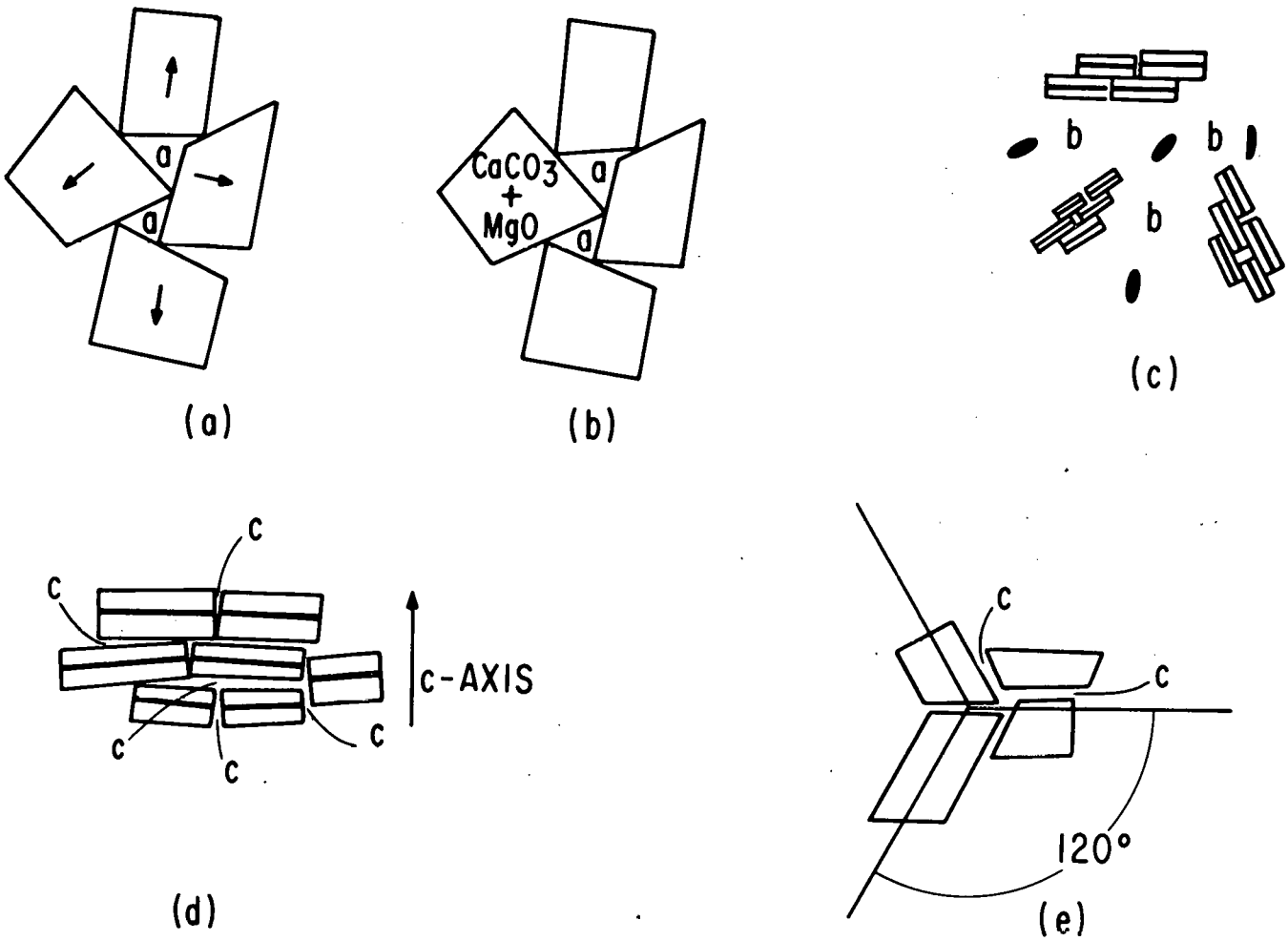

Fig. 35. Schematic Representation of the Structural Characteristics of Dolomite During Sulfation. a) Dolomite before half-calcination, b) dolomite after half-calcination, c) aggregation characteristics, d) non-uniform orientation of crystallite normal to the c-axis, e) non-uniform orientation in the a-a plane of hexagonal axis. (see text for details)

indicated in Fig. 35d by the heavy shading. It is now necessary to define new voids--the spaces that occur between unaligned crystallites of $CaCO_3$. These are labelled c and could constitute regions of defects and various vacancies--points where one might expect high reactivity to SO_2. The stringers of MgO could act as barriers to the diffusion of SO_2, thereby leading to nonuniform sulfation of a calcite crystal.

It is instructive to examine the structure of dolomite and to consider a mechanism of breakdown during the half-calcination process. This leads to a plausible interpretation of the origin of the stringers and to various methods for breaking down the MgO formation.

Calcite, $CaCO_3$, possesses rhombohedral symmetry. The rhombohedral angle is 46°6', as distinct from the cleavage rhomb angle of 101°55'. However, it is convenient to describe the structure in terms of hexagonal symmetry. Dolomite, $CaMg(CO_3)_2$, is also rhombohedral, but can, in a similar manner, be referred to hexagonal symmetry. The hexagonal cell dimensions are (including $MgCO_3$):

	a(Å)	c(Å)
$CaCO_3$	4.99	17.06
$CaMg(CO_3)_2$	4.80	16.00
$MgCO_3$	4.62	14.99

Although the structures of calcite and dolomite are similar, basic differences in symmetry serve to indicate that the two materials are to be considered as distinct compounds. The space group of calcite is D^6_{3d} - $R\bar{3}c$ while that of dolomite is C^2_{3i} - $R\bar{3}$. The alternation of Ca and Mg atoms along the threefold axes lowers the symmetry. In the following, only the structure of dolomite is considered. A visual representation of the structure of calcite can be obtained by replacing Mg with Ca atoms.

Dolomite $CaMg(CO_3)_2$ Z = 3

Coordinates: $000, \frac{1}{3}\frac{2}{3}\frac{2}{3}, \frac{2}{3}\frac{1}{3}\frac{1}{3} +$

Ca in (3a) 000

Mg in (3b) $00\frac{1}{2}$

C in (6c) $\pm 00u$, $u \sim 1/4$

O in (18f) $\pm(x,y,z)(\bar{y},x-y,z)(y-x,\bar{x},z)$ with

$x = 0.2374$, $y = -0.0347$, $z = 0.2440$

In Fig. 36, the Ca^{++} positions lead to extended sheets of Ca^{++} ions normal to the c-axis. Each Ca^{++} is bonded to one of the oxygen atoms of a triangular array of oxygen atoms distributed about the point $\frac{2}{3}\frac{1}{3}$ 1.43. These

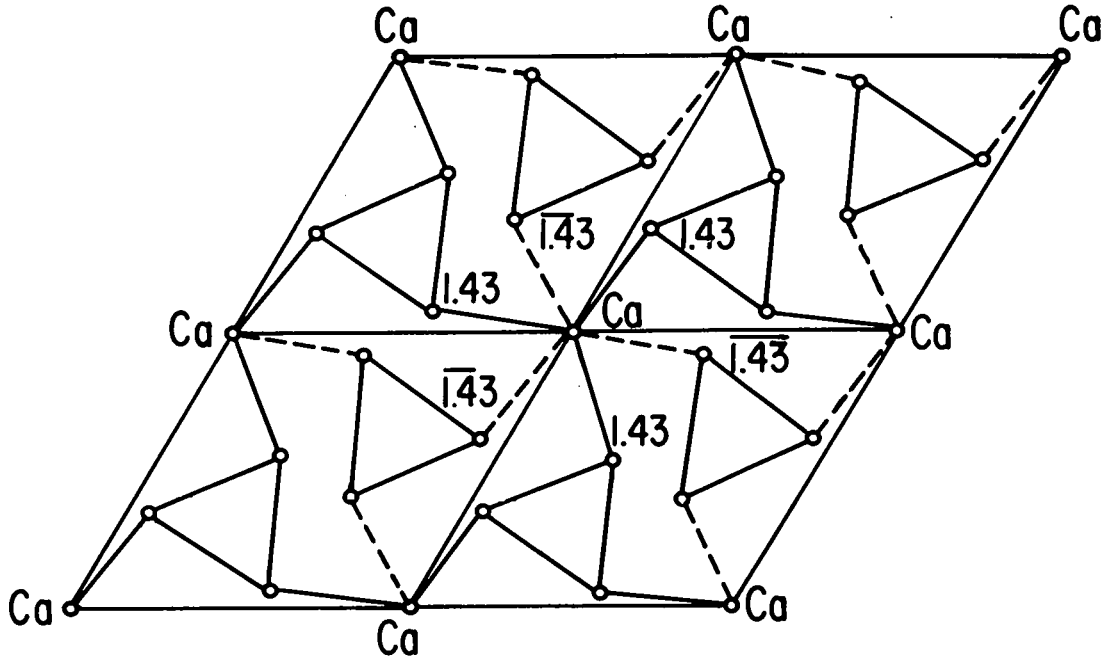

Fig. 36. Schematic Representation of the Cross Section of a Dolomite Crystal taken normal to the c-axis showing Ca^{++} at the 000 positions (see text)

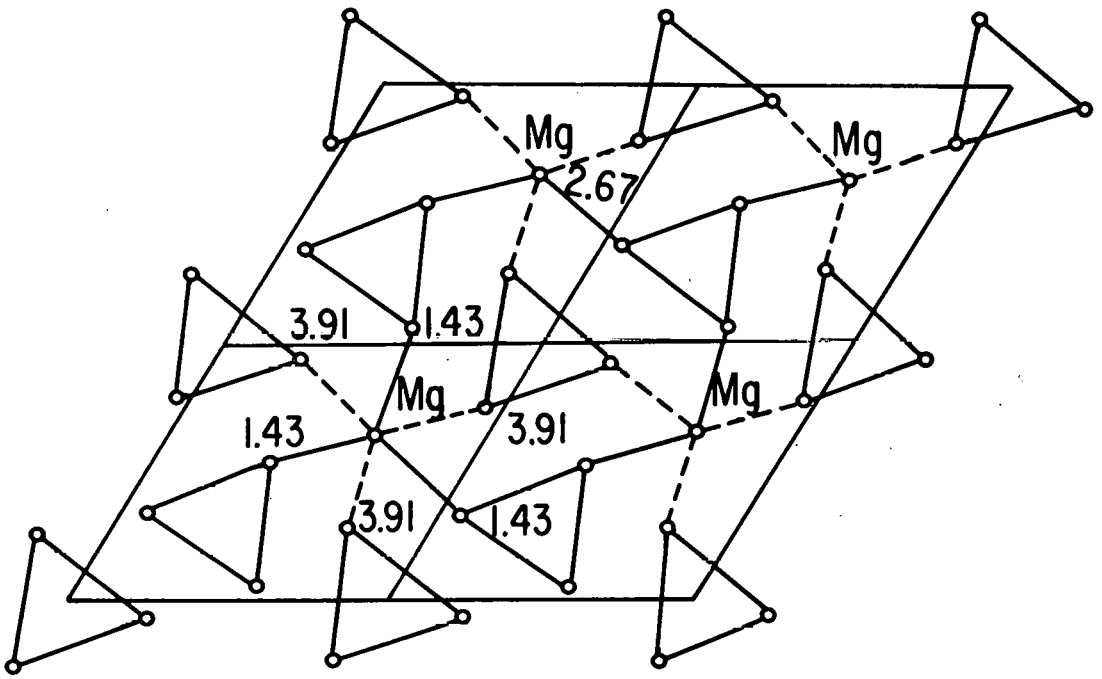

Fig. 37. Schematic Representation of the Cross Section of a Dolomite Crystal Taken Normal to the c axis showing Mg^{++} at the $\frac{1}{3}\ \frac{2}{3}$ 2.67 position (see text)

triangular arrays are the oxygen atoms of the $CO_3^=$ ion. (The carbon positions are omitted for clarity.) Another oxygen array is distributed about the point $\frac{1}{3}\ \frac{2}{3}$ 1.43. All arrays at z = +1.43 Å are extended sheets of oxygen atoms normal to the c-axis. Each Ca^{++} ion is, therefore, bonded to 6 oxygen atoms.

As shown in Fig. 37, Mg^{++} ions appear at positions $\frac{1}{3}\ \frac{2}{3}$ 2.67. Clearly, each Mg^{++} ion is bonded also to oxygen atoms at a height of z = 1.43 Å. However, more $CO_3^=$ groups arise at a height of 3.91 Å, and are distributed about the points 0, 0, 3.91. Consequently, each Mg^{++} ion is also bonded to 6 oxygens. As before, the oxygens at z = 3.91 Å form extended sheets normal to the c-axis. This buildup of sheets of atoms, with Mg^{++} and Ca^{++} ions sharing the same neighboring oxygen atoms, continues the entire length of the c-axis (c = 16.00 Å) within the unit cell. A view normal to the c-axis is shown in Fig. 38.

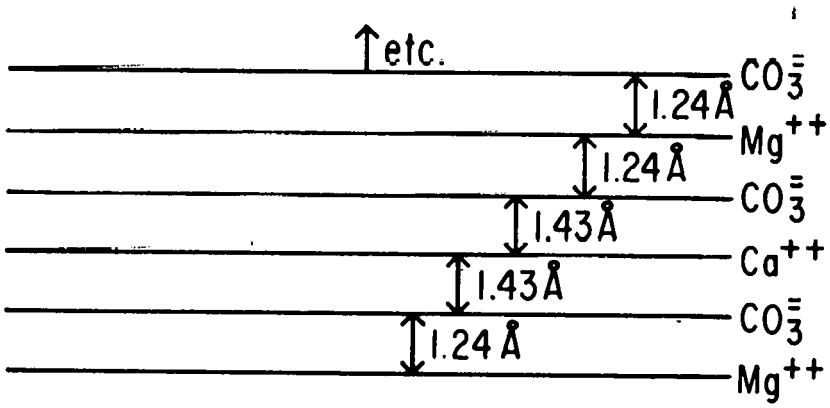

Fig. 38. Distribution of Ions Normal to c-axis Hexagonal

The shorter distance between Mg^{++} - $CO_3^=$ planes arises from the smaller radius of the magnesium ion. The above layering, of course, extends throughout the entire (macroscopic) crystal of dolomite.

Since each Ca^{++} and Mg^{++} ion shares a common oxygen atom, then, in half-calcining, each $CO_3^=$ ion must break down to form $O^=$ ions. An alternative way to view this is to remember that the oxygen atoms are symmetry equivalent; that is, they are derived from an 18-fold set. Figure 39 is a view of a possible mechanism for half-calcination based upon the above structure.

In Fig. 39, each $CO_3^=$ ion is depicted as breaking down to $O^=$ ions. A Mg^{++} ion combines with $O^=$ to form MgO, and since Mg^{++} ions are near each other (corresponding to reasonable metal-metal distances), MgO nuclei can form readily. On the other hand, $CaCO_3$ should form easily since it is stable under the half-calcining conditions and the Ca^{++} positions are close to those in the related dolomite configuration. Diffusion of Mg^{++} ions or MgO from neighboring sheets can occur, but in this case, the formation of calcite sheets can act as barriers to the diffusion. Hence, there may be a limited

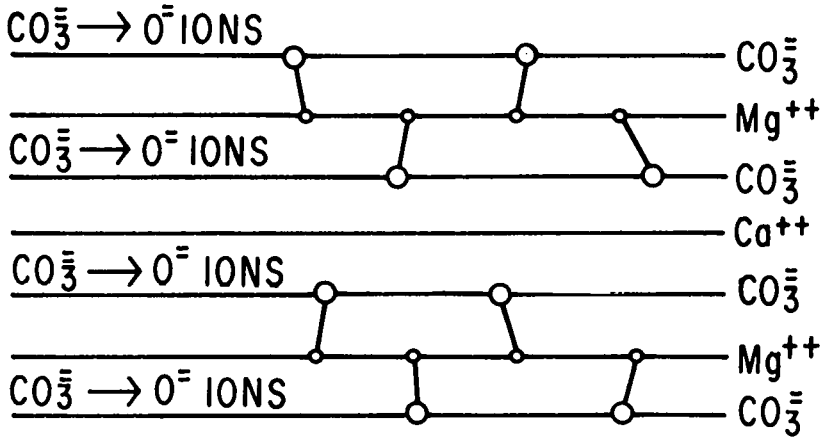

Fig. 39. Formation of Phases

buildup of MgO crystallites along the c-axis, but extended sheets (stringers) could occur in two dimensions normal to c. An idealized situation is shown in Fig. 40. However, dolomite is expected to exhibit a mosaic structure, a feature in common with many crystals. This leads to various faults consisting of defects and dislocations. These regions can become pathways for diffusion of MgO to build up to macroscopic thickness. Limits of growth imposed by the alternation of MgO and $CaCO_3$ would, therefore, account for the small crystallites observed for these phases. However, there is a difference in the subsequent steps associated with half-calcining. MgO is cubic with a structure not compatible with that of either dolomite or calcite. On the other hand, calcite not only is compatible, but exhibits 3 equivalent directions. As indicated above, the 104 reflection of calcite was found to be "spotty". This plane corresponds to the 3 natural cleavage faces of CaCO and the spottiness arises from the tendency of the crystallites to align normal to the 104 direction. If we consider that the dolomite crystals have some mosaic character and that, in addition, new defects are introduced during the calcination, it might be expected that the re-formed crystals of $CaCO_3$ will show configurations as indicated in Fig. 35d in which sections of crystals are displaced along the c-axis. In addition to the various defects, dolomite may contain impurity ions that can replace Ca and Mg atoms at the cation structure sites. At elevated temperature, the thermal motion may become so anisotropic that certain metal-oxygen bonds may break preferentially during half-calcination. This will not change substantially the features of the model presented here.

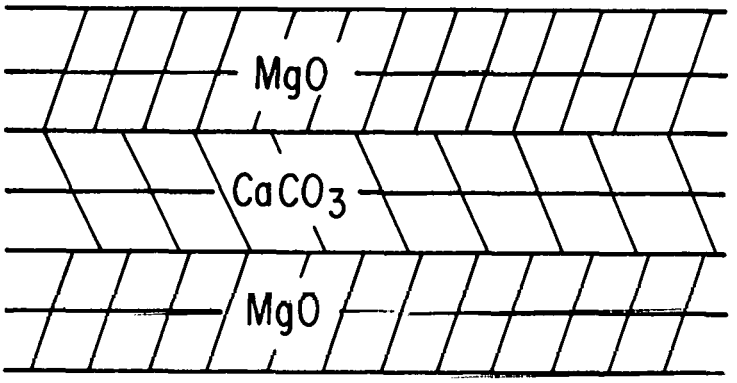

Fig. 40. Layering of Phases

Thus, stacking disorder within a crystallite and stacking disorder between the crystallites can be considered, the latter arising from their attempt to align. Another disorder arises, however, by virtue of the symmetry. This is shown in Fig. 35e. In this case, misalignment can arise in a direction normal to c. In this figure, the extended sheets of MgO are in the plane of the figure.

The model suggests that MgO (and $CaCO_3$ as well) could form extended and nearly 2-dimensional sheets. The aggregated sheets could well constitute the stringers observed optically. The tendency for the calcite sheets to form oriented "crystals," but leading to misalignment could also account for the undulatory nature of the extinction under polarized light. The model, in addition, suggests that a variety of pores could exist. Of particular interest to us is the pore configuration shown in Fig. 35d and 35e. We have defined the regions c as pores. Strictly speaking, these are regions of incomplete bonding -- unsatisfied bonding -- because of structure discontinuity across a boundary and may be the origin of van der Waals or other bonding to cause orientation along specified crystallographic directions. The pores c could well be regions of high reactivity to SO_2.

The model developed above has been established on the basis of limited X-ray diffraction and microscopic studies and consequently has many limitations. The pore blockage and barrier diffusion schemes are oversimplified. Changing molecular volumes produce dynamic changes in channeling and pore makeup. The

formation of $CaSO_4$ apparently does not follow a simple process. Reports on rared studies of sulfation[7] show the buildup of complex sulfates on the faces of CaO. These layers of sulfates could well be responsible for some limitations of continued sulfation. One must also consider the nature of processes responsible for stone hardness and adherence. Possibly, the formation of stable intermediate compounds, developed by an epitaxial mechanism, may lead to adherence, and the epitaxial layers could also participate as diffusion barriers. Finally, as will be shown, the degree of preferred orientation of the calcite will vary with calcining conditions. Thus, Fig. 35c, 35d, and 35e may not be truly representative of the grain makeup. The model should, therefore, be looked upon as a guide, subject to modification as more information is obtained.

Half-Calcination Reaction

In experiments carried out to help establish a structural model, it was noted that the $CaSO_4$ seemed to exhibit a crystallite size and disorder such as that present in the $CaCO_3$ -- certainly, the small crystallite size. Substantial hardening of the stone occurs following sulfation without too much change in shape. It was suspected, therefore, that some of the larger pore configurations are maintained during sulfation. However, other pore or channel arrangements must change continuously, since the molecular volumes of CaO, $CaCO_3$, and $CaSO_4$ differ, leading to different space-filling requirements as reactions progress. It seems evident, therefore, that after cycling of the additive through sulfation and regeneration reactions and returning to a starting material, the regenerated starting material could exhibit quite a modified micropore configuration over that present in the original half-calcined additive. A question thus arises whether a starting material with good sulfation characteristics can return to a starting material with the same quality behavior -- that is, can a good morphology be retained?

Preliminary results on the carbonation reaction presented below suggest that the regeneration process does not go to completion. This raises the question of whether the morphology of half-calcined dolomite can have an effect on the extent of regeneration reactions. To resolve some of these problems, several experiments have been designed to study the modification of starting dolomite in order to obtain morphological information on the half-calcined 1337 dolomite that can be correlated later with rates of the chemical reactions of interest. The experimental variables for the half-calcination reaction, Eq. 1, are temperature and CO_2 partial pressure.

To initiate a systematic study of the calcination reaction and the morphology of the resulting half-calcined material, the following series of experiments was performed: Type 1337 dolomite was half-calcined at one atmosphere pressure in an environment of 100% CO_2 at 640°C, 660°C, 680°C, 700°C, 720°C, and 740°C. In addition, an experiment was performed in which 1337 dolomite was half-calcined in an environment of 40% CO_2 at 640°C. The kinetic results obtained are shown in Fig. 41 and 42, where percent conversion is plotted against time. Some error may exist in these plots because of the manner in which percent conversion was calculated. Since many of the experiments did not go to completion, it was not possible to determine what weight loss cor-

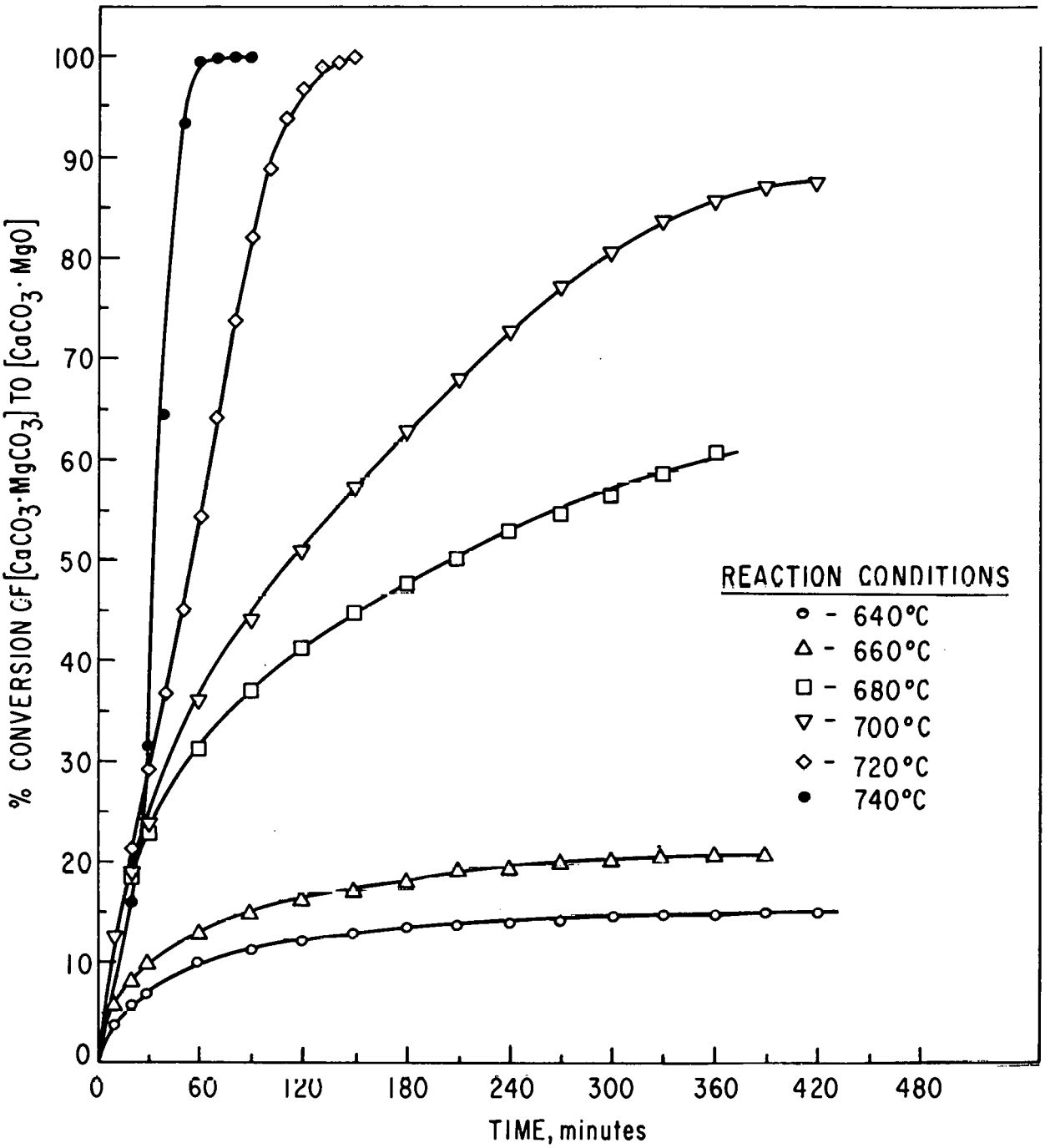

Fig. 41. Plots of % Conversion vs Time for Half-Calcination of 1337 Dolomite under 100% CO_2 Environment as a Function of Temperature

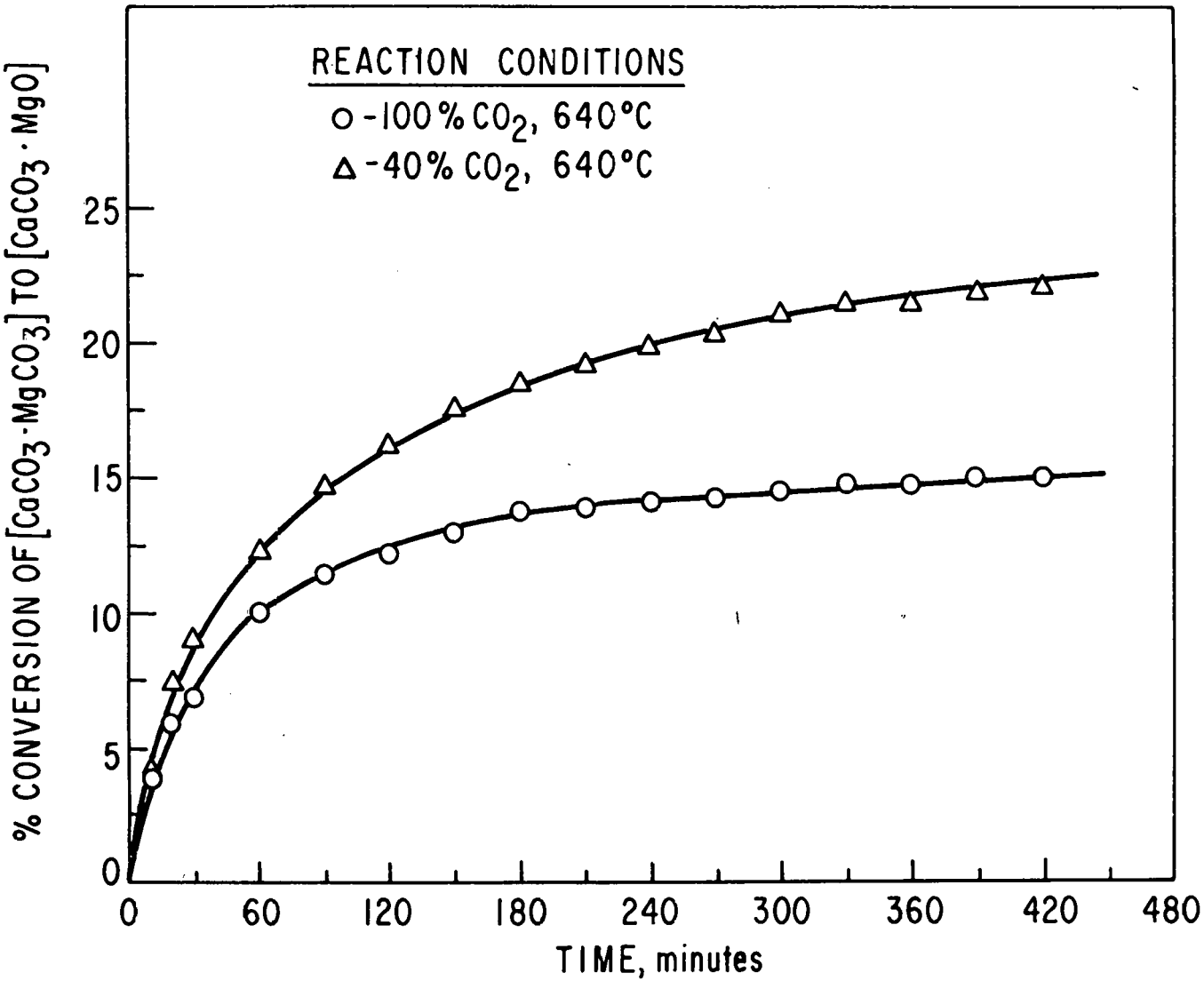

Fig. 42. Plots of % Conversion vs Time for Half-Calcination of 1337 Dolomite at 640°C as a Function % CO_2 Environment

responded to exactly 100% conversion. A common value was chosen for these calculations corresponding to an average value obtained from many previous half-calcination experiments.

The half-calcination technique employed in this program in the past has been to heat the dolomite in an environment of 40% CO_2 at 800°C at a rate of about 25°C/min. Under these experimental conditions, the half-calcination reaction is completed in 20 to 25 min. From Fig. 41, it can be seen that the reacton rate is much lower in the environment of 100% CO_2, even at the highest temperature, 740°C. It is also apparent that the rate for 100% CO_2 increases rapidly with temperature, particularly at temperatures above 660°C. From Fig. 42, it is apparent that the reaction rate increases with decreasing CO_2 partial pressure at 640°C.

A summary of the X-ray diffraction analysis of stones from these half-calcination experiments is given in Table 6.

For the experiments carried out in 100% CO_2, the following morphological trends are significant: The $CaCO_3$ pseudo-crystal size varies from very large at low temperature to small at high temperatures, or alternatively, the extent of $CaCO_3$ crystallite preferred orientation varies with temperature, with the degree of orientation decreasing as temperature increases. It is noted that the indication of fairly large pseudo-crystals from the X-ray data may in fact be due to very small crystallites, perhaps 1000Å or so in size, that are highly oriented to form pseudo-crystals. The rapid dropoff in the intensities of the diffraction lines observed indicates some disorder. A microscopic investigation will yield more information on this.

In 100% CO_2, the MgO crystallite size remains small regardless of the temperature. However, there is some indication that the overall intensities of the MgO lines in the half-calcined dolomite may vary from experiment to experiment. Visual examination of the lines suggests that, in some cases, particularly at large scattering angles, the lines may show some sharpening. If the increase in peak intensity observed is a consequence of crystal growth, this can be determined from line width measurements. This qualitative observation will be pursued by further investigation.

A comparison of the extreme cases between 100% CO_2 at 640°C and 40% CO_2 at 800°C indicates a large difference in morphology. 100% CO_2 at 640°C results in the largest pseudo-crystals (very oriented) of $CaCO_3$, whereas 40% CO_2 at 800°C results in small pseudo-crystals of $CaCO_3$ (slight preferred orientation). The effect of CO_2 partial pressure at 640°C is much less dramatic in that half-calcination with 40% CO_2 rather than 100% CO_2, leading to smaller pseudo-crystals of $CaCO_3$ -- although the pseudo-crystals are still relatively oriented.

These results do show that the morphology of half-calcined dolomite can be controlled to some extent by choosing the conditions under which the reaction is carried out. Comparison of kinetic data and resultant morphology of half-calcined stones makes it obvious that when the reaction is performed under conditions for which the reaction rate is low, the morphology indicates larger pseudo-crystals of $CaCO_3$. It remains to be determined whether or not the MgO structure is being affected in a similar fashion.

Table 6. Summary of X-Ray Diffraction Analysis of 1337 Dolomite Stones from Half-Calcination Reaction Experiments

Sample History	$CaMg(CO_3)_2$		MgO		$CaCO_3$		Quartz
	crystallite size[a]	quantity	crystallite size	quantity	crystallite size[b]	quantity	
100% CO_2 at 640°C for approx. 7 hr	large	major	small	very minor	larger, very oriented	minor	
100% CO_2 at 660°C for approx. 7 hr	large		small	minor +	large, oriented	minor +	very minor
100% CO_2 at 680°C for approx. 6 hr	large	decrease	small	medium	large, less oriented	medium	medium
100% CO_2 at 700°C for approx. 2 1/4 hr	large		small	medium	medium, slight orientation	medium	
100% CO_2 at 700°C for approx. 7 hr	large	minor	small	major	small, slight orientation	major	very minor
100% CO_2 at 720°C for 2 1/3 hr	-----	none	small	major	small, slight orientation	major	
100% CO_2 at 740°C for 1/2 hr	----	none	small	major	small, slight orientation	major	
40% CO_2 at 800°C for approx. 25 min.		none	~1000A	major	small, slight orientation	major	trace
40% CO_2 at 640°C for approx. 7 hr	large	major	small	minor	large, oriented	minor	

[a] It should be noted that the origin of the apparently larger dolomite crystals may be the result of initial decomposition of the finely divided $CaMg(CO_3)_2$ so that the larger crystals stand out in the diffraction pattern.

[b] Lack of resolution of the α,α_2 doublet serves to indicate that the crystallite size is of the order of 1000Å in all experiments. However, they undergo preferred orientation so as to simulate single crystals. At the beginning of this series, the orientation is pronounced enough to produce fairly well defined pseudocrystals. However, as the temperature increases, the pseudocrystals become smaller, with the orientation becoming more random.

Sulfation During Half-Calcination

In the previous section, the studies of half-calcination were intended to isolate those properties of $CaCO_3$ (and possibly MgO) related to crystallite size and degree of preferred orientation which might have a bearing on the kinetics of reactions.

The following experiments also were suggested by the structural model. In this model, it is proposed that MgO stringers in the calcite crystallites formed from a dolomite crystal could act as barriers to SO_2 diffusion into $CaCO_3$. Such an occurrence could explain the nonuniform sulfation of $CaCO_3$ crystallites. The purpose of the experiments described here was to determine if free Mg^{++} ions or MgO molecules not yet fully aggregated into the characteristic three-dimensional structure would react with SO_2 and O_2 during the reaction time of the half-calcination process. To evaluate this, experiments were performed as follows: The flow of the sulfation reaction gas mixture over the 1337 dolomite stones was started at a temperature below that at which the half-calcination reaction would normally begin and then the temperature was raised to that at which half-calcination under 40% CO_2 partial pressure would proceed. In this experiment, sulfation and half-calcination reactions were thus proceeding simultaneously (closely simulating conditions in a fluidized-bed combustion process).

X-ray diffraction analysis of the resulting reaction product showed the presence of a new phase not previously reported in the sulfation of sorbent additives -- $Mg_3Ca(SO_4)_4$. This compound was first identified by Rowe *et al.*[8] After the X-ray studies in the above sulfation-half-calcination experiment, the compound was also identified by optical microscopic study of the reacted stone. Its distribution in the stone was established, and microscopic amounts were removed for additional X-ray investigation, leading to verification of the identity of the phase. The amount of the compound formed varied from experiment to experiment, but in at least one case a substantial amount was formed. In addition, in a recent experiment in which a synthetic dolomite of composition [$CaCO_3 \cdot MgCO_3$], was half-calcined and then sulfated, examination showed a very substantial amount of $Mg_3Ca(SO_4)_4$. The experiment using synthetic dolomite suggests that the binary compound can be formed under various reaction conditions. Therefore, it is concluded that the chemistry associated with the formation of this compound may be a new and significant variable in the cyclic use of dolomite in sulfur emission control chemistry. The formation of $Mg_3Ca(SO_4)_4$ could indicate a breakdown of the MgO sheets or stringers. This merits further study, but, for the present, difficulty is encountered in making a quantitative estimate of the amount of the compound present. However, information from optical microscopy is available on the location of the compound within the particles. Figures 43 and 44 show representative pictures of particles containing the compound. The occurrence of the binary sulfate, $Mg_3Ca(SO_4)_4$, is found to be confined to those surfaces within the particles that are exposed to the gas during the reaction (darkened areas), and it occurs as thin rims on the peripheries and on the walls of interior cavities. In addition, $CaSO_4$ and MgO have always been present as associated phases on X-ray samples taken from these rims. The occurrence of this phase is of interest for two reasons: (a) sulfation during calcination is the more realistic behavior of dolomite in a fluidized bed, and (b) we note that the mineral huntite, $Mg_3Ca(CO_3)_4$, occurs in nature. One might speculate that the huntite might

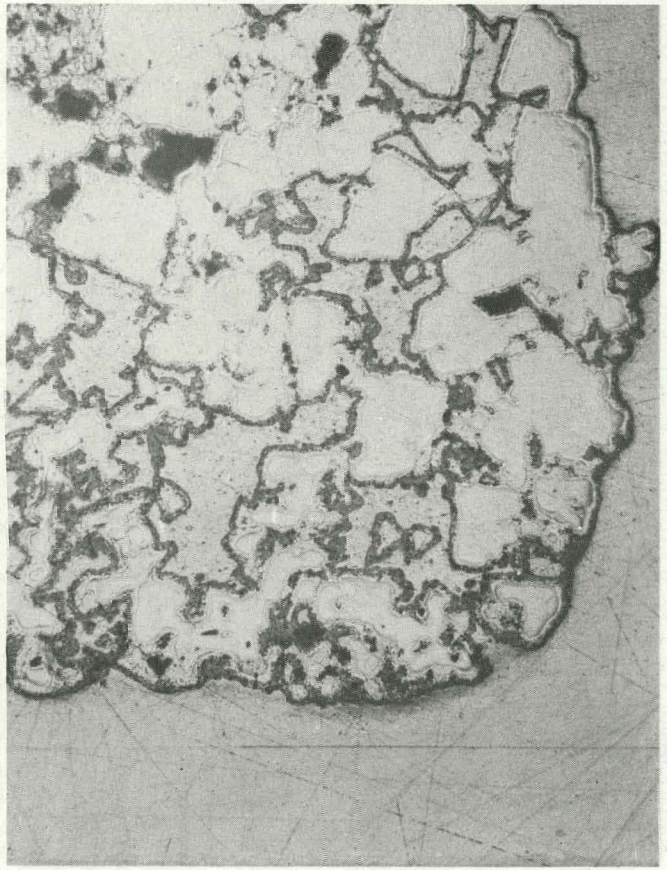

Fig. 43. 1337 Dolomite Particle Showing Location of [$CaSO_4 \cdot 3MgSO_4$] within the Particle. Dark ribbons are [$CaSO_4 \cdot 3MgSO_4$] and have been discolored by exposing sample to air.

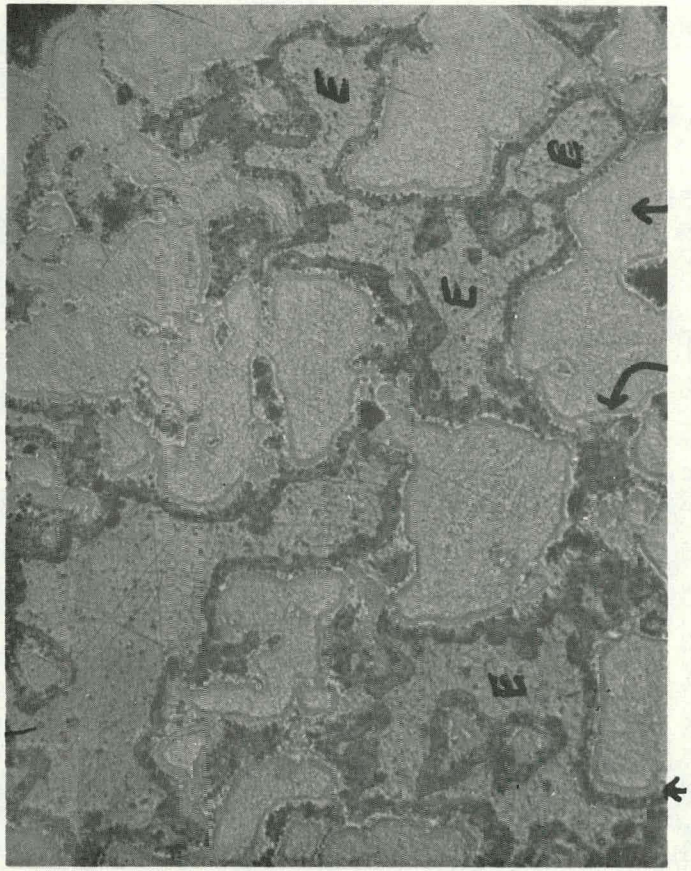

Fig. 44. Another 1337 Dolomite Particle Showing Location of [$CaSO_4 \cdot 3MgSO_4$] within the Particle. Samples were recovered from the points labeled 1, 2, and 3 with the following results: 1, Calcite - strong, MgO - medium strong, anhydrite - weak; 2, anhydrite and MgO; 3, $CaSO_4 \cdot 3MgSO_4$.

have been formed as a transient species and that this phase reacts with SO_2.

It is hoped that $Mg_3Ca(SO_4)_4$ and $Mg_3Ca(CO_3)_4$ can be prepared in sufficient quantity to study their properties, particularly to note whether the carbonate reacts with SO_2 directly to the sulfate double salt. If this occurs, a pretreatment of the dolomite that would lead to the production of substantial amounts of $Mg_3Ca(CO_3)_4$ might be considered.

Sulfate-Sulfide Regeneration Method

The feasibility of the solid-solid reaction

$$3CaSO_4 + CaS \rightarrow 4CaO + 4SO_2 \qquad (20)$$

is documented.[1,10,11] In fact, the reaction has been used as a method of producing SO_2. In addition, this reaction has been the subject of study from time to time as a possible scheme for regenerating dolomite or limestone.[1,11] However, the literature shows no detailed examination of the process - perhaps due to the fact that it entails a solid-solid reaction in which the reaction itself would be dependent on pore size and the associated separation of the reacting phases.

The initial interest in this reaction was based on the observation that a sulfated synthetic dolomite showed no visible pore structure, thereby suggesting that the reacting solid species would be in intimate contact. In addition, microscopic observations indicated that the sulfation reaction in 1337 dolomite is occurring in small grains, separated by the larger pores. Based on this information, it was speculated that the large pores found in dolomite may not necessarily play such an important role in the various diffusion processes. To examine this speculation, a series of preliminary TGA/X-ray diffraction experiments have been performed employing 1337 dolomite.

The procedure used in these experiments was as follows: A sample of the 1337 dolomite was sulfated completely following half-calcination. This was followed by reduction with H_2 at 900°C to reduce the sulfate form of the stones to the sulfide with a 3:1 molar ratio as required by the subsequent regeneration reaction given by Eq. 6

$$3[CaSO_4 \cdot MgO] + [CaS \cdot MgO] \rightarrow 4[CaO \cdot MgO] + 4SO_2 \qquad (6)$$

This step was followed by heating the stones, which contained both CaS and $CaSO_4$, under pure He at one atmosphere to about 950°C. Stones were removed at various stages of reaction 6 for X-ray diffraction analysis.

A number of problems were encountered in these preliminary experiments. In initial attempts, the dolomite particles were not completely sulfated because of instrumental problems. This resulted in a substantial amount of residual CaO in the stones before the solid-solid reaction took place. In addition, in the regeneration reaction, many or all of the phases (MgO, CaO, $CaCO_3$, $CaSO_4$, CaS, etc.) are present in the X-ray diffraction patterns of the dolomite, leading to difficulty in interpreting the data patterns. In the past, a visual examination of the X-ray diffraction patterns has permitted semiquantitative estimates of growth or decrease of chemical species during a reaction. However,

In dealing with this regeneration reaction, it became necessary to develop a method for quantitative measurements of various phases present in the X-ray diffraction patterns. A description of the X-ray technique developed for this purpose will appear elsewhere.[12]

In other work, two reactions which produce sulfur from sulfated dolomite were studied in boat reactor experiments. These included one in which elemental sulfur is a product:

$$3\ CaS + CaSO_4 \rightarrow 4\ CaO + 2S_2 \qquad (21)$$

as well as that in which sulfur dioxide is a product:

$$CaS + 3CaSO_4 \rightarrow 4CaO + 4SO_2 \qquad (22)$$

In the Sulfuric Acid-Cement Process,[9] both reactions proceed at about the same rate in the temperature range of 900 to 1000°C (1650-1832°F); at higher temperatures, reaction 22 is strongly favored.[9] The reactions are carried out in a neutral atmosphere.

In preliminary experiments, chemically pure CaS powder was mixed with either pure $CaSO_4$ or sulfated dolomite from the combustor. The reactions were carried out in porcelain boats in a quartz tube reactor. A flowing nitrogen cover gas passed through a water-cooled condenser to collect condensables.

In an experiment using appropriate stoichiometric ratios of reagent chemicals indicated by reaction 21 and a temperature of 900°C (∿1650°F), elemental sulfur was collected in the condenser. The amount produced (<0.01 g) did not approach the theoretically possible yield, even after four hours. In this experiment, the sulfur began collecting in the condenser at ∿600°C (∿1110°F). Another experiment was performed at 700°C (∿1300°F), but little additional sulfur yield resulted. X-ray diffraction analysis of the boat contents after the experiments indicated that the reaction had proceeded to a lesser degree at 700°C than at 900°C.

In a study of SO_2-producing reaction 22, the reactant temperature was increased gradually from 375 to 950°C (∿700 to 1750°F). Higher temperatures were not used because the maximum furnace temperature was 950°C. The greatest production was found at the highest temperature.

In the final experiments, CaS was reacted at 950°C with either reagent grade $CaSO_4$ or with ground, sulfated dolomite particles from a combustion experiment. The off-gas was analyzed for sulfur dioxide content (all SO_2 was collected), and the composition of the resulting solids of one experiment was determined. The table below lists the reactants, the conditions, the amounts of SO_2 released, and the products observed.

Exper. No.	Reactants	Mole Ratio $CaSO_4$:CaS	SO_2, Total Produced, mmol	% of Theoretical	Products
CAS-7	$CaSO_4$;CaS	3:1	2.8	28.6	Not determined
CAS-9	Sulfated Dolomite; CaS	3:1	5.9	73.8	CaO;$CaSO_4$

It was concluded that reaction 22 is more favorable kinetically than is reaction 21, under the conditions explored. In view of the release of sulfur and the simplicity of operation, further experimentation is warranted.

Preliminary studies have indicated that CaO can be produced by the overall reaction represented by Eq. 6. As an example of these results, one experiment will be described in some detail. In this experiment (identified as H-65), a half-calcined and sulfated dolomite sample was partially reduced to produce CaS. The stones were then heated under helium at 945°C for various times and aliquots were isolated for the X-ray study. In Table 7, percentage volumes observed in these aliquots are shown in the fourth column. These values are reduced to give weights, M, based on the formula $Ca_{1.14}Mg_{0.86}(CO_3)_2$. All weights for $CaCO_3$ and $CaSO_4$ are reduced in the sixth column to give a CaO equivalent.

The results presented in Table 7 cannot as yet be explained in detail. Thus, for H-65-A, substantial amounts of CaO and $CaCO_3$ are observed - not only was 100% sulfation not achieved, but no $CaCO_3$ should have been present. In H-65-B, the effect of the high temperature, in the absence of CO_2, was to convert the $CaCO_3$ to CaO. The 29.1 g of CaO found in H-65-B corresponds well to the 28.8 equivalent grams of CaO found in H-65-A. The TGA weight loss arose from the CaS production. In H-65-C, no major change was observed, although a weight loss was observed in the TGA. For H-65-D, an additional weight loss was observed, but the X-ray diffraction pattern again shows no major change. It should be pointed out at this stage that an assumption is being made that the amount of MgO in the sample remains fixed with time. How true this is remains to be determined for, as reported above, detectable amounts of a double salt $Mg_3Ca(SO_4)_4$ may be formed when sulfation is carried on during half-calcination. H-65-B was conducted under conditions where such a phase could develop; hence, consideration should be placed primarily on the buildup of the CaO. In run H-65-E, a very substantial increase in the CaO content was observed, even though CaS was also detected. An anomaly arises in H-65-F, for although the CaO content remained essentially the same as that of H-65-E, very little CaS was detected. It is believed that much of the irregular behavior stems from the nonuniform response of individual stones to the sulfation and regeneration steps. Future experiments will use larger samples to ensure more representative analytical results.

In Fig. 45, the percentage of the maximum attainable CaO content (based on a CaO max of 63.93 g) with time is shown. Despite anomalies, there is no doubt that the amount of CaO now present is about 70% of maximum. Unfortunately, the starting content of CaO was 42%. The extent to which CaO can be formed when the initial CaO content is zero (*i.e.*, 100% sulfation) remains to be determined. However, the results of other experiments to date have been equally encouraging in indicating that the solid-solid regeneration reaction does indeed proceed.

Table 7. Application of X-Ray Technique to Products of Solid-Solid Regeneration Reaction

Sample	Sample History	Calcium Species	Volume, %	Weight, g	CaO, $M_{equivalent}$	Comments
H-65-A	Half-Calcined sulfated to constant weight, CO_2 removed to calcine remaining $CaCO_3$	CaO	14	8.95	8.95 | 28.8	
		$CaCO_3$	31	35.37	19.82 |	
		$CaSO_4$	69.5	107.7	44.39	
H-65-B	H-65-A partially reduced	CaO	45.5	29.1	29.1	
		$CaSO_4$	33	51.2	21.1	(CaS observed)
H-65-C	H-65-B heated under He for 15 min.	CaO	48	30.69	30.69	
		$CaSO_4$	25.5	39.55	16.30	(CaS observed)
H-65-D	H-65-B heated under He for approx. 36 min.	CaO	42	26.85	26.85	
		$CaSO_4$	31	48.08	19.82	(CaS observed)
H-65-E	H-65-B heated under He for approx. 61 min.	CaO	74	47.31	47.31	
		$CaSO_4$	21	32.57	13.43	(CaS observed)
H-65-F	H-65-B heated under He for approx. 89 min.	CaO	64.5	41.2	41.2	
		$CaSO_4$	24.5	38.0	15.7	(little CaS present)

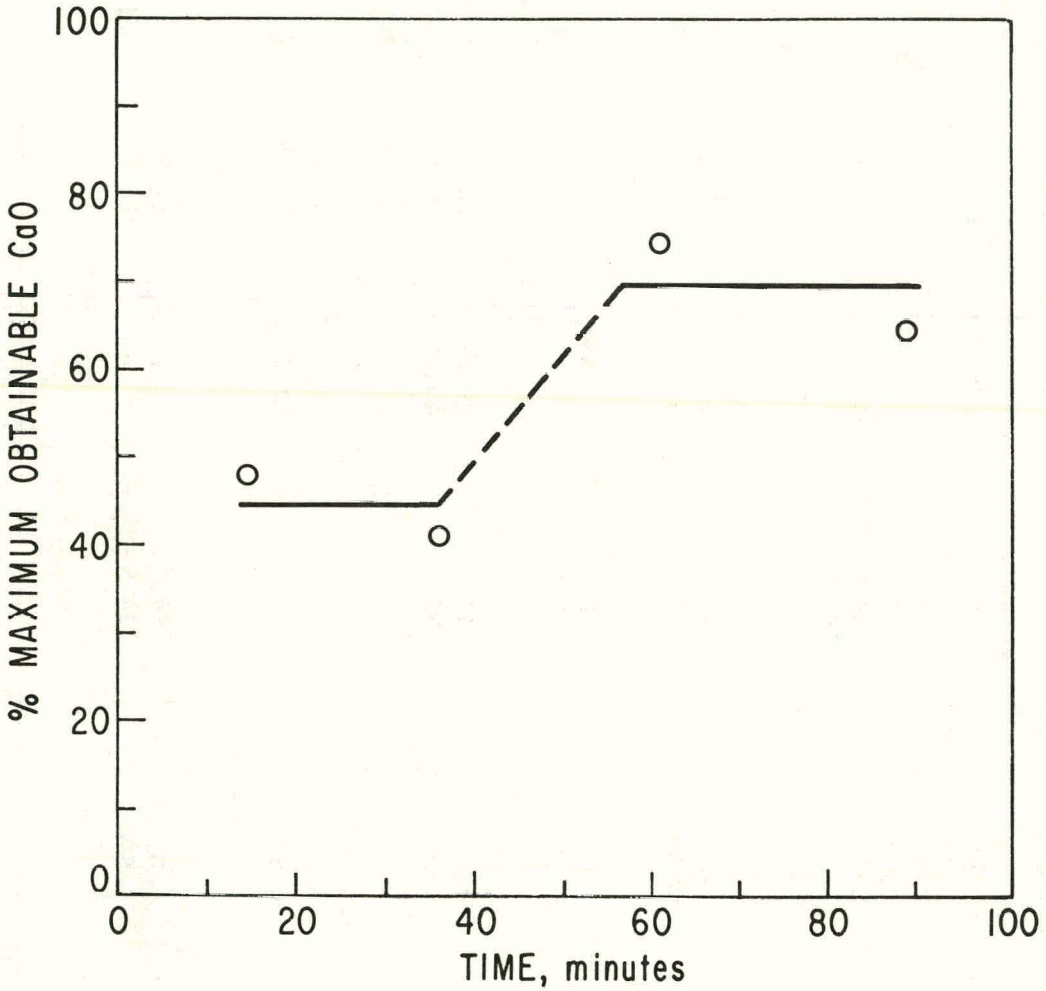

Fig. 45. Percent of Maximum Attainable CaO vs Reaction Time

Stone Adherence

The original dolomite stones are soft and easily fragmented. They are composed of an aggregate of small crystals ranging in size from 30 to 300 microns (1337 dolomite). The X-ray diffraction patterns indicate, however, that finely divided dolomite is also present. The adherence of the stone may be attributed to an intergrowth of the crystals or perhaps to some bonding involving a hydrate.

As reported above in the section on the sulfation reaction, the half-calcined stones develop grains of about the same size as the crystals from which they were derived, but the stones still show adherence. Two sources of bonding may be considered at this stage.

Firstly, the calcite crystallites maintain a preferred orientation relative to the original dolomite crystal[5,6] so that the general shape of the original crystal persists. Observations of the persistence in grain size were based on a microscopic study of a limited number of stones. It is established, however, that the crystallites can be substantially randomized by proper choice of the calcining conditions. Nevertheless, some preferred orientation is always observed. Hence, if this persistence in orientation is assumed, it can be surmised that individual clusters (grains) adhere to other grains by way of van der Waals or other forces.

Second, the presence of alpha-quartz may permit the formation of stable silicates that could act as a cement. There is some merit in this consideration, since in dolomite stones with high alpha-quartz content, the silica can react at high temperatures to form a calcium magnesium silicate. This has been observed in X-ray studies.

Following sulfation, or even on regeneration and sulfation, adherence is still maintained and there is a noticeable hardening of the stones. The hardening is very pronounced in one of the synthetic dolomites. The integrity of the stones is maintained in spite of the very large molecular volume changes taking place during the various reactions. Bonding may arise from the following causes:

i. A $CaSO_4$-CaS eutectic may form. This has been suggested in the literature.[13]

ii. A stable $CaSO_4$ hydrate may form and persist between the grains

iii. A Mg-Ca complex may develop at the interfaces of the grains.

iv. An expitaxial bond may form. M. J. Law *et al.*[7] have carried out an infrared study of the sorption of SO_2 on CaO. This work has led to the identification of $(S_xO_y)^{-n}$ species resulting from polymerization. Although their temperature conditions do not correspond to present TGA operating requirements, the study does suggest that an epitaxial relationship may exist, leading to bonding.

In a number of cases, as shown in Fig. 46, the microscopic studies have revealed the presence of narrow bands around the grains containing the reactants. The bands generally are only a few microns in width and do not lend themselves to study. However, if a reasonably large band does appear, an attempt will be made to remove the material for examination.

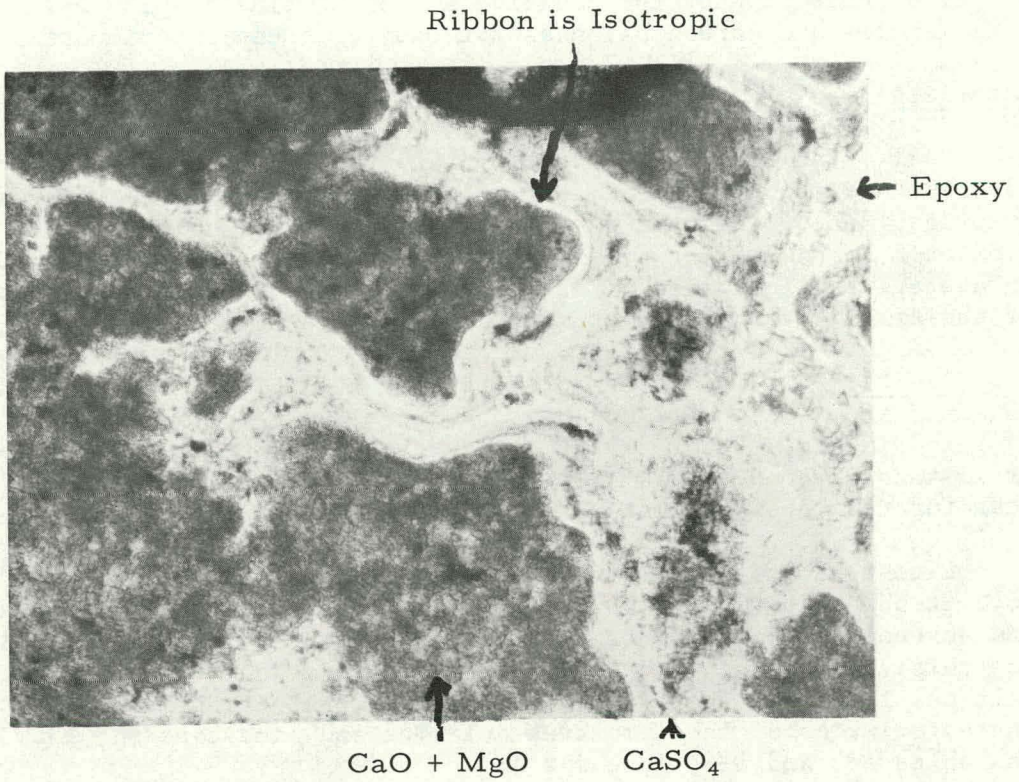

Fig. 46. Thin Section Enlargement (305x) of 1337 Stone in Reduced State, Exhibiting Unidentified Isotopic Bands Surrounding Grains

BENCH-SCALE, PRESSURIZED, FLUIDIZED-BED COMBUSTION EXPERIMENTS

Experiments were performed in the ANL, 6-in.-dia, pressurized fluidized-bed combustor to demonstrate the feasibility and potential of fluidized-bed combustion at elevated pressures (up to 10 atm).

The specific objectives of the experiments were: to evaluate the effect of a higher bed temperature, 1750°F/955°C instead of 1650°F/900°C, on sulfur retention and NO flue gas levels, to compare the sulfur retention capabilities of limestone and dolomite, and to evaluate the effect of excess combustion air on sulfur retention by the additive and on NO flue gas levels. Combustion efficiencies and carbon balances for many of these experiments are reported.

Materials

Coal. The combustion experiments were made with a high-volatile bituminous Pittsburg seam coal from the Consolidation Coal Company Arkwright mine. The coal was fed to the combustor as received. It contained 2.82 wt % S and 7.68 wt % ash and had a heating value of 13,700 Btu/lb and an average particle size of 323 μm. Chemical and physical characteristics of the Arkwright coal are presented in Table A-2, Appendix A.

Additive. A Tymochtee dolomite (∿50 wt % $CaCO_3$ and ∿40 wt % $MgCO_3$) obtained from C. E. Duff and Sons, Huntsville, Ohio, was used in the C- and EA- experiments. Prior to its use in the combustor, the dolomite was air-dried and screened to -14 +100 mesh for the C-experiments and to -14 +30 mesh for the EA-experiments.

Limestone No. 1359 (∿96% $CaCO_3$ and ∿1% $MgCO_3$) obtained from M. J. Grove Co., Stephen City, Va., was used in the LC-experiments. It was air-dried and screened to -14 +100 mesh. In one experiment in which the limestone was calcined to study the effect of precalcination, the size range of the calcined limestone was -14 +45 mesh. Data on the chemical and physical characteristics of the Tymochtee dolomite and limestone No. 1359 are presented in Tables A-3 and A-4, Appendix A.

Bench-Scale Equipment

The experimental equipment and instrumentation consist of a 6-in.-dia, fluidized-bed combustor that can be operated at pressures up to 10 atm, a compressor to provide fluidizing-combustion air, a preheater for the fluidizing-combustion air, peripheral-sealed rotary feeders for metering solids into an air stream entering the combustor, two cyclone separators and two filters in series for solids removal from the flue gas, associated heating and cooling arrangements and controls, and temperature- and pressure-sensing and display devices. A simplified schematic flowsheet of the combustion equipment is presented in Fig. 47.

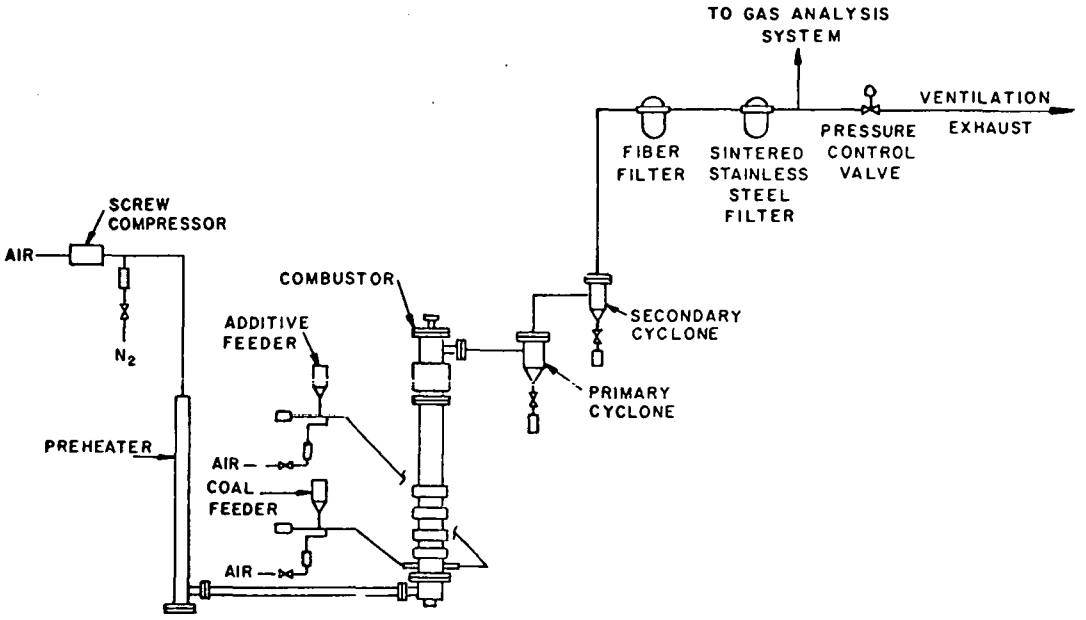

Fig. 47. Simplified Equipment Flowsheet of Bench-Scale Fluidized-Bed Combustor and Associated Equipment.

Details of the fluidized-bed combustor are illustrated in Fig. 48. The reaction vessel consists of a 6-in.-dia, Schedule 40 pipe (Type 316 SS), approximately 11 ft long. The reactor is centrally contained inside a 9-ft section of 12-in.-dia Schedule 10 pipe (Type 304 SS). A bellows expansion joint is incorporated into the outer shell to accommodate differential thermal expansion between the pipes. A bubble-type gas distributor is flanged to the bottom of the inner vessel. Fluidizing-air inlets, thermocouples for monitoring bed temperatures, solids feed lines, and solids removal lines are accommodated by the gas distributor. The coal and additive feed lines extend 2 in. above the top surface of the distributor plate and are angled 20° from the vertical. A constant bed height is maintained in the combustor by use of either a 36-in.- or 48-in.-high standpipe. The 6-in.-dia pipe is alternately wrapped with resistance-type heating elements and cooling coils onto which a layer of heat-conducting copper and then an overlay of oxidation-resistant stainless steel have been applied. Additional cooling capacity is provided by five internal, hairpin-shaped coils that extend down from the flanged top of the combustor to within 12 in. of the top surface of the gas distributor. The coolant is water entrained in air.

Fluidizing-combustion air is supplied by a 75-hp, screw-type compressor capable of delivering 100 cfm at 150 psig. The air can be heated to approximately 1000°F (540°C) in a 6-in.-dia, 10-ft-tall preheater containing eight 2700-watt, clamshell-type heaters.

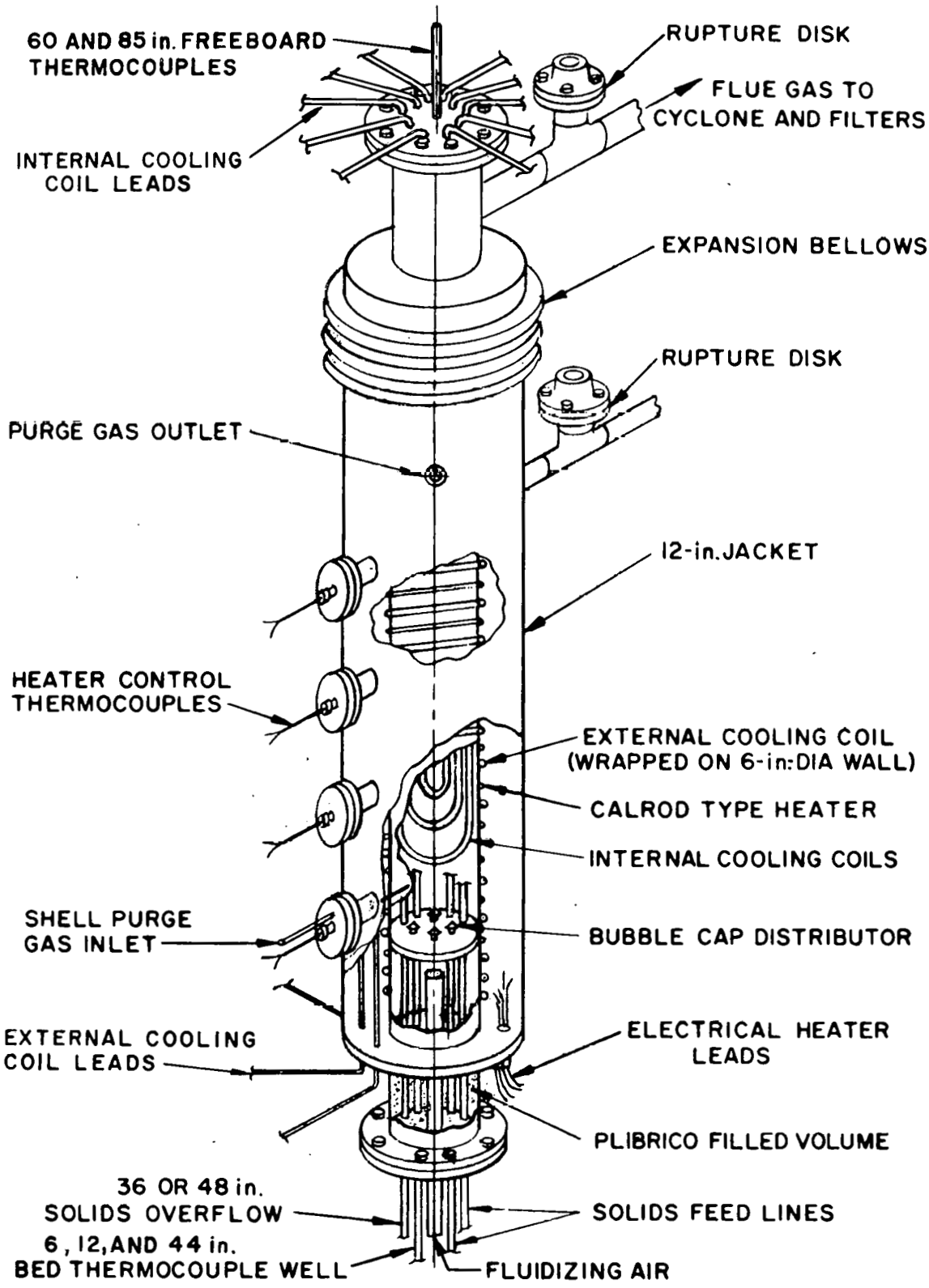

Fig. 48. Details of the 6-in.-dia, Pressurized, Fluidized-Bed Reactor

Coal and either dolomite or limestone additive are pneumatically fed from hoppers to the combustor, using two 10-in.-dia rotary valve feeders. The feeders and hoppers are mounted on platform-type scales.

The flue gas is sampled continuously and is analyzed for the components of primary importance. Continuous determinations of nitrogen oxide, sulfur dioxide, methane, and carbon monoxide are made, using infrared analyzers. Oxygen is also monitored continuously, using a paramagnetic analyzer. Intermittent carbon dioxide analyses of the flue gas are made by gas chromatography. Prior to and during each experiment, the response of each analytical instrument is checked using standard gas mixtures of flue-gas components in nitrogen. Batch samples of the flue gas can be taken and analyzed for components of secondary importance.

The combustion system is equipped with a Hewlett-Packard 2010C data acquisition system to monitor and record temperature, pressure, gas flow, and flue-gas concentration data for subsequent data handling and analysis.

Experimental Procedure

The experimental procedure, although subject to minor variations, was basically as follows: a preweighed amount (~15 kg) of either partially sulfated additive from a previous experiment or fresh unsulfated additive was charged to the reactor to provide an initial bed of material. The starting bed temperature was then raised to about 800°F (430°C) by passing fluidizing air, preheated to between 800-900°F (430-480°C), through the combustor and simultaneously employing the resistance heaters on the combustor wall. Once the bed temperature reached 430°C, the system was brought to the desired operating pressure and coal entrained in a transport air stream was injected into the bed. To prevent the possibility of carbon accumulation in the fluidized bed during startup, coal was initially injected in small, intermittent amounts until ignition and sustained combustion were confirmed by a rapidly increasing temperature and a changing flue-gas composition. Continuous injection of coal was then initiated and the bed temperature was raised to a selected combustion temperature. The bed temperature was maintained by the use of external and internal cooling coils.

Injection of the sulfur-accepting additive was begun when the bed reached operating temperature. The air, coal, and additive feed rates were adjusted to give a specified mole ratio of calcium in the additive to sulfur in the coal, a specified superficial gas velocity, and a specified level of oxygen in the flue gas leaving the combustor. Sulfated additive was removed from the combustor by means of a standpipe to maintain a constant fluidized-bed level.

Experimental Results and Discussion

Effect of Bed Temperature of 955°C on Sulfur Retention and NO Flue-Gas Level. Combustion experiments designed to measure the effect of a higher combustor temperature (955°C/1750°F) on the sulfur retention capability of dolomite and limestone and on the NO level in the flue gas

were performed. BET surface area measurements were made for -25 +35 mesh Tymochtee dolomite and limestone No. 1359. Dolomite in the air-dried, half-calcined ($CaCO_3 \cdot MgO$), and fully calcined ($CaO \cdot MgO$) states had surface areas of 2.14, 4.05, and 8.23 m^2/g, respectively. Limestone in the air-dried and fully calcined (CaO) states had surface areas of 0.35 and 3.56 m^2/g. At 955°C and at the CO_2 partial pressure present in the bed, the $CaCO_3$ in the additive calcines (see Table 8 for carbonate contents of spent additives), larger internal openings in the additive result, and an increase in sulfur retention capability is possible. In these experiments, Arkwright coal was combusted. Tymochtee dolomite in the C-experiments and limestone No. 1359 in the LC-experiments were used to retain the SO_2. The results for these experiments are given in Table 8. All experiments were done at a pressure of eight atmospheres, a gas velocity of 3.5 ft/sec, and with $\sim$3% O_2 in the flue gas. In experiment C-2, a sulfur retention of 96% was obtained with a SO_2 concentration of 80 ppm in the dry flue gas. The operating temperature and dry flue gas analysis are given in Fig. 49. Using the numerical correlation of the VAR-series (Ref. 14, p. 33) of experiments which were performed at temperatures of 790-900°C/1450-1650°F and in which only half-calcination of the Tymochtee dolomite is thought to have occurred, a sulfur retention of 89% with a SO_2 concentration of 240 ppm in the flue gas was predicted.

Experiment C-3A was performed at a Ca/S mole ratio near unity and a temperature of 955°C to further investigate the temperature effect. Because the initial bed of this experiment was the final bed of experiment C-2, it was found that three hours was sufficient time to reach steady state (*i.e.*, constant SO_2 concentration in the flue gas) at which time experiment C-3A was terminated. The experimental results for C-3A are given in Table 8. The SO_2 concentration in the dry flue gas was 300 ppm, which corresponds to a total sulfur retention of 87%. The predicted SO_2 effluent concentration based on the numerical correlation of the VAR-experiments was 420 ppm, which corresponds to a sulfur retention of only 82%. At these Ca/S mole ratios and a temperature of 955°C, the fully calcined dolomite additive has a greater SO_2 retention capability than the projected value based on the half-calcined Tymochtee dolomite experiments.

Experiment C-3B (see Table 8) was performed under conditions similar to those used in experiment C-3A with the exception of bed temperature, 900°C. At this temperature and with $\sim$15% CO_2 in the dry flue gas, the $CaCO_3$ in the dolomite additive does not fully calcine. As expected, the measured SO_2 concentration in the dry flue gas of 375 ppm (sulfur retention of 82%) for experiment C-3B was very close to the predicted value of 355 ppm, which is based on the VAR experiments for half-calcined dolomite. At 900°C and $\sim$15% CO_2 in the dry flue gas, the $CaCO_3$ should not calcine extensively. The carbonate contents of the sulfated dolomite from C-2 and C-3 (a 900°C experiment) are given in Table 8.

The effect of calcination on sulfur retention in a fluidized-bed coal combustor was also tested with limestone No. 1359 additive. In experiment LC-1, limestone No. 1359 and Arkwright coal were simultaneously fed to the combustor at rates that corresponded to a Ca/S mole ratio of 1.8. The bed temperature was 955°C. Because this limestone feed rate ($\sim$4 lb/hr)

Table 8. Operating Conditions and Flue-Gas Analysis for Coal Combustion Experiments to Test the Effect of Temperature on Sulfur Retention by Limestone No. 1359 and Tymochtee Dolomite.

Equipment: 6-in.-dia, pressurized fluidized-bed combustor
Gas Velocity, ft/sec: 3.5
Pressure, psig: 105

Experiment	Additive	Run Time, hr	Ca/S Mole Ratio	Bed Temp, °C	Carbonate in Sulfated Additive, %	Experimental/Predicted[a] SO_2 Flue-Gas Concentration, ppm	Experimental/Predicted[a] Sulfur Retention, %	Flue-Gas Analysis NO, ppm	Flue-Gas Analysis O_2, %
C-2	dolomite	13	1.5	955	0.2	80/240	96/89	135	3.0
C-3A	dolomite	3	1.1	955	--	300/420	87/82	130	2.8
C-3B	dolomite	7	1.2	900	--	375/355	82/83	130	3.0
C-3C	dolomite	2.3	0.8	900	4.4	515/[b]	75/[b]	130	3.0
LC-1	limestone	11	1.8	955	0.7	675/[c]	72/[c]	84	2.9
LC-2A	limestone	3.5	1.4	955	0.7	900/[c]	63/[c]	110	2.8
LC-3A	limestone	7	1.5	900	14	920/[c]	62/[c]	95	2.9
LC-5	limestone	9.5	1.4	900	20	1000/[c]	56/[c]	93	3.2

[a] Predicted values based on empirical correlation of SO_2 flue-gas levels observed for combustion experiments with half-calcined dolomite.

[b] This is beyond the range of the empirical correlation from the VAR-series.

[c] No correlation has yet been obtained for limestone experiments.

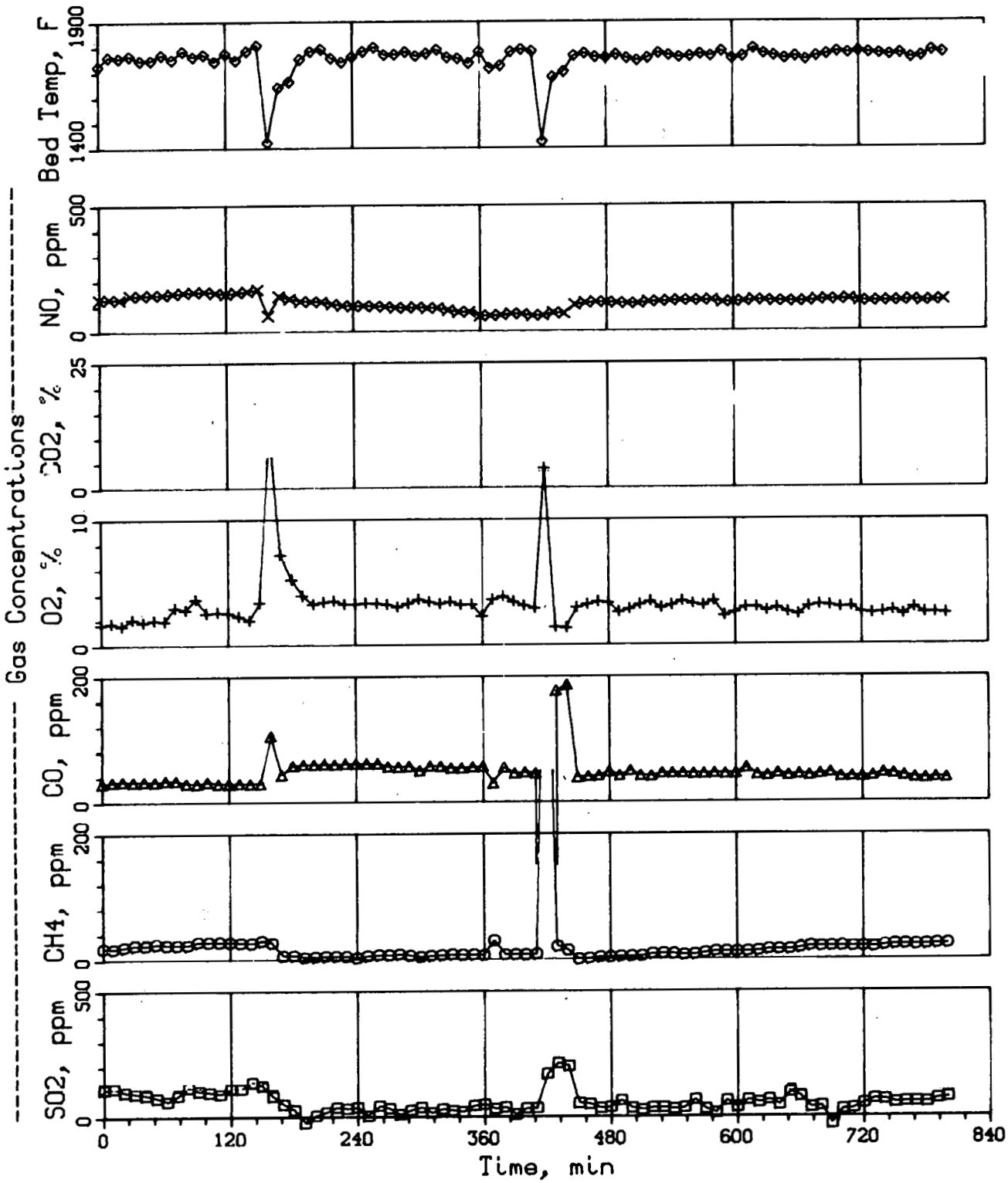

Fig. 49. Bed Temperature and Gas Concentrations in Flue Gas, Experiment C-2

was below the minimum feed-rate capacity of the additive feeder, the additive was fed semicontinuously to the combustor. The duration of this experiment was 11 hr. At quasi-steady state, the average SO_2 concentration in the dry flue gas was 675 ppm and the average NO concentration was 84 ppm. The total sulfur retention was 72%. These results are given in Table 8. The operating temperature and the dry flue gas analysis for the duration of LC-1 are plotted in Fig. 50.

Another shorter experiment, LC-2A, was completed with limestone No. 1359 at 955°C. Because the initial bed in this experiment was the final bed of LC-1, the experimental time required to reach steady state was shorter. Experiment LC-2A was performed with a Ca/S mole ratio of ∿1.4, and the other experimental conditions were equal to those of experiment LC-1. The low mass feed rate of the limestone again made the feed rate difficult to control. The quasi-steady state average SO_2 concentration in the dry flue gas was 900 ppm, which corresponds to a sulfur retention of 63%.

Experiment LC-3A was performed at a Ca/S mole ratio of 1.5 and a nominal combustor temperature of 900°C. The coal was burned in a fluidized bed of uncalcined limestone No. 1359. The steady state duration of this experiment was seven hours. The operating temperature and flue-gas analysis data are plotted in Fig. 51. In experiment LC-3A, a total sulfur retention of 62% was obtained and the SO_2 concentration in the dry flue gas was 920 ppm. This may be compared with the results of experiment LC-2A (performed at a combustor temperature of 955°C and a Ca/S mole ratio of 1.4) in which the total sulfur retention was 63% and the SO_2 concentration in the dry flue gas was 900 ppm. The results at 900°C and 955°C are not noticeably different. The effect of higher temperature and/or calcination of the $CaCO_3$ has less effect on the extent of sulfation in the limestone additive than on the sulfation of the dolomite. The carbonate concentrations of the sulfated limestone additives from the above LC-experiments are given in Table 8.

An additional experiment (LC-5) using precalcined limestone feed was performed at a bed temperature of 900°C and a Ca/S mole ratio of 1.4. Limestone No. 1359 for this experiment was precalcined at atmospheric pressure and 815°C in the 6-in.-dia combustor during the combustion of kerosene, a low-sulfur fuel. Table 9 presents the sieve analysis and the carbonate contents for the calcined limestone that was used for experiment LC-5 and for the uncalcined limestone that was used for the remaining LC-experiments. The average additive feed particle diameter for the precalcined limestone was 850 microns, as compared with 700 microns for the uncalcined feed limestone. Operating data for this experiment are shown in Fig. 52. A total sulfur retention of 56% was obtained, and the SO_2 concentration observed in the dry flue gas was 1000 ppm. A comparison of the results for experiments LC-5 and LC-3A shows a small detrimental effect on sulfur retention in the precalcined experiment (LC-5). The difference in sulfur retention can be attributed to the fact that larger additive particles were used in LC-5. Larger additive particles do not sulfate as well as smaller ones.

The NO concentration in the flue gas remained almost constant (∿100 ppm) for all LC-experiments.

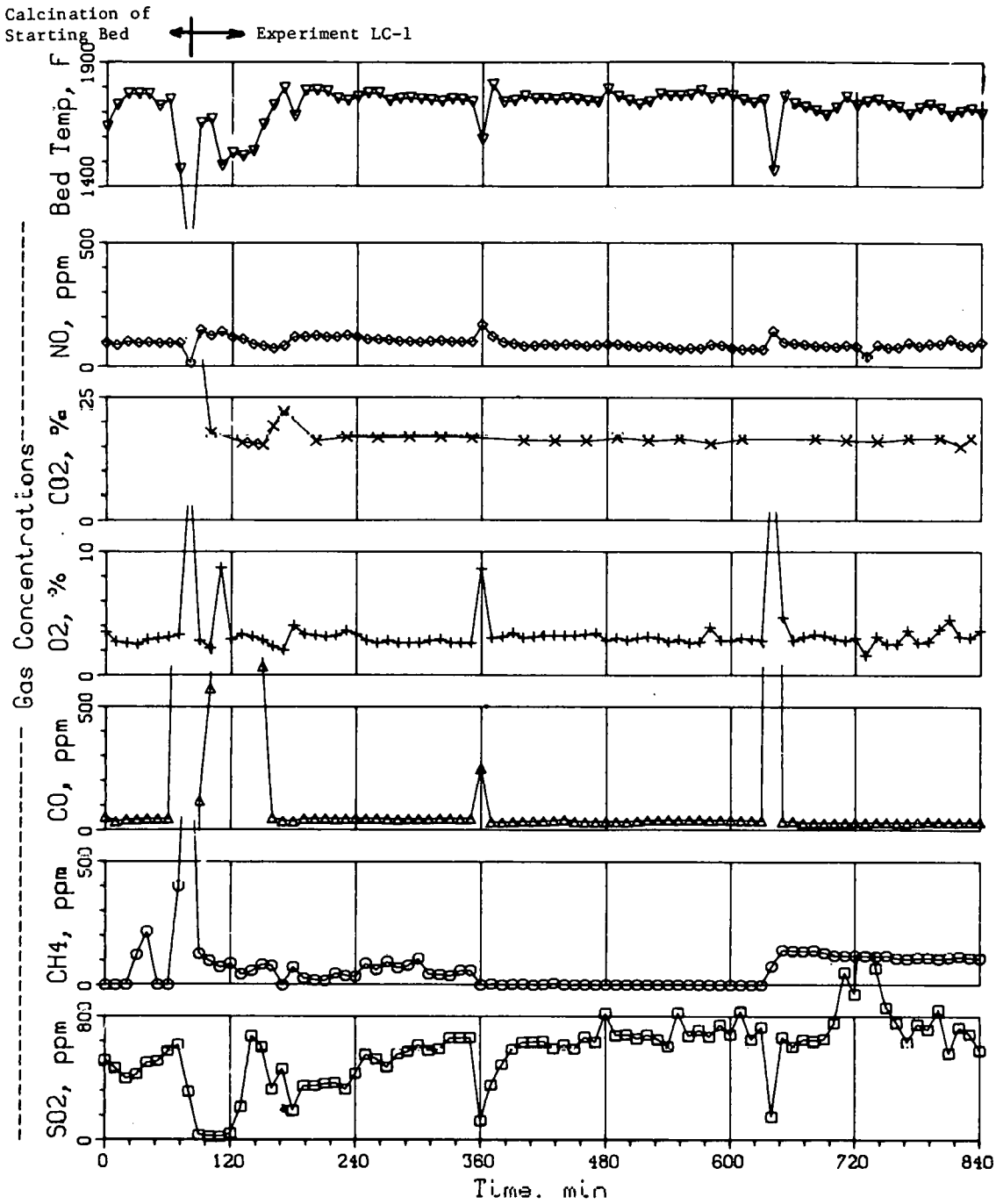

Fig. 50. Bed Temperature and Gas Concentrations in Flue Gas, Experiment LC-1

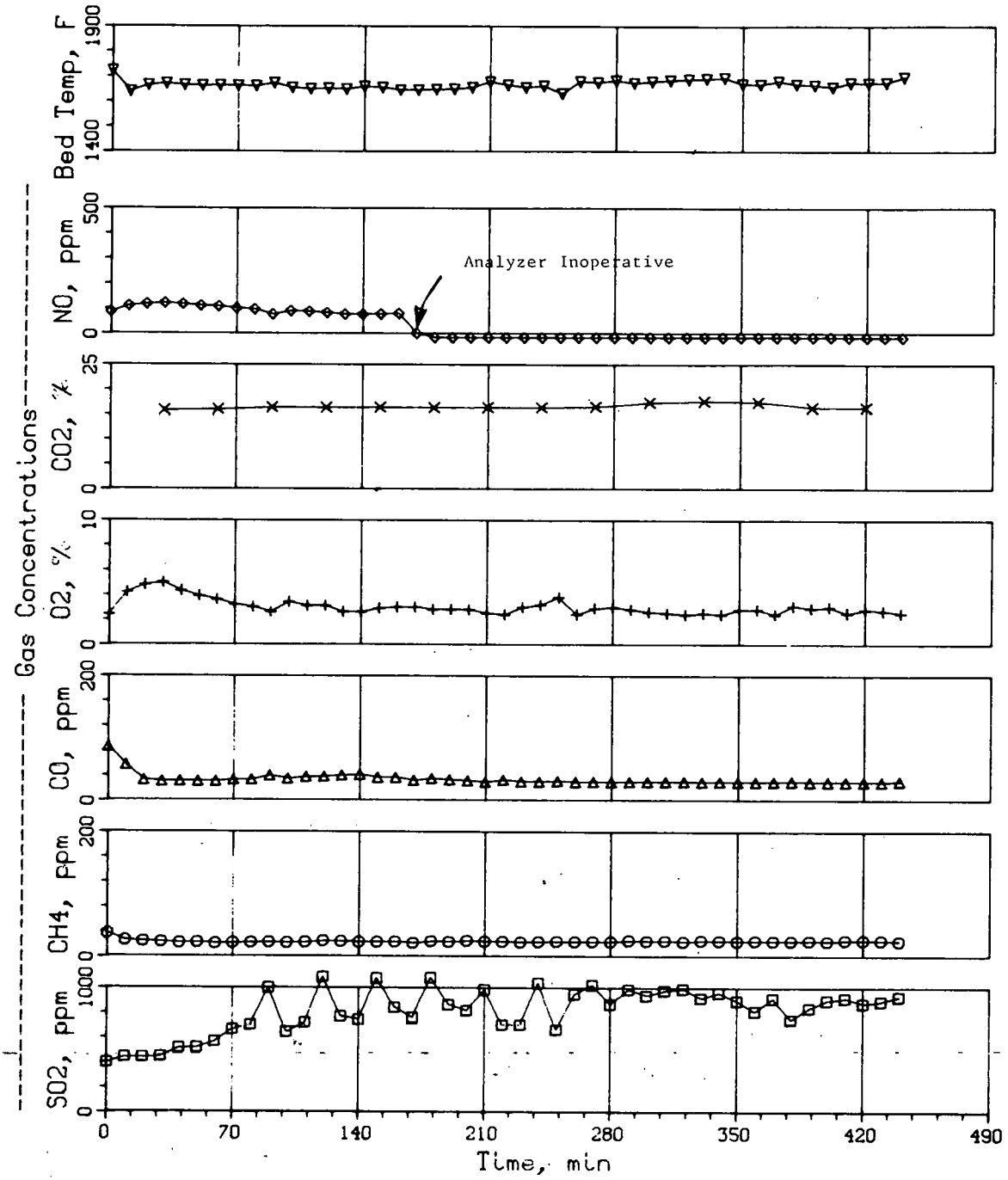

Fig. 51. Bed Temperature and Gas Concentrations in Flue Gas, Experiment LC-3A

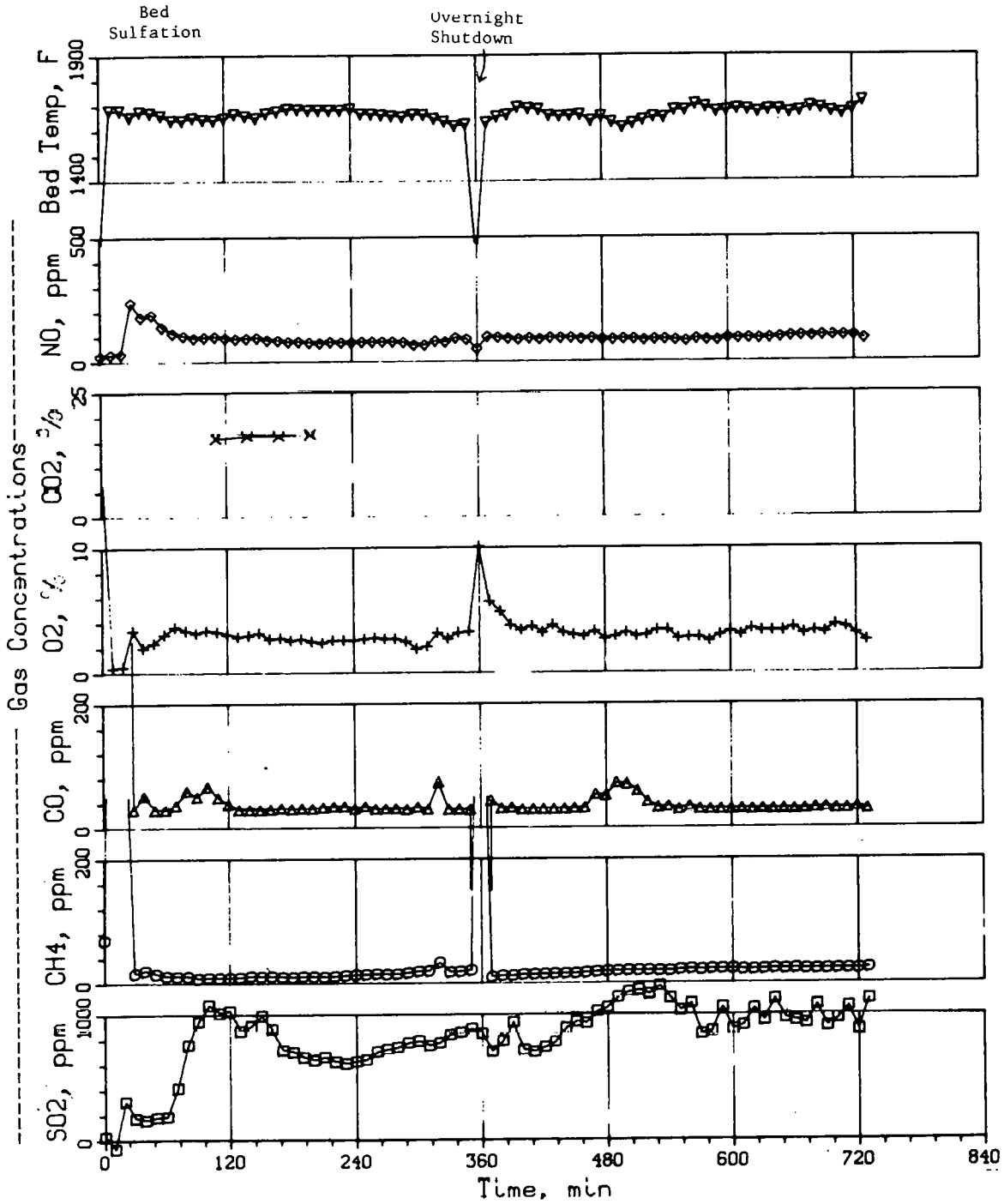

Fig. 52. Bed Temperature and Gas Concentrations in Flue Gas, Experiment LC-5

Table 9. Composition and Particle-Size Range of Calcined and Uncalcined Limestone No. 1359 in Experiment LC-5

	Composition	
	Uncalcined	Calcined
	95% $CaCO_3$ 0.95% $MgCO_3$	85% CaO 8.9% $CaCO_3$ 0.6% MgO
Particle-Size Range, U.S. Sieve Size	Uncalcined, wt %	Calcined, wt %
+14	0	0
-14 +25	46	56
-25 +35	16	37
-35 +45	15	6
-45	22	1
Mean Particle Diameter, μm	700	850

The limestone feed rate range for the above LC-experiments was 2 to 4.5 lb/hr. These rates are less than the minimum continuous feed rate of the additive feeder; hence, additive was fed semicontinuously to the combustor.

Comparison of the Sulfur Retention Capability of Limestone and Dolomite. A series of experiments to compare the sulfur retention capability of limestone with that of dolomite was completed. The results of some of these experiments are presented above.

Experiment LC-2B was designed specifically to compare the sulfur retention capability of limestone No. 1359 with that of an earlier experiment (C-2) with Tymochtee dolomite on an equal mass-feed basis. The experimental conditions were the same for both experiments and included a combustor temperature of 955°C and a mass feed rate of 7.7 lb/hr. The operating temperature and flue-gas analysis data for LC-2B are plotted in Fig. 53. A total sulfur retention of 77% was obtained with the limestone additive in LC-2B, as compared with a sulfur retention of 96% obtained with the dolomite additive in experiment C-2. These results are given in Table 10, along with those previously given for experiment C-2.

Experiments LC-1, LC-2A, LC-3A, LC-5, and LC-2B were performed to compare the sulfur retention capability of limestone No. 1359 to Tymochtee dolomite on a molar-feed basis. None of these experiments were performed with a high mass-feed rate.

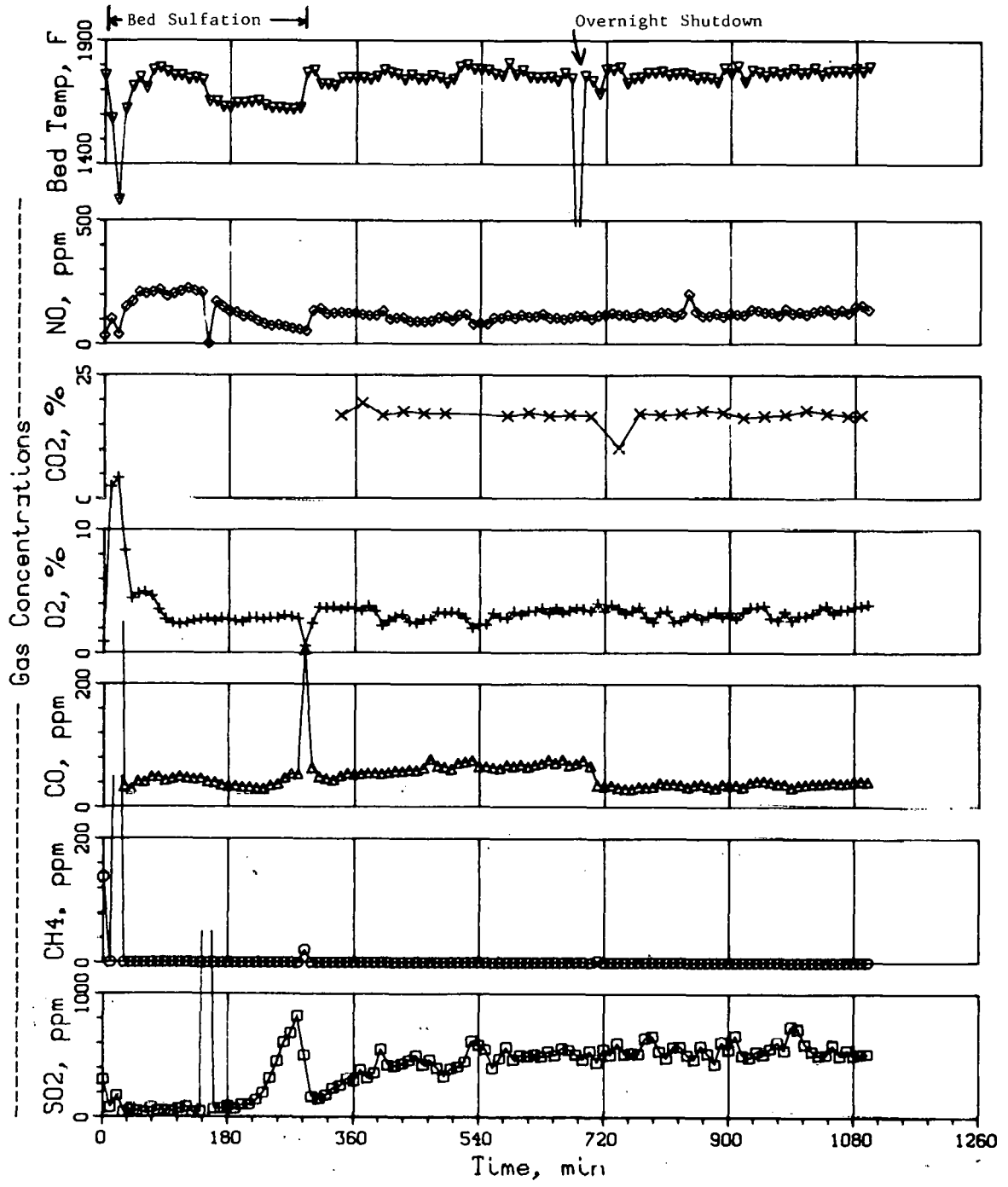

Fig. 53. Bed Temperature and Gas Concentrations in Flue Gas, Experiment LC-2B

Table 10. Operating Conditions and Flue-Gas Analysis for Experiments LC-2B and C-2 (Which Compare the Sulfur Retention Capabilities of Limestone and Dolomite) and Experiment LC-6.

Combustor: ANL, 6-in.-dia
Bed Temp, °C: 955
Pressure, psig: 105
Gas Velocity, ft/sec: 3.5
Additive size range, mesh: -14 +100

Exp.	Additive	Additive Mass Feed Rate, lb/hr	Run Time, hr	Ca/S Mole Ratio	Sulfur Retention, %	Flue-Gas Analysis		
						SO_2, ppm	NO, ppm	O_2, %
LC-2B	Limestone No. 1359	7.7	12	2.7	77	500	130	3.2
C-2	Tymochtee Dolomite	7.7	13	1.5	96	80	135	3.0
LC-6	Limestone No. 1359	11.3	8	4.0	85	335	150	3.1

Experiment LC-6 with limestone No. 1359 and Arkwright coal was performed at a high mass additive feed rate (11.3 lb/hr) to test the limiting sulfur retention capability of limestone at low additive utilization conditions. This feed rate corresponds to a Ca/S mole ratio of 4. The experiment was performed at 955°C. A total sulfur retention of 85% was obtained (Table 10); the SO_2 concentration and NO concentration in the dry flue gas were 355 and 150 ppm, respectively. The flue gas analysis for the duration of the experiment is plotted in Fig. 54.

The total sulfur retention obtained from all the experiments with limestone and dolomite additives which were performed in the C-series and the LC-series have been plotted in Fig. 55 on a molar-feed (Ca/S mole ratio) basis and in Fig. 56, on a mass-feed (lb additive/lb sulfur) basis. At 955°C, the sulfur retention capability of Tymochtee dolomite was superior to that of limestone No. 1359 on both a molar-feed and a mass-feed basis. At higher mass-feed rates, the difference between the sulfur retention capabilities of dolomite and limestone was further accentuated (Fig. 56). The difference in retention is probably due to the formation of a more impervious sulfate layer on the limestone additive.

At 955°C the NO concentration in the dry flue gas ranged from 130 to 135 ppm for the C-series experiments (using dolomite) and from 84 to 150 ppm for the LC-series (using limestone). The additive type does not seem to affect NO emission from a fluidized coal combustor at the experimental conditions used.

Effect of Excess Combustion Air on Sulfur Retention and Flue-Gas NO Level. In fluidized-bed combustion studies conducted by Westinghouse,[15] pressurized combustor systems coupled with the use of combined power cycles (steam and gas turbines) were found to increase the overall plant efficiency (ratio of electric power to coal energy) above that of conventional power plants and atmospheric fluidized-bed systems. A variety of operating schemes (varying the ratio of power generated by gas turbines to that generated by steam turbines) has been proposed. It is highly possible that amounts of air greater than those normally used for combustion (~17% excess air) will be required in these systems.

To test the effect on SO_2 retention and flue-gas NO level of various excess-air combustion conditions, the EA-series of experiments was performed. These experiments were designed to test the effect of Ca/S mole feed ratio on sulfur retention at different excess air combustion conditions. Most of the operating conditions remained constant for all EA-experiments and are given in Table 11. Experiments were all performed at 900°C, a pressure of 8 atm absolute, and a nominal gas velocity of 4.5 ft/sec. Arkwright coal was combusted, and Tymochtee dolomite additive (-14 +30 mesh) was used. The percent excess air was varied between experiments by varying the feed rate of coal with a constant gas feed rate. The nominal height of the fluidized bed for these experiments was 3 ft.

Experiment EA-4 was designed to find the highest excess-air conditions that could be maintained in the 6-in.-dia pressurized combustor at a fixed fluidizing-gas velocity. At high excess-air conditions, the energy released

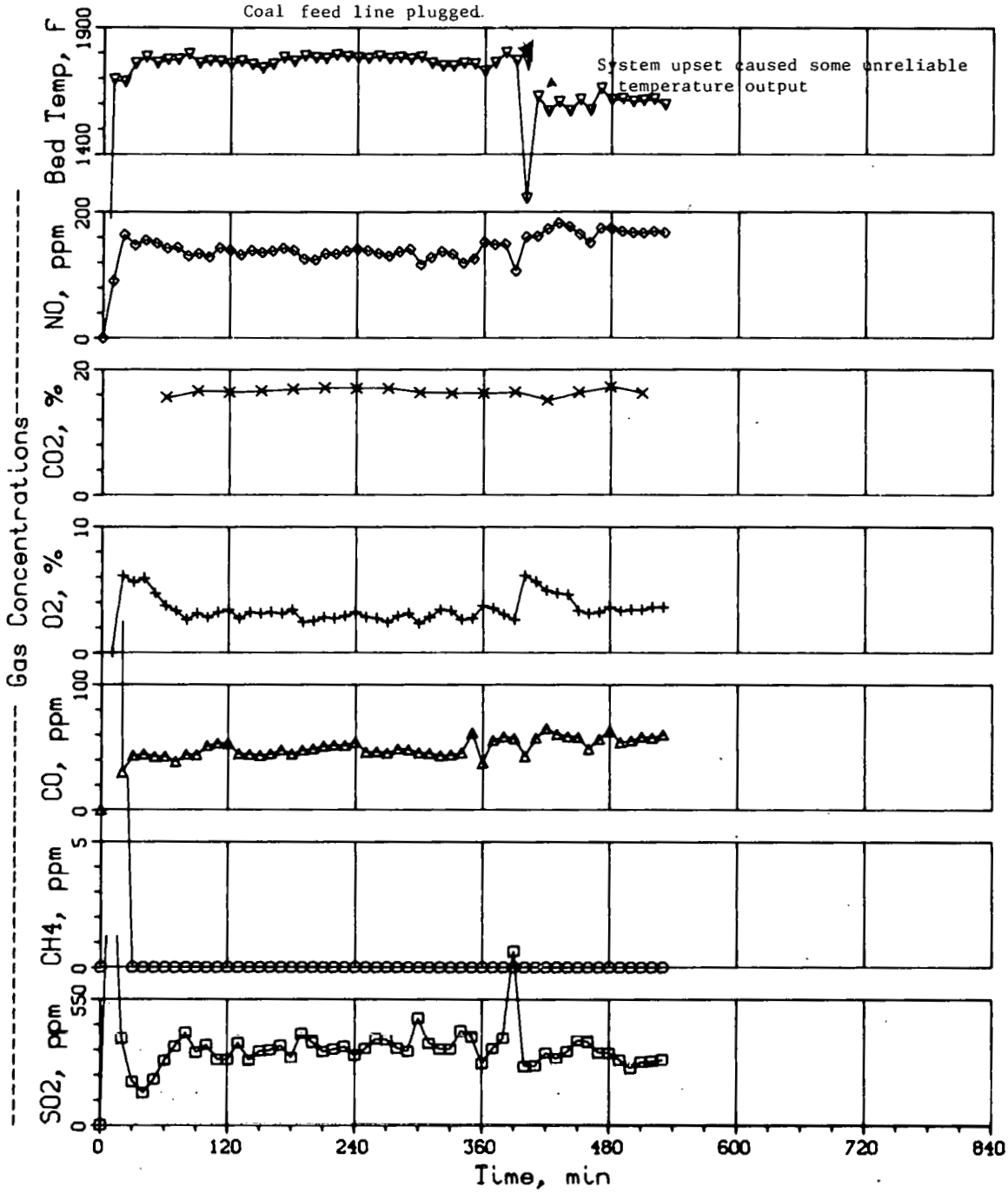

Fig. 54. Bed Temperature and Gas Concentrations in Flue Gas, Experiment LC-6

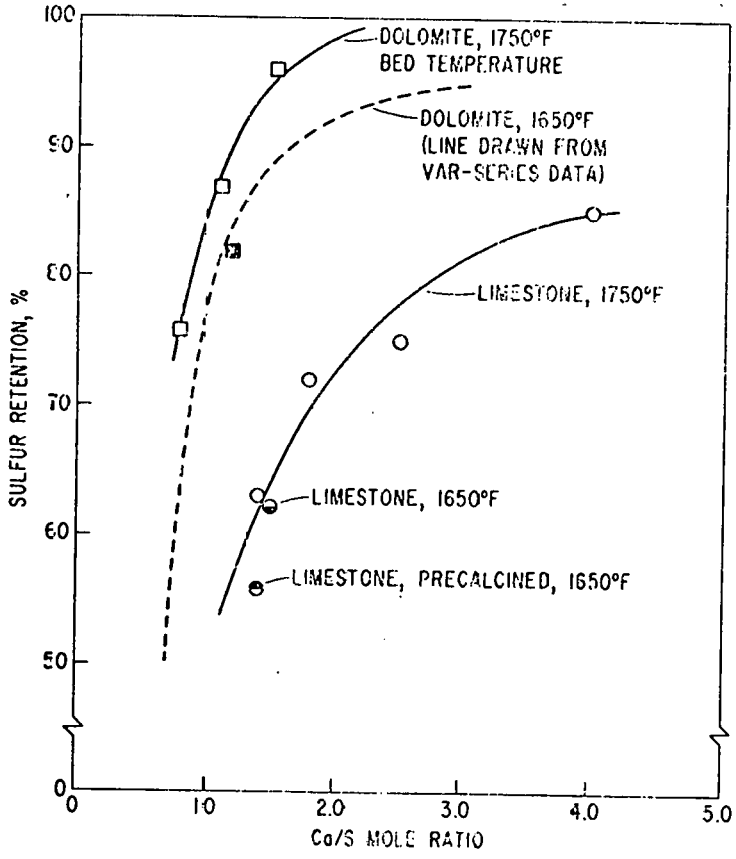

Fig. 55. Comparison of the Sulfur Retention Capabilities of Tymochtee Dolomite and 1359 Limestone on a Molar Feed Basis at 955°C

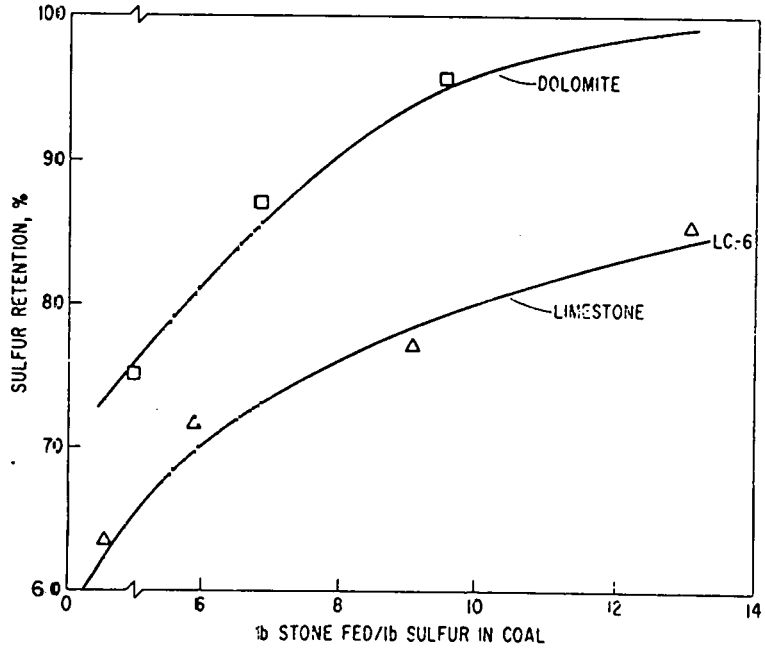

Fig. 56. Comparison of the Sulfur Retention Capabilities of Tymochtee Dolomite and 1359 Limestone on a Mass Feed Basis at 955°C

Table 11. Operating Conditions and Flue-Gas Analysis for Coal Combustion Experiments Designed to Test the Effect of Excess-Air Combustion Conditions.

Bed Temp, °C: 900
Pressure, psig: 105
Nominal Gas Velocity, ft/sec: 4.5

Coal: Arkwright
Additive: Tymochtee Dolomite (-14 +30 mesh)

Exp.	Run Time, hr	Excess Air, %	Air Feed Rate, cfm[a]	Coal Feed Rate, lb/hr	Ca/S Mole Ratio	Sulfur Retention, %	Flue-Gas Analysis			
							SO_2, lb/10^6 Btu	SO_2, ppm	O_2, %	NO, ppm
EA-1	14	17	98	42.8	1.4	83	0.70	392	3.1	160
EA-3	12	44	96	34.3	1.1	76	0.98	448	6.0	b
EA-2	12	44	98	32.5	1.4	71	1.2	512	6.4	211
EA-8	6.5	44	98	34.8	1.9	86	0.58	265	6.1	182
EA-5	6	44	95	33.3	2.9	93	0.28	128	6.0	215
EA-4	15	75	98	23.1	1.3	57	1.78	570	8.6	245
EA-9	10	75	98	27.7	1.5	86	0.57	206	8.9	180
EA-6	8	75	98	27.8	2.1	93	0.26	112	9.3	266
EA-7	6	75	96	30.3	2.9	92	0.32	120	8.5	190

[a] cfm at 70°F and 1 atm

[b] NO analyzer not working properly

by coal combustion per cubic foot of fluidized bed is less than it would be at low excess-air conditions (3% O_2 in the dry flue gas). Heat removal from the combustor by the cooling water was minimized to determine the highest permissible excess-air conditions in this experiment. Only sufficient coolant to maintain a safe-operating wall temperature of less than 1200°F (650°C) (design temperature) was circulated at the combustor wall. For the operating conditions given in Table 11, the highest possible percent excess air in the 6-in.-dia pressurized combustor was found to be 75%. Experiment EA-4 was performed at this condition. (Combustors with refractory liners can be operated at higher excess-air levels because heat losses are smaller.) The flue-gas analysis and the nominal fluidized-bed temperature for the duration of experiment EA-4 are presented graphically in Fig. 57.

The results for all EA-experiments are given in Table 11. In experiment EA-4, with 75% excess air, a total sulfur retention of 57% was obtained; the sulfur dioxide concentration in the dry flue gas was 570 ppm and the oxygen concentration was 8.6%. In experiment EA-2, with 44% excess air, the total sulfur retention increased to 71%, but the sulfur dioxide concentration in the dry flue gas did not change markedly; the SO_2 concentration in the dry flue gas was 512 ppm and the oxygen concentration was 6.4%. Experiment EA-1 was performed at the normal excess-air conditions of 17% (3% O_2 in the dry flue gas). The total sulfur retention was 83%, and the sulfur dioxide concentration in the dry flue gas was 392 ppm. The predicted total sulfur retention from the empirical correlation of past experiments (VAR-series) is 85% for EA-1. In the current EA-series of experiments, the nominal size distribution of the dolomite was -14 +30 in comparison to a nominal size distribution of -14 +100 mesh in the VAR-series of experiments.[14] The slightly lower sulfur retention found in EA-1 probably resulted from the use of coarser dolomite particles. The extent of sulfation is greater for smaller dolomite particles.

Experiments EA-3, EA-5, and EA-8 were performed to test the effect of Ca/S mole ratio on sulfur retention at a fixed excess combustion air value of 44%. Calcium to sulfur mole ratios of 1.1 and 2.9 were used for experiments EA-3 and EA-5, respectively. The experimental conditions and the results for these experiments are given in Table 11. A sulfur retention of 76% was obtained in experiment EA-3. This retention is unexpectedly slightly higher than that obtained for EA-2, which was performed at a Ca/S mole ratio of 1.4. The SO_2 content of the exhaust gas from EA-3 was 0.98 $lb/10^6$ Btu, close to the EPA standard of 1.2 $lb/10^6$ Btu. In experiment EA-5, the total sulfur retention was 93% and the SO_2 content of the dry flue gas was 0.28 $lb/10^6$ Btu. The operating temperature and flue gas analysis data for EA-3 and EA-5 are plotted in Fig. 58 and 59, respectively. Experiment EA-8 was performed with a Ca/S mole ratio of 1.9; a total sulfur retention of 86% was obtained. The operating temperature and flue gas analysis for EA-8 are plotted in Fig. 60.

Experiments EA-9, -6, and -7 were performed with Ca/S mole feed ratios of 1.5, 2.1, and 2.9, respectively, and an excess combustion air condition of 75%. Sulfur retentions were 86% for EA-9, 93% for EA-6, and 92% for EA-7. The bed temperatures and flue gas compositions during these three experiments are plotted in Fig. 61, 62, and 63.

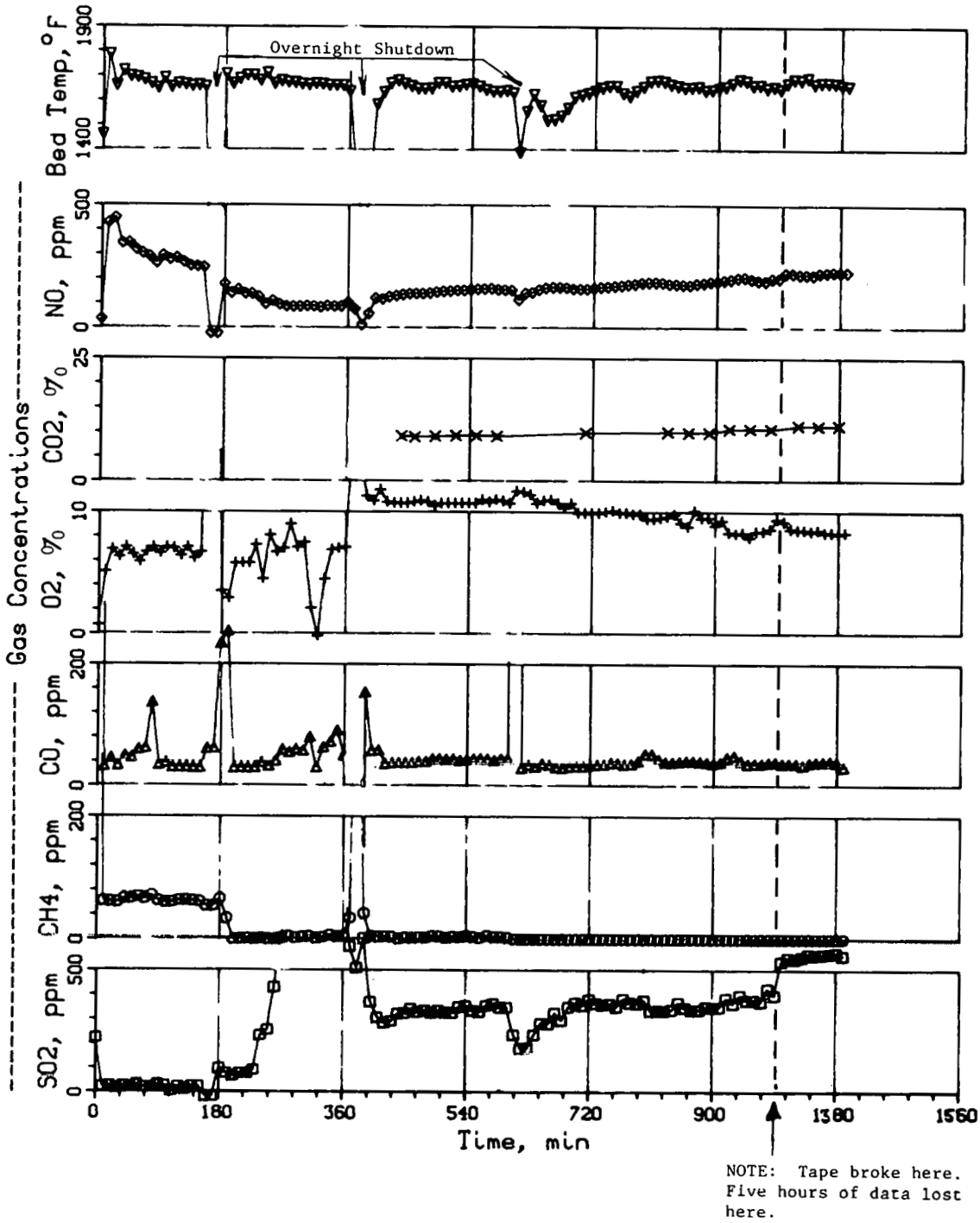

Fig. 57. Bed Temperature and Gas Concentrations in Flue Gas, Experiment EA-4

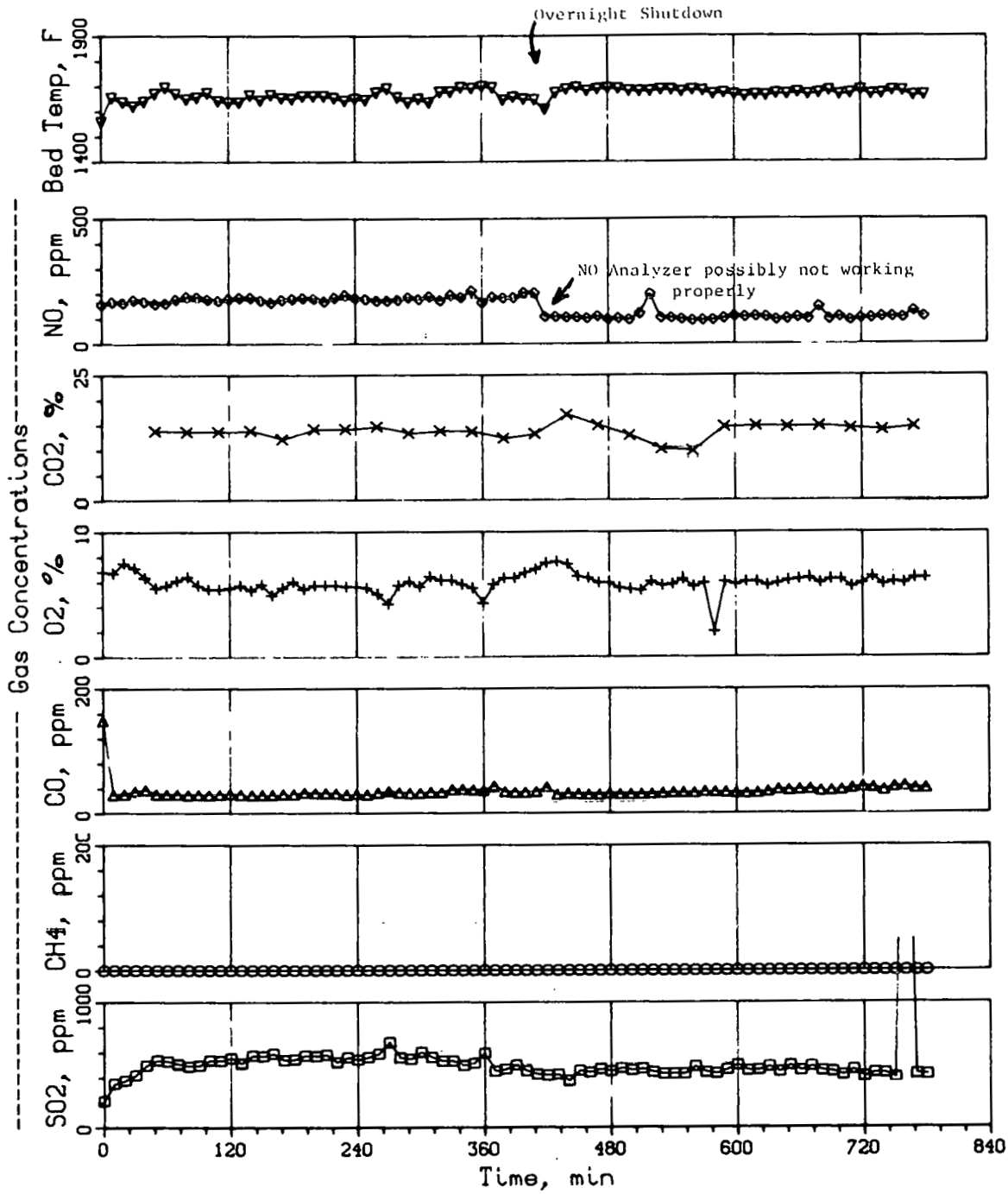

Fig. 58. Bed Temperature and Gas Concentrations in Flue Gas, Experiment EA-3

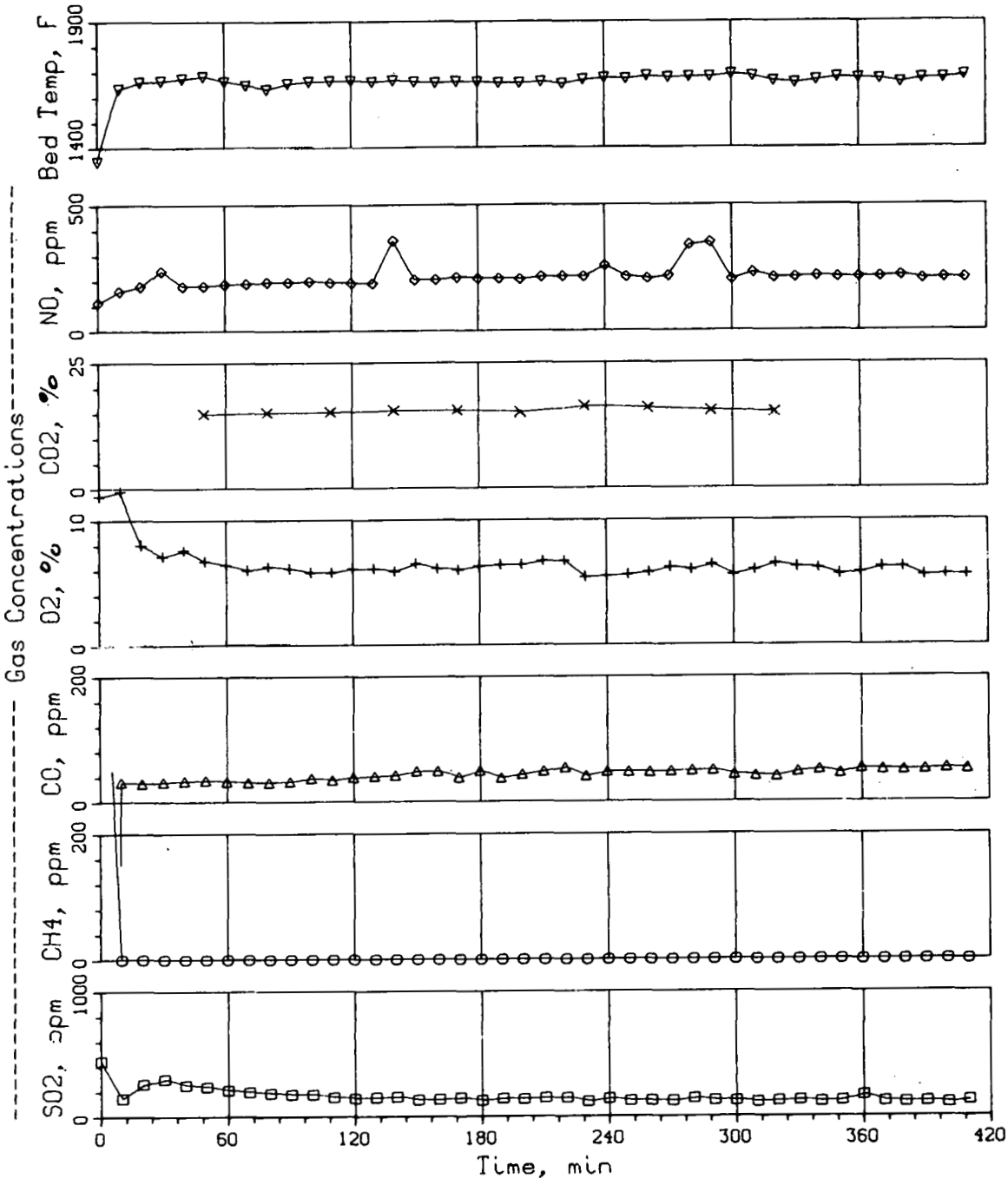

Fig. 59 . Bed Temperature and Gas Concentrations in Flue Gas, Experiment EA-5

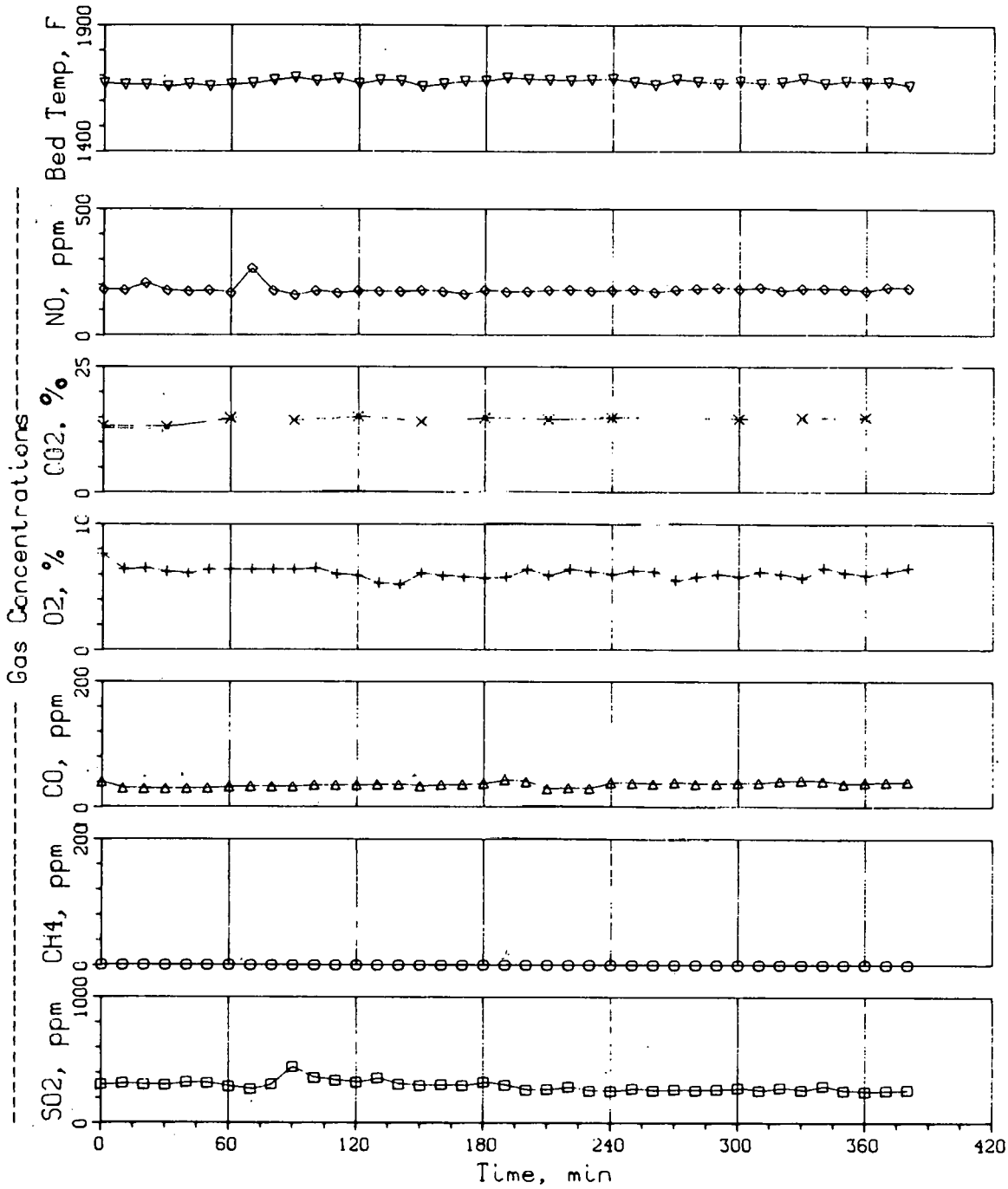

Fig. 60. Bed Temperature and Gas Concentrations in Flue Gas, Experiment EA-8

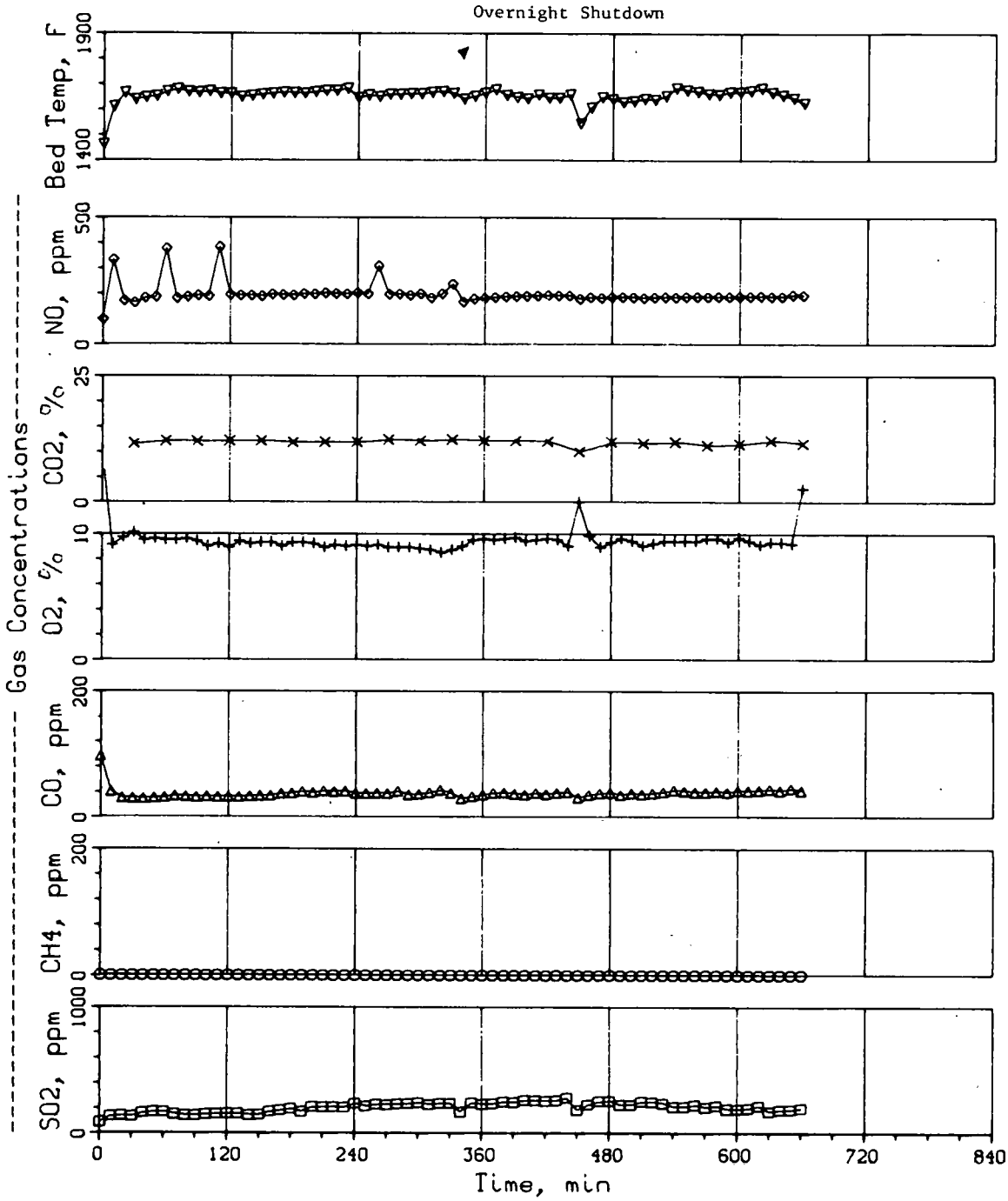

Fig. 61. Bed Temperature and Gas Concentrations in Flue Gas, Experiment EA-9

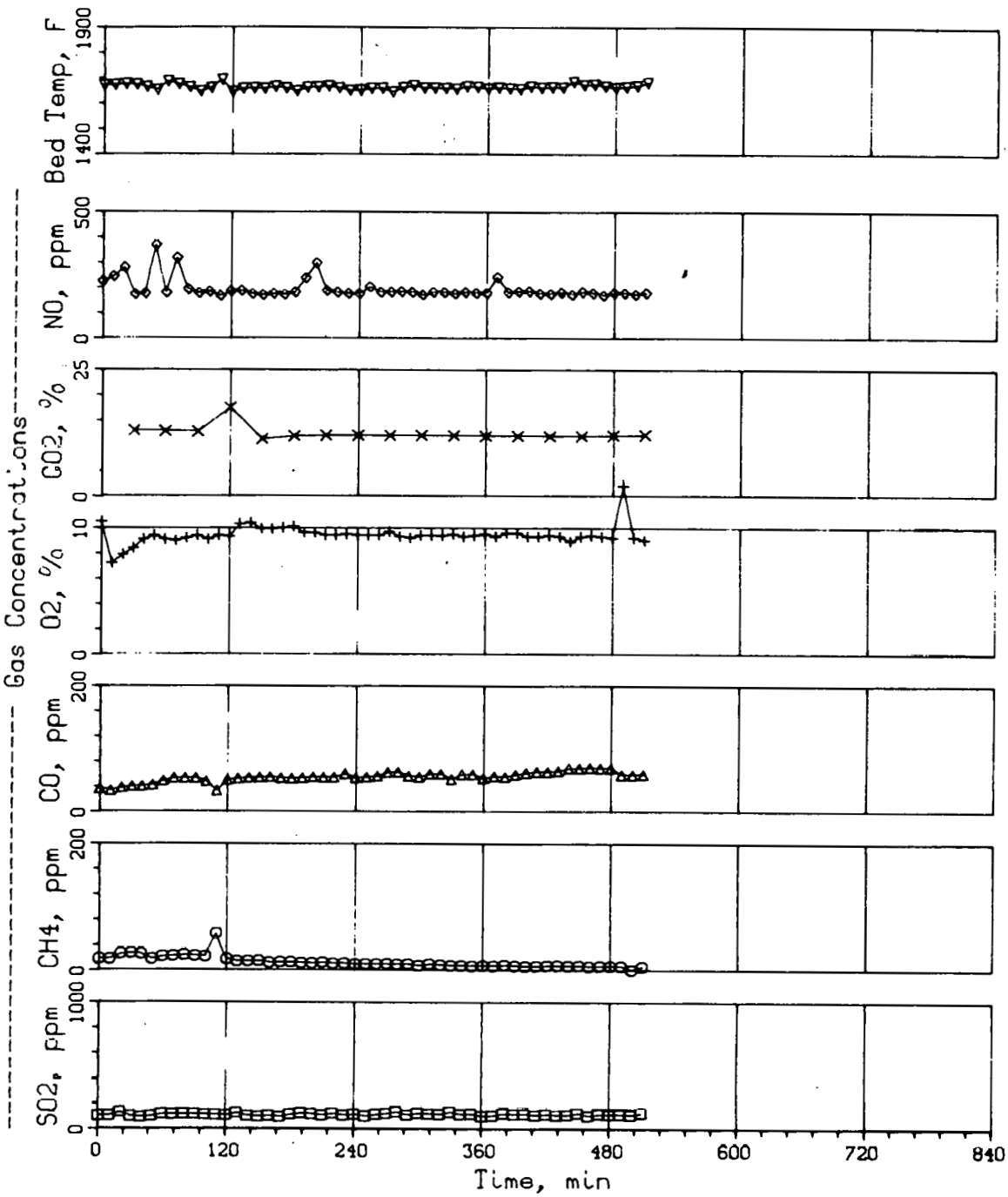

Fig. 62. Bed Temperature and Gas Concentrations in Flue Gas, Experiment EA-6

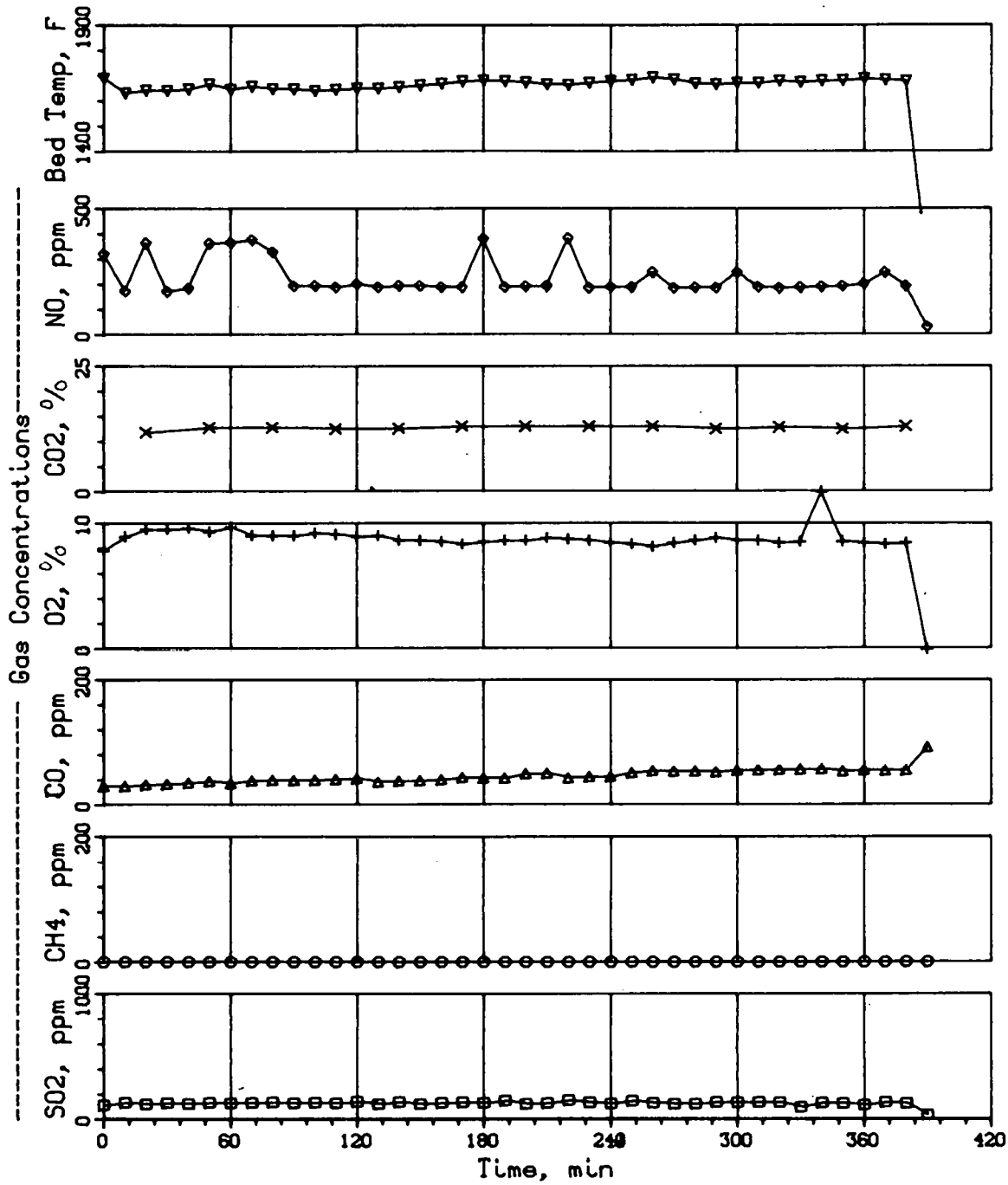

Fig. 63. Bed Temperature and Gas Concentrations in Flue Gas, Experiment EA-7

All total sulfur retentions obtained in the EA-series are plotted as a function of Ca/S mole feed ratio in Fig. 64. In the excess air range investigated (17-75%), the effect of excess combustion air is not pronounced enough to show any real and consistent effect on the sulfur retention capability of dolomite; except for EA-4 (the lowest point), the effect seems to be equivalent in magnitude to experimental deviations.

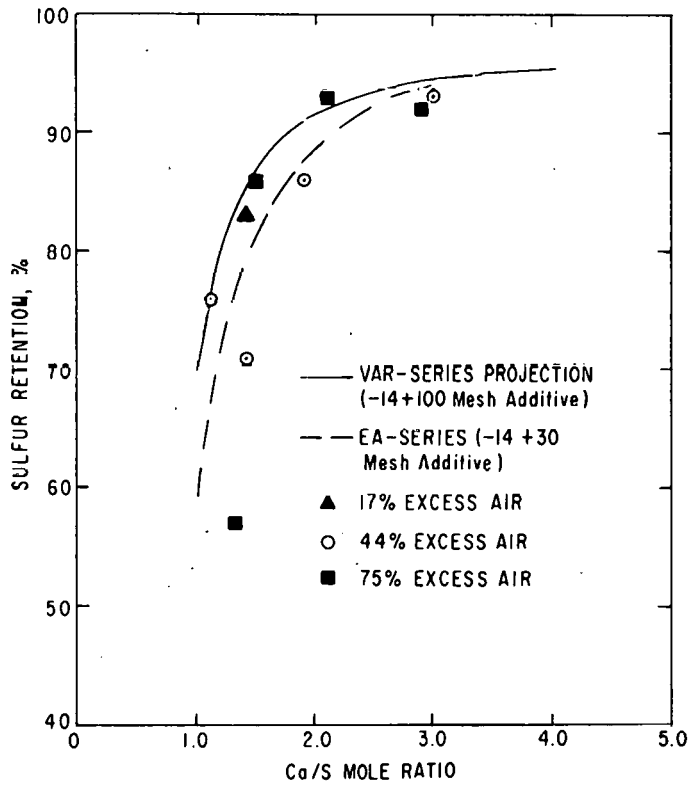

Fig. 64. Effect of Ca/S Mole Ratio on the Sulfur Retention Capability of Tymochtee Dolomite at 900°C, A Fluidizing-Gas Velocity of 4.5 ft/sec, and Various Excess Combustion Air Conditions

The NO concentration in the dry flue gas for the entire EA-series of experiments was found to increase with O_2 concentration, as expected. At ∿3% O_2 in the dry flue gas, the NO concentration was 160 ppm; at ∿6% O_2 it averaged ∿200 ppm; and at ∿9% O_2 it averaged 220 ppm. The above NO results from the EA-series are in qualitative agreement with the results published by the National Research Development Corporation[16] on the effect of O_2 concentration on NO emission levels from fluidized beds.

Combustion Efficiency and Carbon Balance Calculations. Carbon balances and combustion efficiencies were calculated for some C-series dolomite runs and LC-series limestone runs (Table 12). For these experiments, the carbon balances ranged from 96 to 103%. The calculated carbon balances for the C-, LC-, and EA-experiments are given with the sulfur balances in Appendix C. For the C- and LC-experiments at 900°C, the combustion efficiencies ranged

Table 12. Operating Conditions, Carbon Balance, and Combustion Efficiency For C- and LC-Experiments

Pressure, psig: 105
Bed Height, ft: 3
Excess Air: 17%

Coal: Arkwright (2.82% Sulfur)
Additive: Limestone 1359 (-14 +100 mesh), LC-Experiments
Tymochtee Dolomite (-14 +100 mesh), C-Experiments
Gas Velocity, ft/sec: 3.5

Experiment	Bed Temp, °C	Ca/S Mole Ratio	Carbon Balance, %	Combustion Efficiency, %
C-2	955	1.5	96	97
C-3A, C-3B, C-3C	900, 955	1.1	102	88
LC-1	955	1.8	97	94
LC-2B	955	2.7	103	96
LC-3A	900	1.5	103	91

from 88 to 91%; at 955°C, the range was 94 to 97%. These values, when compared with combustion efficiencies for the VAR-series of experiments (Ref. 14, Table 6), are low. The VAR-experiments predict combustion efficiencies of over 95% at 900°C; however, in the VAR-series only one experiment was performed at this temperature (900°C) and a fluidizing gas velocity of 3.5 ft/sec which were used in the C- and LC-experiments.

Carbon balances and combustion efficiencies have been calculated for some of the excess air experiments. The calculated combustion efficiences for these experiments (Table 13) lie within an acceptable range of 85 to 97%. As excess air increased, the combustion efficiencies increased (Fig. 65). By adding other ANL combustion efficiency data at 17% excess air conditions, a more representative line can be drawn through the data. Close agreement has been found between the correlated combustion efficiency data as a function of excess air and that obtained by Exxon[17] (Fig. 65).

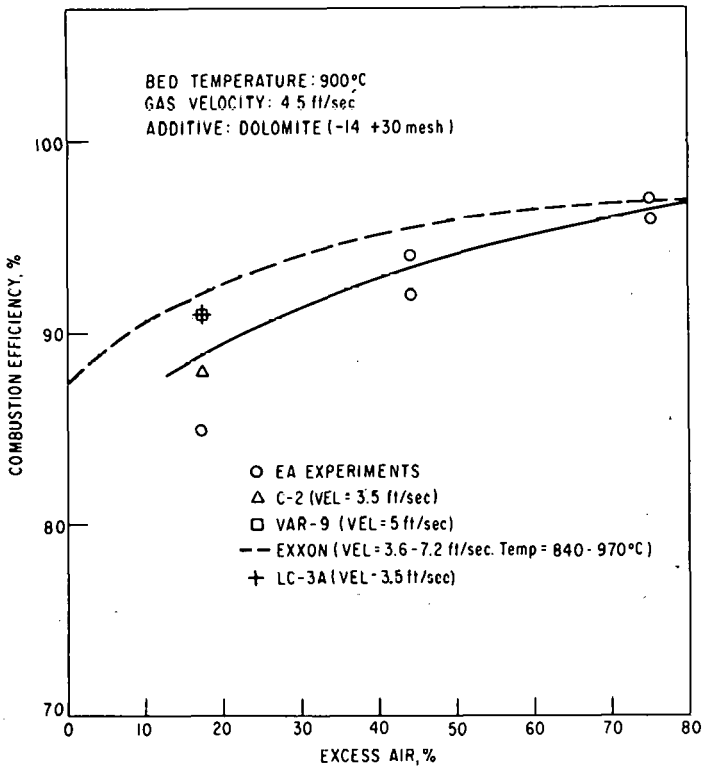

Fig. 65. Effect of Excess Air on Combustion Efficiency

Bed Temperature: 900°C
Gas Velocity: 4.5 ft/sec
Additive: Dolomite (-14 +30 mesh)

Table 13. Operating Conditions, Carbon Balances, and Combustion Efficiencies for Excess-Air Experiments

Bed Temp, °C: 900
Pressure, psig: 105
Gas Velocity, ft/sec: 4.5

Coal: Arkwright (2.82% sulfur)
Additive: Tymochtee dolomite (-14 +30 mesh)
Bed Height, ft: 3

Experiment	Excess Air, %	Ca/S Mole Ratio	Carbon Balance, %	Combustion Efficiency, %
EA-1	17	1.4	107	85
EA-2	44	1.4	101	92
EA-4	75	1.3	114	97
EA-5	44	2.9	97	94
EA-6	75	2.1	97	96

Concentration of COS in Flue Gas. Interest has been expressed in determining the concentrations of carbonyl sulfide (COS) being released in fluidized-bed combustion experiments. Since process analytical instrumentation is not available to perform this determination directly, flue-gas samples of several combustion experiments were taken and were submitted for mass spectrographic analysis of this component. These experiments included C-2, EA-9, EA-7, EA-5, LC-3A, and LC-4. In all cases, the COS concentration was found to be below the detectable limit of 100 ppm.

Processing of Combustor Data. The programs written at ANL to plot data generated in combustion experiments were modified to allow the use of Integrated Software Corporation's (ISC) plotting routines (DISSPLA) now available. In addition to the plot of flue-gas composition and bed temperature, the program plots four additional types of graphs from the experimental data. Figures 66 and 67, for example, show the temperatures recorded at various locations in the combustor off-gas system during a combustion run. In Fig. 68 the pressures and the calculated fluidizing-gas velocity in the combustor system are plotted. In the fourth type of graph (Fig. 69), the flow rates, the Ca/S mole ratio (calculated from the coal and additive hopper weight changes), and the percentage of SO_2 removed from the flue gas are plotted. In order to make these calculations, it was necessary to modify the program that interprets the paper tape from the HP2010C data logger so that the coal and additive hopper weights would be included in the data set.

In addition to the plots, several modifications were made to simplify use of the program. Originally, the time scale was calculated by hand and placed in the program with a text editor, and the experiment number had to be placed in the program before plotting. These two steps have been eliminated by suitable modifications that automatically scale the time axis and read the experiment number as data. In addition, the ordinates in some plots (for example, Fig. 63 and 68) have been automatically scaled. The self-scaling procedure provides useful scales in all but a few cases by calculating the average value and the standard deviation for each variable in an experimental run.

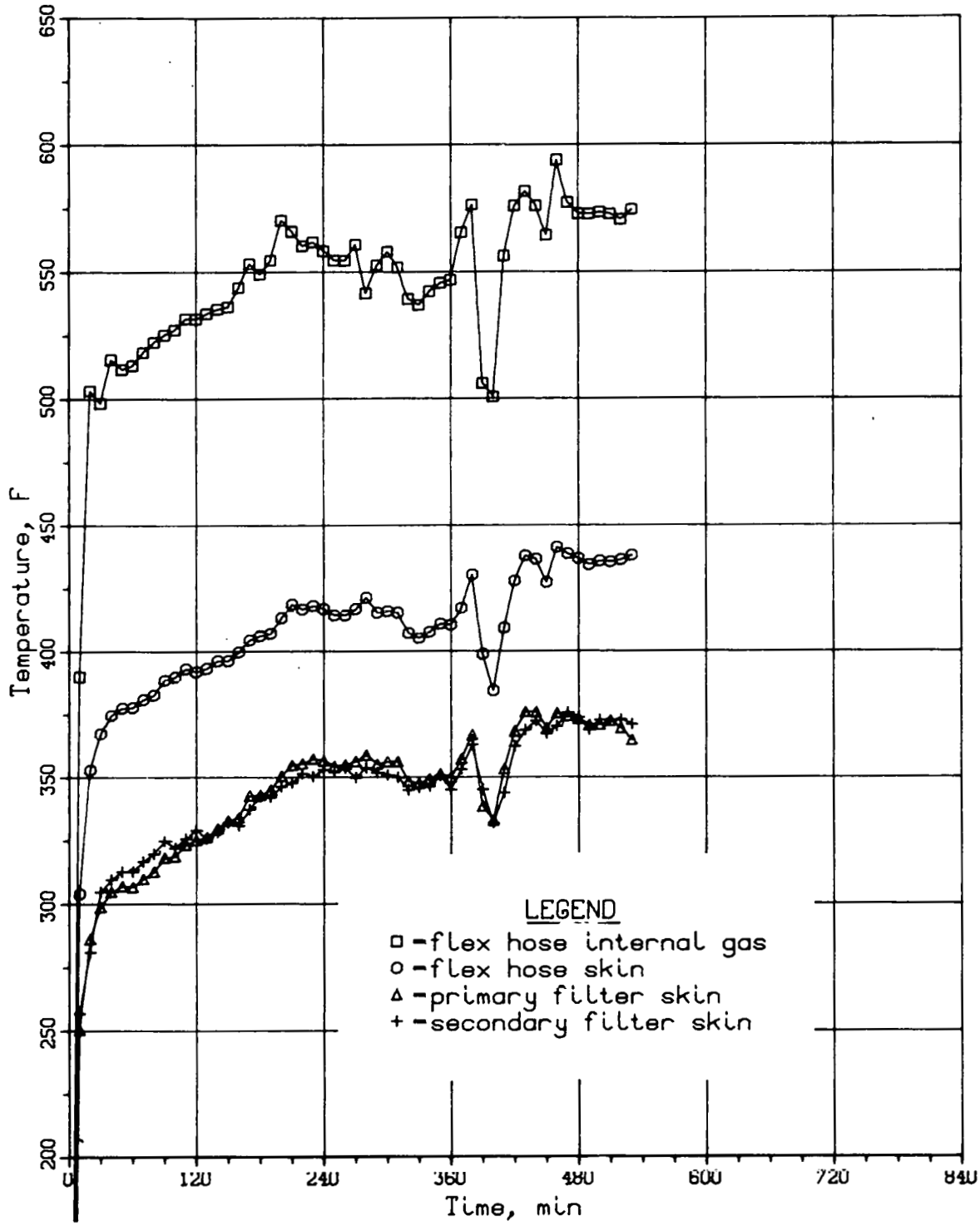

Fig. 66. Temperatures in the Combustor Off-Gas System, Experiment LC-6

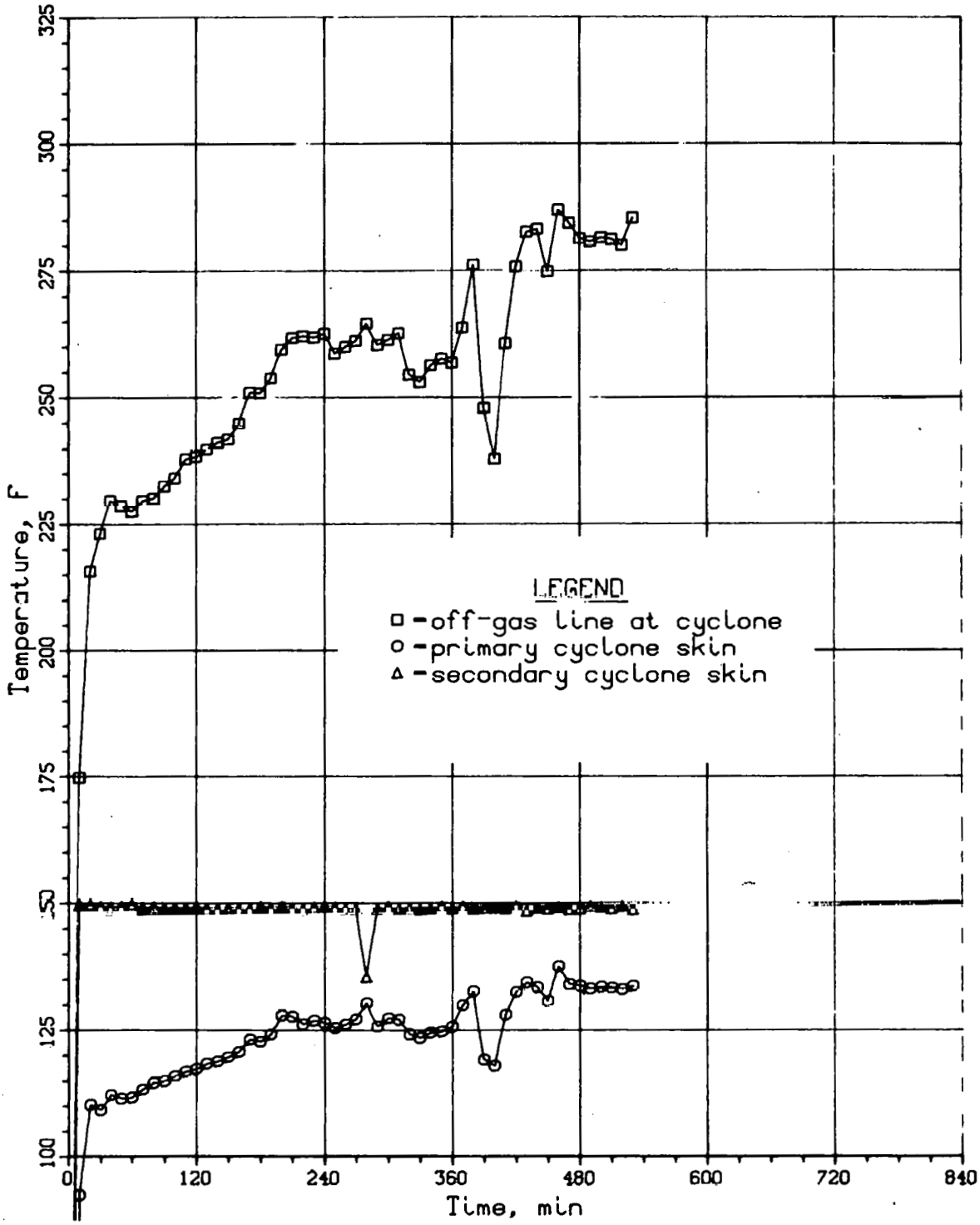

Fig. 67. Temperatures in the Combustor Off-Gas System, Experiment LC-6

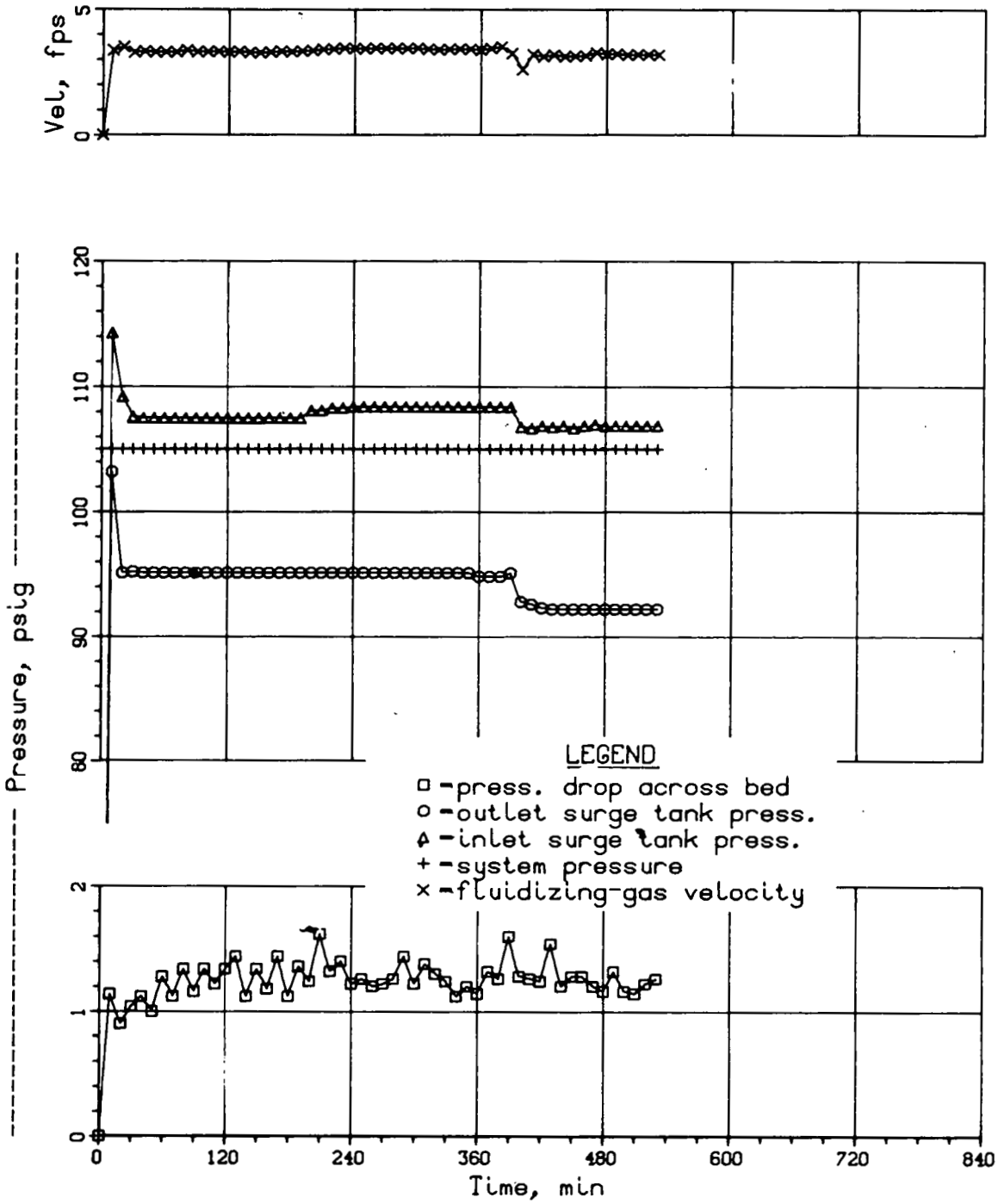

Fig. 68. Fluidizing-Gas Velocity and Pressures in the Combustor System, Experiment LC-6

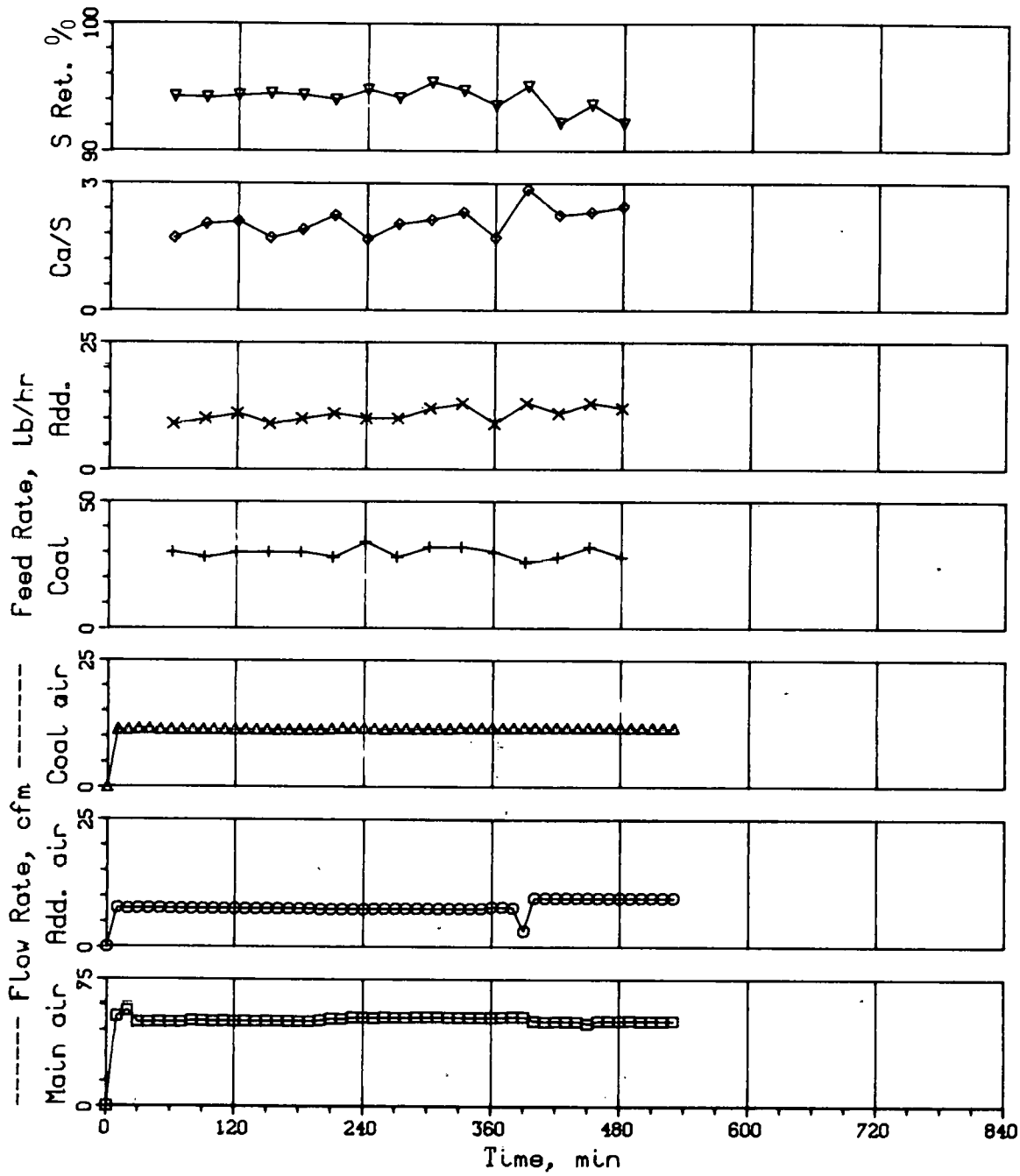

Fig. 69. Flow Rates, Feed Rates, Ca/S Mole Ratio, and Sulfur Retention, Experiment LC-6

The Determination of Inorganic Constituents in the Effluent Gas from Coal Combustion

Past experience from operation of coal-fired boilers and gas turbines has shown that some of the elements carried by the combustion gas cause severe metal corrosion.[18,19] Due to a potential application of the pressurized fluidized-bed combustion gas to a combined-cycle power generation system, a study is necessary to determine which species that may be deleterious to turbine components exist in the vapor phase or are carried on the ultrafine particulates in the hot (870°C) combustion gas. If the fine solids can not be removed by conventional particulate-removing units, they may condense on the gas turbine blades or vanes and react with turbine material, resulting in corrosion problems.

The purpose of this study is to determine quantitatively which elements are present in the hot combustion gas of coal, in either volatile or particulate form, and to differentiate between volatile and particulate species. Our interest is to identify the compound form and the amount of particulate species and to determine the amount and the form of condensable species. The experiments will be designed to obtain a material elemental balance on a batch basis.

This report presents an outline of the experimental program and general descriptions of the laboratory-scale reactor that will be used for this study.

Experimental Approach. The experimental approach is to use a cold trap to collect the condensable inorganic species present in an effluent combustion gas. To differentiate between volatile and particulate species, a hot filter, located upstream from the cold trap, will be used to remove particulates from the hot combustion gas. The condensates obtained from the cold trap and the particulates retained by the filter will be analyzed.

Experimental Equipment and Procedure. A laboratory-scale experimental apparatus using either fluidized-bed combustion or batch-type fixed-bed combustion was considered for this study. These two types of combustion were compared.

The fluidized-bed system would provide experimental conditions more closely simulating the pressurized fluidized-bed combustor being operated presently in this division. However, several disadvantages can also be visualized with this type of combustion system insofar as a study on a laboratory scale is concerned. It would require

substantially more air input for fluidization, and significant amounts of fly ash and particulate would be carried out by the upward flowing flue gas. All of these would cause a heavy load on the filter, limiting the choice of filter. A fluidized-bed system would also require more complicated set-ups for operation, such as feeding system, controls for fluidization, and so forth.

A batch-type fixed-bed combustion would have the following advantages over the fluidized bed: simplicity of operation, smaller gas throughputs, and the feature of providing better material balances. Based on this comparison, the batch-type system was chosen for first consideration in this study.

The conceptual experimental unit, shown in Fig. 70, is designed for operation at a maximum pressure of two atmospheres absolute and a maximum temperature of 900°C (1650°F). It is a 3 1/2-in.-ID horizontal tubular reactor and consists of four sections: preheating, combustion, filtration, and cold trap sections.

At the beginning of an experiment, the entire system will be pressurized to a desired value, and the preheating and filtration sections will be heated to the temperature at which the coal will be combusted, about 870°C (1600°F). The filtration section will be heated by an externally heated tubular furnace. The preheating section will be heated internally. Internal heating provides two advantages: Firstly, it allows for a lower wall temperature, and secondly, cooling coils can be applied. As a consequence, much less heat is conducted through the wall to the end flange, allowing a smaller flange to be used. In addition, due to a lower wall temperature, this preheating section can be heated to a higher temperature internally and preheating of the inlet air can be more efficient. A Lindberg Heavi-Duty K-type heating element (maximum temperature limit of 1205°C) will be used in the preheater section, and a baffle will be provided which allows the air to be heated by passing twice through the hot zone.

During the startup stage, when there is no airflow, the combustion section (in which the coal sample is located) will be maintained as cool as possible to prevent devolatilization of the coal. To accomplish this, baffles or radiation shields will be located on both ends of this section to reduce radiation and convection heat transfers inside the tube. The sample pan will be kept at a sufficient distance from the heat sources on both sides of the pan so that the heat inflow to the sample will be minimized. The cooled induction coils, which are subsequently used to heat the combustion section, together with forced air flow from a fan, will also help to cool the combustion section during this stage of operation.

In this system, the coal sample will be brought to its combustion temperature rapidly by induction heating and combustion with the preheated air. The combustion temperature, which is one of the important

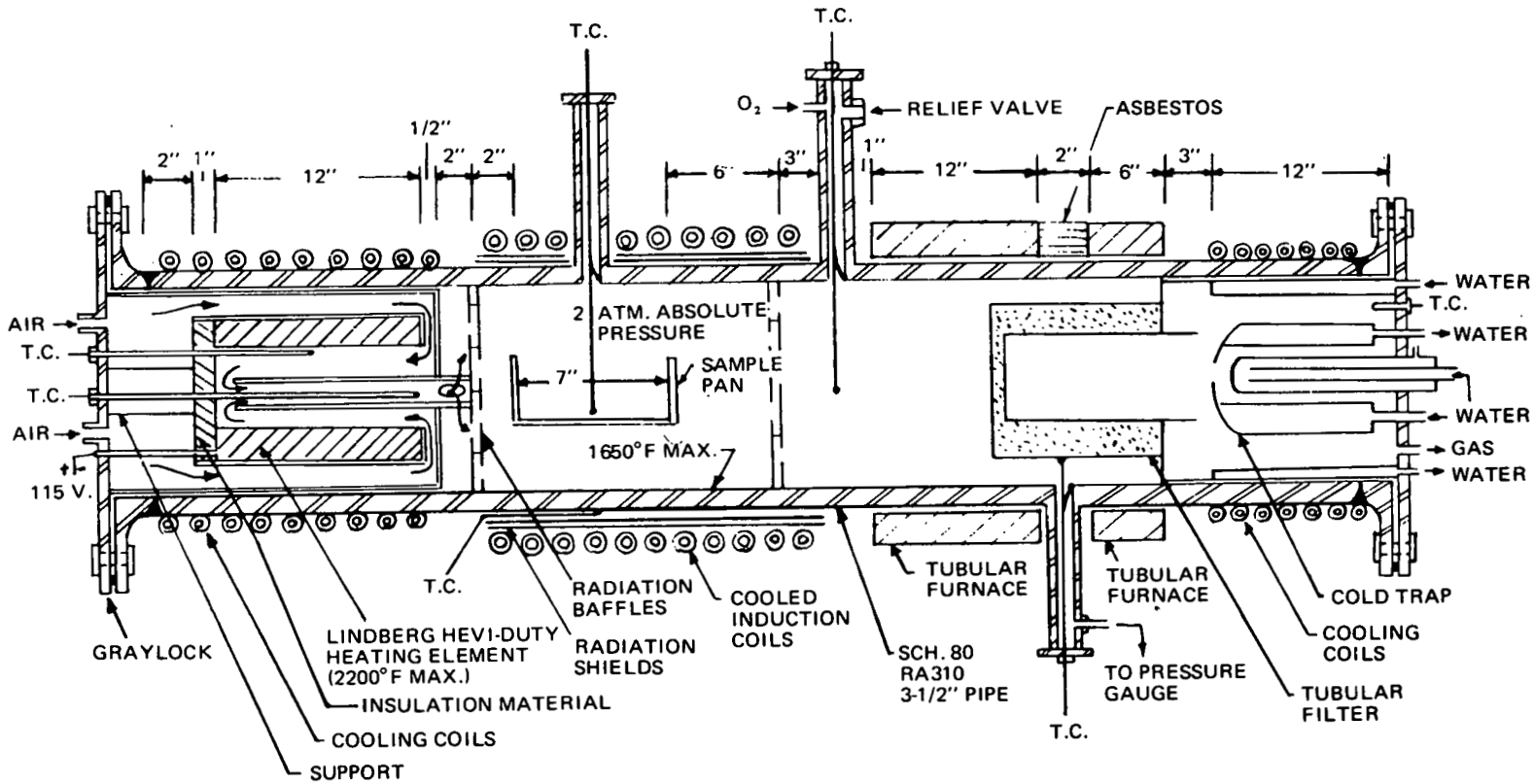

Fig. 70. Conceptual Experimental Unit for the Determination of Inorganic Constituents in the Effluent Gas from Coal Combustion

variables that must be carefully controlled, can be regulated by controlling the amount of oxygen flowing into the system. Increasing the heat-dissipating area by spreading out the sample in the sample pan and by dilution of the coal sample with additives such as limestone or dolomite may also help control the combustion temperature. Dilution of the coal sample with additives would also provide environments in coal combustion simulating the pressurized fluidized-bed system, as well as a more uniformly distributed temperature in the bed.

The hot combustion gas will be maintained at the combustion temperature in the section containing the filter. To minimize the likelihood of clogging of the filter by evolved volatile matter and condensation of tars on the cold trap during the early heating stage, secondary oxygen will be introduced into the system upstream from the filtration section. It may be necessary to add some packing in front of the filter to catalyze combustion. The combustion gas will then be directed immediately to impinge on a cooled metal trap. This trap will be kept at a low enough temperature to condense all inorganic species present except gases such as SO_2, CO, CO_2, etc. The condensates will be mechanically removed from the trap surface for analysis.

The detailed design and engineering drawings of this combustion unit have been completed. Review of the design is under way. The specification for fabrication of the unit is being written.

Analytical Consideration. The amount of coal combusted and the size of the experimental unit are very much dependent on the methods available for the analysis of the condensates and particulates collected. Many of the inorganic constituents in coal are present in only trace amounts. For these, sensitive analytical methods must be used.

X-ray diffraction is probably the most powerful method and is the most widely employed to identify unknown compounds in a collected solid. Consequently, X-ray diffraction should be a first method considered for identification of the phases or the compound forms in the collected samples. The X-ray diffractometer available in this division requires a minimum amount of 2 mg of sample containing at least 5% of the compound being analyzed. A coal sample size of the order of 100 grams is needed for combustion in order to collect enough condensates for X-ray diffraction analysis. Since X-ray diffraction is a nondestructive method, the condensate may also be examined under an optical microscope by the use of liquids of various indexes of refraction. Therefore, optical microscopy examination can be used as a supplement to X-ray diffraction to help identify collected species.

Mass spectrometry has been widely used for the determination of compounds. For the purpose of this study, the "hot" combustion gas after filtration can be introduced directly into the mass spectrometer. The spectrum obtained would yield information concerning the compounds existing in the vapor phase as such. One problem which might be

encountered for this study using this method is that some of the compounds present at higher concentration in the combustion gas may mask the spectrum of the lower concentration constituents, resulting in interpretive difficulty. However, proper selection of ionization voltage might eliminate some of the constituents from the mass spectrum.

Theoretically, both X-ray diffraction and mass spectrometry are adaptable to quantitative determination of a compound in a mixture; however, practical application of these methods to quantitative analysis is generally fraught with difficulties. Therefore, qualitative identification and quantitative assay are also required.

For trace element analysis, several analytical methods are available. Among them are atomic absorption, emission spectrometry, X-ray fluorescence, neutron activation analysis, spectrographic analysis by proton bombardment (SAPB), and scanning electron microscopy. All of these methods (except SAPB, which can be performed by an outside laboratory) are available in this laboratory. Analytical techniques have been developed in this division for some elements and others have been reported in the technical literature.[20] The analytical sensitivity of these methods is generally high. For example, atomic absorption can detect sodium in a mixture containing as little as 1 μg Na; emission spectrometry can sense as little as 0.01 μg Na.[21] The detection limit of trace elements for some methods has been reported by Ruch, Gluskoter, and Shimp.[20]

Filtration Consideration. Due to a significant role played by the filtration unit in this system, its availability is a key to the success of this study. Elevated-temperature operation and the requirement of resistance to chemical attack restrict the choice of filter material. After several communications with filter-producing companies, a commercially available filter called Kellundite, a product of Electro Refractories & Abrasives, Division of Ferro Corporation, was found. Kellundite is a ceramically bonded fused aluminum oxide. It withstands a maximum temperature of 1100°C and is very resistant to chemical attack except by fluorine. Because the fluorine concentration of the coal is sufficiently low (61 ppm is the mean analytical value for 101 Illinois coals,) the amount of hydrofluoric acid vapor in the combustion gas is expected to be low enough to permit utilization of this filter. Kellundite has sufficient strength and high air permeability. Several shapes and sizes with many choices of grade are available.

Kellundite FAO-10 filter, which has a nominal retention of 10-micron particles, has been ordered. Receipt by the middle of June is expected.

Induction Heating Facilities. A Tacco 30-kW, 10,000-cycle induction heating unit, loaned by the Materials Science Division for the duration of this experimental program, has been moved to this building and is being installed.

Choice of Reactor Material. The choice of reactor material is dependent upon (1) availability and (2) material properties suited for utilization at temperatures up to 900°C (1650°F), at a maximum pressure of 2 absolute atmospheres, and in corrosive environments. Great effort has been made to discuss our requirement with steel companies specializing in high-temperature alloy steels. Of the stainless steels (types 304, 316, and 310) considered, type 310 was finally chosen. Type 310 stainless steel shows the following advantages over types 304 and 316 steels: (1) higher values of tensile strength and yield strength,[23] (2) high creep strength, and especially (3) a high scaling resistance temperature--1038°C (1900°F) as compared with 843°C (1550°F) for types 304 and 316.[23] Type 310 stainless steel has excellent resistance to oxidation. Because of its high chromium content, it is suitable for use in sulfurous atmospheres. This alloy steel also shows resistance to moderately carburizing atmospheres and has excellent weldability. It can be readily joined either to itself or to other metals by standard welding procedures.

Both 3 1/2-in. and 1/2-in. nominal diameter, schedule 80 type 310 seamless stainless steel pipes needed for the construction of the combustion unit have been received from Rolled Alloys, Inc.

Scope of Study. During the first phase of this study, we will investigate the volatilization of inorganic species during the combustion of coal. Some pure volatile compounds of elements expected to be present in the hot combustion gas of coal will be first heated to test the system. The combustion of coal with and without additives (alumina, limestone, or dolomite) will be studied under various conditions to evaluate the effects of the operating variables--coal rank, particle size of of coal, combustion temperature, and ratio of coal to additive.

Identification of the vapor forms will be done by analysis of the condensate retained on the cold trap. Coal, the particulate retained by the filter, and the condensate will be analyzed for trace elements, both qualitatively and quantitatively. A material balance on a batch basis will be determined for these elements.

The second phase of this study will be an extension of this work to the gasification of coal. This phase of study is needed because a low-Btu combined cycle plant has attractive advantages as a new power generation system in the near future,[24] and inorganic constituents and particulates in the hot, low-Btu gas are expected to cause serious corrosion and erosion problems on the turbine blades.

Insofar as this phase of study is concerned, no significant modification of the system is necessary, except the addition of some simple equipment for steam feeding and safety. Scopes of the study in the first phase and this phase will be similar.

Systematic Study of the Volatility of Trace Elements in Coal

The effluent gases from coal combustion are known to contain trace elements, some of which are toxic to human beings, animals, and plants,

and some of which cause severe metal corrosion in coal-fired boilers and gas turbines. The evolution of these trace elements has been generally believed to be due to the volatilization of elements and compounds at high temperatures. Therefore, knowledge of the temperatures at which these trace elements start to volatilize and of the rates of volatilization is essential to study of their thermal behavior.

Ruch, Gluskoter, and Shimp[20] studied trace element volatility by ashing coal in a muffle furnace at 300 to 700°C (570-1290°F). The trace elements studied included B, Pb, Mo, V, Zn, Ni, Co, Cu, Cd, Mn, Cr, Be, Ge, and Sr. These workers reported that losses of 33% and up to 25% were observed for Mo and V, respectively, and that no significant losses in samples ashed up to 700°C (1290°F) were noticed for the other elements. Guidoboni[25] has conducted a study of the volatilization of some trace elements in coal by comparing wet-ashing using acid solution and dry-ashing in a furnace at 850°C (1560°F). The results indicate that the trace elements studied, namely, Cu, Ni, Mn, Zn, Cd, Pb, V, Ag, and Li, do not exhibit significant losses during dry-ashing. Similar results were also observed by Kometani[26] for the elements, Pb, Zn, Fe, Cu, Cd, Ni, Mn, Cr, Co, and V, when airborne particulate matter was dry-ashed at 500°C (930°F). All of these volatilization studies were performed at relatively low temperature ranges; therefore, the information is not applicable to the case of coal being subjected to high temperatures (900 to 1000°C or 1650 to 1830°F) such as those generally used in a practical coal combustion furnace. The evolution of trace elements is expected to be greatly increased when coal is combusted at higher temperatures.

Data on the volatility of trace elements at practical coal combustion conditions are sparse in the technical literature. A study to obtain this information is under way. The effect of gasification conditions on the volatility of trace elements will also be included in this study. The information obtained would offer a real understanding of the thermal behavior of these trace elements under the similar conditions which are to be used in coal combustion and gasification. This study is also intended to obtain data supporting the study covered above and can also be considered to be a preliminary investigation for that study.

In the following sections, the experimental program is outlined and the analytical methods for this study are described.

Experimental. This study includes (1) dry-ashing of a coal at various temperatures under both combustion and gasification conditions and (2) analysis of the resulting ashes for the trace elements of interest.

Trace elements in coal are essentially chemically incorporated in the mineral matter of coal. These elements can be retained in the ash while the carbon is oxidized at low temperature with atomic oxygen.[20] Low-temperature ashing will be used to remove carbon from the coal and concentrate the elements in the ash prior to analysis. An important analytical advantage of low-temperature ash (LTA) is that trace elements in the ash are concentrated to 10 or more times their amount in coal. The high-temperature ashing of a coal will be performed in a ceramic tubular furnace with a simple setup of gas inlet controls, as shown in Fig. 71.

The gas, containing a controlled amount of oxygen, can either be introduced directly into the ashing chamber to provide combustion conditions or can be bubbled through a water evaporator prior to its being directed into the ashing chamber to provide gasification conditions. The water evaporator is made of glass. The amount of water vapor carried out by the air is regulated by the water temperature in the evaporator, which is heated externally by a heating tape, and is measured gravimetrically in separate measurements by the use of $CaCl_2$ as an absorbent agent.

The variables of temperature, time, and the composition of gases will be studied to evaluate their effects on the volatility of trace elements. Herrin (No. 6) coal (Illinois coal) was found to be representative of all Illinois coals from the viewpoint of content of major minerals[27] and therefore has been chosen for this study. Coal in the size range of -200 mesh will be used.

Analysis of Coal Ash. Good analytical procedures for coal ash constitute the key factor in this study. Therefore, a survey of the technical literature on the methods for analysis of trace elements in coal ash has been performed. The methods employed by Ruch, Gluskoter, and Shimp[20] are an important guide for this work. For the trace elements of interest, the analytical methods applicable to both coal and coal ash are tabulated in Table 14. It may be seen in this table that no appropriate method has been developed for analyzing chlorine and sulfur in ash. However, the methods applicable to coal are thought to be applicable to ash analysis. Information on these procedures is available. When possible, two analytical methods will be used for each trace element in a parallel manner so that the results can be double-checked.

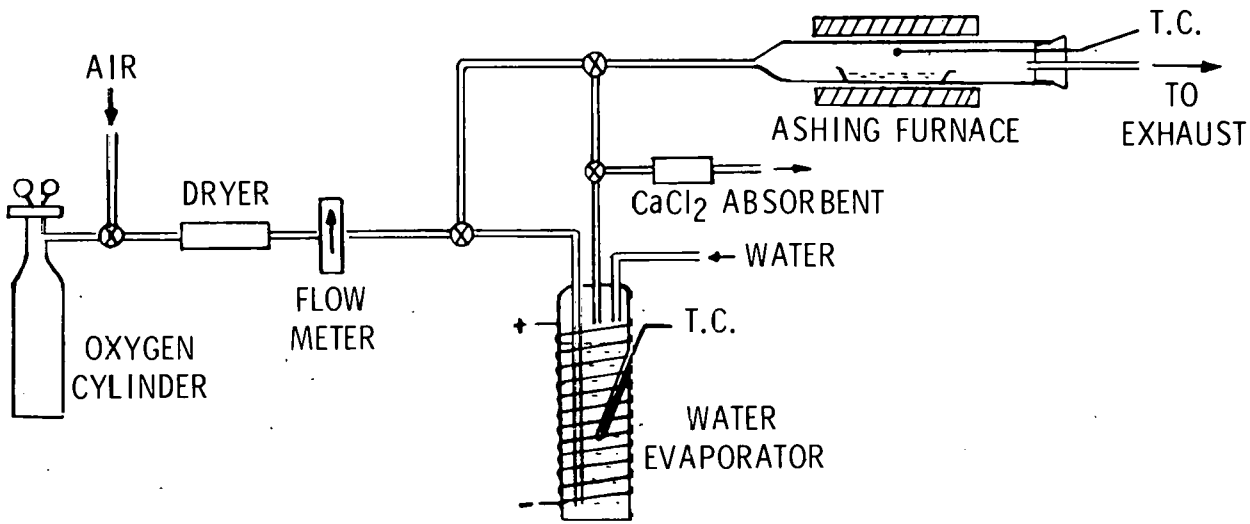

Fig. 71. Apparatus for Ashing of Coal Samples

Table 14. Analytical Methods for Trace Elements in Coal and Ash

Element	Analytical Method[a]		Detection Limit (ppm)		Reference
	Coal	Ash	Coal	Ash	
Na	NAA		0.5		20,28
	FPA	FPA			29,30,31
		AA			32
		XRS			33
	SA	SA			34,35
	(SSMS)[b]	(SSMS)[b]			25,36
	SAPB	SAPB			37
K	XRF	XRF	9		20,38
		FPA			31
		XRS			33
	AA	AA			32,39
	SA	SA			33,34,39
	(SSMS)[b]	(SSMS)[b]			25,36
	SAPB	(SAPB)[b]			37
V	XRF	XRF	0.5		20
	OESA	OESA	5	45	20
	SSMS	SSMS			25,36
	SA	SA			41
	SAPB	(SAPB)[b]	1		37
Ca	XRF	XRF	12		20,38
	AA	AA			31,39
	SA	SA			35
	(SSMS)[b]	(SSMS)[b]			25,36
	SAPB	(SAPB)[b]			37
Cl	XRF		36		20
	NAA				28
	ASTM (Eschka & Bomb)				42
	SAPB	(SAPB)[b]			37
S	XRF		72		20
	ASTM (Eschka & Bomb)				43

[a]
NAA -- Neutron Activation Analysis
FPA -- Flame Photometric Analysis
AA -- Atomic Absorption
XRS -- X-Ray Spectrography
SA -- Spectrographic Analysis
SSMS - Spark Source Mass Spectrometry
OESA - Optical Emission Spectrographic Analysis
XRF -- X-Ray Fluorescence
ASTM - American Society for Testing & Materials
SAPB -- Spectrographic Analysis by Proton Bombardment

[b]
Possibly applicable.

TRACE-ELEMENT DISTRIBUTION STUDIES

Trace elements, such as mercury, lead, and beryllium, emitted from fossil-fueled power plants, incinerators, and industrial sources are receiving increased attention as potentially dangerous air pollutants. The process of coal combustion releases trace elements to the environment as vapors and/or in association with particulate emissions. Although a substantial fraction of the trace elements present in the coal during combustion is retained with the fly ash removed by emission control devices, significant quantities of trace elements (such as mercury) may still be emitted as vapors or in association with submicron-size particles that are not efficiently removed by present day devices.

Recent investigations have demonstrated that several of the trace elements (such as lead, cadmium, arsenic, and nickel) preferentially concentrate in the smallest particles emitted from conventional coal-fired power plants.[44,45] The enrichment of trace elements in the finer fly ash from conventional power plants has been attributed to the volatilization of the elements (or their compounds) in the combustion zone of the furnace and their subsequent condensation or adsorption onto suspended fly ash particles; this would result in relatively higher concentrations of the trace elements in the finer particles, which have higher surface-to-mass ratios.[44,45]

Since fluidized-bed combustion is carried out at temperatures of 855-955°C (1550-1750°F) well below those of conventional coal-fired power plants and in the presence of an additive for sulfur dioxide removal (which may also act as sorbent for trace elements), an investigation was made at ANL to evaluate the potential of fluidized-bed combustion for reducing trace-element emissions as compared with conventional combustors. The trace elements of primary interest in the investigation were mercury, fluorine, beryllium, and lead. Mass balances were made around ANL's 6-in.-dia, pressurized, fluidized-bed combustor for the following trace and minor elements: Hg, F, Be, Pb, As, Br, Co, Cr, Fe, K, La, Mn, Na, and Sc. All solid materials charged to or recovered from the combustor, including particulate matter entrained in the flue gas from the unit, were analyzed. Also, the flue gas was analyzed for both mercury and fluoride emissions The results of these analyses were used to evaluate the potential loss to the environment of the various trace elements by volatilization.

Additional results are presented here on four combustion experiments, TRACE-3, -4B, -5A, and -6, for which some results were reported in the preceding annual report.[14] Nominal operating conditions for experiments TRACE-3 and TRACE-4B were a bed temperature of 845°C (1550°F), 10 atm pressure, and 4% O_2 in the dry flue gas, as compared with values of 900°C (1650°C), 8 atm, and 3% O_2 for experiments TRACE-5A and TRACE-6. In experiments TRACE-3 and TRACE-5A, Arkwright coal was combusted in a fluidized bed of Alundum (electrically fused Al_2O_3 grain, Type 38, from the Norton Company), whereas in experiments TRACE-4B and TRACE-6, Arkwright coal was combusted in a fluidized bed of Tymochtee dolomite.

Mass balances for mercury, lead, beryllium, fluorine, and sodium, presented and discussed in the preceding annual report [14] are presented again. Material balances determined for nine additional trace and minor elements also re presented. The concentrations of the trace elements in the coal and fly sh samples from successive stages of gas-particle separators (primary cyclone,

secondary cyclone, and filter) were adjusted to a combustible-matter-free basis and compared for significant differences in concentration between coal and ash samples and among successively finer samples of ash. This analysis was performed to detect evidences of preferential concentration in the samples of finely divided fly ash. Insofar as possible, attempts have been made to compare the results reported here with similar results reported by other investigators for conventional coal-fired power plants. In addition, results on testing of the sampling train used to measure mercury levels in the flue gas from the combustor are reported.

Analytical Methods

Wet chemical techniques were employed to measure the concentrations of the four trace elements of primary interest in the investigation: mercury and lead by atomic absorption, beryllium by fluorimetry, and fluorine by specific ion electrode. The concentrations of the remaining trace elements measured were obtained by neutron activation analysis. The details of the analytical procedures have been presented in considerably more detail elsewhere (Ref. 14, p. 73, 130-133).

Table 15 compares the analytical results obtained by ANL and by an independent laboratory for samples of Illinois No. 6 seam coal and the unquenched ash of the coal obtained from a Lurgi gasifier. The trace element results of the two laboratories agree with each other within the precision of the measurements in all cases, except for cobalt and lead in the No. 6 coal and for mercury, manganese, and lead in the ash.

In the two instances of disagreement in the lead values, the ANL results are considered more likely to be correct. The impressive overall agreement, which includes a number of cases for which different analytical methods were used, indicates that the methods used are reliable and strengthens the conclusions that can be drawn from the results reported here.

Results

Representative trace element concentration data are presented in Table 16 for combustion experiment TRACE-3, which was carried out at a temperature of 845°C (1550°F) in an alumina bed. With the data from Table 16 and similar data from the other three combustion experiments, mass balances were determined for the following trace and minor elements: Hg, Pb, Be, F, As, Br, Co, Cr, K, La, Mn, Na, Sc, and Fe. The results of these calculations are presented in Table 17.

The first two lines in Table 17 present the mass balances for mercury and fluorine based on the analysis of solid samples and the flue gas. The mercury balances, which exhibited an average recovery of only 38%, are particularly disappointing. The fluorine balances of 120 and 110% recovery for the experiments at 845°C are reasonably acceptable values; the recoveries of 180 and 240% for the experiments at 900°C are unaccountably high. The poor balances obtained for both the mercury and the fluorine have been attributed to problems with the flue-gas analysis, rather than with the analysis of the solid samples. (The results of testing of the sampling train used to measure mercury levels in the flue gas from the combustor are presented elsewhere in this section of the report.)

Table 15. Comparison of Trace Element Concentrations in Illinois No. 6 Seam Coal and in the Unquenched Gasifier Ash of the Coal as Determined by ANL and by an Independent Laboratory.

Element	Coal		Ash	
	Independent[a] ppm	Argonne[b] ppm	Independent[a] ppm	Argonne[b] ppm
Ag	0.3		3.8	
As	1.0	2.1 ±1.0 C	0.1	
B	132		622	
Be	1.8	1.55 ±0.8	14	13.4 ±0.7
Br		4.1 0.7 B		
Cd	<0.3		<0.3	
Ce				38 ±4 A
Co	4.3	3.2 ±0.5 B	40	34 ±3 A
Cr	22	18.3 ±2.7 B	705	806 ±81 A
Cu	12		239	
Dy				8.5 ±1.3 B
Eu		0.2 ±0.1 C		
F	79	79 ±16		5.2 ±1.0
Fe (x10^4)		1.2 ±0.1 A		13 ±1 A
Hg	1.00[c]	1.18 ±0.12	0.04	0.007 ±0.001
K (x10^3)		1.5 ±0.1 A		16 ±2 A
La		3.9 ±0.4 A		40 ±20 C
Li	9.2		74	
Mn	20	18.6 ±1.9 A	243	156 ±16 A
Mo	7		6	
Na (x10^2)		3.0 ±0.3 A		27 ±3 A
Ne	14		456	
Pb	12	8.0 ±0.8	96	46.0 ±2.3
Sb	0.1	D	0.2	
Sc		2.1 ±0.2 A		34 ±2 A
Se		D		
Sm		0.005 ±0.003 C		
Tb				3.1 ±1.6 C
V	29		301	
Yb		1.4 ±0.7 C		11 ±2 B
Zn (x10^2)	0.43	D	4.69	D

[a] The precision of the independent laboratory results is estimated to be ±10% in all cases.

[b] The accuracy of the Argonne results for mercury is estimated to be ±10%; the precision of the Argonne results for beryllium is ±5%, for lead ±10%, for fluorine ±20%. The confidence ratings shown for the Argonne results obtained by neutron activation analysis correspond to the following accuracy levels: A ±10%, B ±15%, C ±50%, and D identification only.

[c] Not representative of the seam; contamination suspected.

Table 16. Trace Element Concentrations in Samples From Experiment TR-3 on a Combustible-Matter-Free Basis

Combustion Temperature:	1550°F	Coal :	Arkwright		
Pressure :	10 atm	Bed Material:	Alumina (Al_2O_3)		
Gas Velocity :	2.4 ft/sec				

	Concentration, ppm[a]					
Element	Starting Bed	Coal	Final Bed	Primary Cyclone	Secondary Cyclone	Flue Gas
As		5 B	3.5 B	25.B		
Ba		D		350 C	860 B	
Be	0.8	0.7	0.8	2.6	6.0	
Br	6 B	13 B			3 B	
Ce		D	C	19 C	13 C	
Co		1.8 B		11 B	19 A	
Cr		100 A	12 C	180 A	300 A	
Dy		0.2 B		1.8 C	2.9 A	
F	100	25		20	10	8.1
Fe	240 A	$1x10^4$ A	$5.5x10^3$ A	$5.9x10^4$ A	$3.6x10^4$ A	
Ga	110 A					
Hf	1.7 A		97 A	2.9 C	6 C	
Hg	<0.005	0.15	<0.005	0.46	0.46	0.32 ppb
K		580 C	660 B	$3.7x10^3$ C	$5x10^3$ C	
La		4.2 A	3.7 A	31 A	52 A	
Mn	D	26 A	39 B	110 B	140 B	
Na	$1.7x10^3$ A	690 A	$1.3x10^3$ A	$4.1x10^3$ A	$7.2x10^3$ A	
Pb	1.1	29	51	95	260	
Sb		0.3 C	0.7 B	3 C	6.2 B	
Sc	0.03 A	1.7 A	1.8 A	9 A	19 A	
Sm		0.8 A	0.1 C	D		
Yb			5.2 B	4 C	7.5 C	
Zn	D					
Zr			340 B			

[a]ppm = parts per million followed by absolute error rating for neutron activation determinations: A = ≤10%, B = ≤15%, C = ≤50%, D = identification only.

Table 17. Mass Balances for Trace and Minor Elements Around ANL 6-in.-dia, Pressurized, Fluidized-Bed Combustor

	Recovery,[a] %				
	Combustion in Alumina Bed		Combustion in Dolomite Bed		Average[b]
Element	TR-3	TR-5A	TR-4B	TR-6	
Mass Balances Based on Solids and Flue-Gas Analysis					
Hg	56	29	43	25	38
F	120	180	110	240	160
Mass Balances Based on Solids Analysis Only					
Hg	37	26	9	20	23
F	5	23	62	56	36
Pb	110	120	78	95	100
Be	63	56	71	87	69
As	85	I[c]	85	>83	85
Br	0	I	36	I	18
Co	79	100	88	96	91
Cr	27	64	83	120	74
Fe	92	120	95	92	100
K	120	I	77	74	90
La	120	>74	89	I	104
Mn	110	170	110	I	130
Na	79	120	85	100	96
Sc	110	110	83	88	98

[a] Percent of element entering combustor accounted for in product streams.

[b] Average recovery for experiments in which a balance was determined.

[c] I means indeterminate due to incomplete concentration data for some samples.

The remainder of Table 17 lists the material balances based on solid samples only for those elements (including mercury and fluorine) for which sufficient analytical data were available. Retention of the relatively volatile elements, mercury, arsenic, fluorine, and bromine, in the solids indicates a definite potential for fluidized-bed combustion to reduce the emissions of these elements.

The average retention of 23% for mercury in the solid effluents from the combustor (Table 17) is higher than the results reported by other investigators. Billings *et al.*[46] made a mercury balance around a 660-MWe coal-fired power station and reported a mercury retention of only 10% in the ash and emission of 90% of the mercury in the vapor phase.

The recovery of arsenic (~85%) is another good indication that fluidized-bed combustion, because of its lower combustion temperatures, has the potential for retaining trace elements by reducing their volatilization as compared with combustion in conventional coal-fired boilers. Bolton *et al.*[47] reported a recovery for arsenic of only 40 to 50% in the particulate phases for a mass balance made around a conventional 290-MWe cyclone-fed boiler. Similarly, Attari[48] estimated a retention of only 35% for arsenic in the solid effluents from the Illinois Institute of Gas Technology's HyGas (high-Btu coal gasification) pilot plant.

The most significant observation that can be made from the fluorine balances is that the retention of the fluorine in the solid phases leaving the combustor was considerably higher when additive was used in the experiment. The reported recoveries of fluorine in the solid samples were 56 and 62% for combustion with additive present and only 23 and 5% for combustion in an alumina bed. Further indication of the effect of additive is that the fluorine concentration increased from only 14 ppm in the fresh dolomite to as high as 350 ppm in the partially sulfated dolomite, indicating a significant retention of fluorine by the additive.

Like the fluorine results, the bromine mass balances suggest that the additive may also be effective in reducing bromine emissions. The concentration data for bromine (not presented here) indicated only marginal increases, however, in the concentration of bromine in partially sulfated samples (starting bed, final bed, and overflow samples) as compared with the concentration of bromine in the unreacted dolomite stone fed to the combustor. Thus, the reported bromine retention of 36% for experiment TRACE-4B with additive present (Table 17) represents a retention of bromine only slightly greater than the retention of the fraction of bromine (25%) entering the system with the unreacted additive.

Seven of the remaining ten elements reported on (Mn, Co, Fe, K, La, Na, and Sc) had material balances of 100 $\pm$ 10%, indicating within analytical accuracies essentially no losses by volatilization. The relatively low recoveries of beryllium and chromium are suspect since complete recoveries of chromium have been reported for coal-processing units operated at much higher temperatures and since beryllium is reportedly less volatile than chromium.[47,49] Except for one unaccountably high recovery value for manganese, this element also exhibited a recovery of 100 $\pm$ 10%.

The significance of these results is emphasized in Table 18, which compares the projected trace element emissions from conventional and fluidized-bed

Table 18. Projected Emissions of Trace Elements from Conventional and Fluidized-Bed Combustors Expressed as a Percentage of the Element Entering the System

Element	Conventional Combustion[a]	Fluidized-Bed Combustion
Hg	90	80
F	90-100 (estimated)	40
Br	100 (estimated)	65
As	50-60	15
Pb	0-60	0-20
Be	Not available	20-40
Sc	10	0
Cr	0	25
Co	10-20	0-20
Na	20	5
K	30	10
Fe, La, Mn	0	0

[a] Projected from data in the literature[45-47] on trace-element emissions from conventional power plants.

combustion systems based on currently available data. With the exception of the projected emissions for chromium, the emissions from fluidized-bed combustion are consistently as low or lower than those projected for conventional combustor.

The trace-element data were further analyzed to qualitatively assess concentration versus particle-size effects and to determine whether fluidized-bed combustion has the potential of reducing the preferential concentration or enrichment of trace elements in the finer particulate matter. The concentrations of the trace elements in the coal and fly ash samples from successive stages of gas-particle separators (primary cyclone, secondary cyclone, and filter) were adjusted to a combustible-matter-free basis and compared for significant differences in concentration between coal and ash samples and among successively finer samples of ash. The coal analyses were corrected on the basis of the ash content of the coal, whereas the analyses of the ash samples were corrected to a carbon-free, sulfur-free basis. This analysis was made for the two combustion experiments carried out in a fluidized bed of alumina (TRACE-5A and TRACE-3). The results of the calculations are presented in Table 19.

The following observations can be made on the basis of the concentration values reported in Table 19:

1. The concentrations of lead and beryllium were essentially uniform among the samples, indicating that no enrichment of these elements occurred in the finer fly ash. In a study conducted in a conventional power plant, the concentration of lead in the electrostatic precipitator ash was one order of magnitude higher than the concentration of the lead in the coarser ash removed in the mechanical separator.[45]

2. The concentration of chromium in the ash products of combustion for both experiments is significantly lower than the concentration of chromium in the coal. This is reflected in the relatively poor material balances reported for chromium in Table 17. There does not, however, appear to be any significant increase in chromium concentration in the fly ash with decreasing particle size, as would be expected if the chromium were indeed being lost by volatilization.

3. Sodium and potassium show no increase in concentration in the fly ash as compared with their respective concentrations in the coal for experiment TRACE-3, (made at a bed temperature of ∿845°C). This tends to suggest that neither the sodium nor the potassium was volatilized during combustion at 845°C. The concentration of sodium does, however, appear to have increased significantly with decreasing particle size for experiment TRACE-5A, which was carried out at a combustion temperature of ∿900°C. In this experiment, the combustible-matter-free concentration of sodium increased from ∿1.2 wt % in the relatively coarser primary cyclone fly ash to ∿2.5 wt % in the much finer filter fly ash.

4. The concentrations of several elements (such as barium, cobalt, lanthanum, antimony, scandium, and tantalum) show slight tendencies to increase with decreasing particle size of the ash. For barium and tantalum, the rather large absolute errors of the concentration values greatly reduce the significance of the observed increases in concentration.

5. In experiments TRACE-3 and TRACE-5 (Table 19), the concentration of iron in the primary cyclone fly ash is about the same as the iron concentration in the

Table 19. Trace Element Concentrations in Arkwright Coal and in Ash Samples Recovered During Combustion Experiments TR-3 and TR-5A on a Combustible-Matter-Free Basis

	Concentration, ppm					
		TR-3		TR-5A		
Element	Coal	Primary Cyclone	Secondary Cyclone	Primary Cyclone	Secondary Cyclone	Filter
As	63 ± 9	52 ± 8	N.D.[a]	N.D.	D[b]	N.D.
Ba	D	740 ± 370	1200 ± 180	940 ± 140	1200 ± 600	1800 ± 900
Be	9.1 ± 0.9	5.4 ± 0.5	8.7 ± 0.9	3.6 ± 0.4	8.2 ± 0.8	7.9 ± 0.8
Ce	D	40 ± 20	19 ± 10	51 ± 26	26 ± 13	25 ± 12
Co	23 ± 3	23 ± 3	28 ± 3	22 ± 3	26 ± 3	33 ± 3
Cr	1,300 ± 130	390 ± 39	430 ± 43	880 ± 88	560 ± 56	560 ± 56
Dy	2.5 ± 0.4	3.8 ± 0.9	4.2 ± 0.4	N.D.	3.7 ± 1.8	5.6 ± 2.8
F	350 ± 70	42 ± 8	15 ± 3	55 ± 11	15 ± 3	5.7 ± 1.1
Fe[c]	13 ± 1	12 ± 1	5.2 ± 0.5	15 ± 2	7.4 ± 0.7	7.3 ± 0.7
Hf	N.D.	6.1 ± 3.0	8.7 ± 4.4	4.7 ± 2.4	7.6 ± 1.1	N.D.
Hg	1.4 ± 0.1	1.0 ± 0.1	0.7 ± 0.07	0.23 ± 0.02	0.48 ± 0.05	0.51 ± 0.05
K	7,300 ± 3,600	7,700 ± 3,800	7,200 ± 3,600	N.D.	N.D.	11,000 ± 5,500
La	53 ± 5	65 ± 6	75 ± 8	45 ± 22	N.D.	D
Mn	330 ± 33	230 ± 34	210 ± 32	550 ± 280	250 ± 38	290 ± 140
Na[c]	0.9 ± 0.1	0.9 ± 0.1	1.0 ± 0.1	1.2 ± 0.1	1.6 ± 0.2	2.5 ± 0.2
Pb	21 ± 0.2	-	-	23 ± 0.2	16 ± 0.2	25 ± 0.2
Pb	380 ± 38	200 ± 20	300 ± 38	-	-	-
Sb	3.8 ± 1.9	6.3 ± 3.2	8.9 ± 1.3	N.D.	N.D.	N.D.
Sc	21 ± 2	19 ± 2	28 ± 3	20 ± 2	30 ± 3	36 ± 4
Ta	N.D.	N.D.	N.D.	1.6 ± 0.8	3.7 ± 1.8	4.5 ± 2.2

[a] N.D. = not detected.

[b] D = detected qualitatively.

[c] Concentrations in wt %.

coal on an ash basis. In succeeding stages of particulate removal, however, the iron concentration decreases by approximately a factor of two. This suggests the possibility that the segregation of certain trace and minor elements by particle size in the resulting fly ash might be a function of the grain size of the discrete phases of mineral matter that host the various trace elements in coal instead of being simply the consequence of volatilization during combustion. For example, sphalerite (ZnS) has been identified as the host mineral for cadmium, as well as zinc, and has been found in relatively large, discrete grains in the low-temperature ashes of several coals.[49] A separate phase, possibly galena (PbS), was found in the very fine fraction of the low-temperature ash of yet another coal.[49]

The above experimental results demonstrate the definite potential of fluidized-bed combustion for reducing trace-element emissions as compared with conventional coal-fired power plants. The lower combustion temperatures and the presence of additive for sulfur dioxide removal are instrumental in reducing trace-element emissions by volatilization, which also results in minimizing the preferential concentration of trace elements in the finer fly ash particles.

Testing of Mercury Sampling Train

As reported above, mercury material balances for the trace-element combustion experiments, expressed as the percent of mercury entering the combustor that could be accounted for in the combustion products, ranged from a low of 29% to a high of 56%. Earlier work to determine the cause of the poor recovery of Hg was reported in the preceding annual report.[14] In additional work to determine the cause of the poor material balances and to possibly improve the sampling procedure, a thorough evaluation of the mercury sampling components used in the TRACE-5A and -6 experiments was made. In these experiments, the flue gas was successively passed through a scrubber solution containing 400 ml of 7% Na_2CO_3, 15.5 g of gold (in two separate coils of 10-mil-dia wire), and a scrubber containing 200 ml of 0.1M iodine monochloride (ICl) solution. Mercury was found in the carbonate solutions and on the gold, but none was found in the ICl solution.

Two laboratory experiments, MERC-1 and MERC-2, were completed to determine the suitability and efficiency of this sampling apparatus as an effective mercury recovery system. The apparatus is illustrated in Fig. 72. A carefully weighed amount of elemental mercury was placed in the mercury vapor generator and passed into the same combination of scrubbers and gold coils used in TRACE-5A and -6. The procedure in MERC-1 consisted of vaporizing 1.55 mg of mercury and passing it through the sampling train in a pure nitrogen carrier stream. In the MERC-2 experiment, 2.10 mg of mercury was vaporized, but, by controlled splitting of the nitrogen carrier gas, only ~250 μg of mercury was transported to the train.

A subsequent experiment, MERC-4, was performed to determine any effect of using flue gas as carrier gas. The procedure of MERC-1 and -2 was duplicated except that the flue gas from experiment EA-1 was used as the carrier gas instead of nitrogen gas.

The results of the three experiments are given in Table 20. Based on these data, the following conclusions were made:

1. When no potential interferences were present (as was the case in MERC-1 and -2 when pure nitrogen carrier was used), essentially full recovery of mercury

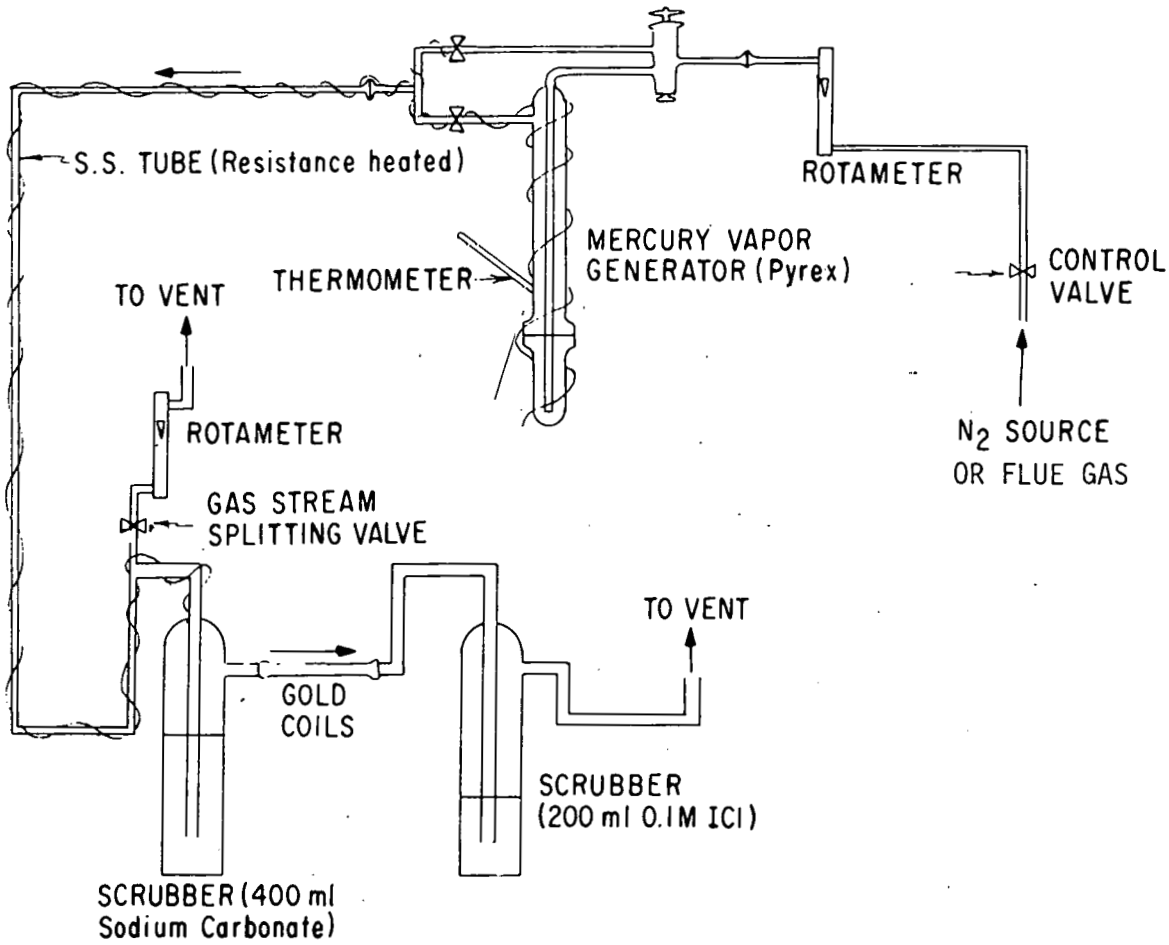

Fig. 72. Schematic Drawing of Testing Apparatus for Mercury Sampling

Table 20. Mercury Recoveries in Experiments MERC-1, -2, and -4

Experiment	Carrier Gas	Mercury In, µg	Mercury Recovered		
			Part of Train	µg	Recovery, %
MERC-1	N_2	1550	Na_2CO_3 solution	36	2
			Gold Foil	330	22
			ICl solution	1250	83
			Total	1616	107
MERC-2	N_2	247	Na_2CO_3 solution	0.28	--
			Gold Foil	72.0	29
			ICl solution	150.0	61
			Total	222.3	80
MERC-4	Flue Gas, Combustion Experiment EA-1	920	Na_2CO_3 solution	25.7	3
			Gold Foil	54.0	6
			ICl solution	687.0	75
			Total	766.7	84

(at least up to 1.50 mg) was achieved with this sampling system.

2. Even though the 7% sodium carbonate solution was the first absorber to contact the mercury, essentially all of the mercury in the stream passed through this solution. Apparently, the mercury concentration in the gas stream is so low that it cannot be condensed in the scrubber and a chemical reaction is required to remove the mercury from the gas.

3. The amount of mercury removed from the stream by the gold was less than one-half of that which came in contact with it. Essentially none of the Hg passed the ICl solution. This indicates that the ICl solution is quite efficient (in the absence of interferences) and that gold cannot be used alone to obtain full recovery.

4. The total mercury recovery in MERC-4 was again good, taking into account uncertainties in microgram weighing and analytical procedures. Whereas it had been noted in previous experimental work that quantities of mercury added to ICl solutions that had been contacted with flue gas could not be fully accounted for by subsequent mercury analyses, no problem was encountered in recovering the mercury "spiked" into the flue-gas-contacted ICl solution after experiment MERC-4. Thus the low mercury balances in the TRACE experiments are not due to interferences from flue-gas components passing through the train; other explanations must be found.

THE PROPERTIES OF A DOLOMITE BED OF A RANGE OF PARTICLE SIZES AND SHAPES AT MINIMUM FLUIDIZATION

Introduction

Coal can be burned in excess air in a pressurized fluidized bed of dolomite or limestone particles. The latter react with the sulfur compounds formed as a result of coal combustion and thereby reduce environmental pollution. The efficiency for sulfur retention in this process and adequate mathematical modeling appropriate for its scale-up demand, among other things, the proper understanding of the characteristics of a fluidized bed consisting of a wide range of particle sizes and shapes.

The results of a series of fluidization experiments performed in the ANL, 6-in.-dia, fluidized-bed reactor (normally used as a combustor) in the temperature and pressure ranges of 20-425°C/70-800°F and 26-121 psia are reported. In particular, the bed voidage at fluidization, the mean sphericity of the particles, and the minimum velocities were determined. Some comments are also made concerning the quality of fluidization of a bed of a range of particle sizes and shapes. These results are correlated on the basis of the Ergun relation. Other methods available in the literature and often employed for predicting the minimum fluidization velocity of a bed of single-size spherical particles are examined here for their applicability to a bed of a range of particle sizes and shapes. Knowledge of the minimum fluidization velocity facilitates the modeling of the reaction kinetics of a fluidized-bed reactor since it permits the determination of the gas in the bubble phase as an excess over that required for minimum fluidization.

Experimentation

The experiments were performed on the ANL bench-scale equipment designed for operation at pressures up to 10 atm. It consists of a fluidized-bed reactor (Fig. 48), a compressor for supplying fluidizing-combustion air, a preheater for this air, coal and additive feeders (for use in combustion runs), and an off-gas system. The latter consists of two cyclones, filters, gas sampling equipment, and a pressure let-down valve. The system is thoroughly instrumented and is equipped with an automatic data-logging system. The reactor consists of a 6-in.-dia stainless steel pipe, 11 ft long. The exterior of the pipe is wrapped with electrical heaters to heat the bed from room temperature to a desired temperature and up to the coal ignition temperature at the start of a coal combustion experiment. Also wrapped around this surface are external cooling coils to cool the bed during coal combustion. Additional cooling is provided by hairpin coils immersed in the fluidized bed. In these experiments, with combustion absent, no cooling of the bed was required. In this work, the bed was charged with a known amount of dolomite and then was operated as a batch reactor. A nominally constant bed level of 36 in. was maintained in the reactor by use of an internal overflow pipe.

Pressure taps installed in the reactor permitted measurements of pressure drops across the entire bed, as well as across two points (6 in. apart) in the bed. From these data, the height of the bed can be determined as a function of the fluidizing air velocity.

A knowledge of the dependence of the pressure drop across the bed, ΔP, on the gas velocity, u, yields information on the structure of a fixed or fluidized bed. For small values of u, ΔP is proportional to the gas velocity. As u increases, ΔP increases until u reaches the value u_{mf}, the minimum fluidization velocity. At this point, ΔP attains its maximum value, $\Delta P_{max}=W/A$. Here W is the weight of the bed and A is the effective cross-sectional area. As the gas velocity is increased beyond u_{mf}, gas bubbles form. Because a bubbling bed can easily deform, the pressure drop can remain constant over a range of u values above u_{mf}. However, under certain conditions the bubbles grow by coalescence to a diameter almost equal to the bed diameter before they escape from the bed and large pressure fluctuations occur. Also, channeling may occur in the bed and a large fraction of the bed remain unfluidized, in which case the ΔP_{max} is less than W/A. Furthermore, anomalous pressure drops may be observed if circulation patterns are set up within the bed and cause energy to be lost by friction among the solid bed particles and between the particles and the walls containing the fluidized bed. It is clear, therefore, that a plot of ΔP versus u is a useful indicator of the nature or quality of fluidization. Fluidization experiments made to gain insight into the quality of fluidization and to determine the minimum fluidizing velocity are next reported.

The reactor was charged with 14.9 kg of partially sulfated dolomite. The particle size distribution as obtained by sieve analysis is given in Table 21, as is the mass-weighted average particle diameter, $\bar{d}_p$, computed from the following relation:

$$\bar{d}_p = \frac{1}{\sum_i (x/d_p)_i} \qquad (1)$$

Here x is the weight fraction of particles in a size range i of diameter d_p. Seven fluidization experiments were conducted with this bed, using various combinations of temperature (20-425°C) and pressure (26-121 psia). Pressure drop measurements were obtained for both increasing and decreasing gas velocities. For each experiment, a straight line was drawn from the origin through the ΔP points that represented decreasing values of u. The intersection of this line with the line representing W/A was regarded as characterizing the minimum fluidization velocity. The experimental values of u_{mf} are listed in Table 22. On the whole, W/A was found to be a good measure of ΔP_{max} if the range of uncertainties associated with the various measurements was taken into consideration. Also, a detectable hysteresis effect in

Table 21. Particle-Size Distribution of Partially Sulfated Dolomite Bed Material Before and After the Seven Fluidization Runs

U. S. Sieve No.	Size Range, mm	Weight Fraction in the Range	
		Before	After
+14	> 1.41	0.0188	0.0192
-14 +25	1.41 - 0.71	0.5563	0.6347
-25 +35	0.71 - 0.50	0.2402	0.2071
-35 +45	0.50 - 0.35	0.1435	0.1026
-45 +80	0.35 - 0.177	0.0412	0.0249
-80 +170	0.177- 0.088	0.0000	0.0115
	Average Particle Diameter, μm	704	730

Table 22. Experimental Values of u_{mf}, L_{mf}, $\bar{\varepsilon}_{mf}$, $Re_{p,mf}$, and $\bar{\phi}_s$ at Various Temperatures and Pressures

Experiment No.	Temp, °C	Pressure, psia	u_{mf}, ft/sec	L_{mf}, ft	$\bar{\varepsilon}_{mf}$	$Re_{p,mf}$	$\bar{\phi}_s$
2	20	30	1.18	2.96	0.631	36	--
3	20	121	0.755	3.25	0.662	92	--
4	20	72	0.91	3.25	0.663	70	--
5	265 ± 5	26	1.18	3.18	0.657	12	0.3635
6	250 ± 14	120	0.77	3.20	0.659	33	--
7	380 ± 30	120	0.765	3.00	0.636	23	--
8	425 ± 14	73	0.85	3.00	0.636	14	0.3634
Mean	--	--	--	--	0.65	--	0.364

room temperature experiments was found, i.e., the ΔP values for a specific u were larger when the gas velocity was being increased than when the velocity was being decreased. Significantly, this effect became negligible when the pressure and/or temperature was increased. Also, a "hump" in the plot of ΔP versus u that was observed in the data pertaining to 70°F and 30 psia disappeared for runs at higher pressures and/or temperatures. In almost all cases, the data for ΔP are reasonably consistent for value of $u \leq u_{mf}$, but at larger values of u, an appreciable scatter in ΔP values is evident. In some cases, the scatter cannot be explained by the error limits of our measurements. These plots suggest that the observed response is not always characteristic of a bubbling bed; the large fluctuations may indicate slugging in the bed.

After the series of runs was completed, the bed was drained and weighed; its weight was only 4.5% less than its initial weight. No significant amount of material was found in the primary cyclone. Sieve analysis of a sample from the drained bed yielded the particle-size distribution reported in the fourth column of Table 21. The average particle diameter for the material originally fed, computed from equation 1, was found to be 704 μm. Since the average particle diameter after the runs was 730 μm, we regard the weight of the bed as constant for all runs. Also, the dolomite bed particles were found to have a smooth size distribution; consequently, the onset of fluidization and the plots of ΔP versus u may be interpreted in terms of a bed of uniform size particles of diameter $\bar{d}_p$. In the calculations described later, a mean value of 717 μm is used for $\bar{d}_p$

The experimental u_{mf} values reported in Table 22 indicate that at a given temperature, u_{mf} decreases with increasing pressure. These data also suggest that at a pressure of 8 atm, u_{mf} is almost independent of temperature in the range 20-380°C. These results also indicate that u_{mf} is almost independent of temperature at about 2 and 5 atm. Thus, in the pressure range of current measurements, u_{mf} appears to be almost independent of temperature. Also listed in this table are the values of the height of the fluidized bed at minimum fluidization, L_{mf}, as obtained from pressure drop measurements. It is interesting to note that these values are consistent with the height (3 ft) of the overflow pipe in the reactor.

Correlation for Minimum Fluidization Velocity

Correlation of these observed values of u_{mf}, L_{mf}, and ΔP_{mf} as a function of temperature and pressure on the basis of Ergun's correlation[50] for the pressure drop across a fixed and fluidized bed was attempted.

The theoretical basis of Ergun's correlation is based on works which are reviewed by Carman,[51] and the numerical constants and general form of the correlation are substantiated by a large body of experimental work of Chilton and Colburn,[52] Leva et al.,[53], [54] Ergun and Orning,[55] and others. The experiments in almost all cases were performed on particles of a single size or a narrow size distribution. The Ergun correlation for a fixed bed based on data mostly obtained at room temperature and atmospheric pressure is as follows:

$$\frac{\Delta P g_c}{L} = 150 \frac{(1-\bar{\varepsilon})^2 \mu u}{\bar{\varepsilon}^3 \bar{D}_p^2} + 1.75 \frac{(1-\bar{\varepsilon}) \rho_g u^2}{\bar{\varepsilon}^3 \bar{D}_p} \qquad (2)$$

Here ΔP is the pressure drop across a bed of height, L; $\bar{\varepsilon}$ is the mean void fraction (voidage); u is the superficial gas velocity; μ is the gas viscosity; ρ_g is the gas density; g_c is the conversion factor and is equal to 980g cm/(g-wt)(sec^2); and $\bar{D}_p$, the mean particle diameter, is defined in terms of S_v, the specific surface of the solid particles (i.e., the solid particle surface area per unit volume of the solid) as follows:

$$\bar{D}_p = (6/S_v) = \bar{\phi}_s \bar{d}_p \qquad (3)$$

Equation 3, involving the mean shape factor, $\bar{\phi}_s$, and the mean particle diameter, $\bar{d}_p$, defined by equation 1, is used here to interpret the behavior of a bed composed of nonspherical particles of a wide size distribution. The weight fraction in the size interval of average diameter, d_p, is obtained in this work by sieve analysis. If d_p is the diameter of the sphere having the same volume as that of the particle, the shape factor, ϕ_s, would represent the sphericity of the particle.

Equation 2 may be applied[55,56] to a fluidized bed at minimum fluidization as follows:

$$\frac{\Delta P_{mf} g_c}{L_{mf}} = 150 \frac{(1-\bar{\varepsilon}_{mf})^2 \mu u_{mf}}{\bar{\varepsilon}_{mf}^3 (\bar{\phi}_s \bar{d}_p)^2} + 1.75 \frac{(1-\bar{\varepsilon}_{mf}) \rho_g u_{mf}^2}{\bar{\varepsilon}_{mf}^3 (\bar{\phi}_s \bar{d}_p)} \qquad (4)$$

where the subscript mf signifies minimum fluidization. Furthermore, ΔP_{mf} is equal to the buoyant weight of the dolomite particles per unit area:

$$\Delta P_{mf} g_c = (\rho_s - \rho_g)(1-\bar{\varepsilon}_{mf}) L_{mf} g \qquad (5)$$

where ρ_s is the solid particle density and g is the acceleration due to gravity.

The plots of ΔP versus u (not included here) indicated that the quantity, Q, at minimum fluidization, defined as

$$Q = \Delta P_{mf}(A/W) \tag{6}$$

is unity for all seven experiments and that therefore

$$P_{mf}=W/A \tag{7}$$

The density of fresh and unsulfated dolomite particles was experimentally determined to be 2.749 ± 0.004 g/cc. The density was determined by the weight loss of a known amount of dolomite in water. A trace of surfactant was added to the water prior to the determination. Equations 5 and 7 are employed to compute $\bar{\epsilon}_{mf}$, and these values of $\bar{\epsilon}_{mf}$ are reported in Table 22.

It is clear that for the range of particle sizes and operating conditions of temperature and pressure employed in the experiments, the use of the mean value of 0.65 for bed voidage, $\bar{\epsilon}_{mf}$, at minimum fluidizing conditions is adequate for calculations. The voidage of a mixture of particles with a wide size distribution is difficult to estimate because the fines can fit into the voids between the large particles and thus decrease voidage. On the other hand, it has been shown[51,57] that the particles pack more loosely near the walls as a result of air velocity near the walls differing from that in the middle section. The latter effect increases as the ratio of the particle diameter to the bed diameter increases. In our bed, additional enhancement of this effect is a result of the presence of hairpin cooling coils. If segregation of the particles occurs, the voidage can vary appreciably along the height of the bed as a result of the larger particles being packed tighter at the bottom of the bed and more and more light particles populating the upper regions of the bed. This results in the voidage increasing with height. It thus appears that the concept of mean bed porosity (voidage) is artificial in fluidized-bed operations involving a wide range of particle sizes.

The particle Reynolds number, Re_p, is defined as

$$Re_p = \bar{d}_p \rho_g \, u/\mu \tag{8}$$

When Re_p is smaller than 20, the rightmost term of equation 4, which represents the kinetic energy losses, is negligibly small. Under such conditions, the observed pressure drop is almost completely accounted for by the viscous effect, so that at minimum fluidization,

$$\frac{\Delta P_{mf} g_c}{L_{mf}} = 150 \frac{(1-\bar{\varepsilon}_{mf})^2 \mu u_{mf}}{\varepsilon_{mf}^3 (\bar{\phi}_s \bar{d}_p)^2} \tag{9}$$

as long as

$$Re_{p,mf} = \frac{\bar{d}_p \rho g \, u_{mf}}{\mu} < 20 \tag{10}$$

The Reynolds numbers at minimum fluidization velocity, $Re_{p,mf}$, computed for the various experiments are listed in Table 23. For experiments 5 and 8, the condition of equation 10 is satisfied. Equation 9, in conjunction with equation 7, is employed to compute the mean particle sphericity, $\bar{\phi}_s$, and the results are given in the eighth column of Table 23. The agreement between the two values is fortuitously good, but their apparent small magnitudes are somewhat puzzling at first sight. The calculated values of particle sphericity, ϕ_s, from microscopic measurements summarized by Carman[51] suggest that such low values are characteristic of fibers and flakes. The low values of $\bar{\phi}_s$ are due to the use of $\bar{d}_p$ values as determined by sieve analysis. To illustrate the point, let us assume that the value of $\bar{\phi}_s$ is 0.6. Then on the basis of our experimental value for $\bar{\phi}_s$, the diameters determined by screen analysis must be multiplied by about 0.61 to obtain the diameters of the equivalent spheres that would have the same volume as the particles. These numerical figures would agree with the exact calculations if the dolomite particles should have approximately a disk shape with a thickness one-third of the disk radius. Further, it must be kept in mind that the accuracy of the correlation of equation 2, even for well-behaved packed beds, is estimated to be $\pm$25%. We thus regard the mean shape-size factor, $\bar{\phi}_s \bar{d}_p$, as a semiempirical adjustable parameter, and this concept should prove useful if equation 4 emerges as a successful correlating relation for u_{mf}. This concept is evaluated below.

The mean fluidizing velocities computed for the operating conditions corresponding to experiments 2, 3, 4, 6, and 8 from equation 4 are listed in Table 23, column 5. These calculated values agree with the directly measured values (listed in column 4 of Table 23), within an average absolute deviation and a maximum deviation of 2.7 and 4.5 percent, respectively. This agreement is regarded as satisfactory because the accuracy of the experimental u_{mf} values is estimated to be $\pm$5 percent. It also follows from this good agreement between the two sets of u_{mf} values that similar good agreement would probably be obtained for $\bar{\phi}_s$, if the data on the remaining runs (all at $Re_{p,mf} > 20$) were to be employed. The point to be stressed is the success of the Ergun correlation with this semi-empirically determined shape-size factor in quantitatively predicting the temperature and pressure dependence of u_{mf}. Thus, experimental trends, one indicating that at a given temperature, u_{mf} decreases with increasing pressure and the other that

Table 23. Experimental and Calculated Values of Minimum Fluidization Velocity

Experiment No.	Temp, °C	Pressure, atm	u_{mf}, cm/sec			
			Exptl	Calculated		
				Eq. 4	Eq. 15	Eq. 17
2	20	2.04	36.0	37.7	31.1	45.6
3	20	8.23	23.0	23.4	20.5	45.5
4	20	4.90	27.7	27.3	24.0	45.5
5	265 ± 5	1.77	36.0	--	26.4	30.0
6	240 ± 15	8.16	23.5	24.1	22.9	30.5
7	380 ± 30	8.16	23.3	24.4	20.4	26.3
8	425 ± 15	4.97	25.9	--	21.5	25.2

at a given pressure, u_{mf} is almost independent of temperature, are quantitatively confirmed by the Ergun relation. The interpolation within the range of the operating variables, as well as a modest amount of extrapolation, seems warranted and reliable enough for engineering design calculations.

In the above treatment we have assumed that there is no flocculation or clustering of small particles.[58] However, if flocculation or clustering occurs, $\bar{d}_p$ will increase and this will lead to smaller pressure drops on the basis of equation 4. A smaller pressure drop will also result with any increase in $\bar{\phi}_s$. The Ergun relation can be broadened by adding a third term on the right-hand side of equation 4. This term should include the influence of hairpin cooling coils, thermowells, and the walls of the reactor, because these present a different type of surface to the fluid than do the bed particles.[51] Ergun[50] noted the inapplicability of equation 4 to systems involving mixtures of different size particles when the ratio of tube diameter to average particle size is less than 10. For the larger particles in our feed, the configuration of our reactor (with cooling coils immersed in the bed) simulate such conditions. However, the cooling coils and the thermowells located close to the reactor walls occupy only about 15 percent of the reactor cross section. Thus, apparently only a small portion, at most, of any probable discrepancy can be attributed to this source. The view of treating $\bar{\phi}_s$ as an adjustable parameter in the Ergun relation appears to be expedient at the present time.

Calculation of Minimum Fluidization Velocity

Our experimentally determined values of minimum fluidization velocity will now be discussed in the light of various procedures described in the literature for their prediction and correlation.

The various correlation methods developed for minimum fluidization velocity and hence appropriate for its calculation are described by Leva[59] and Frantz.[60] Some of the more recent correlations are due to Narsimhan,[61] Frantz,[62] and Wen and Yu.[63,64] Of these methods, the expressions given by Narsimhan[61] and Wen and Yu[63] are tested against sufficient experimental data and are consequently fairly reliable. For computing the minimum fluidization velocity for the operating conditions of the series of seven runs described above, use of the expression of Wen and Yu[63] is preferred because it is based on more realistic estimates[64] of minimum fluidization voidage and the particle shape factor.

By combining equations 4 and 5, we get

$$150 \frac{(1-\bar{\varepsilon}_{mf})^2 \mu u_{mf}}{\bar{\varepsilon}_{mf}^3 (\bar{\phi}_s \bar{d}_p)^2} + 1.75 \frac{(1-\bar{\varepsilon}_{mf}) \rho_g u_{mf}^2}{\bar{\varepsilon}_{mf}^3 (\bar{\phi}_s \bar{d}_p)} - g(\rho_s - \rho_g)(1-\bar{\varepsilon}_{mf}) = 0 \qquad (11)$$

Equation 11 can be rearranged by introducing the particle Reynolds number at minimum fluidization, $Re_{p,mf}$, and the Galileo number, Ga, so that

$$150 \frac{(1-\bar{\varepsilon}_{mf})}{\bar{\phi}_s^2 \bar{\varepsilon}_{mf}^3} Re_{p,mf} + 1.75 \frac{Re_{p,mf}^2}{\bar{\phi}_s \bar{\varepsilon}_{mf}^3} - Ga = 0 \qquad (12)$$

where

$$Ga = \frac{\bar{d}_p^3 \rho_g (\rho_s - \rho_g) g}{\mu^2} \qquad (13)$$

Wen and Yu[63] suggested, on the basis of experimental data available in the literature, that the two groups of $\bar{\phi}_s$ and $\bar{\varepsilon}_{mf}$ occurring in equation 12 be approximated by the following relations:

$$\frac{(1-\bar{\varepsilon}_{mf})}{\bar{\phi}_s^2 \bar{\varepsilon}_{mf}^3} \simeq 11 \text{ and } \frac{1}{\bar{\phi} \bar{\varepsilon}_{mf}^3} \simeq 14 \qquad (14)$$

Our experimental $\bar{\varepsilon}_{mf}$ and $\bar{\phi}_s$ values give, for the two groups of equation 14, the values of 9.6 and 10, respectively. The two sets of numerical values are only in fair agreement with each other, and it is interesting to examine the following simplified version of equation 12 obtained on the basis of equation 14 for predicting u_{mf}:

$$u_{mf} = \frac{\mu}{\bar{d}_p \rho_g} \left\{ [(33.7)^2 + 0.0408\ Ga]^{1/2} - 33.7 \right\} \tag{15}$$

Values calculated by the use of equation 15 are given in column 6 of Table 23; it will be noticed that the relation of equation 15 consistently underestimates the values of u_{mf} by about 15 percent. This is to be regarded as satisfactory agreement since a statistical evaluation of equation 15 with 284 data points by Wen and Yu[63] yielded a standard deviation of 34 percent and an average deviation of $\pm$25 percent. However, this comparison of theory and experiment does emphasize the importance of using accurate $\bar{\varepsilon}_{mf}$ and $\bar{\phi}_s$ values in estimating u_{mf} based on equation 12.

If $Re_{p,mf}$ is less than twenty, the second term of equation 11 representing the kinetic energy losses is negligibly smaller than the first term referring to the viscous losses, and equation 11 simplifies to:

$$u_{mf} = \frac{(\bar{\phi}_s \bar{d}_p)^2\ g(\rho_s - \rho_g)\ \bar{\varepsilon}_{mf}^3}{150\ \mu\ (1-\bar{\varepsilon}_{mf})} \tag{16}$$

Equation 16 in conjunction with equation 14 further simplifies to the following:

$$u_{mf} = \frac{(\bar{\phi}_s \bar{d}_p)^2\ g(\rho_s - \rho_g)}{1650\ \mu} \tag{17}$$

In our experiments, $Re_{p,mf}$ ranges from 12 to 92 if $\bar{d}_p$ is based on the nominal apertures of the sieves used in the particle size analysis. In establishing the limit for equation 16 in terms of $Re_{p,mf}$, the size dimension used was the diameter of an equivalent sphere that has the same volume as the actual particle. We may consequently expect only moderate success for equation 17 in correlating our measured u_{mf} values. Values computed from equation 17 are reported in the seventh column of Table 23, and these values are generally larger than the experimental values given in the fourth column of this table. Alternative values for the numerical coefficient in equation 17 have been recommended. Davidson and Harrison[65] and Davies and Richardson[66] recommended values of 1233 and 1282, respectively. Such choices would further worsen the agreement between the computed and experimental values.

Another important feature to note concerning equation 17 is its inability to reproduce the observed pressure and temperature dependencies of u_{mf}. Mii, Yoshida, and Kunii[67] reported the inability of equation 16 to reproduce their experimentally determined u_{mf} values as a function of temperature in the range 20-800°C; the calculated values were greater than the values they observed. Mii et al. data pertain to graphite spheres of 0.20 to 0.40 mm diameter at ambient pressure. On the other hand, the work of Singh, Rigby, and Callcott,[68] who used silica sand with a mean particle size of 200 μm in the temperature range 288-973°K at ambient pressure, confirms the appropriateness of equation 17 with a value of 1386±90 for the numerical constant. The primary motivation of their work[68] was to confirm the dependence of u_{mf} on μ as given by equation 16 and equation 17. Broughton[69] suggests the use of equation 17 with 1440 as the numerical coefficient for computing u_{mf} with a maximum error of 15%. Broughton[69] also explains why Mii et al. data[47] may be in error.

It follows from the above analysis that the application of equation 16 or equation 17 to a system at a pressure higher than ambient is inappropriate, though the majority of literature evidence supports their adequacy for representing the dependencies of u_{mf} on temperature and viscosity of the fluidizing gas at ambient pressure and for low Reynolds number.

For a particle Reynolds number smaller than 5, Leva[70] has suggested a relation similar to that of equation 17 except that the numerical factor is replaced with 1429 $Re_{p,mf}^{0.063}$. This correlation has been extensively tested by Kunz[71] for fluid cracking catalysts and spherical glass beads but is not employed here bacause it is only valid for systems characterized by very low Reynolds numbers.

The Ergun correlation at minimum fluidization as given by equation 4 may be rearranged in the following linear form:

$$f_v = \frac{\Delta P_{mf} g_c \bar{\phi}_s^2 \bar{d}_p^2 \bar{\varepsilon}_{mf}^3}{L_{mf} \mu u_{mf} (1-\bar{\varepsilon}_{mf})^2} = 150 + 1.75\ Re'_{p,mf} \qquad (18)$$

where

$$Re'_{p,mf} = \frac{\bar{\phi}_s}{(1-\bar{\varepsilon}_{mf})} Re_{p,mf} \qquad (19)$$

Here f_v is the viscous friction factor and is dimensionless. The modified Reynolds number, $Re'_{p,mf}$, is defined in terms of (1) the Reynolds number given by equation 10, (2) the mean sphericity, $\bar{\phi}_s$, which is one for spherical particles, and (3) the mean bed voidage, $\bar{\varepsilon}_{mf}$.

Hicks[72] has shown that for spherical particles, the above relation of equation 18 is not in accordance with the observed pressure drop for $Re_{p,mf}$ greater than 500. He recommends a nonlinear relation for f_v in the range $300 < Re_p/(1-\varepsilon) < 60{,}000$. In our experiments with nonspherical ($\bar{\phi}_s = 0.364$) dolomite particles of a size range from slightly greater than 14 mesh (U.S. Sieve No.) to +170, the maximum value of $Re'_{p,mf}$ is about 95. The validity of the linear relation of equation 18 in interpreting our experimental data is then in conformity with the findings of Hicks.

In contrast to the Ergun relation of equation 11 derived by consideration of pressure drop, Wen and Yu[63] developed a correlation on the basis of drag force considerations. They found that the drag force, F_k, of a fluid acting on a single spherical particle in a multiparticle system is related by the following relation to the drag force, F_{ks}, of the same fluid on this particle when situated in an infinite expanse of fluid:

$$F_k = \bar{\varepsilon}^{4.7} F_{ks} \tag{20}$$

Further, by assuming the validity of the above relation at minimum fluidization, Wen and Yu[63] equated the drag and the buoyance forces acting on the particle with the gravitational force and derived a correlation that is valid for Reynolds numbers up to 1000, particle diameters ranging from 0.001524 to 0.635 cm, ρ_s from 1.06 to 11.25 g/cc, fluid density from 0.818 to 1.135 g/cc, and μ from 1.0 to 15.01 centipoise. This correlation, after modification to apply to a wide size range of nonspherical particles, becomes:

$$\bar{\varepsilon}_{mf}^{4.7}\, \bar{\phi}_s^2 Ga = 18\, Re_{p,mf} + 2.70\, \bar{\phi}_s^{0.687} (Re_{p,mf})^{1.687} \tag{21}$$

The validity of equation 21 was checked on the basis of results of the same series of seven runs for which data are reported in Table 23, and the results given in Table 24 were obtained. The modified correlation is shown to be adequate by this comparison of theory and experiment, and the average absolute deviation of 9.4% is about the same as that found by Wen and Yu.[63] This result also substantiates that the correlations obtained for u_{mf} on the basis of either pressure drop or drag forces for a wide range of nonspherical particles give similar results. A similar conclusion is derived by Wen and Yu[63] for spherical particles of a moderate size range.

Zenz[73,74] generated plots of $(Re_p/C_D)^{1/3}$ versus $(C_D Re_p^2)^{1/3}$ as a function of bed voidage to describe particulate fluidization characteristics of spherical particles. Here C_D is the drag coefficient. For a bed composed of nonspherical particles of a wide size range, Zenz's relations are modified as follows:

Table 24. Demonstration of the Validity of Equation 21

Experiment No.	$Re_{p,mf}$	X[a]	Y[b]	Dev., %
5	12	289	305	5.2
8	14	390	368	5.6
7	23	734	681	10
6	33	1238	1086	12
2	36	1327	1217	8.3
4	70	3295	3008	8.7
3	92	5264	4428	16

a $X \equiv \bar{\epsilon}_{mf}^{4.7}\ \bar{\phi}_s^2 Ga$

b $Y \equiv 18\ Re_{p,mf} + 2.70\ \bar{\phi}_s^{0.687}\ (Re_{p,mf})^{1.687}$

$$\left[\frac{Re_p}{C_D}\right]^{1/3} = u\ \frac{4}{3}\left[\frac{\mu(\rho_s-\rho_g)g}{\rho_g^2}\right]^{-1/3} \tag{22}$$

and

$$(C_D Re_p^2)^{1/3} = \bar{\phi}_s \bar{d}_p \left[\frac{3}{4}\frac{\mu^2}{\rho_g(\rho_s-\rho_g)g}\right]^{1/3} \tag{23}$$

Zenz's procedure is employed here with equation 22 and equation 23 to check whether the plot of our data, taken at minimum fluidization for different temperature and pressure conditions of the bed, is consistent with the plots of Zenz. The experimental data (plotted in Fig. 73) pertain to a mean bed voidage of 0.650. The suggested functional dependence of this plot implies at least qualitative correctness of the theory of drag forces acting on particles at minimum fluidization. This analysis also validates the extension of the procedure suggested by Zenz for spherical particles to nonspherical particles of a wide size range as included in equation 22 and equation 23. Also given in Fig. 73 are the two plots approximately

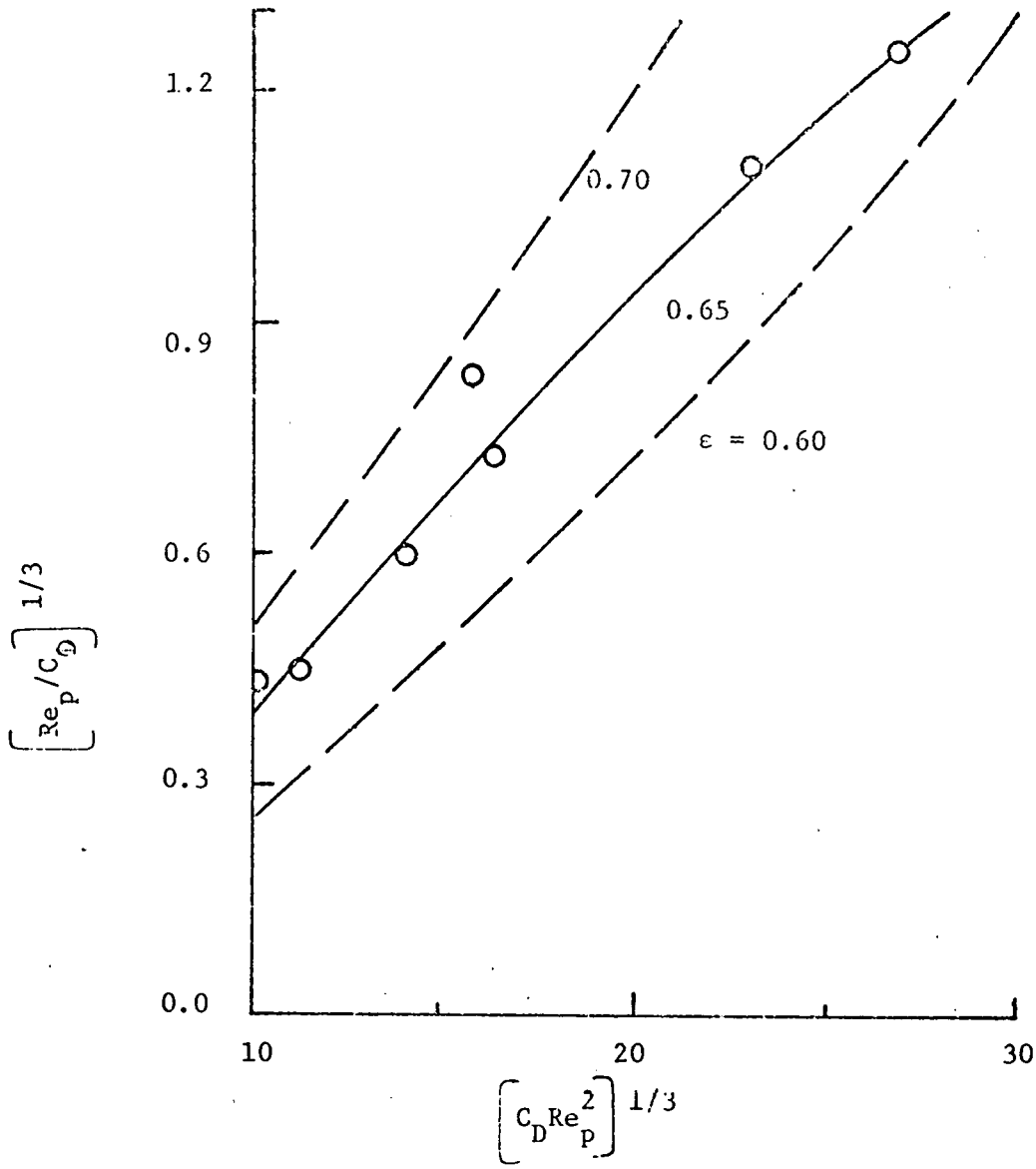

Fig. 73. A Correlation Plot for Particulate Fluidization. Circles are our experimental points, and the continuous curve is a smooth plot through them. Broken curves are approximate reproductions from Zenz and Othmer.[74]

reproduced from the graph given by Zenz and Othmer[74] for bed voidage values of 0.60 and 0.70 for spherical particles. Zenz and Othmer generated these curves by smoothing the available literature data. Their agreement with our results, as contained in Fig. 73, reflects the consistency of our measured u_{mf} values and the adopted characterization procedure for nonspherical particles of a wide size range with the literature values of particulate fluidization and sedimentation data on spherical particles.

Andersson[75] developed a modified version of the pressure drop correlation of Ergun by introducing a tortuosity factor, q, a cross section factor, Z, and an inertial drag coefficient, C_i. His final result for the particulate fluidized bed composed of uniform size spheres, when modified for the nonspherical particles of a wide size range, becomes

$$\frac{\Delta P}{L} = 36Zq^2 \frac{(1-\bar{\varepsilon})^2 \mu u}{\bar{\varepsilon}^3 (\bar{\phi}_s \bar{d}_p)^2} + 6C_i q^3 \frac{(1-\bar{\varepsilon})\rho_g u_{mf}^2}{\bar{\varepsilon}^3 (\bar{\phi}_s \bar{d}_p)} \tag{24}$$

Here

$$q = 1.71 \left(\frac{1-\bar{\varepsilon}}{\bar{\varepsilon}} \right)^{0.15}, \tag{25}$$

$$Zq^2 = \frac{1}{2(1-\bar{\varepsilon})\, \bar{\varepsilon}^{1.59}}, \tag{26}$$

and

$$C_1 = 4.5/8 \tag{27}$$

Calculated values of ΔP by use of these expressions agree with the observed values for experiments 2, 3, 4, 6, and 7 within the percentage deviations of 15, 5.6, 7.7, 16.3, and 20, respectively. The experimental values were each greater than the corresponding calculated results. This is regarded as fair agreement since the mean value of sphericity was computed from Ergun correlation at low Reynolds number by using the observed pressure drops. Further, since the correlations of equation 24 through equation 27 are based on data for spherical particles, their validity for our system is only approximate. Nevertheless, the above calculations are revealing and substantiate to a large extent the present approach of employing mean ε, d_p, and ϕ_s values to describe a bed of a wide size range of nonspherical particles.

Quality of Fluidization

Another important aspect of modeling studies lies in the adequate understanding of the dispersion of solid particles in the gas, i.e., the quality of fluidization of the bed. Suitable criteria for determining the quality of fluidization have been developed by combining theoretical analysis with experimental data. Thus, Wilhelm and Kwauk[76] report that at maximum fluidization, the Froude number, defined as

$$Fr_{mf} = u_{mf}^2/d_p g \tag{28}$$

is smaller than 0.13 for smooth or particulate fluidization and is greater than 0.13 for bubbling or aggregative fluidization. Richardson[77] puts this Froude number for the transition between particulate and aggregative fluidization as unity. For our experiments, the Froude numbers, computed by means of equation 28 with $\bar{d}_p$, range from 7.7 to 18.4. This suggests that, even at minimum fluidizing condition, the bed as a whole may not be smoothly fluidized and that at least parts of it are in a state of bubbling fluidization. This is further confirmed by applying the criteria of Romero and Johanson,[78] who suggested that the product of the following four dimensionless groups:

$$(Fr_{mf})(Re_{p,mf}) \{ (\rho_s-\rho_g)/\rho_g) \} (L_{mf}/d_t) \tag{29}$$

should be smaller than 100 or greater than 100 for a smooth or a bubbling fluidized bed, respectively. For our runs, this product is much larger, about 10^6. In equation 29, d_t is the diameter of the reactor. Although the basis of these criteria is sound, some caution is essential in the quantitative application, because these limits were established by experiments on particles of the same size, in many cases with spherical or nearly spherical particles, and in relatively shallow beds.

A logical inference on deep beds of particles of wide size distribution such as those employed in this work is that smooth fluidization occurs at the bottom of the bed, where the pressure is high and gas velocity low, and that bubbling fluidization occurs at the top, where the terminal velocity[57] for the smallest size particles is twice the superficial gas velocity. As a result, these small particles are not likely to be permanently thrown out of the bed. The pressure drop for a range of fluidizing-gas velocities greater than that required for the bed at minimum fluidization has been observed to be approximately constant; this is consistent with the conjectured quality of fluidization. Because the pressure fluctuations are rather modest, we exclude the possibility that slugging is occurring. Furthermore, in view of the validity of equation 7, the prospects for channeling or for establishing circulation patterns within the bed are somewhat remote. Although these conclusions clearly follow from the present work and are consistent with the accumulated experience in the literature, they are strictly valid only for particle-size distributions similar to those given in Table 21.

REVAMPING OF THE BENCH-SCALE, PRESSURIZED, FLUIDIZED-BED COMBUSTION SYSTEM

The existing 6-in.-dia, pressurized, fluidized-bed combustor is limited to operating at combustion temperatures ranging from 790 to 955°C (1450 to 1750°F), fluidizing-gas velocities from 2 to 5 ft/sec, bed depths of 3 to 4 ft, and additive particle sizes below 14 U.S. mesh (1.41 mm). A new 6-in.-dia combustor is being designed for installation and use in studying the effects of much higher gas velocities, deeper beds, and larger additive particle sizes. The new combustor will be capable of operating at conditions to be used for a full-size, pressurized combustor incorporated into a combined cycle. In a combined cycle, the flue gas from the combustor, which is at high temperature, is expanded through a gas turbine.

In the existing combustor, the temperature of the flue gas decreases several hundred degrees Centrigrade in the freeboard area of the combustor, and the flue-gas system is not designed to withstand combustion-zone temperatures. Concentrations of elements harmful to turbine blades, as well as concentrations and sizes of particles, in the flue gas are to be determined at flue-gas temperatures expected in a full-size unit. It is planned, therefore, to replace the present combustor flue-gas system (piping, cyclones, and filters) with equipment suitable for operation at temperatures up to 900°C (1650°F).

Design of New Combustor

The design operating conditions for the proposed new combustor are presented in Table 25. A conceptual drawing of the combustor design is presented in Fig. 74.

Table 25. Design Parameters of New 6-in.-dia Combustor

Parameter	Range or Limit
Pressure	≤10 atm abs.
Temperature	835-955°C (1550-1750°F)
Gas Velocity	6-10 ft/sec
Bed Height	6-8 ft
Excess Air	15-100%
Ca/S Ratio	≤6:1
Additive Size	-0.25 in.
Coal Size	-7 U.S. mesh (0.111 in.)

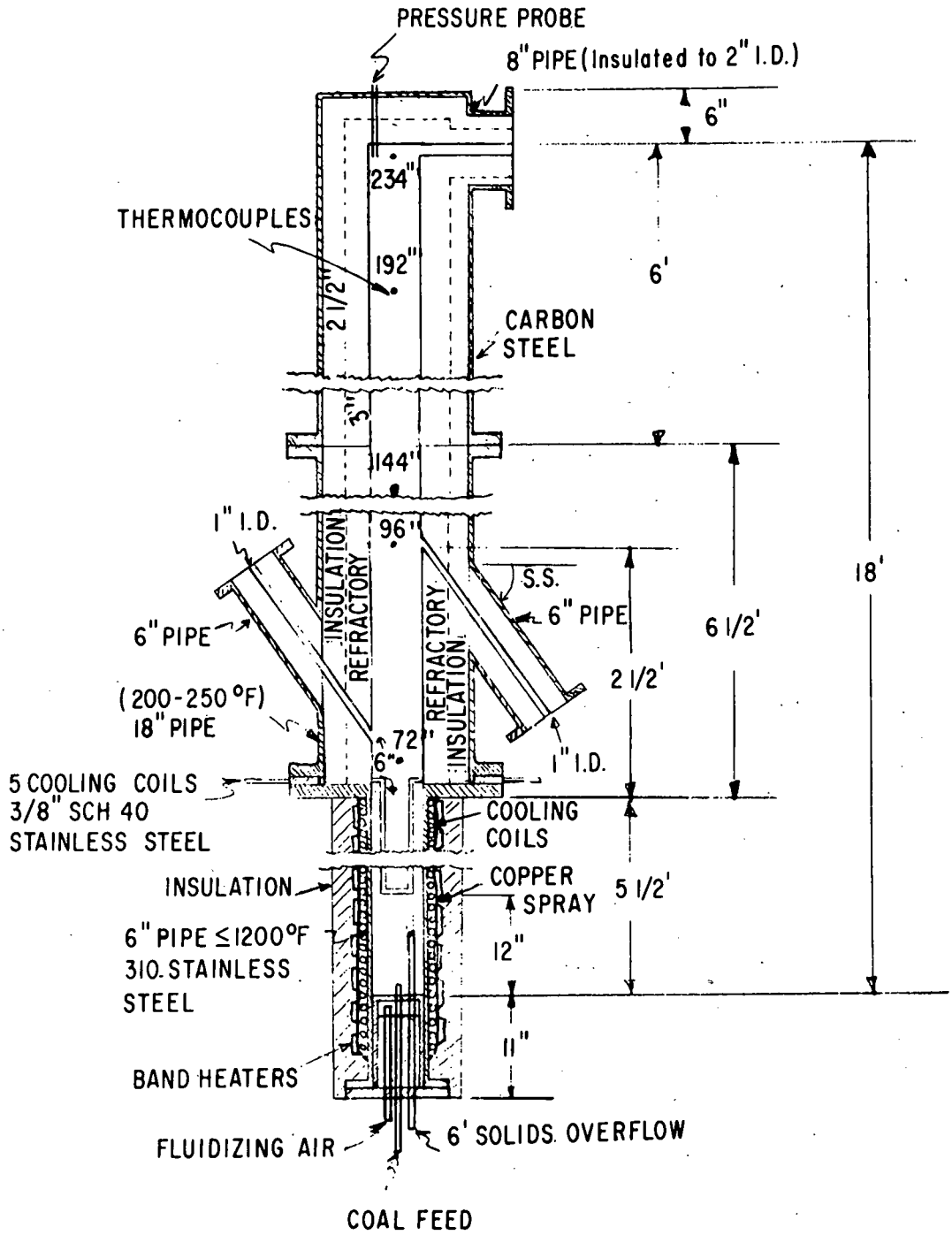

Fig. 74. Conceptual 6-in.-dia Combustor

The lower section of the combustor consists of a 6-in.-dia, schedule 40, stainless steel pipe approximately 6.5 ft long. A bubble-type gas distributor is flanged to the bottom of the lower section and accommodates fluidizing-air inlets, a coal feed line, thermocouples for monitoring bed temperature (not shown in Fig. 74), and a 6-ft standpipe for maintaining a constant bed level. The 6-in.-dia pipe will be wrapped with cooling coils onto which a layer of heat-conducting copper and then an overlay of oxidation-resistant stainless steel will be applied. Strip heaters will then be banded to the heat-conducting overlay for use during startup of the combustor. This arrangement should facilitate the replacement of heaters in the event of burnout. The active lower section of the combustor will then be insulated to eliminate heat losses during startup of the unit.

Additional cooling capacity will be provided by five internal, hairpin-shaped cooling coils that enter the combustor through a flat-plate ring section positioned between the flanges connecting the lower and middle sections of the combustor. The cooling coils will extend downward in the combustor to within 12 in. of the top surface of the gas distributor. Maintenance of the internal cooling coils should be considerably easier in the new combustor than in the existing unit.

The middle and upper sections of the new combustor consist of nominal 18-in.-dia, schedule 30, carbon steel pipe lined with insulation and refractory to an inside diameter of 6 in. The refractory/insulation lining is designed to limit the temperature drop of the flue gas to $\leq$30°C in the freeboard section of the combustor. The inner refractory liner (3 in. thick) will be Plicast Ero-zist, a high-density erosion-resistant castable from the Plibrico Company. The insulation between the refractory and the steel shell will be WRP-X ($\sim$2.5 in. thick) from Refractory Products Company.

The middle section of the combustor has two side arms, one for the feeding of additive and the other for withdrawing solids during runs made at a bed depth of 8 ft. Feeding of the additive by gravity eliminates the high flow rates of air that would be needed to pneumatically transport 0.25-in. additive particles into the combustor, which has a relatively small cross section.

The overall height of 16 ft between the gas distributor and the off-gas port is designed to avoid slugs of material being carried up the reactor and into the off-gas lines. The relatively high gas velocity of 10 ft/sec in a 6-in.-dia unit will undoubtedly result in slugging of the bed material with bed levels of 6 or 8 ft.[79] Therefore, a maximum freeboard was provided to permit dissipation of the slugs.

Flue-Gas System

The proposed new flue-gas system (off-gas system) is illustrated in Fig. 75. The system is being designed to operate at temperatures up to 900°C/1650°F, with an anticipated drop in flue-gas temperature of $\sim$55°C through the system. The primary and secondary cyclones will consist of refractory-lined steel shells that will either serve as cyclones themselves or house cyclones of stainless steel construction. Vendors are being requested to submit bids for these items.

After the flue gas passes through the primary cyclone and the secondary cyclone, the flue gas passing through the main flue-gas system will be quenched to a temperature of 400°F (205°C), filtered to remove the fine particulate solids, and then vented to the atmosphere. Devices will be installed, however, to take a sample of the hot flue gas from the secondary cyclone and to pass it through experimental filters to study the removal of fine particulate matter at high temperatures.

As indicated in Fig. 75, several sample ports will be located in the off-gas system for measuring both the concentrations of flue-gas constituents and the concentrations of particulate solids in the flue gas.

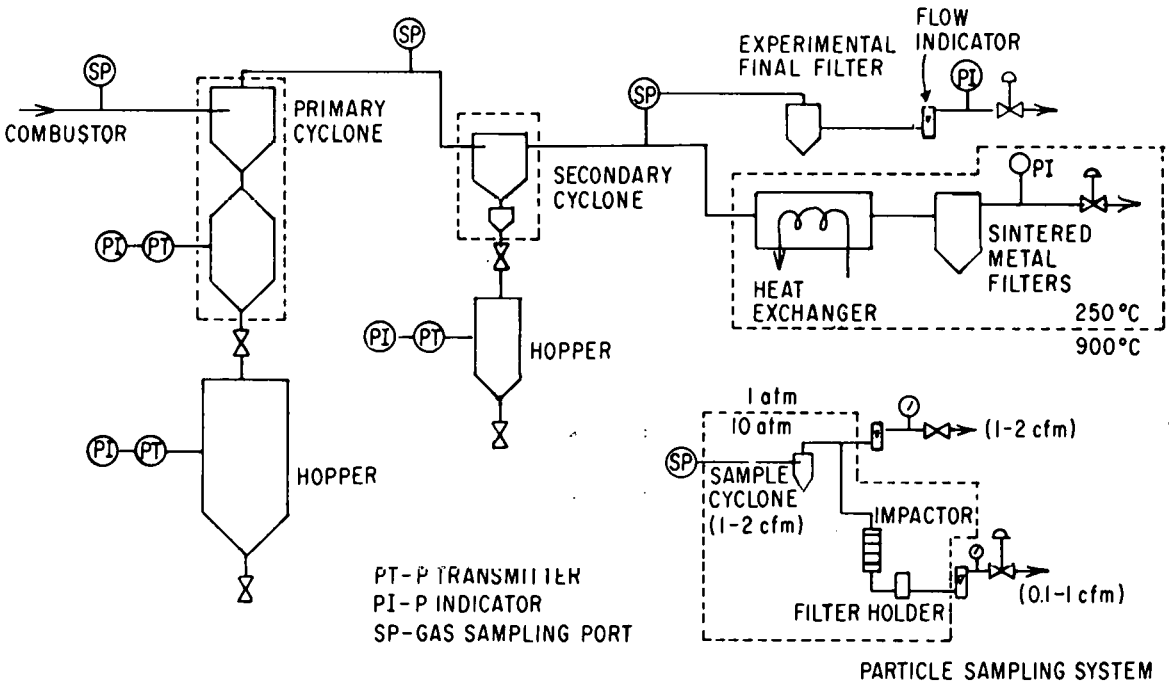

Fig. 75. Hot Off-Gas System (Designed for Operation at 900°C)

SEPARATION OF COMBUSTION AND REGENERATION SYSTEMS

The 6-in.-dia, pressurized, fluidized-bed combustor and the 3-in.-dia, pressurized, fluidized-bed regenerator currently utilize several components in common. Equipment common to both units includes the inlet and outlet surge tanks, the gas preheater, the additive solids-feeder, the off-gas system (cyclones, filters, pressure-control valve, etc.), and the off-gas analysis system. Due to the dual function of these components, the two units cannot be operated simultaneously.

Modifications of both units and installation of additional equipment are in progress in order to physically separate the combustor and the regenerator and to provide each unit with its own auxiliary components. These modifications will permit concurrent investigations of both the combustion process and the regeneration process, thus increasing research capabilities relating to both processes.

Efforts to implement the necessary modifications were begun during the past year with the following significant accomplishments:

1. A new regenerator support structure with associated access platforms was erected except for the safety stairways. The stairways were received and are scheduled to be installed after experiments being conducted with the regenerator in its current location are completed. The new support structure measures about 10 1/2 ft by 18 1/2 ft, with two access platforms, one located 7 ft and the other 14 ft above floor level.

2. Service requisitions were issued for all of the required fabricated components (surge tanks, sulfated-additive feed hoppers, gas preheater, cyclone receiver vessels, and cyclone reinforcements allowing the use of operating pressures up to 10 atm absolute). Fabrication of all of these components except the gas preheater is complete. The design of the gas preheater required extensive review for conformance to appropriate ASME Boiler and Pressure Vessel Codes prior to fabrication. A fabrication schedule for this unit is currently being formulated.

3. Purchase orders were issued for commercially available major components being procured from outside vendors. These components include a sulfated-sorbent solids feeder, an electronic digital scale (for measuring the feed rate of sulfated sorbent to the regenerator), a sintered-metal cartridge-type final filter assembly, an off-gas conditioning system (to be used in conjunction with the off-gas analytical instrument train), and various analytical instruments (for determining the concentration in the regenerator off-gas of O_2, SO_2, CO, CO_2, H_2, total hydrocarbons, H_2S, $NO\text{-}NO_x$, and H_2O). All of these purchased components (except the sorbent solids feeder and the off-gas conditioning system) have been received.

4. Installation drawings were prepared to specify the locations of the major process components within the existing laboratory facility.

Included in these drawings is the routing and interconnection of the various process and instrument piping required for the new regeneration system. Location of the piping was optimized for easy access for operating and maintenance purposes. The necessary valves, fittings, and pipe were procured, and arrangements were made for the installation of the various lines.

5. An itemized list was prepared of the work required to provide the necessary electrical services for the new regeneration-system process and control circuitry, and installation of the services was initiated.

ACKNOWLEDGMENTS

We gratefully acknowledge the help given by Mr. L. Burris and Mr. D. S. Webster in directing and reviewing this program and to Dr. N. Dudey and his analytical staff for analyzing samples submitted to them.

REFERENCES

1. G. J. Vogel *et al.*, "A Development Program on Pressurized Fluidized-Bed Combustion," Interim Report No. 2 for Period July 1, 1974 - Oct. 1, 1974, ANL/ES-CEN-1008.

2. G. J. Vogel *et al.*, "Reduction of Atmospheric Pollution by the Application of Fluidized-Bed Combustion and Regeneration of Sulfur-Containing Additives, Annual Report July 1971 - June 1972, "ANL/ES-CEN-1005 and EPA-R2-73-253.

3. J. D. Wheeloch and R. D. Boylen, "Reductive Decomposition of Gypsum by Carbon Monoxide," Ind. Eng. Chem. 52, 215 (March 1960).

4. "Chemical Engineering Division Physical Inorganic Chemistry Annual Report, July 1973 - June 1974, "USAEC Report ANL-8123, pp. 47-52 (1974); R. T. Yang, P. T. Cunningham, W. I. Wilson, and S. A. Johnson, Adv. Chem. Series 139, 149 (1975).

5. H. Wilsdorf and R. Haul, Nature 167, 945 (1951).

6. R. Haul and H. Wilsdorf, Acta Crystallogr. 5, 250 (1952).

7. M. J. Law *et al.*, Environ. Sci. Technol. 5, 1191 (1971).

8. J. J. Rowe, G. W. Morey, and C. C. Silber, J. Nucl. Chem. 29, 925 (1967).

9. Kirk-Othmer, Encyclopedia of Chemical Technology, Vol. 19, p. 357 (1969).

10. B. Neumann, Z. Angew. Chem. 39, 1537 (1926).

11. R. C. Hoke *et al.*, Combustion, 6-12 (January 1975).

12. "Chemical Engineering Division Environmental Chemistry Annual Report, July 1974 - June 1975," USERDA Report ANL-75-51, in preparation.

13. D. L. Keairns *et al.*, EPA Contract No. 68-02-0217, Westinghouse Research Laboratories (December 1973).

14. G. J. Vogel *et al.*, "Reduction of Atmospheric Pollution by the Application of Fluidized-Bed Combustion and Regeneration of Sulfur-Containing Additives, Annual Report July 1973 - June 1974," ANL/ES-CEN-1007 and EPA-650/2-74-104.

15. Evaluation of the Fluidized-Bed Combustion Process, "Final Report," OAP Contract 70-9, Westinghouse Research Laboratory (November 1971).

16. "Pressurized Fluidized-Bed Combustion," National Research and Development Corp., Final Report to OCR, Contract No. 14-32-0001-1511 (November 1973).

17. Exxon Corp., Private communication.

18. R. J. Bishop, "The Formation of Alkali-Rich Deposits by a High-Chlorine Coal," J. Inst. Fuel 40, 51 (1968).

19. W. T. Reid, External Corrosion and Deposit--Boilers and Gas Turbines, American Elsevier Publishing Co., Inc., New York (1971).

20. R. R. Ruch, H. H. Gluskoter, and N. F. Shimp, "Occurrence and Distribution of Potentially Volatile Trace Elements in Coal," Environmental Geological Notes, No. 72, Final Report, Illinois State Geological Survey (August 1974).

21. Analytical Group, Chemical Engineering Division, Argonne National Laboratory, private communication.

22. Douglas F. Miner and John B. Seastone, Handbook of Engineering Materials, 1st Ed., John Wiley & Sons, Inc. New York, pp. 2-131 to 2-136 (1955).

23. "Metals," Reference Issue of Machine Design Journal, p. 38 (Dec. 14, 1967).

24. L. Agosta, H. F. Illiam, R. M. Lundberg, and O. G. Tranby, "Low BTU Gas for Power Station Emission Control," Chem. Eng. Progr. 69 No. 3, 65 (1973).

25. R. J. Guidoboni, "Determination of Trace Elements in Coal and Coal Ash by Spark Source Mass Spectrometry," Anal. Chem. 45, No. 7, 1275 (1973).

26. T. Y. Kometani, J. L. Bove, B. Nathanson, S. Siebenberg, and M. Magyar, "Dry Ashing of Airborne Particulate Matter on Paper and Glass Fiber Filters for Trace Metal Analysis by Atomic Absorption Spectrometry," Environ. Sci. Technol. 6, No. 7, 617 (1972).

27. C. P. Rao, and H. J. Gluskoter, "Occurrence and Distribution of Minerals in Illinois Coals," Illinois State Geological Survey, Circular 476 (1973).

28. H. J. Gluskoter and R. R. Ruch, "Chlorine and Sodium in Illinois Coals as Determined by Neutron Activation Analysis," Fuel 50, 65-76 (1971).

29. R. A. Durie, "Direct Determination of Sodium Content of Victorian Brown Coal," Fuel 40, 146 (1961).

30. K. Govindaraju, "Rapid Flame Photometric Determination of Sodium and Potassium in Silicate Rocks," Appl. Spectosc. 20, No. 5, 302-304 (1966).

31. P. J. Jackson and A. C. Smith, "A Rapid Method for Determining Potassium and Sodium in Coal Ash and Related Materials," J. Appl. Chem. 6, 547 (1956).

32. R. B. Muter and C. F. Cockrell, "The Analysis of Sodium, Potassium, Calcium and Magnesium in Siliceous Coal Ash and Related Materials by Atomic Absorption Spectroscopy," Appl. Spectrosc. 23, No. 5, 493 (1969).

33. A. Volborth, "Dual Grinding and X-Ray Analysis of all Major Oxides in Rocks to Obtain True Composition," Appl. Spectrosc. 19, No. 1, 1 (1965).

34. C. H. Anderson and C. D. Beatty, "Spectrographic Determination of Sodium and Potassium in Coal Ashes," Anal. Chem. 26, No. 8, 1369 (1954).

35. R. G. Hunter and A. J. W. Headlee, "Spectrographic Analysis of Coal and Coal Ash," Anal. Chem. 22, No. 3, 441-445 (1950).

36. T. Kessler, A. G. Sharkey, Jr, and R. A. Friedel, "Spark Source Mass Spectrometer Investigation of Coal Particles and Coal Ash," U.S. Bureau of Mines Rep. TPR 42, Pittsburgh, Pa. (September 1971).

37. Dr. Gunnar Kullerud, Head, Department of Geoscience, Purdue University, personal communication (Apr. 23, 1975).

38. H. J. Rose, Jr, I. Adler, and F. J. Flanagan, "Z-Ray Fluorescence Analysis of the Light Elements in Rock and Minerals," Appl. Spectrosc. 17, No. 4, 81 (1963).

39. A. M. Hartstein, R. W. Freedman, and D. W. Platter, "Novel Wet-Digestion Procedure for Trace-Metal Analysis of Coal by Atomic Absorption," Anal. Chem. 45, No. 3, 611 (1973).

40. A. F. Rekus, "The Spectrographic Determination of Potassium in Coal Ash," Appl. Spectrosc. 12, No. 5, 141-142 (1958).

41. R. L. O'Neil and N. H. Suhr, "Determination of Trace Elements in Lignite Ashes," Appl. Spectrosc. 14, No. 2, 45 (1960).

42. H. J. Gluskoter, and O. W. Ree, "Chlorine in Illinois Coal," Illinois State Geological Survey, Circular 372 (1964).

43. "Methods of Analyzing and Testing Coal and Coke," U.S. Bureau of Mines, Bulletin 638 (1967).

44. D. F. S. Natusch, J. R. Wallace, and C. A. Evans, Jr., "Toxic Trace Elements: preferential concentration in respirable particles," Science 181 (4121), 202 (1974).

45. J. W. Kaakinen, R. M. Jordan, and R. E. West, "Trace element study in a pulverized-coal-fired power plant," preprint of paper presented at the 67th annual meeting of the Air Pollution Control Association, Denver, Colorado (June 9-13, 1974).

46. C. E. Billings, A. M. Sacco, W. R. Matson, R. M. Griffin, W. R. Coniglio, and R. A. Hanley, "Mercury balance on a large pulverized coal-fired furnace," J. Air Poll. Contr. Assoc. 23 (9), 773 (1973).

47. N. E. Bolton, J. A. Carter, J. F. Emergy, C. Feldman, W. Fulkerson, L. D. Hulett, and W. S. Lyon, "Trace element mass balance around a coal-fired steam plant," in Preprints of papers presented at 166th National Meeting, American Chemical society, Division of Fuel Chemistry 18 (4), 114 (1973).

48. A. Attari, "Fate of trace constituents of coal during gasification," Environmental Protection Agency Report EPA-650/2-73-004 (1973).

49. R. R. Ruch, H. J. Gluskoter, and N. F. Shimp, "Occurrence and Distribution of Potentially Volatile Trace Elements in Coal: An Interim Report," Environmental Geology Note No. 61, Illinois State Geological Survey (1973).

50. S. Ergun, Chem. Eng. Progr. 48, 89-94, (1952).

51. P. C. Carman, Trans. Inst. Chem. Eng. 15, 150-66 (1937).

52. T. H. Chilton and A. P. Colburn, Trans. Am. Inst. Chem. Eng. 26, 178-96 (1931).

53. M. Leva, Chem. Eng. Progr. 43, 549-554 (1947).

54. M. Leva and M. Grummer, Chem. Eng. Progr. 43, 633-38, 713-18 (1947).

55. S. Ergun and A. A. Orning, Ind. Eng. Chem. 41, 1179-84 (1949).

56. D. Kunii and O. Levenspiel, Fluidization Engineering, Ch. 3, John Wiley & Sons, Inc., New York (1969).

57. L. E. Brownell and D. L. Katz, Chem. Eng. Progr. 43, 537-48, (1947).

58. R. D. Morse, Ind. Eng. Chem. 41, 1117-24 (1949).

59. M. Leva, Fluidization, Chapter 3, p. 62, McGraw-Hill Book Co., Inc., New York (1959).

60. J. F. Frantz, Chem. Eng. 69, 161-78 (1962).

61. G. Narsimhan, A.I.Ch.E. J. 11, 550-4 (1965).

62. J. F. Frantz, Chem. Eng. Progr. Sym. Series 62, No. 62, 21-31 (1966).

63. C. Y. Wen and Y. H. Yu, Chem. Eng. Progr. Sym. Series 62, No. 62, 100-11 (1966).

64. C. Y. Wen and Y. H. Yu, A.I.Ch.E. J. 12, 610-12 (1966).

65. J. F. Davidson and D. Harrison, Fluidized Particles, p. 14, Cambridge University Press, London (1963).

66. L. Davies and J. F. Richardson, Trans. Inst. Chem. Eng. 44, T293-T305 (1966).

67. T. Mii, K. Yoshida, and D. Kunii, J. Chem. Eng. Japan 6, 100-2 (1972).

68. B. Singh, G. R. Rigby, and T. G. Callcott, Trans. Inst. Chem. Eng. 51, 93-6 (1973).

69. J. Broughton, Trans. Inst. Eng. 52, 105-7 (1974).

70. Reference 59, p. 64, equation 3-24.

71. R. G. Kunz, Powder Technol. 4, 156-62 (1970-71).

72. R. E. Hicks, Ind. Eng. Chem. Fundam. 9, 500-2 (1970).

73. F. A. Zenz, Petrol. Refiner 36, 147-55 (1957).

74. F. A. Zenz and D. F. Othmer, Fluidization and Fluid-Particle Systems, Reinhold Publishing Corporation, New York, Ch. 7 (1960).

75. K. E. Bertil Andersson, Chem. Eng. Sci. 15, 276-97 (1971).

76. R. H. Wilhelm and M. Kwauk, Chem. Eng. Progr. 44, 201-18 (1948).

77. J. R. Richardson, Fluidization, Ch. 2, p. 26, J. F. Davidson and D. Harrison, Eds., Academic Press, New York (1971).

78. J. B. Romero and L. N. Johanson, Chem. Eng. Progr. Symp. Ser. 58(38), 28-37 (1962).

79. A. Skopp, M. S. Nutkis, G. A. Hammons, and R. R. Bertrand, "Studies of the Fluidized Lime-Bed Coal Combustion Desulfurization System. Part I: Design of the High Pressure Fluidized Bed Combustion Lime Regeneration Pilot Plant Unit - The FBCR Miniplant. Part II: Factors Affecting NO_x Formation and Control in Fluidized Bed Combustion," EPA Report APTD-1116 or PB-210246 (December 1971).

APPENDIX A. CHARACTERISTICS OF RAW MATERIALS USED IN FLUIDIZED-BED COMBUSTION EXPERIMENTS

Table A-1. Particle-Size Distribution and Chemical Characteristics of Type-38 Alundum Grain Obtained from the Norton Company

Sieve Analysis	
U.S. Sieve No.	Wt % on Sieve
+14	0.0
-14 +25	15.7
-25 +35	73.3
-35 +45	11.0
-45 +80	0.0
Total	100.0

Typical Chemical Analysis	
Component	Wt %
Al_2O_3	99.49
SiO_2	0.05
Fe_2O_3	0.10
TiO_2	0.01
Na_2O	0.35

Table A-2. Particle-Size Distribution and Chemical Characteristics of Arkwright Coal

Sieve Analysis	
U.S. Sieve No.	% on Sieve
+14	0.0
-14 +25	8.0
-25 +35	14.2
-35 +45	12.3
-45 +80	24.7
-80 +170	17.9
-170	23.0
Mean Particle Dia:	323 μm

	Proximate Analysis (wt %)	
	As Received	Dry Basis
Moisture	2.89	--
Volatile Matter	38.51	39.66
Fixed Carbon	50.92	52.43
Ash	7.68	7.91
	100.00	100.00
Sulfur, wt %	2.82	2.90
Heating value, Btu/lb	13,706	14,114

	Ultimate Analysis (wt %)
Carbon	77.14
Hydrogen	5.23
Sulfur	2.90
Nitrogen	1.66
Chlorine	0.19
Ash	7.91
Oxygen (by difference)	4.97

Table A-3. Particle-Size Distribution and Chemical Characteristics of Tymochtee Dolomite

	Sieve Analysis	
C-Experiments	U.S. Sieve No.	% on Sieve
	+14	0.4
	-14 +25	48.6
	-25 +35	19.9
	-35 +45	18.8
	-45 +80	11.7
	-80 +170	0.4
	-170	0.4
	Average Particle Size:	750 µm
EA-Experiments	U.S. Sieve No.	% on Sieve
	+14	0
	-14 +20	33.51
	-20 +25	26.52
	-25 +30	19.00
	-30 +35	10.79
	-35 +45	9.80
	-45	0.38
	Average Particle Size:	803 µm

Component	Chemical Analysis (wt %)
Ca	20.0
Mg	11.3
CO_2	38.5
H_2O	0.2

Derived Composition	
$CaCO_3$	50.0
$MgCO_3$	39.1

Table A-4. Particle-Size Distribution and Chemical Characteristics of Limestone No. 1359, M. J. Grove Lime Co., Stephen City, Va.

Sieve Analysis	
U.S. Sieve No.	% on Sieve
+14	0.63
-14 +25	45.80
-25 +35	16.36
-35 +45	15.10
-45 +80	15.17
-80 +170	5.82
-170	1.13
Average Particle Size:	700 μm

Component	Chemical Analysis (wt %)
Ca	38.3
Mg	0.29
CO_2	39
H_2O	1.56

Derived Composition	
$CaCO_3$	95.8
$MgCO_3$	1.0

APPENDIX B: OPERATING CONDITIONS FOR FAC-EXPERIMENTS

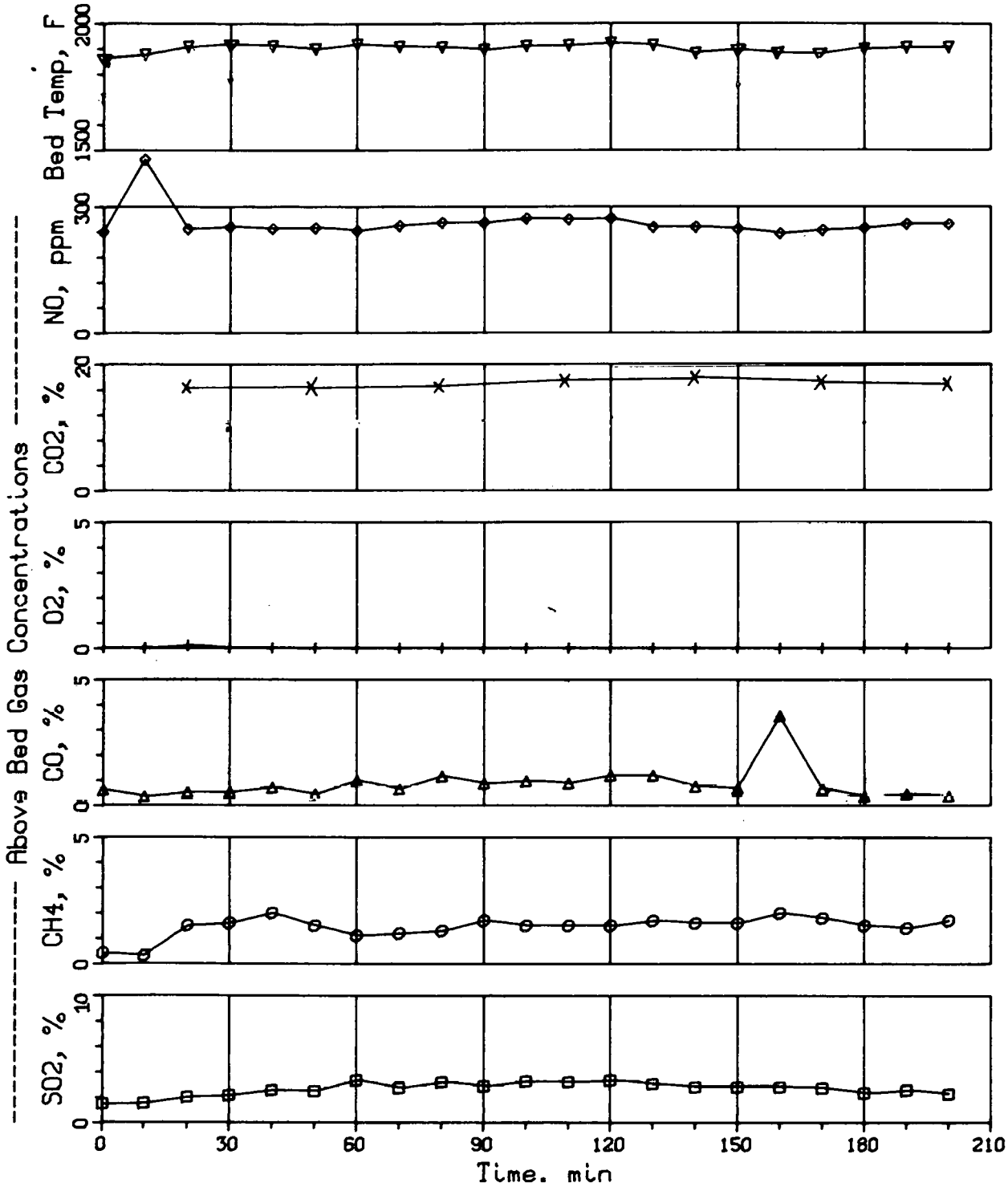

Fig. B-1. Bed Temperature and Gas Concentrations in Off-Gas, Experiment FAC-1R1

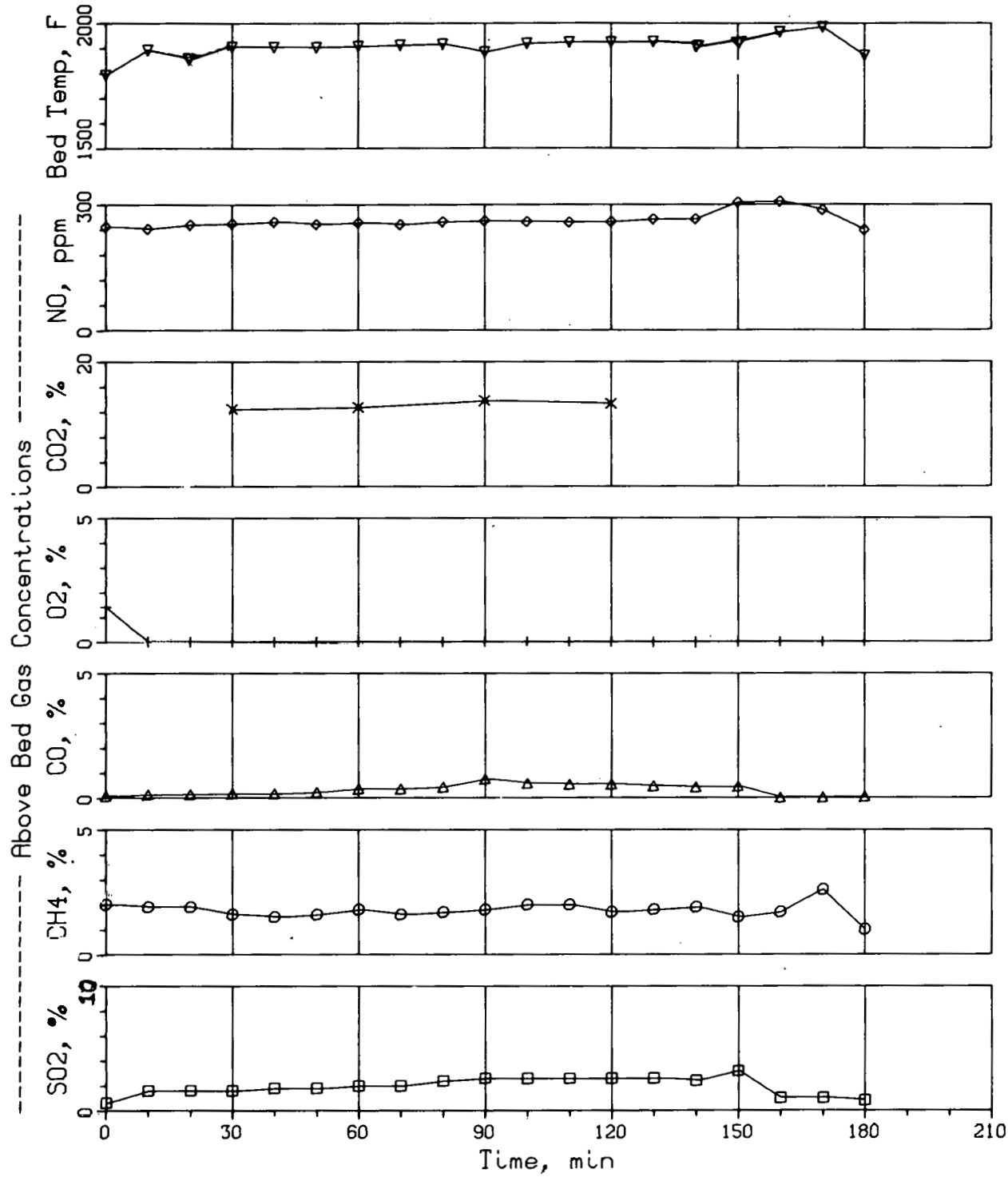

Fig. B-2. Bed Temperature and Gas Concentrations in Off-Gas, Experiment FAC-1R2

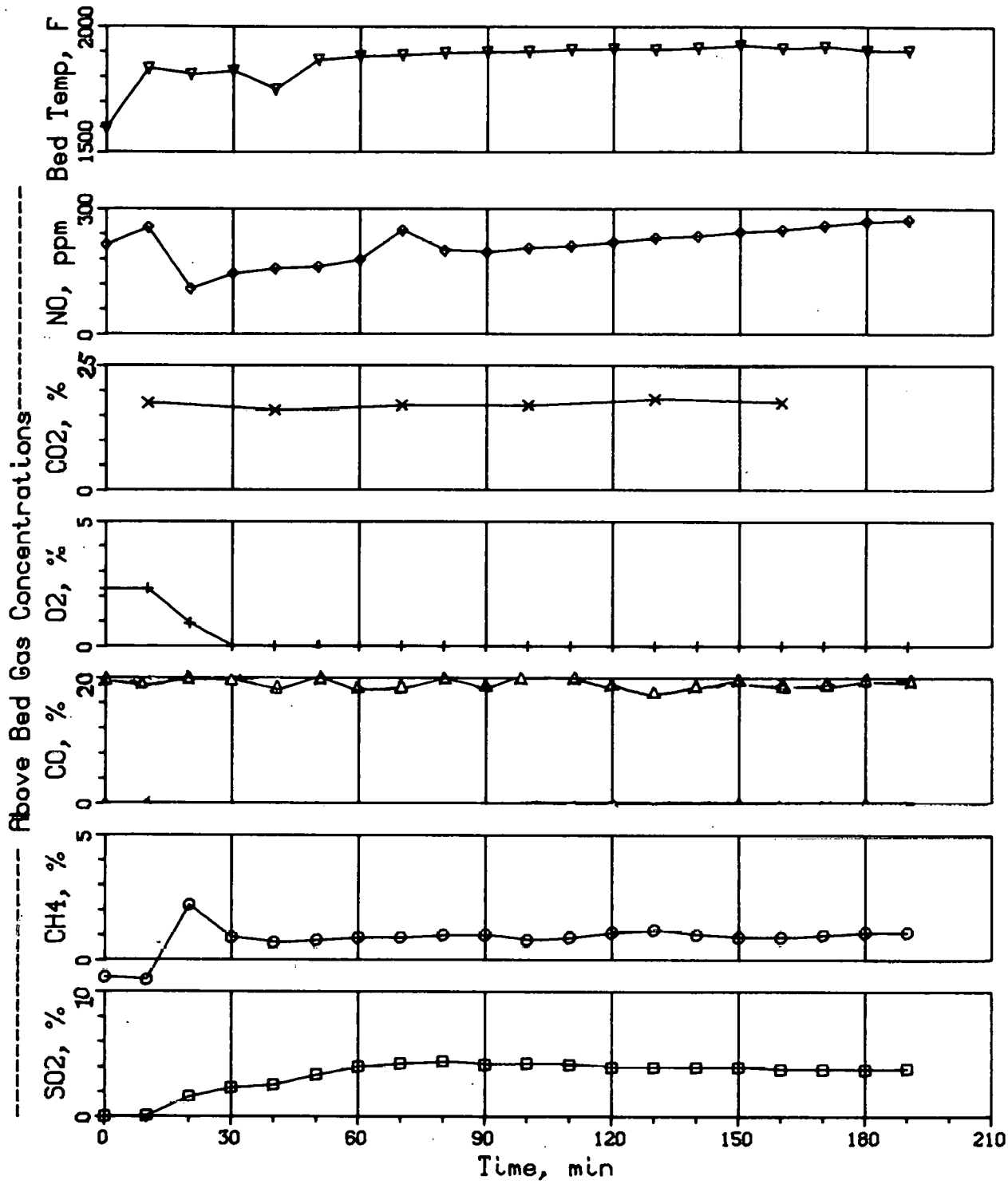

Fig. B-3. Bed Temperature and Gas Concentrations in Off-Gas, Experiment FAC-3

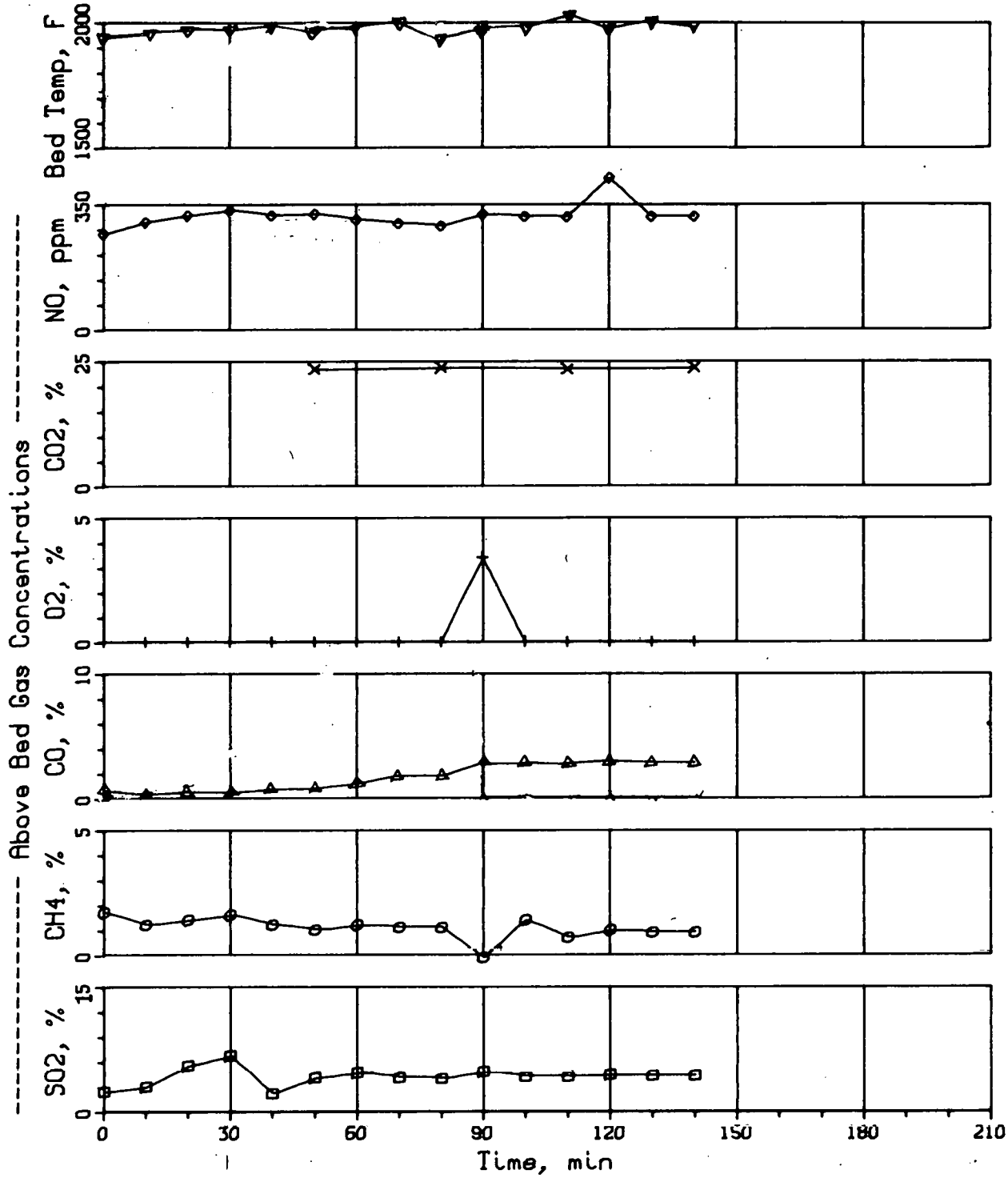

Fig. B-4. Bed Temperature and Gas Concentrations in Off-Gas, Experiment FAC-4

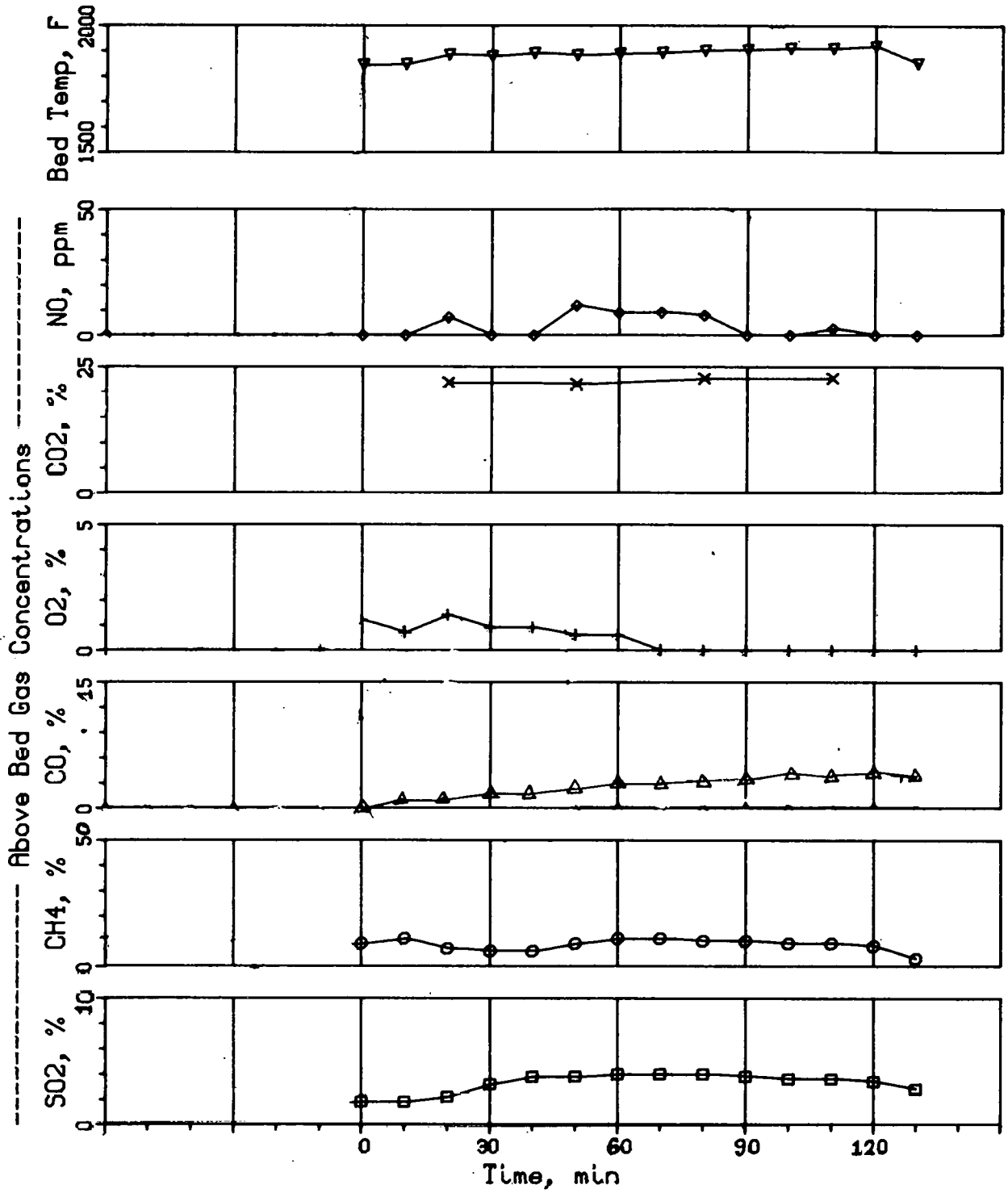

Fig. B-5. Bed Temperature and Gas Concentrations in Off-Gas, Experiment FAC-5

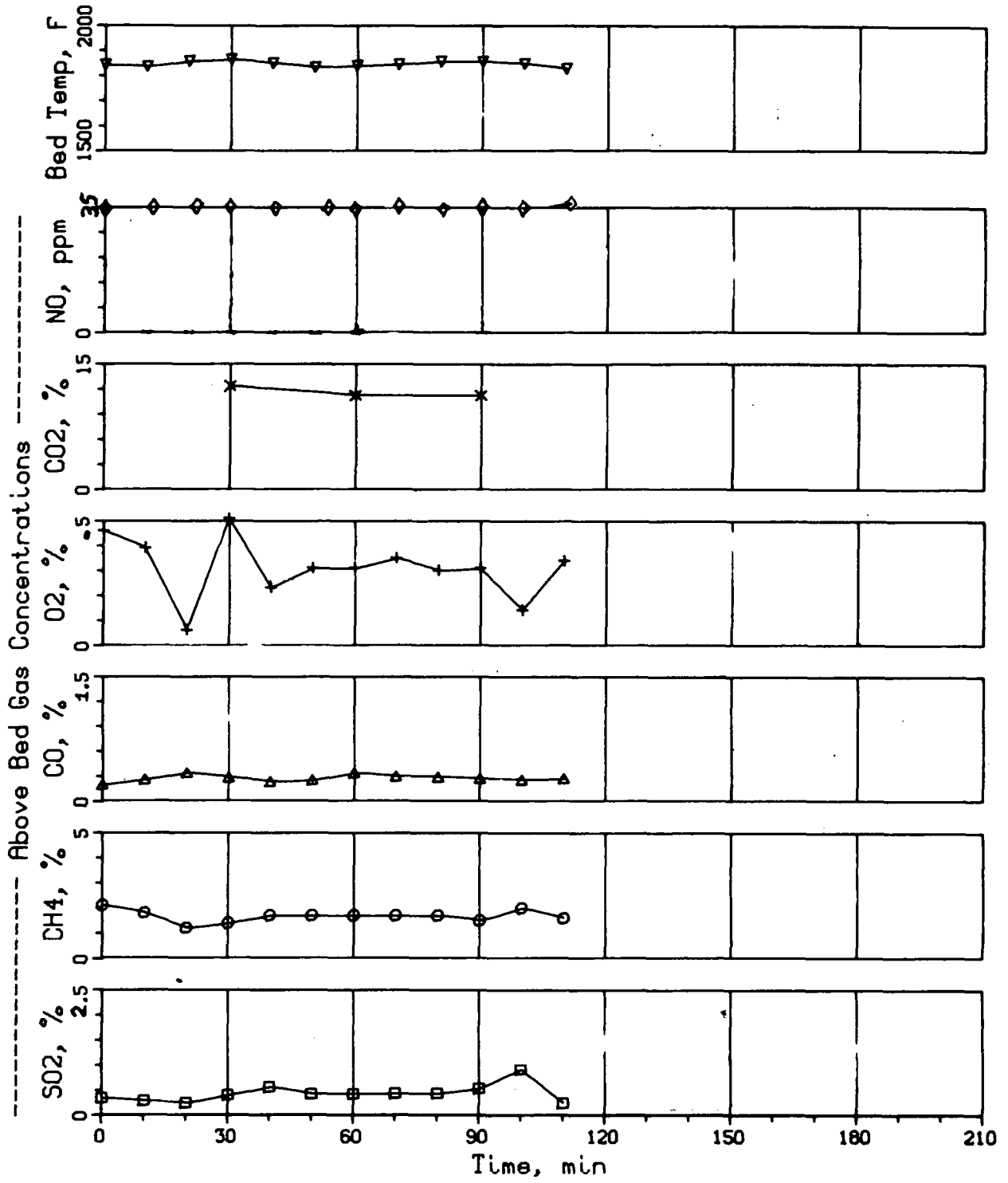

Fig. B-6. Bed Temperature and Gas Concentrations in Off-Gas, Experiment FAC-8

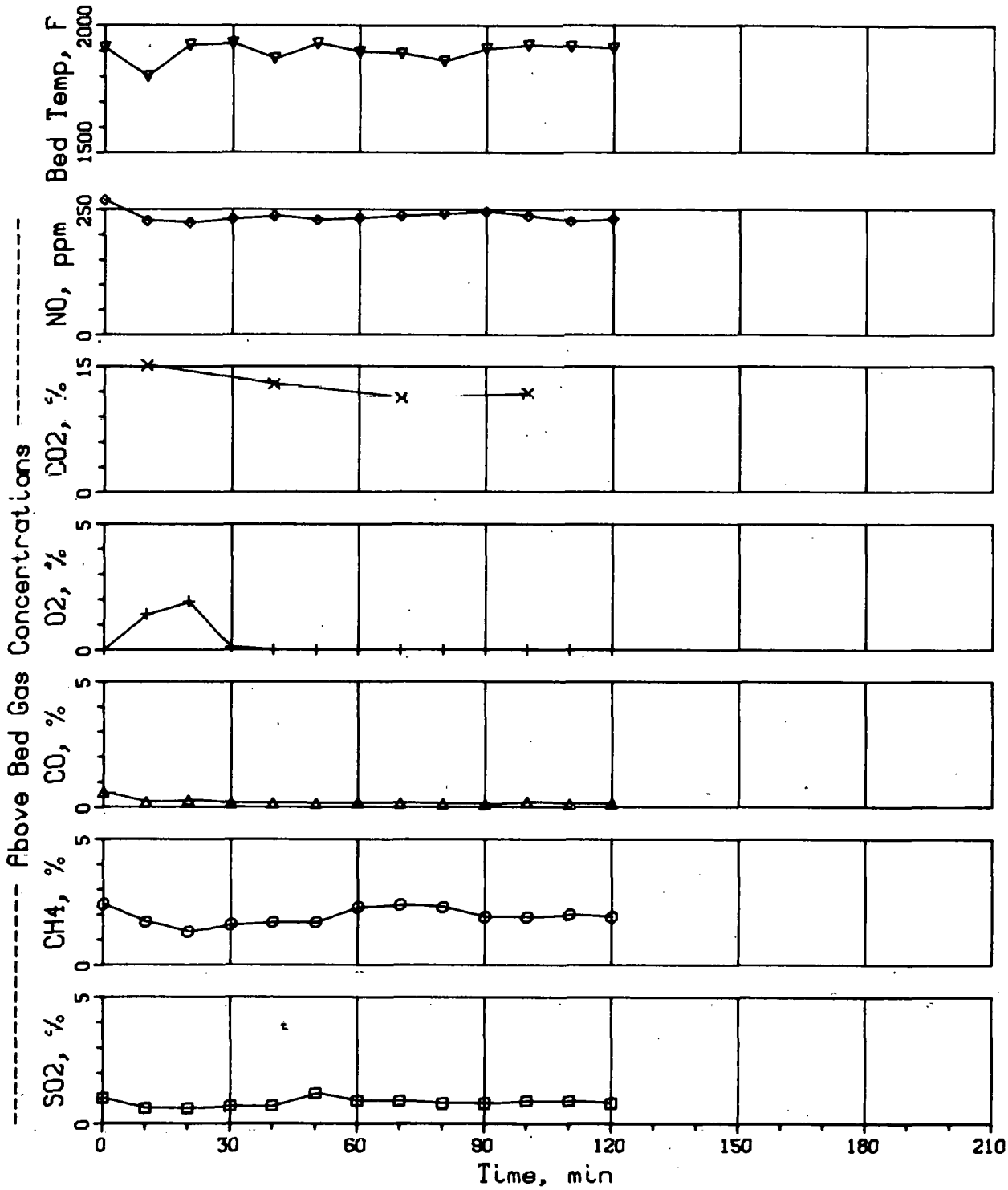

Fig. B-7. Bed Temperature and Gas Concentrations in Off-Gas, Experiment FAC-9

APPENDIX C. CARBON, SULFUR, AND CALCIUM BALANCES FOR C-, LC-, and EA- EXPERIMENTS

Table C-1. Carbon and Sulfur Material Balances for Experiment C-2

Bed Temperature, °C: 955
Ca/S Mole Ratio: 1.5
Gas Velocity, ft/sec: 3.5
Flue-Gas O_2, %: 3

Source of Material	Weight, g	Carbon, wt %	Carbon, g	Sulfur, wt %	Sulfur, g
Material in					
Starting bed[a]	15,770	10.5	1,656	0.3	47.3
Coal	199,100	74.91	149,145	2.82	5614.6
Dolomite Additive	56,700	10.5	5,954	0.3	170.1
			156,755		5832.0
Material out					
Final bed	13,413	0.4	57.7	11.06	1483.5
Bed overflow	17,978	0.5	89.9	10.34	1858.9
Primary cyclone	40,350	9.2	3,712.2	7.24	2921.3
Secondary cyclone	415	7.6	31.5	3.36	13.9
Primary filter	1,180	6.2	73.2	3.55	41.9
Flue gas[b]			147,060.6[c]		234.0[d]
			151,025		6,319.5
	% Balance		96.3%		112%

[a] Unsulfated dolomite.

[b] Avg. flue-gas flow rate, (cfm @21°C (70°F) and 1 atm) = 72

[c] Calculated for avg. CO conc. of 48 ppm plus avg. CO_2 conc. of 15%.

[d] Calculated for avg. SO_2 conc. of 80 ppm.

Table C-2. Carbon and Sulfur Material Balances for Experiment C-3A, C-3B, C-3C

Bed Temperature, °C: 900
Ca/S Mole Ratio: 1.1
Gas Velocity, ft/sec: 3.5
Flue-Gas O_2, %: 2.8-3.0

Source of Material	Weight, g	Carbon, wt %	Carbon, g	Sulfur, wt %	Sulfur, g
Material in					
Starting bed[a]	12,483	10.5	1,311	11.06	1,381
Coal	166,500	74.9	124,725	2.82	4,695
Dolomite additive	31,800	10.5	3,339	0.3	95.4
			129375		6,171
Material out					
Final bed	15,121	1.2	181	12.45	1,883
Bed overflow	11,397	1.3	148	10.99	1,253
Primary cyclone	29,399	41.9	12,318	2.48	729
Secondary cyclone	4,375	34.7	1,518	3.23	141
Primary filter	3,485	18.5	645	3.18	111
Flue gas[b]	72,200		116,000[c]		781[d]
			130,810		4,898
% Balance			101		79.4

[a] Partially sulfated dolomite, source experiment C-2.

[b] Avg. flue-gas flow rate, (cfm @ 21°C and 1 atm) = 72.2

[c] Calculated for avg. CO conc. of 35 ppm plus avg. CO_2 conc. of 16%.

[d] Calculated for avg. SO_2 conc. of 360 ppm.

Table C-3. Carbon and Sulfur Material Balances for Experiment LC-1

Bed Temperature, °C: 955
Ca/S Mole Ratio = 1.75
Gas Velocity, ft/sec = 3.5
Flue-Gas O_2, % = 3

Source of Material	Weight, g	Carbon, wt %	Carbon, g	Sulfur, wt %	Sulfur, g
Material in					
Starting bed[a]	14,501	11.4	1653	-	-
Coal	147,200	74.9	130413	2.82	4,912
Limestone additive	23,100	11.4	2633	-	-
			134699		4,912
Material out					
Final bed	15,793	0.8	126	10.33	1,631
Bed overflow	2,422	1.8	44	8.48	205
Primary cyclone	29,394	26.1	7672	3.32	976
Secondary cyclone	2,080	10.9	227	5.32	111
Primary filter	3,474	13.3	462	4.10	142
Flue gas[b]			122000[c]		1,533[d]
			130531		4,598
% Balance			97		94

[a] Unsulfated limestone No. 1359.

[b] Avg. flue-gas flow rate, (cfm @ 21°C and 1 atm) = 72

[c] Calculated for avg. CO conc. of 40 ppm plus avg. CO_2 conc. of 16%.

[d] Calculated for avg. SO_2 conc. of 675 ppm.

Table C-4. Carbon, Sulfur, and Calcium Material Balances for Experiment LC-2B

Bed Temperature, °C: 955
Ca/S Mole Ratio = 2.7
Gas Velocity, ft/sec = 3.5
Flue-Gas O_2, % =

Source of Material	Weight, g	Carbon, wt %	Carbon, g	Sulfur, wt %	Sulfur, g	Calcium, wt %	Calcium, g
Material in							
Starting bed[a]	15,000	12.0	1,800	-	-	39.1	5,865
Coal	243,230	74.91	182,129	2.82	6,859	0.26	632
Limestone additive	70,535	12.0	8,464	-	-	39.1	27,579
			192,393		6,859		34,076
Material out							
Final bed	15,873	4.37	694	9.40	1,492		
Bed overflow	7,485	6.36	476	7.86	588		
Primary cyclone	43,458	16.69	7,253	4.76	2,069		
Secondary cyclone	966	12.86	124	3.94	38		
Primary filter	916	10.94	100	5.44	50		
Flue gas[b]			189,901[c]		1501.3[d]		
			198,548		5738		
	% Balance		103.2		84		

[a] Unsulfated Limestone No. 1359.

[b] Avg. flue-gas flow rate, (cfm @ 21°C and 1 atm) = 72.1

[c] Calculated for avg. CO conc. of 50 ppm plus avg. CO_2 conc. of 17%.

[d] Calculated for avg. SO_2 conc. of 504 ppm.

Table C-5. Carbon and Sulfur Material Balances for Experiment LC-3A

Bed Temperature, °C = 900
Ca/S Mole Ratio = 1.5
Gas Velocity, ft/sec = 3.5
Flue-Gas O_2, % = 2.9

Source of Material	Weight, g	Carbon, wt %	Carbon, g	Sulfur, wt %	Sulfur, g	Calcium, wt %	Calcium, g
Material in							
Starting bed[a]	17,500	5.9	1,033	~10.71	~1,874		
Coal	108,864	74.91	81,550	2.82	3,070	0.26	283
Limestone additive	16,783	12.0	2,014			39.1	6,562
			84,597		4,944		
Material out							
Final bed	16,240	5.89	957	10.71	1,739		
Bed overflow	4,272	6.40	273	10.15	434		
Primary cyclone	24,512	28.26	6,927	5.72	1,402		
Secondary cyclone	1,085	18.96	206	3.44	37		
Primary filter	396	13.24	52	5.38	21		
Flue gas[b]			79,234[c]		1,176[d]		
			87,649		4,809		
	% Balance		103.6		97.3		

[a] Partially sulfated limestone, source experiment LC-3.

[b] Avg. flue-gas flow rate, cfm @ 21°C and 1 atm = 75.5

[c] Calculated for avg. CO conc. of 31 ppm plus avg. CO_2 conc. of 16.54%.

[d] Calculated for avg. SO_2 conc. of 920 ppm.

Table C-6. Carbon and Sulfur Material Balances for Experiment EA-1

Bed Temperature, °C = 900
Ca/S Mole Ratio = 1.4
Gas Velocity, ft/sec = 4.5
Flue-Gas O_2, % = 3.57

Source of Material	Weight, g	Carbon, wt %	Carbon, g	Sulfur, wt %	Sulfur, g
Material in					
Starting bed[a]	15,026	10.5	1578	11.4	1713
Coal	299,400	74.91	224281	2.82	8443
Dolomite additive	78,500	10.5	8342	0.3	236
			234102		10392
Material out					
Final bed	16,074	1.24	199	10.90	1752
Bed overflow	7,717	0.81	63	11.36	877
Primary cyclone	92,225	35.82	33035	3.75	3458
Secondary cyclone	3,695	14.31	529	4.60	170
Primary filter	2,086	8.56	179	6.28	131
Flue gas[b]			216083[c]		1366[d]
			250088		7754
	% Balance		106.8		74.6

[a] Partially sulfated dolomite, source experiment EA-2.

[b] Avg. flue-gas flow rate, (cfm @ 21°C and 1 atm) = 98.

[c] Calculated for avg. CO conc. of 30 ppm plus avg. CO_2 conc. of 16.8%.

[d] Calculated for avg. SO_2 conc. of 392 ppm.

Table C-7. Carbon and Sulfur Material Balances for Experiment EA-2

Bed Temperature, °C = 900
Ca/S Mole Ratio = 1.4
Gas Velocity, ft/sec = 4.5
Flue-Gas O_2, % = 9.24

Source of Material	Weight, g	Carbon, wt %	Carbon, g	Sulfur, wt %	Sulfur, g
Material in					
Starting bed[a]	14,730	10.5	1,547	12.47	1837
Coal	200,000	74.91	159,820	2.82	5640
Dolomite additive	52,200	10.5	5,481	0.3	157
			166,848		7634
Material out					
Final bed	15,026	.34	51.1	11.40	1713
Bed overflow	7,547	.52	39.2	11.33	855
Primary cyclone	66,763	19.18	12,805.0	5.34	3565
Secondary cyclone	2,123	9.31	197.7	4.26	90
Primary filter	1,021	2.3	23.5	6.70	68
Flue gas[b]			156,057.0[c]		1520[d]
			169,174.0		7811
	% Balance		101.4		102.3

[a] Partially sulfated dolomite, source experiment EA-4.

[b] Avg. flue-gas flow rate, (cfm @ 21°C and 1 atm) = 98

[c] Calculated for avg. CO conc. of 40 ppm plus avg. CO_2 conc. of 14.2%.

[d] Calculated for avg. SO_2 conc. of 512 ppm.

Table C-8. Carbon and Sulfur Material Balances for Experiment EA-4

Bed Temperature, °C = 900
Ca/S Mole Ratio = 1.3
Gas Velocity, ft/sec = 45
Flue-Gas O_2, % = 15.75

Source of Material	Weight, g	Carbon, wt %	Carbon, g	Sulfur, wt %	Sulfur, g
Material in					
Starting bed[a]	15,000	10.5	1,575	0.3	45
Coal	212,700	74.9	159,333	2.82	5998
Dolomite additive	46,700	10.5	4,903	0.3	140
			165,811		6183
Material out					
Final bed	14,730	0.15	22.1	12.97	1837
Bed overflow	6,846	0.726	49.7	11.61	795
Primary cyclone	34,594	11.87	4,103.0	4.72	1633
Secondary cyclone	1,654	6.94	114.8	4.38	72
Primary filter	2,710	4.94	133.9	6.00	162
Flue gas[b]			185,099.0[c]		2497[d]
			189,523		6998
	% Balance		114		113.2

[a] Unsulfated dolomite.

[b] Avg. flue-gas flow rate, (cfm @ 21°C and 1 atm) = 98

[c] Calculated for avg. CO conc. of 40 ppm plus avg. CO_2 conc. of 10.2%.

[d] Calculated for avg. SO_2 conc. of 510 ppm.

Table C-9. Carbon and Sulfur Material Balances for Experiment EA-5.

Bed Temperature, °C = 900
Ca/S Mole Ratio = 2.9
Gas Velocity, ft/sec = 4.5
Flue-Gas O_2, % = 9.24

Source of Material	Weight, g	Carbon, wt %	Carbon, g	Sulfur, wt %	Sulfur, g
Material in					
Starting bed[a]	15,540	∿3.4	∿528	∿9.7	1,507
Coal	102,967	74.91	77,133	2.82	2,904
Dolomite additive	48,535	10.5	5,096	0.3	146
			82,757		4,557
Material out					
Final bed	14,650	3.36	492	9.67	1,417
Bed overflow	3,602	0.82	30	11.40	411
Primary cyclone	40,587	10.06	4,083	6.66	2,703
Secondary cyclone	1,507	9.82	148	4.49	68
Primary filter	493	4.59	23	6.62	33
Flue gas[b]			74,890[c]		188[d]
			79,666		4,820
	% Balance		96.3		105.8

[a] Partially sulfated dolomite, source experiment EA-3.

[b] Avg. flue-gas flow rate, (cfm @ 21°C and 1 atm) = 95.

[c] Calculated for avg. CO conc. of 45 ppm plus avg. CO_2 conc. of 15.5%.

[d] Calculated for avg. SO_2 conc. of 128 ppm.

Table C-10. Carbon and Sulfur Material Balances for Experiment EA-6

Bed Temperature, °C = 900
Ca/S Mole Ratio = 2.1
Gas Velocity, ft/sec = 4.5
Flue-Gas O_2, % = 15.75

Source of Material	Weight, g	Carbon, wt %	Carbon, g	Sulfur, wt %	Sulfur, g
Material in					
Starting bed[a]	13,840	0.9	125	10.92	1,511
Coal	107,957	74.91	80,871	2.82	3,044
Limestone additive	44,453	10.5	4,668	0.3	133
			85,664		4,688
Material out					
Final bed	14,643	0.88	129	10.14	1,485
Bed overflow	3,427	3.38	116	10.18	349
Primary cyclone	37,517	7.06	2,649	5.44	2,041
Secondary cyclone	1,222	7.77	95	4.80	59
Primary filter	573	1.44	8	6.28	36
Flue gas[b]			80,275[c]		198[d]
			83,272		4,168
		% Balance	97.2		88.9

[a] Partially sulfated dolomite, source experiment EA-7.

[b] Avg. flue-gas flow rate, (cfm @ 21°C and 1 atm) = 98

[c] Calculated for avg. CO conc. of 60 ppm plus avg. CO_2 conc. of 12.1%.

[d] Calculated for avg. SO_2 conc. of 112 ppm.